UNIVERSITAT DE BARCELONA

Caracterització de la precipitació i canvi climàtic en àrees de muntanya. El cas dels Pirineus

Marc Lemus i Cánovas

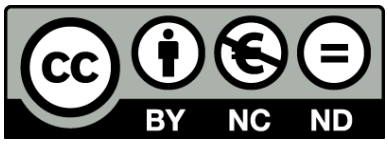

Caracterització de la precipitació i canvi climàtic en àrees de muntanya.

El cas dels Pirineus

Marc Lemus I Cánovas

Programa de doctorat Geografia, Planificació Territorial i Gestió Ambiental

Departament de Geografia

Universitat de Barcelona

Setembre 2021

Climatology Group

Universitat de Barcelona

UNIVERSITAT DE BARCELONA

Programa de Doctorat Geografia, Planificació Territorial i Gestió Ambiental

Departament de Geografia

Caracterització de la precipitació i canvi climàtic en àrees de muntanya. El cas dels Pirineus

Memòria presentada per:
Marc Lemus I Cánovas
per obtenir el títol de doctor

Tesi Doctoral dirigida pels directors:
Dr. Javier Martín Vide
Dr. Joan Albert López Bustins

Tesi Doctoral tutoritzada per:
Dr. Javier Martín Vide

Barcelona, setembre de 2021

Als meus avis i àvies, Pepe, Pepita, Josep Maria i Carme.

Agraïments

Voldria agrair, en primer lloc, tot el suport que m'han brindat els directors d'aquesta tesi doctoral, el Dr. Javier Martín Vide i el Dr. Joan Albert López Bustins. Al Dr. Javier Martín Vide agrair-li tot l'acompanyament fet durant el període predoctoral, tant per la supervisió d'aquesta tesi, com per iniciar-me en el camp de la docència universitària compartint l'assignatura de Geografia Física i Climatologia del Grau de Ciències Ambientals. També li voldria agrair les oportunitats brindades en projectes externs a aquesta tesi doctoral, així com la llibertat total a l'hora de treballar, la qual cosa ha estat un privilegi. Al Dr. Joan Albert López Bustins, amic i director, li agraeixo la seva implicació durant tot el període predoctoral. De fet, si aquesta tesi ha arribat a bon port és gràcies a la motivació que m'ha brindat des que el 2012 vaig iniciar el Grau en Geografia. Ha estat una sort poder comptar amb el seu acompanyament i mestratge durant aquesta etapa, no només des d'un punt de vista professional, si no també personal. Moltes gràcies pel vostre suport en tot aquest irregular recorregut.

També he d'agrair la possibilitat que m'han brindat els dos directors en incorporar-me al Grup de Climatologia, per la integració en els seus projectes de recerca WEMOTOR (CSO2014-55799-C2-1-R) i CLICES (CGL2017-83866-C3-2-R), i per la possibilitat de presentar-me amb ells a la convocatòria predoctoral FPU (FPU2017/02166), la qual m'ha permès dedicar-me a temps complet al món de la recerca i de la docència universitària. Per tant, he de fer extensibles els agraïments al Ministeri d'Universitats de l'estat espanyol, pel finançament rebut durant aquest període. També aprofito per agrair el finançament puntual rebut de l'Institut de Recerca de l'Aigua de la Universitat de Barcelona, així com, per part del Centre de la Neu i la Muntanya d'Andorra de l'Institut d'Estudis Andorrans. Voldria que els meus agraïments arribessin també al Servei Meteorològic de Catalunya, a l'Agència Estatal de Meteorologia i a l'Observatori Pirinenc del Canvi Climàtic, per totes les dades que m'han facilitat i que han permès conduir la tesi doctoral que aquí es presenta.

Pel que fa al Grup de Climatologia, voldria manifestar un gran agraïment a la companya de batalla, Laia Arbiol, amb la qual ha estat més fàcil saldar els contratemps que, inevitablement, apareixen durant aquest període predoctoral. Voldria fer extensibles els agraïments a les companyes que, amb menor freqüència, també han format part del meu dia a dia en aquest grup, i amb les quals he compartit bons moments: La Petia Guintchev i la Núria Casals de l'Institut de l'aigua; i les companyes de grup i laboratori, Mari Carmen Moreno, Maria José Cordobilla, Daniela Sandoval i Laura Malermo.

Una altra persona que ha aplanat el camí del doctorat, i la qual també n'ha motivat la seva temàtica, és la Dra. Laura Trapero, que juntament amb tot l'equip del CENMA, em van acollir generosament l'estiu del 2017 a Andorra, fent possible la meva primer estada de recerca durant els estudis de màster. Posteriorment, a més, em varen finançar dos mesos de recerca abans d'iniciar el contracte FPU, i una nova valuosa experiència.

Lligat al període de màster, també voldria agrair als tècnics de la Unitat de Predicció d'Allaus de l'Institut Cartogràfic i Geològic, l'oportunitat d'estar becat en aquesta important institució. L'últim any de becari va suposar l'embrió de la idea inicial d'aquesta tesi doctoral. Impagable, doncs, l'acompanyament d'en Santi Manguan, Carles Garcia i Glòria Martí durant aquell període.

La possibilitat de realitzar estades de recerca en altres grups d'investigació m'ha donat la possibilitat de conèixer temàtiques que m'eren alienes, així com persones que ara puc considerar amigues. En aquest sentit, voldria expressar el meu sincer agraïment a l'Swen Brands i a en Gonzalo Míguez per fer tan còmoda i profitosa l'estada a Meteogalicia i al Grup de Física No Lineal de la

Universitat de Santiago de Compsotela. D'aquesta estada a Santiago m'emporto també l'amistat d'en Damián, en Martín, en Darío i la Irma. Amb ells vaig poder conèixer els entorns naturals de Galicia, així com el Santiago nocturn.

Seguint amb el recorregut de les estades, durant el mes que vaig estar a la Universitat de Porto, en Dominic Royé va fer de gran amfitrió. Gràcies per tots els recursos oferts durant aquest període sobre el llenguatge R, a part d'ensenyar-me Porto i la seva costa.

Finalment, agrair al Professor Ricardo Machado Trigo la predisposició a acollir-me a l'Instituto Dom Luiz de la Universitat de Lisboa, en temps de pandèmia. Ha estat un plaer poder treballar en el seu equip. D'aquí també m'emporto alguns amics que han fet que l'estada fos entretinguda tot i les restriccions per la pandèmia. Gràcies Álvaro, Carmen, Celia, Paco y Óscar.

Retornant a Barcelona, i concretament al Departament de Geografia, voldria donar les gràcies a tots els companys de doctorat pel recolzament mutu brindat durant aquest període, però sobretot per la sintonia i bon ambient. En especial a: la Laia Arbiol, a l'Eduard Montesinos, la Tania Cearreta, la Julia Garcia, en Carlos Sánchez, la Laia Casanovas, el Miquel Ángel Calero i en Marcos Francos, així com a tots els membre del grup de "Dinars al Lab", és a dir, els anteriors, juntament amb en Dr. Xavier Úbeda i el Dr.Filipe Carvalho, així com la Verónica Gallego. Menció especial al bon amic Albert Santasusagna, amb el qual ha estat un plaer compartir departament.

Com no podia ser d'una altra manera, vull agrair a en Roger Clavero, Raúl Estévez, Martí Oliveras i Carles Masachs, col · legues d'aquella promoció del 2012-13 del Grau en Geografia, la seva amistat i el voler compartir inquietuds científiques però també personals. No vull oblidar-me tampoc de la resta de companys de la carrera.

Ara bé, el que tinc clar de veritat, es que si no fos per la colla d'amics que tinc a Vilanova, això hagués costat molt més. En especial al meu gran amic de tota la vida, en Joan López, que simplement per haver entomat incondicionalment el dur còctel de confinament i cabòries de la meva tesi, ja és mereixedor d'un gran agraïment.

També voldria fer un agraïment especial a l'amic Aleu Pons, que durant la temporada en què hem viscut al pis amb en Joan, s'ha creat una cohesió molt maca entre tots tres, difícil de trencar d'ara en endavant. Voldria agrair a la resta d'amics del grup BBQ el compartir estones de cerveses, cartes, càmpings i sortides en BTT: al Miquel Margalef, al Guillem Serra, a l'Andoni Bengoetxea, a la Milena Rugoso, al Guillem Ramos, a la Gemma Jorquera, al Marc Montané, a l'Adrià Sánchez i a l'Albert Cermeno. Gràcies també, Marc Martínez, per compartir moments "meteofreaks" a la nostra ciutat. Hem de continuar somniant. Algun dia nevarà a Vilanova, creu-me.

En aquest llarg camí, he pogut comptar amb l'acompanyament de l'Ariadna, a la qual li he d'agrair el seu gran suport moral i anímic, així com la seva capacitat per fer menys rudes alguns moment d'aquest període.

Ja per acabar, voldria agrair als meus pares, Rafa i Carme, i a la meva germana, Maria, el suport incondicional brindat des del minut zero d'aquesta vida. Gràcies per inculcar-me la importància de ser constant i rigorós a l'hora de treballar, però sobretot de ser millor persona. També voldria agrair l'amor incondicional que m'han brindat els meus iaios de València, en Pepe i la Pepita, que tot i la llunyania, sempre s'han preocupat perquè jo i la Maria estiguéssim bé. Lògicament, iaia Carme, sempre recordaré la teva manera simpàtica de prendre't les coses, fent broma de qualsevol cosa; o com ens havíeu cuidat tu i el iaio Josep Maria quan estàvem malalts la Maria o jo. Us trobo molt a faltar.

Resum

Per la seva altitud i localització en una àrea de transició climàtica entre el domini temperat i humit de latituds més septentrionals, i el domini càlid i sec de latituds subtropicals, el Pirineu esdevé una àrea d'elevada variabilitat termo-pluviomètrica. El fet anterior, lligat amb l'actual procés de canvi climàtic, reforça l'interès per conèixer els canvis en el comportament dels centres d'acció atmosfèrics que expliquen les dinàmiques pluviomètriques d'aquesta regió. Els objectius generals d'aquesta tesi doctoral s'han centrat a 1) caracteritzar els principals patrons sinòptics que condicionen la pluviometria del Pirineu; 2) construir un entorn repetible que permeti aquesta caracterització mencionada anteriorment, però traslladable a qualsevol indret del planeta; 3) finalment, analitzar les característiques futures del clima pirinenc, centrant la mirada en els períodes perllongats sense precipitació i d'altes temperatures. Els resultats obtinguts han permès caracteritzar sinòpticament les principals situacions sinòptiques que determinen la pluviometria del Pirineu, de forma general, però també per a casos extrems ($\geq$ 100 mm/24h). Fruit d'aquesta relació entre els patrons sinòptics i la precipitació diària, s'ha proposat una metodologia que permet l'obtenció de regions categòriques explicatives dels principals patrons pluviomètrics de la regió, així com establir-ne la seva pròpia tendència pluviomètrica. Precisament, aquestes tendències regionals han permès quantificar un descens estadísticament significatiu de la precipitació anual a l'àrea més meridional del Pirineu. Aquest flux metodològic ha estat implementat en una llibreria en llenguatge de programació R, anomenada synoptReg, la qual cobreix 1) la descàrrega de dades de reanàlisi atmosfèrica; 2) la computació d'una classificació sinòptica; 3) l'espacialització dels valors diaris de precipitació en relació a cada patró sinòptic; i culmina amb 4) la regionalització categòrica d'aquests patrons de precipitació. Finalment, i pel que fa a l'evolució futura de les sequeres meteorològiques –conegudes com a ratxes seques– i de la temperatura màxima extrema que es produeix en el seu interior, en un escenari intermedi d'emissions d'efecte hivernacle (RCP4.5), l'augment del risc induït per aquestes dues variables es veurà incrementat a causa d'un fort augment de la temperatura extrema. En canvi, sota un escenari d'altes emissions (RCP8.5), els riscos futurs induïts per aquests extrems compostos seran conseqüència d'un increment, tant de la temperatura extrema interna, com de la longevitat d'aquests períodes secs de llarga durada, sobretot durant la primavera. D'aquesta manera, aquesta tesi aborda diferents perspectives climàtiques d'elevat interès per a la població pirinenca, però també per a les regions circumdants que es beneficien dels recursos que ofereix la serralada més important de l'Europa central, amb el permís dels Alps.

Abstract

As a result of their altitude and location within a zone of climatic transition between the warm wet domain of the more northern latitudes, on one hand, and the warm dry domain of the subtropical latitudes, on the other, the Pyrenees now constitute an area of high thermo-pluviometric variability. This fact, together with the current process of climate change, calls for more in-depth study of changes in the behaviour of the atmospheric centres of action accounting for the pluviometric dynamics in this region. The general objectives of the present doctoral thesis focus upon 1) characterising the principal synoptic patterns governing pluviometry in the Pyrenees; 2) constructing a reproducible environment to enable the above mentioned characterisation, which can also be applied to any region on the planet; 3) and lastly, on analysing the future characteristics of the climate of the Pyrenees, highlighting prolonged periods with high temperatures and no precipitation. The results obtained have enabled a synoptic characterisation of the main synoptic situations determining the pluviometry of the Pyrenees in general terms, but also in reference to extreme events (≥100 mm/24h). Resulting from this relationship between the synoptic patterns and daily precipitation, a methodology has been proposed which establishes the categorical regions accounting for the principal pluviometric patterns in the zone and reveals their own pluivometric tendencies. Indeed, these regional tendencies have enabled quantification of a statistically significant decrease in annual precipitation in the southernmost area of the Pyrenees. This Methodological flow has been implemented in a library in the R programming language, known as synoptReg, and which addresses 1) downloading of data on atmospheric reanalysis; 2) computing of a synoptic classification; 3) spatialization of daily precipitation values in relation to each synoptic pattern; and finally, 4) a categorical regionalisation of these precipitation patterns. Lastly, with regard to the future evolution of droughts –known as dry spells– and of the extreme maximum temperatures during these, in an intermediate scenario of greenhouse emissions (RCP4.5), the increased risk caused by the combination of these two variables will be even greater due to a sharp increase in extreme temperatures. On the other hand, within a high-emissions scenario (RCP8.5), the future risks caused by these compound extremes will result from an increase in both the maximum extreme temperature and in the duration of these long-lasting dry periods, particularly during the spring. Thus, the present thesis addresses different climatic perspectives of great interest for the population of the Pyrenees area, but also for the surrounding regions that benefit from the resources provided by this mountain range, which is the most important in central Europe, with the exception of the Alps.

Resumen

Por su altitud y localización en un área de transición climática entre el dominio templado y húmedo de latitudes más septentrionales, y el dominio cálido y seco de latitudes subtropicales, el Pirineo se convierte en un área de elevada variabilidad termo-pluviométrica. El hecho anterior, junto con el actual proceso de cambio climático, refuerza el interés por conocer los cambios en el comportamiento de los centros de acción atmosféricos que explican las dinámicas pluviométricas de esta región. Los objetivos generales de esta tesis doctoral se han centrado en 1) caracterizar los principales patrones sinópticos que condicionan la pluviometría del Pirineo; 2) construir un entorno repetible que permita esta caracterización mencionada anteriormente, pero trasladable a cualquier lugar del planeta; 3) finalmente, analizar las características futuras del clima pirenaico, centrando la mirada en los periodos prolongados sin precipitación y de altas temperaturas. Los resultados obtenidos han permitido caracterizar sinópticamente las principales situaciones sinópticas que determinan la pluviometría del Pirineo, de forma general, pero también para casos extremos (≥100 mm/24h). Fruto de esta relación entre los patrones sinópticos y la precipitación diaria, se ha propuesto una metodología que permite la obtención de regiones categóricas explicativas de los principales patrones pluviométricos de la región, así como establecer su propia tendencia pluviométrica. Precisamente, estas tendencias regionales han permitido cuantificar un descenso estadísticamente significativo de la precipitación anual en el área más meridional del Pirineo. Este flujo metodológico ha sido implementado en una librería en lenguaje de programación R, llamada synoptReg, la cual cubre 1) la descarga de datos de reanálisis atmosféricos; 2) la computación de una clasificación sinóptica; 3) la espacialización de los valores diarios de precipitación en relación con cada patrón sinóptico; y culmina con 4) la regionalización categórica de estos patrones de precipitación. Finalmente, y en cuanto a la evolución futura de las sequías meteorológicas -conocidas como rachas secas- y de la temperatura máxima extrema que se produce en su interior, en un escenario intermedio de emisiones de efecto invernadero (RCP4.5), el aumento del riesgo inducido por estas dos variables se verá incrementado debido a un fuerte aumento de la temperatura extrema. En cambio, bajo un escenario de altas emisiones (RCP8.5), los riesgos futuros inducidos por estos extremos compuestos serán consecuencia de un incremento, tanto de la temperatura extrema interna, como de la longevidad de estos períodos secos de larga duración, sobre todo durante la primavera. De este modo, esta tesis aborda diferentes perspectivas climáticas de elevado interés para la población pirenaica, pero también para las regiones circundantes que se benefician de los recursos que ofrece la cordillera más importante de la Europa central, con el permiso de los Alpes.

Índex

Acrònims

ACP Anàlisi de components principals
AEMET Agencia Estatal de Meteorologia
AIC Akaike information criterion
CDF Cumulative distribution function
CENMA Centre d'Estudis de la Neu i la Muntanya d'Andorra
CLIM'PY Caracterització de l'evolució del clima i provisió d'informació per a l'adaptació als Pirineus
CMIP Coupled Model Intercomparison Project
CORDEX Coordinated Regional Climate Downscaling Experiment
CP Component principal
D Duration
ECMWF European Centre for Medium-Range Weather Forecasts
EM Extreme magnitude
EMA Estació meteorològica automàtica
EQM Empirical quantile mapping
ETCCDI Expert Team on Climate Change Detection and Indices
FEDA Forces Elèctriques d'Andorra
FEDER Fons Europoeu de Desenvolupament Regional
GAM Generalized Additive Model
GCM General Circulation Model
GEH Gasos d'efecte hivernacle
GLM Generalized linear model
ICGC Institut Cartogràfic i Geològic de Catalunya
IEA Institut d'Estudis Andorrans
IPCC Intergovernmental Panel on Climate Change
IVT Integrated water vapour transport
M Magnitude
MAE Mean absolute error
MBCn Multivariate bias correction with N-dimensional probability density function transform
MDE Model Digital d'Elevacions
MOS Model output statistics
NCAR National Center for Atmospheric Research
NCEP National Centers for Environmental Prediction
NRMSE Normalized root-mean-square error
OPCC Observatori Pirinenc del Canvi Climàtic
PP Perfect prog
Q Humitat específica / Specific humidity
QDM Quantile delta mapping
RCM Regional Climate Model
RCP Representative Concentration Pathway
RK Regression Kriging
RMSE Root-mean-square error
SLP Pressió atmosfèrica a nivell de mar / Sea level pressure
SMC Servei Meteorològic de Catalunya
SOM Self-organizing maps
SRTM Shuttle Radar Topography Mission
Tx Temperatura màxima
T850: Temperatura a 850 hPa / Temperature at 850 hPa.
U Component zonal del vent / Eastward component of the wind
V Component meridional del vent / Northward component of the wind
WCRP World Climate Research Programme
Z500 Altura geopotencial a 500 hPa / Geopotential Height at 500 hPa

Capítol 1. Introducció

1.1. Motivació

La motivació que dona lloc a aquesta tesi no és una, sinó diverses, però totes elles tenen per objectiu ampliar el coneixement existent del clima del Pirineu, prenent com a objecte d'estudi la precipitació, per excés o absència de la mateixa. D'una banda, la primera d'aquestes motivacions rau a fer possible una cartografia contínua de les característiques pluviomètriques del Pirineu. Aquest fet podria semblar, a priori, bàsic en qualsevol estudi climàtic, no obstant això, disposar de dades confiables per a estudiar els patrons pluviomètrics d'aquesta àrea és, i ha estat, una quimera. Poder oferir una cartografia espacialment contínua i robusta de les principals situacions pluviomètriques està totalment condicionat a la densitat espacial i longitud temporal de les sèries climàtiques disponibles. És per això que un dels reptes d'aquesta tesi doctoral és poder proveir un catàleg de les principals situacions pluviomètriques, vinculades als diferents tipus de circulació atmosfèrica que afecten el conjunt de l'àrea del Pirineu. A més, i des d'una visió geogràfica, es vol proporcionar una cartografia mosaic que resumeixi les principals situacions pluviomètriques. Precisament, el procés d'obtenció d'aquesta cartografia sintètica dels principals patrons de precipitació condicionats a la circulació atmosfèrica ha de ser una alternativa viable a altres aproximacions a l'hora de realitzar regionalitzacions categòriques del clima, sovint computacionalment costoses. Per tant, aquesta motivació rau a desenvolupar una versió computacional low-cost que permeti l'obtenció de regions climàtiques robustes pel Pirineu.

D'altra banda, la motivació anterior dona lloc a una segona. Habitualment, en el camp de la recerca del clima, és complicat trobar investigacions que siguin repetibles i, per tant, que siguin fàcilment exportables a altres àrees d'estudi. Aquestes dificultats es deuen, sobretot, al fet que la immensa majoria de recerques venen mancades de codi o programari obert que permeti la seva repetibilitat, o per la impossibilitat d'accedir a les dades que fan possible la recerca en qüestió. Així doncs, aquesta segona motivació va en la línia d'oferir un marc repetible de bona part d'aquesta tesi doctoral, concretament, de tots els procediments sorgits de la primera motivació.

Finalment, la tercera i última motivació, és ampliar el coneixement que es té sobre els extrems pluviomètrics en aquesta àrea. Les situacions extremes solen ser puntuals en el temps però ocasionant devastadores conseqüències. Un exemple de situació extrema és una precipitació torrencial, el que podem descriure com una gran quantitat de precipitació caiguda en un període curt de temps –minuts, hores, o inclús dies–. Aquestes situacions extremes no tenen perquè estar vinculades a un excés pluviomètric, també poden respondre a un dèficit. En aquest sentit, la visió retrospectiva és molt important per conèixer i entendre les causes d'aquests fenòmens extrems, de la mateixa manera que és clau poder inspeccionar l'evolució futura de tals esdeveniments, per tal d'anticipar situacions altament perjudicials per a la continuïtat de la riquesa ecològica o per al manteniment de les activitats econòmiques d'aquesta àrea.

1.2. Estat de l'art

1.2.1. Disponibilitat de dades en l'estudi de la precipitació i la temperatura

La complexa topografia del Pirineu ha limitat, fins a dia d'avui, un estudi detallat del clima d'aquesta serralada, degut a la manca de sèries climàtiques suficientment llargues per a una caracterització robusta dels diferents ambients climàtics que es troben en aquesta àrea. De fet, aquesta escassetat de sèries climàtiques robustes[1] s'accentua a mesura que ascendim d'altitud, sobretot a partir dels 1500 msnm, cota a partir de la qual no existeixen pràcticament zones habitades. Aquesta mancança de sèries climàtiques en els estrats superiors del Pirineu és un denominador comú en tota la literatura relacionada amb l'estudi del clima mitjançant observacions in situ en aquesta àrea (Maris et al., 2009; Esteban et al., 2010; Pérez-Zanón et al., 2017). És a partir de la dècada de 1990 quan, gràcies a les estacions meteorològiques automàtiques (EMA), és possible monitoritzar de forma més generalitzada el clima dels estrats més elevats d'aquesta serralada. Fins llavors, aquesta monitorització, a cotes elevades, només havia estat possible realitzar-la de forma manual i en escassos observatoris, com ara a Montlluís a 1600 msnm (el Conflent, Catalunya Nord) o a l'observatori de Pic du Midi a 2800 msnm (Alts Pirineus, França), entre els més destacats

Malgrat l'absència d'un banc de sèries climàtiques abundant, això no ha impedit la realització de multitud d'estudis, principalment, sobre la tendència i la variabilitat de la temperatura i la precipitació en diverses subàrees d'aquesta serralada, tals com: el Pirineu central (Vicente-Serrano et al., 2007, Buisan et al., 2016; Pérez-Zanón et al., 2017); el Pirineu francès (Maris et al., 2009); Andorra (Esteban Vea et al., 2012), el Pirineu oriental (Pepin i Kidd, 2007; Bonsoms et al., 2021a); o observatoris concrets (Bücher i Dessens, 1991; Dessens i Bücher, 1997; Serrano-Notivol et al., 2018). Per la notable presència de la coberta de neu en aquesta zona durant el semestre fred de l'any, també destaquen un gran nombre d'estudis dedicats a investigar l'evolució històrica d'aquesta (Lopez-Moreno et al., 2005; Buisan et al., 2015; Lopez-Moreno et al., 2020; Bonsoms et al., 2021b), ja que esdevé un reservori d'aigua durant l'època estival (Añel et al., 2014). Si bé són molts els treballs que estudien les tendències recents de la precipitació i la temperatura, no són tants aquells que centren la mirada en l'estudi de l'evolució de les sequeres com a objecte d'estudi. En aquest sentit, cal destacar el recent treball de Vicente-Serrano et al. (2021), en el qual un dels objectius és determinar la resposta dels sistemes hídrics a la variabilitat de la sequera en la zona central dels Pirineus. Altres estudis, com el de Lopez-Moreno et al. (2009), aborden la qüestió de les ratxes seques -entesa com el número de dies consecutius sense precipitació apreciable-, extraient-ne les principals tendències per a la zona central del Pirineu, juntament amb l'anàlisi d'altres índexs de precipitació. També en la mateixa àrea, Vicente-Serrano i Cuadrat (2007) analitzen les tendències en la intensitat i variabilitat de les sequeres per a la segona meitat del segle XX. Com és observable, existeix una escassa varietat de recerques que treballin sobre els períodes d'absència de precipitació a escala pirinenca –ni que sigui

[1] Sèrie robusta, entesa com a llarga, contínua, sistemàtica, homogènia i precisa.

en alguna de les seves subregions–. Aquesta carència de treballs en l'àmbit pirinenc, contrasta amb l'extensa recerca en l'àmbit de la Península Ibérica (Vicente-Serrano, 2006a; Vicente-Serrano, 2006b; Sánchez et al., 2011; Páscoa et al., 2017; González-Hidalgo et al., 2018 o Páscoa et al., 2021, entre d'altres). En moltes de les recerques anteriorment mencionades, s'inclou l'àrea del Pirineu mitjançant interpolacions espacials amb un escàs nivell de detall espacial i, sovint, sense disposar d'observacions in situ en aquesta regió (Martin-Vide i Gómez, 1999; Lana et al., 2006 i 2008).

Aquesta escassetat d'estudis en l'àrea del Pirineu, es deu bàsicament a la ja mencionada escassetat de dades disponibles. Sortosament, l'Observatori Pirinenc del Canvi Climàtic[2] (OPCC), creat l'any 2010, ha abordat aquesta qüestió promovent un esforç conjunt entre els principals serveis meteorològics i de recerca que hi ha en les regions que comparteixen, administrativament, aquesta serralada. Precisament, una de les principals tasques que ha realitzat l'OPCC ha estat la de recuperar el major nombre possible de sèries climàtiques de temperatura i precipitació a resolució diària, iniciades en qualsevol moment del segle XX. D'aquesta manera, un dels primers resultats obtinguts fou una base de dades homogènia amb 66 sèries termomètriques (Cuadrat et al., 2013) i 139 sèries pluviomètriques (Cuadrat et al., 2014), per al període 1950-2010, amb almenys un 75 % de la longitud de les sèries disponible. Gràcies a successius rescats de sèries climàtiques pels socis de l'OPCC, les millores en el control de qualitat de les sèries, i als processos d'emplenament de forats de les mateixes (Serrano-Notivoli et al., 2017 i 2019a), aquesta iniciativa ha aconseguit generar una base de dades diària de temperatura i precipitació, reticulada a 1km de resolució espacial (Cuadrat et al., 2020). Aquesta tasca desencalla la impossibilitat de realitzar estudis climàtics espacialment detallats i temporalment continus en aquesta àrea.

1.2.2. L'evolució de la temperatura i la precipitació en les últimes dècades

Tots els estudis existents a qualsevol de les àrees del Pirineu mostren un clar increment de la temperatura, independentment de l'estació de l'any (Maris et al., 2009; El Kenawy et al., 2011; Esteban et al., 2012), encara que aquest augment és més moderat en algunes zones ≥ 2000 msnm (Serrano-Notivoli et al., 2018). A l'àrea central del Pirineu, Pérez-Zanón et al. (2017), detecten un increment de 0.11ºC per dècada a nivell regional en el cas de la temperatura màxima, i de 0.06 ºC per dècada en el cas de la temperatura mínima pel període 1910-2013. Aquest increment subtil, passa a ser de 0.57ºC per dècada per a la temperatura màxima i de 0.23ºC per dècada en el cas de la temperatura mínima per al període 1970-2013, el que recalca que l'increment tèrmic s'ha accelerat en les últimes dècades. Aquests dos primers fets: 1) l'increment superior per dècada en la temperatura màxima que en la temperatura mínima; i 2) l'acceleració de l'increment tèrmic a partir de la dècada del 1980; juntament amb 3) l'increment tèrmic per dècada superior durant l'estiu i primavera, que

[2] Projecte interregional cofinançat al 65% pel Fons Europeu de Desenvolupament Regional (FEDER) a través del Programa Interreg V-A Espanya-França-Andorra (POCTEFA 2014-2020) i dirigit per la Universitat de Saragossa, Meteo-France, AEMET, SMC, CSIC, CSBIO, IEA.

durant la tardor i l'hivern, són coherents amb els resultats obtinguts per Serrano-Notivoli et al. (2019b) per a tot l'àmbit del Pirineu.

Pel que fa a l'evolució de la precipitació, aquesta mostra una tendència general a disminuir, encara que amb una variabilitat interanual molt elevada (OPCC, 2013), el que accentua el grau d'incertesa respecte la seva evolució. Aquest fet, juntament amb que 1) els Pirineus estan situats en una àrea de transició entre el domini humit i suau de les latituds mitjanes i la zona àrida del cinturó anticiclònic subtropical; 2) la seva marcada topografia; i 3) la seva ubicació entre dues conques climàticament diferenciades, la mediterrània i la cantàbrica, fan que aquesta zona muntanyosa presenti una pluviometria molt variable. Precisament, Pérez-Zanón et al. (2017) observen una important variabilitat interanual de la pluviometria al sector central dels Pirineus, quantificant una tendència negativa però sense ser estadísticament significativa. Aquesta disminució observada s'accentua durant la segona meitat del segle XX i a principis del segle XXI. Una aproximació interessant que permet reduir la incertesa sobre l'evolució pluviomètrica és la que proposa Esteban et al. (2009), la qual permet conèixer la tendència temporal dels mecanismes físics que poden desencadenar episodis d'inestabilitat i estabilitat atmosfèrica. En aquest sentit, en els resultats d'Esteban et al. (2009) s'observa com les situacions anticiclòniques amb estacionalitat hivernal han augmentat la seva freqüència significativament entre el 1960 i el 2001. De fet, estudis anteriors també detecten un increment de la pressió atmosfèrica al centre d'Europa (Maugeri et al., 2004; Lopez-Bustins et al., 2008). Aquests resultats tenen una elevada coherència amb el descens pluviomètric observat a l'hivern per Pérez-Zanón et al. (2017), superior al de la resta d'estacions de l'any. Lopez-Moreno et al. (2020) també constaten que algunes de les tendències observades en relació a la reducció de la coberta de neu podria estar vinculada a l'augment de la freqüència de situacions sinòptiques anticiclòniques, així com a la disminució de l'ocurrència de les adveccions de l'oest i sud-oest, molt favorables a causar episodis importants d'innivació a la meitat oest del Pirineu (Bonsoms et al., 2021b). La reducció de la precipitació, tot i no ser significativa, té també reflex en l'augment dels períodes secs (Vicente-Serrano et al., 2007). Els resultats obtinguts en l'últim informe del OPCC (OPCC, 2018) venen a consolidar aquests descensos descrits en la literatura.

1.2.3. Estat recent de la recerca sobre projeccions de canvi climàtic al Pirineu

Durant les últimes tres dècades, la resolució espacial dels experiments de models climàtics globals que contribueixen al Coupled Model Intercomparison Project (CMIP) ha augmentat constantment (Taylor et al., 2012; Eyring et al., 2016), aconseguint un nivell de detall de les integracions de models climàtics regionals a escala continental, similars a les proporcionades pel COordinated Regional climate Downscaling EXperiment (CORDEX) (Jacob et al., 2014; Kotlarski et al., 2014; Giorgi, 2019; Demory et al. , 2020), i esdevenint la base quantitativa dels successius informes entregats pel Intergovernmental Panel on Climate Change (IPCC). No obstant això, inclús per a les simulacions dels models regionals del CORDEX, segueix mancant una major resolució espacial per aquells estudis d'impacte en escales local, sobretot en àrees d'orografia complexa. A més,

quan hom té interès en l'exploració d'esdeveniments extrems, és necessari eliminar els biaixos sistemàtics que apareixen a les simulacions dels models climàtics (Maraun et al., 2017a), així com emprar un nombre suficient de models per tal de testar la variabilitat interna de les simulacions i el grau d'incertesa en els resultats (Knutti et al., 2010).

Precisament, corregir el biaix en les simulacions climàtiques és de vital importància per evitar traslladar errades intrínseques del model climàtic, de cara a la projecció futura d'una variable climàtica (Willby i Wigley, 1997). El concepte de correcció del biaix (en anglès, bias correction) és un tipus de post processat dels models climàtics, que rau dins la branca de l'aproximació coneguda com a model output statistics (MOS) (Glahn and Lowry, 1972). La correcció del biaix d'un model climàtic es pot definir com qualsevol mètode capaç d'establir una funció estadística de transferència entre el model i la observació, per a, posteriorment, aplicar aquesta funció de transferència al model climàtic (Maraun i Widmann, 2018a) (Fig. 1).

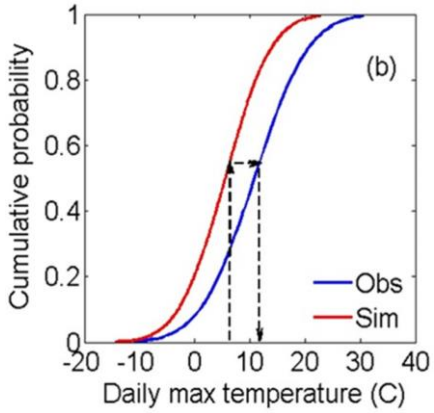

Figura 1. Exemple de correcció del biaix d'una sèrie de temperatura màxima mitjançant la tècnica quantile mapping. La corba de distribució de probabilitat acumulada (CDF) de la temperatura diària simulada pel model climàtic (línia vermella) es força a desplaçar perquè coincideixi amb la CDF de la temperatura diària observada (línia blava). Extret de Modala, 2014.

Sovint, els mètodes de correcció de biaix també s'empren per a la reducció d'escala –procés popularment conegut com a downscaling– de les projeccions climàtiques (Rajczak et al., 2016a; Crespi et al., 2020). No obstant, és una pràctica poc recomanada ja que indueix problemes d'inflació a les sèries corregides (Maraun, 2013), i és incapaç de generar variabilitat diària subescala (Maraun et al., 2017). Aquestes problemàtiques tendeixen a agreujar-se a les zones de muntanya, on molts processos locals poden no estar representats després d'un procés conjunt de correcció del biaix i dowscaling estadístic (Maraun i Widmann, 2018a). Una major garantia a l'hora de reduir l'escala d'un model climàtic és l'aproximació perfect prog (PP), que es defineix com aquell model estadístic que estableix un enllaç entre un o diversos predictors a escala sinòptica, i un predictand observat a escala local. Aquest enllaç estadístic és emprat, posteriorment, per transferir les propietats del model calibrat amb dades observades a les dades projectades a la resolució espacial de les dades observades. Una limitació important és que s'assumeix una relació invariant en el temps entre el predictand i el predictor, quelcom que succeeix també en els mètodes que empren l'aproximació anomenamada model output statistics (MOS). Aquest fet significa que el vincle que s'estableixi entre el predictor i predictand serà sempre el mateix, ara i en el futur.

És aquesta aproximació PP la que s'empra en l'únic estudi que existeix fins a la data de projeccions climàtiques a alta resolució espacial a l'àrea del Pirineu (Amblar-Francés et al., 2020). Amblar-Francés et al. (2020) empren el mètode d'anàlegs i el mètode de regressió lineal múltiple, per tal de projectar la temperatura i la precipitació a 5 km amb un conjunt de models del CMIP5. En aquest treball troben que les temperatures màximes i mínimes mostren una clara tendència a l'augment a tot el Pirineu, sent l'augment de la temperatura màxima superior al de la temperatura mínima. Pel que fa als canvis futurs de la precipitació, aquests no presenten una tendència clara, a causa de la incertesa provinent dels models climàtics. Precisament, conèixer els canvis futurs en la temperatura i la precipitació pirinenca és essencial per entendre, per exemple, la viabilitat futura de les estacions d'esquí. En l'estudi recent de Spandre et al. (2019), s'apunta que, a final del segle XXI, en cap de les 46 estacions d'esquí localitzades al Pirineu serà viable produir-hi neu artificial en les zones més baixes de les estacions.

1.2.4. Els avenços en el camp de la climatologia sinòptica i el seu vincle amb l'escala local

Segons l'Associació Meteorològica Americana (American Meteorological Society, en anglès), la climatologia sinòptica es pot definir com l'estudi del clima des de la perspectiva de la circulació atmosfèrica, amb èmfasi en les connexions entre els patrons de circulació i les diferències climàtiques. Un dels objectius de la climatologia sinòptica és, doncs, entendre les relacions entre la superfície –per exemple, la temperatura o la precipitació d'un indret– i la circulació atmosfèrica (Yarnal, 1993). Amb una escala horitzontal de ~1000 km i una vida útil de ~5-7 dies, les depressions i els anticiclons, que són les principals estructures de l'escala sinòptica de l'atmosfera (Barry, 2005), influeixen en una àmplia varietat de processos ambientals, inclosos els recursos hídrics, els extrems climàtics i meteorològics, o la salut, entre d'altres. En conseqüència, l'anàlisi del clima a escala local sovint comença amb una caracterització dels processos de forçament a escala sinòptica (Dixon et al., 2016). Per tant, els estudis de climatologia sinòptica acostumen a anar acompanyats de diversos mapes que caracteritzen diferents estats atmosfèrics (Yarnal, 1993; Barry i Carleton, 2001), i que ens permeten conèixer quins són els mecanismes físics, per exemple, d'una inusual sequera en una determinada regió del planeta. En definitiva, la climatologia sinòptica contribueix a explicar com l'atmosfera interactua amb el sistema terrestre en el seu conjunt.

Els procediments bàsics d'un estudi sinòptic segons Barry (2005) són: 1) la determinació de tipus o patrons de circulació atmosfèrica; i, 2) l'avaluació estadística de les condicions meteorològiques en relació amb aquests patrons. Ha estat una pràctica comuna distingir un petit nombre de tipus de circulació atmosfèrica a partir dels mapes meteorològics diaris i, seguidament, calcular els valors mitjans de temperatura i el total de precipitació diària d'un conjunt d'estacions meteorològiques per a cada patró sinòptic. De fet, aquests tipus d'estudis s'inicien gairebé des que es van elaborar els primers mapes meteorològics a finals de segle XIX per meteoròlegs tan coneguts com Abercromby (1883) i Van Bebber i Köppen (1895).

En la climatologia sinòptica, el mètode o esquema de classificació a emprar ha estat el motiu principal de diverses recerques durant moltes dècades. S'han utilitzat múltiples variables per classificar els patrons atmosfèrics, inclosa la temperatura, la pressió, el flux d'aire i altres propietats derivades com ara la vorticitat (Ledrew, 1984; Barry, 2005), entre moltes altres. A més, aquestes característiques es classifiquen a diverses escales espacials -globals o regionals- i temporals -anuals, mensuals o diàries, majoritàriament-. La classificació de patrons sinòptics permet a la climatologia sinòptica relacionar-se amb altres disciplines de manera que es puguin analitzar la interacció entre els patrons atmosfèrics i els processos ambientals (Carleton, 1999). Pel que fa a la varietat de mètodes de classificació sinòptica, aquesta és molt àmplia, existint-hi enfocaments subjectius (manuals), objectius (semi-automàtics i automàtics) o híbrids. Les classificacions manuals s'inicien molt aviat (Abercromby, 1883; Van Bebber i Köppen, 1895; Lamb, 1950), basades en l'experiència del propi professional/acadèmic per distingir una sèrie de patrons sinòptics representatius d'una àrea geogràfica determinada. Encara que la majoria dels catàlegs subjectius se centren en l'anàlisi regional (Baur et al. 1944; Lamb, 1972), alguns s'han desenvolupat a major escala (Girs, 1948). Recentment, s'han desenvolupat mètodes de classificació automatitzats i híbrids, i la disciplina continua evolucionant gràcies a una major disponibilitat de dades meteorològiques i models climàtics més complexos. En aquest sentit, Huth et al. (2008) ofereixen una anàlisi detallada de tots els mètodes de classificació sinòptica que existeixen fins, pràcticament, acabar la primera dècada del segle XXI.

L'augment de la capacitat de càlcul, juntament amb l'increment de la complexitat i robustesa de les classificacions sinòptiques, ha provocat que avui dia s'invoquin multitud de mètodes estadístics en la literatura científica (Yarnal et al., 2001). Tècniques com l'anàlisi de components principals i l'anàlisi clúster (per exemple, Esteban et al. 2005), o els mapes auto-organitzats (en anglès, self-organizing maps) (Kohonen et al. 2001; Hewitson i Crane 2002; Sherindan i Lee, 2011), han contribuït a remodelar la disciplina. L'augment en la quantitat i la qualitat de les retícules de reanàlisi atmosfèrica –com ara ERA-5, ERA-Interim, ERA-20C, UERRA, MERRA-2, NCEP-NCAR reanalysis (I i II), entre d'altres– han permès incloure variables atmosfèriques més complexes, com el transport integrat de vapor d'aigua o les components zonals i meridionals del vent a diferents nivells de pressió, per citar-ne dos exemples. També els darrers avenços en les bases de dades de reanàlisi ens fan disposar de variables a una elevada resolució espacial i horària, capaces de detectar estructures mesoescalars.

Com s'ha mencionat anteriorment, hom pot tenir interès a cercar l'impacte que té un tipus de circulació atmosfèrica concret en una variable ambiental o meteorològica –per exemple, la precipitació– sobre una àrea geogràfica determinada. Aquesta seria l'aproximació clàssica, coneguda com circulation-to-environment (de la circulació al medi ambient), emprada en multitud d'estudis la dècada dels 90 (Davies et al., 1990; Hulme i Jones, 1991; Goodes i Paultikof, 1998), fins a l'actualitat (Cortesi et al., 2014; Ramos et al., 2014; Peña-Angulo et al., 2020). El número d'estudis amb aquesta aproximació es disparen cap a la dècada dels 2000 degut a dues raons principals: 1) durant la dècada anterior es consoliden mètodes objectius per a classificar sinòpticament la circulació atmosfèrica, com

són el cas del treballs previs de Jenkinson i Collison (1977), i Jones et al. (1993), els quals objectiven la subjectiva classificació de Lamb (1972) aplicada a les Illes Britàniques; 2) la millora en la capacitat de càlcul a nivell global, permetent així una àmplia aplicació de mètodes més sofisticats de classificació sinòptica -com ara l'anàlisi de components principals- (Esteban et al., 2005; Huth et al., 2008), i la realització d'interpolacions automàtiques que permetin representar la variable objectiu de forma espacialment contínua (Ninyerola et al., 2000; Trigo i DaCamara, 2000; Maheras et al., 2003; entre molts altres). D'altra banda, trobem també un enfocament realitzat des de l'escala local cap a l'escala sinòptica, en el qual es tracta de seleccionar dies d'interès –per exemple, dies amb precipitació que superin un cert llindar–, i crear una classificació sinòptica mitjançant mètodes estadístics multivariants amb aquests dies objectiu. També és possible realitzar la mitjana aritmètica de la variable sinòptica d'interès en els dies en què se supera un llindar determinat en superfície, per així obtenir el mapa sinòptic d'aquella situació (Carro-Calvo et al., 2017). Aquest tipus d'aproximació s'ha aplicat al NE d'Ibèria (Martin-Vide et al., 2008), a Iberia (Lopez-Bustins et al., 2008), al sud d'Europa (Sanchez-Lorenzo et al., 2009; Insua-Costa et al., 2021) i en altres zones del món, com el Japó (Nishiyama e al., 2007) i el nord de Xile (Meseguer-Ruiz et al., 2020), entre d'altres.

En el cas dels Pirineus, existeixen diversos treballs que apliquen l'enfocament circulation-to-environment en diverses subregions d'aquesta àrea, principalment, en el camp de la precipitació: vessant sud del Pirineu (Lopez-Moreno et al., 2007; Buisan et al., 2015); Andorra (Esteban et al., 2009), Pirineu Català (Bonsoms et al., 2021ab). Per contra, són pràcticament inexistents els treballs que condueixen l'enfoc invers en aquesta àrea, tan sols trobant-ne l'estudi d'Esteban et al. (2005), en el qual caracteritzen els patrons atmosfèrics lligats als dies de nevades ≥ 30 cm a Andorra; o el treball de Garcia-Sellès et al. (2009), en el qual a partir dels registres de grans allaus al Pirineu català, es crea un catàleg sinòptic de les situacions promotores d'aquests esdeveniments. Tot i la notable varietat de treballs de climatologia sinòptica en aquesta àrea, es detecten dues mancances principals: 1) un profund buit de coneixement a la meitat nord de la serralada, principalment, al Pirineu francès; 2) la inexistència d'estudis que contemplin com a àrea d'estudi el conjunt del Pirineu. Aquestes dues mancances esmentades anteriorment són també una motivació a l'hora d'ampliar el coneixement que hi ha en aquesta àrea.

Precisament, un dels motius pels quals hi ha carència d'estudis que integrin tot el Pirineu, i que ja s'ha esmentat reiteradament, és la mancança de dades observacionals in situ de les principals variables meteorològiques. Aquesta pobresa de sèries climàtiques contínues, homogènies i llargues, es veu reflectida en l'escàs nombre d'estudis que interpolen alguna variable climàtica en qualsevol de les subàrees del Pirineu (Lopez-Moreno et al., 2007; Esteban et., 2009). Sortosament, amb la posada en marxa del projecte CLIM'PY (Caracterització de l'evolució del clima i provisió d'informació per a l'adaptació als Pirineus) de l'OPCC a finals de l'any 2016, s'inicien les tasques de recuperació, control de qualitat i homogeneïtzació de les sèries climàtiques de tota l'àrea del Pirineu, principalment, de temperatura i precipitació diària. Aquest nou fons de dades, el qual s'ha anat desenvolupant en paral · lel al transcurs d'aquesta tesi doctoral, ha permès estudiar la interacció entre els patrons atmosfèrics i la precipitació a escala pirinenca a un elevat nivell de resolució espacial,

gràcies a l'ús de mètodes de regressió estadística multivariant a l'hora de realitzar les interpolacions espacials.

Cal notar que molts dels estudis que cerquen relacionar l'impacte que tenen els patrons sinòptics en la precipitació d'una àrea acostumen a emprar una malla diària interpolada preexistent (Morata et al., 2006; Casado et al., 2010; Cortesi et al., 2014; Ramos et al., 2014), de manera que no cal utilitzar mètodes d'interpolació espacial per tal de generar superfícies contínues de precipitació. Tot i aquest avantatge, aquestes quadrícules tenen una resolució espacial normalment superior als 10 km, pel que pot mancar cert detall orogràfic en regions geogràficament poc extenses i de topografia complexa. Per atenuar aquesta limitació, o en cas d'inexistència d'una graella diària de precipitació diària, existeixen diversos mètodes d'interpolació que permeten una predicció espacial de la precipitació en zones topogràficament complexes com ho són els Pirineus. La majoria dels estudis que aborden la interpolació de la precipitació o de qualsevol altra variable climàtica influenciada per la topografia del lloc solen fer ús de mètodes de regressió estadística multivariant (Ninyerola et al., 2000; Brunetti et al., 2013). Aquesta tipologia de mètodes permeten, d'entrada, alimentar un model amb predictors geogràfics explicatius de la precipitació, tals com l'altitud, la latitud, la longitud o la distància al mar, entre d'altres. Un ajust adequat d'aquests models pot permetre obtenir valors predits força realistes en aquells punts on no tenim observació. No obstant això, en zones de topografia complexa, molts observatoris s'ajustaran llunyanament a la recta de regressió lineal, implicant una gran diferència entre el valor predit i observat. Aquesta manca de flexibilitat o de linealitat pot suplir-se mitjançant correccions posteriors com la proposada a Ninyerola et al. (2000), en la qual s'interpolen els valors residuals de la regressió de cada observatori amb el mètode d'invers a la distància ponderada (en anglès, inverse distance weighted) o amb una interpolació Spline, per a posteriorment sumar-los al resultat previ de la predicció del model de regressió. D'aquesta manera, s'aconsegueix alleugerar l'error del valor predit en la cel · la corresponent a un observatori n, apropant d'aquesta manera el valor predit a l'observat. Per contra, aquest mètode pot implicar errors en altres zones on no es disposa d'observatoris, o pot generar artefactes en el mapa resultant, com ara els coneguts ulls de bou (Pesquer et al., 2007). Altres autors, com Peña-Angulo et al. (2016) o Crespi et al. (2018), ajusten aquests residus fent ús del mètode d'interpolació Kriging (Hengl et al., 2007), el qual es basa en l'autocorrelació espacial dels residus. Mitjançant el semivariograma, hom pot ajustar la distància entre els valors residuals de cada parella d'observatoris, partint del principi que dos observatoris propers tindran un residu més similar entre ells que dos observatoris allunyats entre si. El procés de regressió lineal, juntament amb la interpolació dels residus mitjançant alguna de les tipologies de kriging, es coneix popularment com a regressió de Kriging (en anglès, Kriging regression) (Fig. 2).

$$Z(\mathbf{s}) = m(\mathbf{s}) + \varepsilon'(\mathbf{s}) + \varepsilon''$$

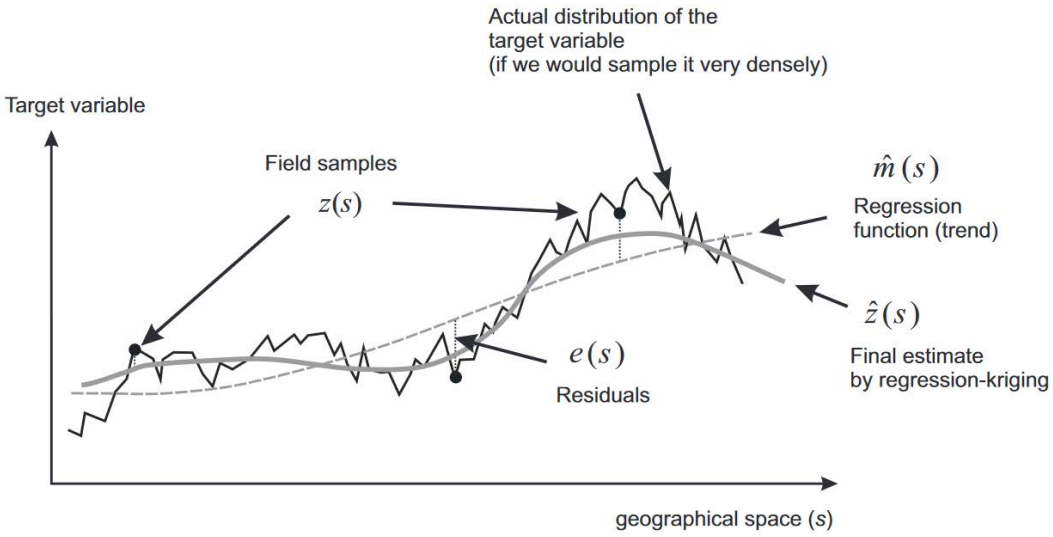

Figura 2. Esquematització de la regressió de Kriging. Extret de Hengl (2009).

En ocasions, els processos naturals no poden ser explicats per relacions lineals i tendeixen a tenir una resposta curvilínia, de manera que cal esperar una possible resposta no lineal de les nostres dades. Els Models Additius Generalitzats (en anglès, generalized additive models, abreviats com a GAM) (Hastie i Tibshirani, 1990) són una extensió semiparamètrica dels Models Lineals Generalitzats (en anglès, generalized linear models, abreviats com a GLM), amb l'avantatge de no representar una forma paramètrica estricta, permetent així una resposta més flexible que en la regressió lineal. En el camp de la interpolació climàtica, hi ha diverses aplicacions que empren aquest mètode semiparamètric: Aalto et al. (2013) utilitzen un GAM per ajustar la precipitació mensual a Finlàndia; Stauffer et al. (2017) ajusten un GAM per a generar una retícula de precipitació diària per a Àustria.

1.2.5. Les regionalitzacions discretes en el camp de la climatologia

Encara que un dels punts forts de la modelització espacial basada en models de regressió implica la possibilitat d'analitzar i visualitzar la complexitat espacial de les variables ambientals, el gran nombre de mapes resultant –per exemple, un per a cada dia; o un per a cada tipus de circulació atmosfèrica– pot dificultar una visió resumida dels seus principals patrons espacials. Per tant, una visió sintètica produïda per l'aplicació d'un mètode de classificació no supervisat –popularment coneguts amb el nom de clustering– pot facilitar el descobriment dels patrons espacials d'un conjunt de dades climàtiques o ambientals de tipologia espacio-temporal. Per exemple, l'algoritme de classificació no supervisada ISODATA (Duda i Hart, 1973), s'utilitza sovint en el camp de la teledetecció en la fase exploratòria de classificació d'imatges satèl · lits (Rahman, 2015). Diversos estudis categoritzen les variables climàtiques mitjançant classificacions no supervisades, emprant en

molts casos, graelles de dades espacio-temporals. En aquest sentit, Zscheischleret al. (2012) utilitzen el mètode de k-means per a realitzar una classificació climàtica global combinant dades mensuals de temperatura, precipitació, i dades derivades de la teledetecció, com ara índexs de vegetació. Un altre treball similar és el presentat per Carro-Calvo et al. (2017), en què l'objectiu principal és la regionalització de l'ozó troposfèric (O_3) estival a Europa. En aquest cas, els autors apliquen de nou la tècnica de clustering k-means per tal de generar regions espacio-temporals d'1×1^{o} per als períodes d'estiu del 1998-2012. Un dels problemes que afloren a l'emprar mètodes no supervisats de classificació sobre dades espacio-temporals és l'alt cost computacional que suposen (Philips, 2002), sobretot, si emprem llargues sèries temporals d'alta resolució espacial i temporal. En aquest sentit, aquesta tesi també vol abordar aquesta qüestió i posar sobre la taula una proposta que afavoreixi la realització de classificacions no supervisades de dades climàtiques i ambientals sense un alt cost computacional.

1.2.6. Sobre l'anàlisi conjunta d'esdeveniments secs i càlids

Les investigacions sobre les ratxes seques o sequeres, així com sobre els fenòmens tèrmics extrems –per exemple, onades de calor–, es basen habitualment en un enfocament individual, i sovint es descuida el caràcter compost de tals fenòmens. En aquest sentit, en el cas de les ratxes –siguin seques o humides–, diversos estudis han examinat la durada de les mateixes i han quantificat les tendències d'aquests esdeveniments en diferents regions del món (Martin-Vide i Gómez, 1999; Zolina et al., 2013; Singh et al., 2014); però el component tèrmic d'aquests episodis no ha estat abordat en ells. De la mateixa manera, trobem diferents estudis sobre temperatures extremes que no avaluen l'efecte de la durada de les mateixes (Diffenbaugh i Ashfaq, 2010; Fonseca et al., 2016; Salameh et al., 2019). En termes generals, els índexs proposats per l'Expert Team on Climate Change Detection and Indices (ETCCDI) del World Climate Research Programme (WCRP) no impliquen l'anàlisi composta dels esdeveniments, una deficiència que pot resultar en una subestimació del risc (Zscheischler et al., 2018).

Com s'ha esmentat anteriorment, l'anàlisi composta d'esdeveniments climàtics permet estimar el risc real induït per l'ocurrència simultània de diversos extrems climàtics; això és d'especial interès en zones fràgils i vulnerables, com les àrees de muntanya, en un context de canvi climàtic antropogènic. En aquest sentit, la zona dels Pirineus, àrea transfronterera entre tres països (Andorra, Espanya i França), posseeix una gran riquesa de recursos naturals i un alt nivell de biodiversitat. No obstant això, alguns estudis ja han abordat els primers impactes de l'escalfament observat en aquesta regió, sobretot en relació amb el declivi dels boscos de muntanya (Camarero, 2017). A més, la major freqüència de períodes secs i de sequeres també han provocat la defoliació dels boscos d'avets (Abies alba) en aquesta regió (Gazol et al., 2020). Per tant, és urgent realitzar una anàlisi composta dels períodes secs extrems i dels esdeveniments de temperatures càlides extremes, és a dir, la combinació de la durada (D) i la magnitud (M); tal com es conceptualitza a Manning et al., (2019), amb la

finalitat de determinar si aquests esdeveniments compostos s'estendran més en el futur i si suposen altres riscos, com els incendis forestals o les pèrdues de rendiment dels cultius.

Pel que fa a l'anàlisi composta dels esdeveniments secs i càlids, estudis anteriors han posat de manifest un augment de la freqüència i extensió geogràfica d'aquests esdeveniments durant els últims anys en diverses zones, com els Estats Units (Mazdiyasni i AghaKouchak, 2015), Índia (Sharma i Mujumdar, 2017) o la Xina (Wu et al., 2019). No obstant, Manning et al. (2019) observen que aquests increments en els esdeveniments compostos secs i càlids són a causa, principalment, d'un pes superior en l'augment tèrmic que no pas per la prolongació de la durada dels períodes secs. Diversos estudis recents se centren, principalment, en els canvis observats en aquests esdeveniments compostos (Hao et al., 2019; Manning et al., 2019; Wu et al., 2019). No obstant això, són menors les anàlisis que han emprat models climàtics per avaluar el risc futur de la concurrència d'aquests extrems (Zscheischler i Seneviratne, 2017; Lu et al., 2018; Wu et al., 2020). Zscheischler i Seneviratne (2017) utilitzen la funció de distribució multivariada de probabilitat de Copula per avaluar els canvis en la probabilitat d'ocurrència futura d'esdeveniments compostos secs i càlids; en aquest treball, els autors empren diversos models climàtics globals del CMIP5 que els permet quantificar un increment en la probabilitat d'ocurrència d'aquests esdeveniments en la majoria de les regions del món. Per tant, les investigacions anteriors han posat de manifest un augment general d'aquest tipus d'esdeveniments, però sovint no aborden el pes intern que tenen cada una de les variables que contribueixen o conformen aquests esdeveniments extrems compostos. Precisament, en aquesta tesi, s'intenta explicar l'evolució històrica i futura d'aquests esdeveniments secs i càlids a l'àrea del Pirineu, així com els canvis interns de les variables que formen aquest extrem compost en els diversos escenaris futurs de canvi climàtic.

1.3. Objectius

1.3.1. Objectius generals

Les tres motivacions mencionades a l'inici d'aquesta tesi doctoral (secció 1.1), són traslladables als tres objectius generals al voltant dels quals s'ha desenvolupat la present tesi doctoral:

- OG1: Caracteritzar els principals patrons pluviomètrics de l'àrea pirinenca des d'un punt de vista sinòptic. Conèixer la magnitud, la distribució espacial i temporal de la precipitació associada als tipus de circulació atmosfèrica és essencial per millorar la gestió dels recursos hídrics i per desenvolupar estratègies destinades a reduir l'impacte dels riscos naturals en les zones de muntanya, tals com les allaus, els despreniments i les inundacions, entre d'altres riscos hidrogeològics. A més, caracteritzar les tipologies sinòptiques vinculades als esdeveniments extrems pluviomètrics, siguin per excés o absència, proporciona una visió global de les principals situacions que desencadenen riscos naturals sobre l'àrea pirinenca, i alhora esdevenen un recurs útil en la predicció meteorològica, ja que permeten establir una analogia entre les situacions passades i les pronosticades, i el seu impacte en l'escala local.

- OG2: Proveir un entorn repetible que permeti la caracterització pluviomètrica des d'un punt de vista sinòptic de qualsevol indret del planeta. Cal proporcionar un marc repetible en el qual qualsevol investigador o tècnic pugui computar una classificació sinòptica objectiva i en pugui establir el vincle amb l'escala local, mitjançant la variable climàtica/ambiental de la seva preferència.

- OG3: Analitzar les característiques dels períodes perllongats d'absència de precipitació i, alhora, d'altes temperatures. Per la gran riquesa ecològica i de recursos naturals que ofereix el Pirineu, és molt important conèixer quin és i quin serà l'impacte del canvi climàtic en aquest àrea. Estudiar l'evolució recent i futura de la longitud dels períodes secs primaverals i estivals, i les temperatures extremes en el seu interior, així com els mecanismes físics que els causen, ha de servir per traslladar a la societat l'estat de vulnerabilitat al qual s'enfronta aquesta àrea en els propers anys a causa del canvi climàtic antròpic.

1.3.2. Objectius específics

A continuació, es detallen una sèrie d'objectius específics que permeten vertebrar els objectius generals i estructurar els resultats presentats:

- OE1: Proposar una metodologia que permeti l'obtenció objectiva de regions pluviomètriques uniformes i autoexplicatives mitjançant el vincle dels patrons sinòptics amb la precipitació diària. Els patrons pluviomètrics a escala pirinenca poden ser descrits per un notable número de situacions sinòptiques. En aquest sentit, i per a sintetitzar l'impacte de la circulació atmosfèrica en la pluviometria pirinenca, es formula un flux de treball per a l'obtenció d'una cartografia categòrica que expliqui aquest vincle entre la llarga escala i l'escala local, per al cas del Pirineu, però que també sigui extrapolable a altres regions del planeta.

- OE2: Desenvolupar una llibreria en el llenguatge de programació R que permeti repetir l'objectiu OE1, i en definitiva l'OG2, en qualsevol punt del planeta de forma totalment automatitzada. Proporcionar una nova eina d'accés obert per a l'estudi de la climatologia sinòptica i els seus vincles amb l'escala local, en llenguatge de programació R. Aquest objectiu específic és d'elevada importància per fer extensible els mètodes emprats en aquesta tesi doctoral a la resta de comunitat científica del camp de la climatologia i disciplines afins.

- OE3: Identificar les causes sinòptiques atribuïbles als esdeveniments torrencials. Sovint els serveis meteorològics necessiten disposar d'unes situacions sinòptiques de referència per a la previsió de situacions meteorològiques de risc. En aquest cas, a partir d'una aproximació environment-to-circulation es pretén obtenir un catàleg de situacions sinòptiques que descriuen els dies de més de 100 mm de precipitació.

- OE4: Projectar al futur l'evolució de les ratxes seques de llarga durada conjuntament amb l'ocurrència de temperatures màximes extremes. Disposar de les projeccions per a esdeveniments extrems és fonamental per a vertebrar les actuacions d'adaptació i mitigació enfront al canvi climàtic. En aquest sentit, mitjançant una prèvia correcció del biaix de les projeccions climàtiques, s'estableix l'evolució bivariada de la futura durada de les ratxes seques longeves, conjuntament amb els extrems de temperatura màxima en el si d'aquestes ratxes seques. Aquest tipus de situacions poden esdevenir punts d'ignició de catàstrofes naturals com ara grans incendis forestals.

1.4. Estructura de la tesi

Aquesta tesi doctoral, la qual es presenta com un compendi d'articles, està estructurada en 5 capítols diferents. En el Capítol 1 s'inclou la motivació per a realitzar aquesta tesi doctoral, així com l'estat l'art de les qüestions desenvolupades durant la present investigació, els objectius i l'estructura de la mateixa. El Capítol 2 s'ha dedicat a explicar l'origen i les característiques de les diverses tipologies de fonts que s'han emprat –observacions in-situ i reticulades, models de reanàlisi atmosfèrica, i models climàtics regionals, entre les més rellevants–. De la mateixa manera, s'han repassat les diverses metodologies aplicades per al control de qualitat de les dades in-situ, per al còmput de les classificacions sinòptiques, així com per als mètodes d'interpolació espacial de variables climàtiques, entre d'altres. El Capítol 3 és el que dona lloc als resultats d'aquesta tesi doctoral, i on apareixen les publicacions que formen part del compendi d'articles presentat. Cada una de les 5 publicacions presentades dona resposta als objectius plantejats en la secció 1.3:

L'objectiu general OG1 i l'objectiu específic OE1 són abordats en els dos treballs citats a continuació. En ambdós treballs s'estudia l'impacte que tenen els patrons sinòptics per a un període temporal llong en la precipitació diària. En el primer d'ells (Lemus-Canovas et al., 2019a), s'aborda aquesta qüestió a escala del Pirineu català i enfocant-se en les temporades hivernals entre el 1991 i el 2015, ja que l'objectiu és proveir de les situacions sinòptiques més freqüents durant la temporada d'allaus i el seu impacte en els patrons espacials de precipitació. Finalment, s'estableix una regionalització categòrica que permet comparar-la a les regions nivoclimàtiques emprades per la unitat d'allaus en el butlletí diari de predicció d'allaus que emet l'Institut Cartogràfic i Geològic de Catalunya (ICGC). En el mateix sentit, el segon estudi (Lemus-Canovas et al., 2019b) té uns objectius similars, ja que també contempla vincular les situacions sinòptiques més comunes del període 1961-2010 a la precipitació diària, però per a tota l'àrea del Pirineu. A més, en aquesta recerca es proposa una metodologia per obtenir una regionalització que permet descriure la pluviometria pirinenca mitjançant 8 regions diferents.

- Lemus-Canovas, M., Ninyerola, M., Lopez-Bustins, J. A., Manguan, S., & Garcia-Sellés, C. (2019a). A mixed application of an objective synoptic classification and spatial regression models for deriving winter precipitation regimes in the Eastern Pyrenees. International Journal of Climatology, 39(4), 2244–2259. https://doi.org/10.1002/joc.5948

- Lemus-Canovas, M., Lopez-Bustins, J. A., Trapero, L., & Martin-Vide, J. (2019b). Combining circulation weather types and daily precipitation modelling to derive climatic precipitation regions in the Pyrenees. Atmospheric Research, 220. doi: 10.1016/j.atmosres.2019.01.018

També formant part de l'objectiu general OG1, però de l'objectiu específic OE3, trobem el tercer treball (Lemus-Canovas et al., 2021) d'aquest compendi d'articles. En aquest cas, a partir dels dies amb precipitació torrencial (precipitació diària ≥ 100 mm), es classifiquen els principals patrons sinòptics als quals se'ls atribueix aquests volums diaris de precipitació.

- Lemus-Canovas, M., Lopez-Bustins, J. A., Martín-Vide, J., Halifa-Marin, A., Insua-Costa, D., Martinez-Artigas, J., Trapero, L., Serrano-Notivoli, R., & Cuadrat, J. M. (2021). Characterisation of Extreme Precipitation Events in the Pyrenees: From the Local to the Synoptic Scale. Atmosphere, 12(6), 665. https://doi.org/10.3390/atmos12060665

En el quart article (Lemus-Canovas et al., 2019c), es treballa sobre els objectius generals OG1 i OG2 i els objectius específics OE1 i OE2. En aquest últim treball, es presenta la llibreria R synoptReg que permet computar una classificació sinòptica objectiva, espacialitzar-ne la precipitació diària –o qualsevol altra variable ambiental contínua– en funció dels patrons sinòptics sorgits durant el procés de classificació i, per últim, establir-ne una regionalització categòrica que sigui capaç de sintetitzar les principals característiques pluviomètriques –o de qualsevol altra variable ambiental–.

- Lemus-Canovas, M., Lopez-Bustins, J. A., Martin-Vide, J., & Royé, D. (2019c). synoptReg: An R package for computing a synoptic climate classification and a spatial regionalization of environmental data. Environmental Modelling and Software, 118, 114–119. https://doi.org/10.1016/j.envsoft.2019.04.006

El cinquè, i últim article, (Lemus-Canovas i Lopez-Bustins, 2021) cobreix l'objectiu general OG3, i l'objectiu específic OE4. En ell s'aborda l'evolució recent i futura dels períodes consecutius sense precipitació i de les temperatures màximes extremes que es donen al seu interior, mitjançant un enfocament bivariat. A més, també se'n descriuen els seus mecanismes físics.

- Lemus-Canovas, M., & Lopez-Bustins, J. A. (2021). Assessing internal changes in the future structure of dry–hot compound events: the case of the Pyrenees. Natural Hazards and Earth System Sciences, 21(6), 1721–1738. https://doi.org/10.5194/nhess-21-1721-2021

A continuació dels resultats, s'exposen les principals conclusions a les quals s'ha arribat, primerament en català, i posteriorment en anglès, per tal d'optar a la menció internacional de doctorat. Així doncs, les conclusions, que formen el quart i cinquè capítol, són el resultat de donar resposta als objectius plantejats en aquesta tesi doctoral. Addicionalment, en aquests dos capítols també s'inclouen els últims avenços realitzats per l'autor, que, per una qüestió temporal, no han pogut presentar-se formalment en forma de publicació científica.

Finalment, hi ha dos apèndixs. En el primer, es presenta el material suplementari de cada un dels articles que conformen aquesta tesi doctoral, i en el segon s'inclou un llistat amb les contribucions realitzades durant el període predoctoral, incloent-hi les publicacions en revistes indexades, la docència realitzada, les presentacions orals i els pòsters presentats en congressos i jornades, així com altres mèrits també rellevants.

Capítol 2. Dades i mètodes

Aquesta secció ha de permetre al lector obtenir una visió global del conjunt de dades i metodologies emprades en aquesta recerca. Sovint, aquestes fonts han procedit de diverses bases de dades, així com s'ha fet ús de diferents metodologies, ja sigui per a realitzar les classificacions sinòptiques objectives; per dur a terme interpolacions estadístiques; o postprocessar els desajustos intrínsecs dels models climàtics, entre d'altres. Precisament, amb l'ànim d'esquematitzar tots els processos duts a terme en aquesta tesi doctoral, la Figura 3 presenta les principals tipologies de dades emprades (quadres blancs), les metodologies o els processos conduïts (quadres grisos), i els resultats obtinguts (quadres de groc pàl · lid). Les fletxes indiquen la direcció del flux de treball, posant, a la vegada, de manifest quins són els nexes d'unió entre els diversos treballs produïts. Finalment, el quadre de color maragda pàl · lid, el qual engloba diverses tipologies de dades, mètodes i resultats, mostra l'àrea repetible d'aquesta tesi doctoral. A partir d'aquesta esquematització, es vertebren els diversos apartats que venen a continuació.

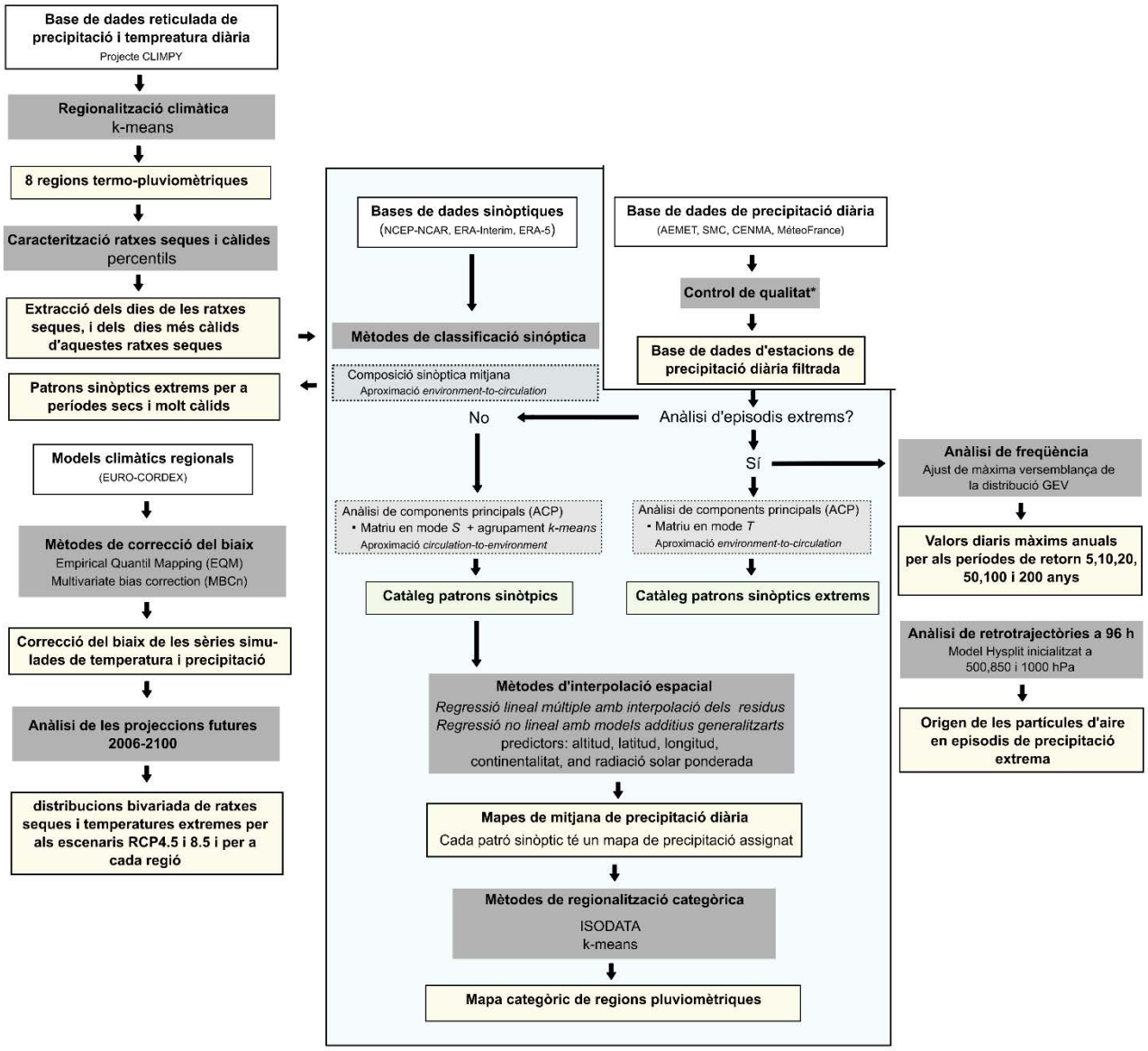

Figura 3. Esquematització de les bases de dades (quadres blancs) i metodologies (quadres grisos) emprades, així com els resultats obtinguts en cada un dels processos (quadres groc pàl · lid). El quadre maragda pàl · lid engloba la secció repetible de la tesi doctoral.

2.1. Dades

2.1.1. Sèries de precipitació i temperatura diària

La quantitat i longitud de les sèries climàtiques emprades en aquesta tesi han variat durant el seu transcurs arran de dos motius principals: 1) els avenços en el projecte interregional CLIM'PY, que és el que proveeix les dades observacionals a escala pirinenca; 2) l'objectiu de cada estudi presentat. En funció d'aquests objectius, s'ha donat una major o menor flexibilitat a l'hora de filtrar els valors que manquen en aquestes sèries i, per tant, fent variar el nombre de sèries finals a emprar en les anàlisis realitzades; i finalment, 3) l'àrea geogràfica treballada.

Aquests tres motius mencionats donen lloc a un desglossament de les dades observades emprades en cada un dels diferents estudis, i sintetitzats en la Taula 1.

- En el treball realitzat a Lemus-Canovas et al. (2019a), s'empren un total de 105 sèries diàries de precipitació al Pirineu oriental, proveïdes pel Servei Meteorològic de Catalunya (SMC), per l'Agència Estatal de Meteorologia (AEMET) i per les Forces Elèctriques d'Andorra (FEDA). En aquesta ocasió, el període d'estudi engloba les temporades hivernals (octubre-maig), entre el 1990 i el 2015. En molts casos, les sèries emprades presenten llacunes internes o sèries més curtes al període mencionat. Posterior al control de qualitat exposat en la secció 2.2.1., l'anàlisi es duu a terme amb 85 sèries diàries.

- A Lemus-Canovas et al. (2019b), la base de dades emprada ja és fruit de l'esforç cooperatiu interregional en el marc del Projecte interregional CLIM'PY. Els mateixos socis d'aquest projecte duen a terme diversos processos d'homogeneïtzació i control de qualitat de les dades de precipitació diària, amb l'objectiu de crear una base de dades climàtica única i d'alta qualitat per a tot el Pirineu. En el moment de la realització del treball, aquesta base de dades incloïa 673 sèries pluviomètriques, les quals cobreixen el període 1950-2015, moltes d'elles presentant discontinuïtats internes, i algunes amb menys de 10 anys de dades diàries disponibles. Per tal d'obtenir els resultats més robustos possibles, en aquest treball es consideren les sèries pluviomètriques dins del període 1961-2010, i que almenys continguin un mínim de 10 anys de dades, amb l'excepció de les estacions a altituds superiors a 1500 msnm, per les quals el llindar establert és una longitud mínima de 7 anys. La gran manca de sèries a cotes elevades propicia l'elevada flexibilitat d'aquest llindar. Un cop finalitzat el filtratge, el nombre final d'estacions distribuïdes per la zona d'estudi, així com per l'àrea circumdant, és de 349, amb la majoria d'aquestes (208) amb un període > 30 anys.

- En l'estudi presentat a Lemus-Canovas et al. (2021), la precipitació diària s'obté de nou de la base de dades del projecte CLIM'PY, que en data d'inici d'aquest treball, ja contenia 1.328 sèries pluviomètriques per al període 1950-2015. Com en els treballs anteriors, aquest període és simplement una referència, ja que la longitud de moltes sèries és variable, presentant diversos buits interns. No obstant això, Serrano-Notivoli et al. (2019) generen una base de dades homogeneïtzada i reomplerta per al període 1950 i 2015, i una altra amb el mateix període de dades, homogeneïtzada però sense reomplir. Per aquest treball s'empra la base de dades homogeneïtzada però amb la presència de buits, ja que en els tests de les dues bases de dades es detecten tendències artificials en aquelles sèries reomplertes, precisament degut a aquest procés (Fig. 4). Aquesta troballa precipita l'ús de les sèries sense reomplir, en les quals es filtraren totes les sèries amb més d'un 90 % de dades diàries, per al període 1981-2015, per tal de no perdre els dies amb una precipitació ≥ 100 mm, objecte d'aquest estudi. Aquest fet implica que el treball es desenvolupa amb 160 sèries diàries.

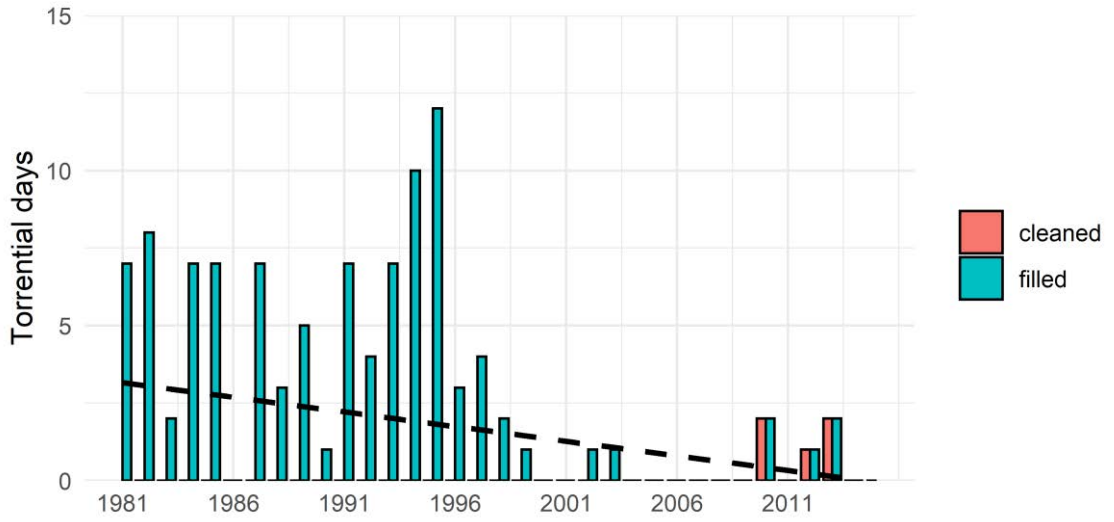

Figura 4. Número de dies torrencials per a la sèrie reomplerta (filled) i la sèrie original homogeneïtzada (cleaned) de l'observatori de la Renclusa (La Ribagorça). S'observa com en aquest cas, s'ha reomplert el 80 % de la sèrie.

- Per als dos estudis restants, s'empren bases de dades reticulades. En el cas de Lemus-Canovas i Lopez-Bustins (2021), s'empra la graella reticulada de precipitació diària i temperatura generada per Cuadrat et al. (2020). Aquesta base reticulada té una resolució espacial d'1km i comprèn el període 1981-2015. Finalment, en el treball de Lemus-Canovas et al. 2019c, es fa servir la base reticulada diària de precipitació a nivell europeu E-OBS (Haylock et al. 2008), que té una resolució espacial de 0.25º (~26km) per al període 1979-2017, per a l'àrea dels Alps, amb finalitats demostratives.

Taula 1. Descripció de les dades observacionals de precipitació i temperatura emprades per a l'àrea del Pirineu en els 5 treballs presentats.

Referència	Observacions	Període temporal	Resolució
Lemus-Canovas et al. (2018)	85 sèries de precipitació diària	1990-2015 (temporades hivernals)	
Lemus-Canovas et al. (2019a)	349 sèries de precipitació diària	1961-2010	
Lemus-Canovas et al. (2019b)	Malla EOBS. precipitació diària	1979-2017	~26km
Lemus-Canovas i Lopez-Bustins (2021)	Malla CLIM'PY. precipitació i temperatura màxima diària	1981-2015	~1km
Lemus-Canovas et al. (2021)	160 sèries de precipitació diària	1981-2015	

2.1.2. Models de reanàlisi atmosfèrica

En el cas dels models de reanàlisi atmosfèrica, s'han emprat diverses bases de dades (Taula 2), bàsicament provinents del Centre Europeu de Prediccions Meteorològiques a Mitjà Termini (ECMWF, European Centre for Medium-Range Weather Forecasts en anglès), i del Centre Nacional per la Previsió Ambiental (NCEP, National Centers for Environmental Prediction en anglès) i del Centre Nacional per a la Investigació Atmosfèrica (NCAR, National Center for Atmospheric Research en anglès). Per a cada un dels treballs presentats en aquesta tesi doctoral, s'han fet servir diverses variables (veure Taula 2), entre les quals, les més emprades han estat la pressió atmosfèrica reduïda a nivell del mar (SLP) i l'altura geopotencial a 500 hPa (Z500). Ambdues variables han esdevingut claus per a constituir les classificacions sinòptiques presentades en aquesta tesi doctoral. El període de dades extret de les bases de dades de reanàlisi ha estat variable en funció de la disponibilitat de les dades observades in-situ.

Cal tenir en compte que la base de dades NCEP/NCAR Reanalysis 2 també s'ha emprat per a la ingesta necessària de dades a l'hora d'inicialitzar el model de partícules Hysplit (Stein et al., 2015).

Taula 2. Descripció de les bases de dades de les reanàlisis atmosfèriques emprades en cada un dels treballs d'aquesta tesi doctoral. SLP és la pressió atmosfèrica en superfície; Z500 és l'altura geopotencial a 500 hPa; T850 correspon a la temperatura a 850 hPa; Q és la humitat específica; U i V són la component zonal i meridional del vent, respectivament. Q, U i V s'empren per als nivells entre 300 i 1000 hPa.

Referència	Base de dades	Variables	Període	Resolució	Àrea
Lemus-Canovas et al. (2018)	NCEP-NCAR Reanalysis 2	SLP, Z500	1990-2015 (temporades hivernals)	2.5	30º–60ºN 30ºW–15ºE
Lemus-Canovas et al. (2019a)	ERA-20C	SLP	1961-2010	1º	30º-55ºN, 12ºW-15ºE
Lemus-Canovas et al. (2019b)	ERA-Interim	SLP	1979-2017	0.75º	30º-60ºN, 10ºW-30ºE
Lemus-Canovas i Lopez-Bustins (2021)	ERA-Interim	Z500,T850	1981-2015	0.25º	30º-70ºN, 30ºW-20ºE
Lemus-Canovas et al. (2021)	ERA-5, NCEP-NCAR Reanalysis I	SLP,Z500, T850, Q, U, V	1981-2015	0.25º, 2.5º	30º-60ºN 20ºW-20ºE

2.1.3. Models de canvi climàtic

S'han emprat sis models climàtics a partir de diferents Models Climàtics Regionals (RCM, Regional Climate Models en anglès), niats a diferents Models de Circulació General (GCM, General Circulation Models en anglès), computats per a l'envolupant d'Europa, en el marc de l'Experiment

regional Coordinat de downscaling del Clima (CORDEX, Coordinated Regional Climate Downscaling Experiment en anglès) (Jacob et al., 2014) (Taula 3). Aquestes projeccions espacialment reticulades cobreixen tot Europa amb una resolució espacial de 0.11° (~12 km) per al període 1981-2005 (experiment històric) i 2006-2100 (escenaris futurs d'emissió de gasos d'efecte hivernacle -GEH-). En la selecció dels models climàtics, s'ha tingut en compte aquells que proporcionen dades suficients per a l'objectiu de la recerca duta a terme, i que ja havien estat emprats en investigacions anteriors (Jacob et al., 2014). Pel que fa a les Trajectòries de Concentracions Representatives (RCPs, Representative Concentration Pathways en anglès) utilitzades, aquestes han estat la RCP4.5 –via d'estabilització sense excés fins a l'estabilització de 4.5 W/m^2 (~650 ppm de CO_2) després del 2100 (Wise et al., 2009)– i el 8.5 –via d'augment del forçament radiatiu que porta a 8.5 W/m^2 (~1370 ppm de CO_2) per al 2100 (Riahi et al., 2007)– .

Taula 3. Models climàtics EURO-CORDEX utilitzats.

Institut	GCM	RCM
CNRM	CNRM-CM5	ALADIN-63
CNRM	CNRM-CM5	RACMO22E
DMI	NCC-NorESM1-M	DMI-HIRHAM5
KNMI	EC-EARTH	RACMO22E
SMHI	IPSL-CM5A-MR	RCA4
SMHI	MPI-ESM-LR	RCA4

2.2. Mètodes

2.2.1. Control de qualitat de les sèries climàtiques observades

Abans d'analitzar qualsevol sèrie climàtica és indispensable assegurar-ne la seva qualitat, mitjançant una sèrie de rutines estadístiques que en garanteixin la seva robustesa. Per tal de comprovar la validesa de les sèries diàries de precipitació, s'ha executat l'extensió del programari lliure RClimdex (Zhang i Yang, 2004), anomenat ExtraQC (Aguilar i Prohom, 2011), el qual ofereix una sèrie d'índexs estadístics per testar-ne la seva qualitat.

El primer d'aquests índexs és el de detecció d'outliers (valors fora de rang). La localització d'aquests valors es realitza en sumar 5 vegades el rang interquartílic (IQR) a aquells dies en què la precipitació supera el tercer quartil (valors > a 3r quartil + 5*IQR.). Aquest procediment, de fàcil aplicació, té la contrapartida de detectar falsos outliers, amb la qual cosa es fa palesa la necessitat de verificar cada un d'aquests casos suposadament fora de rang. A la Figura 5 s'observa la detecció d'un outlier de 367,5 mm/24 h a Darnius (l'Alt Empordà). Revisant l'arxiu de climatologies d'AEMET (Sección de Climatología, 2002), així com la premsa local, és possible validar la veracitat del registre. Aquest fet remarca la necessitat d'una revisió acurada tant estadísticament com manual.

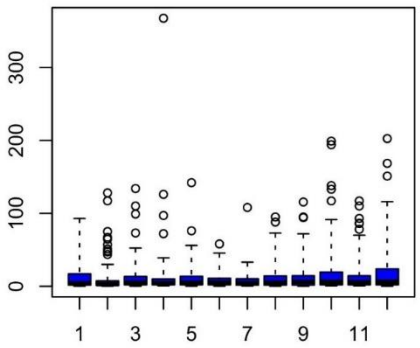

Figura 5. Detecció de falsos outliers a l'observatori pluviomètric de Darnius (l'Alt Empordà).

Seguidament s'ha dut a terme un control de precisió, mitjançant la quantificació de freqüències absolutes per decimal, és a dir, el recompte del nombre de dies amb precipitació decimal 0 fins 9, descartant-se aquells dies amb una precipitació 0.0. Aquest índex permet testar la qualitat de precisió de cada una de les sèries, ja que moltes sèries són arrodonides a 1 mm o 0.5 mm. Un exemple d'aquesta precisió dispar es presenta a la Figura 6.

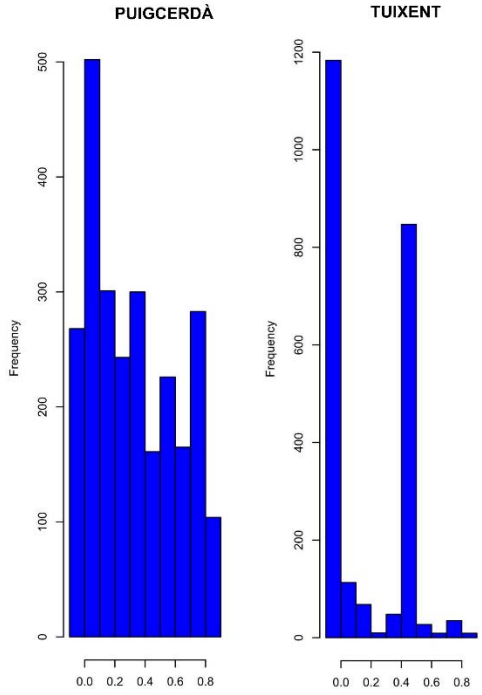

Figura 6. Freqüències absolutes de precisió decimal per valorar la precisió de les sèries pluviomètriques de Tuixent (l'Alt Urgell) i Puigcerdà (la Cerdanya).

Com s'observa en el cas de Tuixent (l'Alt Urgell), la precipitació es registra només en intervals de 0.5 mm, mentre que a Puigcerdà (la Cerdanya) es realitza, generalment, per a tots els decimals. Per últim, mitjançant l'ExtraQC, es realitza un control d'aquells valors anormalment alts i baixos, com ara precipitacions diàries superiors a 200 mm i valors negatius, aquest últim sovint emprat per indicar precipitacions inapreciables o sumatoris de diversos dies. Fora d'aquest programari, s'han emprat dos mètodes proposats per Abaurrea et al. (2004). El primer d'ells és la detecció de falsos

zeros, que es basa en considerar sospitosa aquella sèrie que registra un valor mensual de 0 mm i es produeix una de les següents condicions:

- Almenys un 75 % de les sèries auxiliars (mínim 4) mesuren una precipitació mensual superior a 15 mm.
- Les dues sèries més properes a la sèrie candidata sobrepassen els 10 mm mensuals.

El segon mètode es basa en el desplaçament diari de la data del registre. Per detectar l'existència de desplaçaments reiterats a partir dels valors diaris de cada any, s'estableix un índex que es defineix com la suma anual de les diferències absolutes de la sèrie candidata i l'auxiliar entre les mateixes diferències quan la sèrie candidata es desplaça un dia cap endavant (eq.1):

$$\sum|y_t - x_t| / \sum|y_{t+1} - x_t| \qquad \text{(eq. 1)}$$

On y_t és el valor diari de la sèrie candidata, x_t el valor diari de la sèrie auxiliar. S'aplicarà el mateix procediment però restant un dia a la sèrie candidata (eq.2):

$$\sum|y_t - x_t| / \sum|y_{t-1} - x_t| \qquad \text{(eq. 2)}$$

Aquest índex serà més proper a zero com major sigui la semblança entre la sèrie candidata i l'auxiliar.

2.2.2. Metodologies de classificació sinòptica

Molts conjunts de dades climàtiques són multidimensionals i, per tant, poden ser difícils de visualitzar i interpretar. No obstant això, sovint existeix una dimensionalitat intrínseca més petita en el conjunt de dades, on no es necessiten totes les variables per transmetre la informació més rellevant del conjunt original. Per tant, freqüentment, és d'interès reduir la dimensionalitat de les dades originals. Els mètodes per reduir la dimensionalitat intenten capturar la màxima informació present en aquest conjunt de dades, minimitzant al mateix temps l'error entre les dades originals i la nova representació dimensional inferior (Donoho, 2000).

Un dels mètodes més emprats a l'hora de reduir aquesta dimensionalitat és l'anàlisi de components principals (ACP). Aquest mètode redueix un conjunt de dades que conté un gran nombre de variables a un conjunt de dades que conté menys variables. Aquestes noves variables són combinacions lineals de les originals, i aquestes combinacions lineals s'escullen per representar la màxima variància continguda en les dades originals.

Les dades dels camps atmosfèrics i altres camps geofísics presenten, generalment, grans correlacions entre variables, i l'ACP resulta en una representació molt més compacta de les seves variacions (Wilks, 2019). L'ACP té el potencial de proporcionar una visió sintètica tant de les

variacions espacials com de les temporals exhibides pel camp o camps atmosfèrics que s'estan analitzant, el que pot suggerir noves interpretacions de les dades originals.

La disposició de la matriu de dades originals prèvia a l'aplicació de l'ACP és molt important. En aquest treball s'han emprat dos variants, la matriu en mode espacial (S) i en mode temporal (T). Cada una d'aquestes dues matrius implica objectius i processos diferents a l'hora d'obtenir el catàleg sinòptic. Seguidament, se'n detallen les seves característiques, així com els passos necessaris fins a l'obtenció de la classificació sinòptica.

Catàleg sinòptic a partir d'una matriu en mode S (ACP + k-mitjanes)

Com s'ha comentat anteriorment, la disposició original de la matriu de dades, conformada per tres entitats principals –la variable atmosfèrica, el temps, i l'espai[3]–, és de gran importància en funció de quin sigui el nostre objectiu. En el cas de la matriu en mode S, aquesta té una disposició temps (t) x espai (g), amb l'afegitó de n variables atmosfèriques. Precisament, aquest últim cas, el de treballar amb més d'una variable, no és trivial, ja que aquestes variables poden tenir unitats de mesura diferents i distorsionar el resultat final. Per aquest motiu, quan hom treballa amb més d'una variable, cal estandarditzar-les prèviament, i calcular-ne la matriu de correlacions, en comptes de la de covariàncies. Una representació esquemàtica de la matriu en mode S i la seva disposició es presenta a la Figura 7.

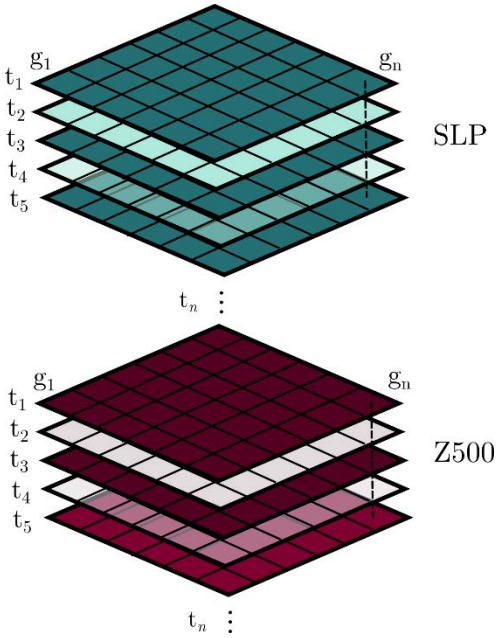

	g_1 (lon_1,lat_1)	g_2 (lon_2,lat_2)	g_3 (lon_3,lat_3)	g_n (lon_n,lat_n)
t_1	SLP(t_1,g_1)	SLP(t_1,g_2)	SLP(t_1,g_3)	SLP(t_1,g_n)
t_2	SLP(t_2,g_1)	SLP(t_2,g_2)	SLP(t_2,g_3)	SLP(t_2,g_n)
t_3	SLP(t_3,g_1)	SLP(t_3,g_2)	SLP(t_3,g_3)	SLP(t_3,g_n)
t_n	...	...	...	...
t_1	Z500(t_1,g_1)	Z500(t_1,g_2)	Z500(t_1,g_3)	Z500(t_1,g_n)
t_2	Z500(t_2,g_1)	Z500(t_2,g_2)	Z500(t_2,g_3)	Z500(t_2,g_n)
t_3	Z500(t_3,g_1)	Z500(t_3,g_2)	Z500(t_3,g_3)	Z500(t_3,g_n)
t_n	...	...	...	...

Figura 7. A l'esquerra representació esquemàtica de la disposició d'un conjunt multidimensional de dades climàtiques a l'hora d'aplicar un ACP en mode S. Les matrius de color verd representen la pressió atmosfèrica en superfície (SLP) i les

[3] Espai entès com les parelles de coordenades que formen la retícula de punts d'un model de reanàlisi atmosfèrica, per exemple.

de color granat, l'altura geopotencial a 500 hPa (Z500). Cada variable te el mateix número de passos temporals (t_n) i de punts de retícula (g_n). A la dreta trobem la disposició de la matriu de dades emprada a l'hora de realitzar aquest ACP en mode S, la qual es concreta en el fet que les variables, o caps de columna, són els punts de retícula, i les files són les observacions de tots els casos de SLP i Z500.

En aplicar l'ACP sobre aquesta matriu de dades s'obté un conjunt de components principals que bàsicament són la combinació lineal –és a dir, una suma ponderada– de tots els parells de coordenades de la retícula. Els pesos en aquesta suma ponderada són correlacions de Pearson –a les quals anomenarem loadings, a partir d'ara–, les quals s'empren a l'hora d'ajustar cada un dels eixos d'aquestes components principals (CPs), per tal d'obtenir el millor ajust en les dades. Cal tenir en compte que, aquests eixos, són ortogonals entre sí. Per tant, el primer component tractarà d'explicar la màxima variància possible sobre les dades originals mitjançant una primera combinació lineal (eq.3):

$$PC1 = \alpha_{1,g_1} slp_{g_1} + \alpha_{1,g_2} slp_{g_2} + \alpha_{1,g_3} slp_{g_3} ... \alpha_{1,g_n} slp_{g_n} \qquad \text{(eq.3)}$$

On, $\alpha_{1,g1}$ és el loading corresponent a la primera component per al primer punt de la retícula, mentre que slp_{g1} és el vector de valors de pressió atmosfèrica en superfície per al primer punt de la retícula. Degut a l'ortogonalitat d'aquestes components, la segona CP serà independent a la primera, mostrant una correlació 0 entre ambdues CPs, i alhora captant la màxima variància possible. La tercera CP, també serà ortogonal a les anteriors, per tant, no estarà correlacionada amb les dues CPs anteriors. Aquest procés continua fins que s'han calculat el total de n components principals, és a dir, el nombre de components principals és el mateix que el nombre original de variables, que en aquest cas són els punts de retícula. En aquest moment, la variància total de totes les components principals igualarà la variància total entre totes les variables. D'aquesta manera, es conserva tota la informació continguda a les dades originals; no es perd cap informació; l'ACP implica només una rotació ortogonal de les dades originals.

En tot cas, el que roman interessant en aquest punt és el fet que els loadings són una clara expressió del pes de cada punt de la retícula en cada CP, és a dir, per al CP1 cada punt de retícula g_n té associat un valor de correlació de Pearson, el que ens permet representar espacialment els modes de variació de la nostra variable. Precisament, per mitjà dels loadings obtinguts en l'ACP en mode S, els patrons de baixa freqüència són fàcilment cartografiables. Ara bé, cal no confondre que aquests patrons espacials en cap cas són tipus de circulació atmosfèrica, ja que la variabilitat captada per aquest procés és baixa (Hewitson i Crane, 1992; Huth, 1996). No obstant això, i com s'ha comentat anteriorment, l'ACP suposa la rotació del conjunt original de dades, el que implica que aquestes observacions es troben en posicions diferents a les originals. Això vol dir que es troben en un nou sistema de coordenades en aquestes components principals. Precisament, aquestes coordenades són la situació en l'espai multivariant de cada un dels nostres dies objectius a classificar, i com de propers es troben cada un d'ells respecte cada centre de coordenada de cada component principal. Aquestes coordenades en l'espai multivariant de l'ACP s'anomenen popularment scores i són calculats com a combinacions lineals de les variables originals i els pesos $\alpha_{i,gn}$. Aquestes coordenades multivariants

permeten, precisament, conèixer el grau de representativitat de cada un dels nostres casos en cada una de les components principals, i alhora cercar grups dins d'aquests casos, els quals estadísticament siguin propers els uns dels altres. És aquesta última particularitat la que permetrà generar una classificació de tipus de circulació, realitzant un previ agrupament mitjançant tècniques de clustering.

Arribats a aquest punt hem definit els dos principals elements que ens permeten caracteritzar estadísticament conjunts de dades climàtiques multidimensionals: els loadings i els scores. Prèviament, ja s'ha mencionat que, particularment, per a una ACP en una matriu S, els loadings no permeten establir patrons sinòptics. Per tant, per assolir la desitjada classificació sinòptica caldrà treballar amb els scores, pels motius ja mencionats anteriorment. No obstant això, prèviament cal decidir quin número de components principals es volen retenir per seguir amb el tractament posterior dels scores. En aquesta recerca s'ha optat per fer ús del Scree test (Catell, 1966), el qual es basa en el canvi de pendent en la línia que uneix els punts que representen percentatges de variància de cada component principal. El punt previ a la caiguda de la variància esdevé el punt de tall. Un cop retingut el número de components principals, hi ha dues opcions: 1) procedir a treballar els scores directament; 2) aplicar una rotació dels eixos de les components principals retingudes. Aquí s'ha optat per la segona opció, ja que una rotació pot afavorir una redistribució de la variància entre les components principals retingudes. Bàsicament, s'espera que les components que explicaven un percentatge menor de variància, amb el reajustament, vegin incrementat el seu pes. Existeixen multitud de tipologies de rotació d'eixos, però en aquest treball s'ha optat per emprar la rotació ortogonal VARIMAX, un algoritme, que precisament té per objectiu cercar la màxima variància per a cada component principal i que ha estat àmpliament usat (Esteban et al., 2006; Martin-Vide et al., 2008; Zachary et al., 2020).

En aquest punt, s'inicia el tractament dels scores rotats, és a dir, aquestes coordenades que han estat rotades inicialment per l'ACP i, posteriorment, mitjançant la rotació VARIMAX. Ara mateix tenim els nostres casos dispersos en l'espai multivariant, pel que és necessari trobar una metodologia que ens els permeti agrupar. Esteban et al. (2005) proposa el mètode de les puntuacions extremes, el qual es basa a trobar els scores positius i negatius per sobre i per sota de +2 i -2, respectivament, per a cada component principal, amb l'objectiu d'establir-los com a centroides d'un futur algoritme de clustering. Aquesta metodologia pot establir fins a dos centroides per CP. Per exemple, en el cas del CP1, en primer lloc se cercarà si hi ha dies amb un score > 2 (CP1+); en cas afirmatiu, es recolliran tots els dies que superin aquest valor i se'n fa la mitjana. Aquesta mitjana no només es realitza amb els casos del CP1, sinó que es fa extensible a la resta de CPs (Taula 4). En cas que no existeixi cap dia amb un score superior a 2, aquest grup queda directament exclòs. Així doncs, n CPs poden esdevenir fins a 2n tipus de circulació, en funció de si es pot establir un centre de coordenades per excés de llindar.

Taula 4. Exemple fictici sobre l'establiment dels centroides de cada grup. En aquest cas es cerquen els scores superiors a 2 en el PC1, i es troben 4 dates diferents. S'extrauen els scores de totes les components (rotades) per aquests dies, i posteriorment se'n realitza la mitjana per obtenir el centre de clúster del primer grup. Aquest procés es realitza de forma iterativa per a l'extrem positiu i negatiu de cada component principal.

Dies	CP1	CP2	CP3	CP4	CP5	CP6
19/02/1993	2.50	1.49	-1.46	-1.00	-0.74	-0.43
06/11/2007	2.49	1.11	-0.14	-0.16	0.67	1.59
21/11/2008	2.70	0.47	-1.91	0.57	0.04	0.59
09/12/2010	2.59	0.87	-1.17	-1.82	0.75	-0.27
X (centroide)	2.57	0.99	-1.17	-0.60	0.18	0.37

Calculats els centres de clúster, es fa ús del mètode d'agrupament K-means per tal de classificar tots els dies d'estudi en cada un dels diferents grups. El mètode de K-means s'aplica sense iteracions, ja que es valora que els centres de clúster establerts amb el mètode de les puntuacions extremes són representatius de cada un dels grups (Esteban et al. 2012). Amb tot, en aplicar el mètode, aquests centres de clúster inicials es recalculen per tal d'agrupar tots els dies, i no deixar-ne cap sense classificar. Els nous centres mantindran uns valors pròxims als inicials, però lleugerament modificats, per així classificar la totalitat de la mostra i obtenir el catàleg sinòptic desitjat.

Catàleg sinòptic a partir d'una matriu en mode T (ACP)

La matriu en mode T és la transposada de la mode S, per tant, en aquest cas tenim que les variables són els dies i els casos són els punts de la retícula (Fig. 8). Per a aquesta tipologia s'obviaran alguns detalls que ja s'han descrit en l'explicació metodològica anterior. L'aplicació de l'ACP en una matriu en mode T implica que els CPs resultants no siguin combinacions lineals entre els punts de la retícula, sinó que ho siguin entre els dies a classificar. Per tant, això suposarà que en aquest cas, els pesos de la combinació lineal de cada CP –tants com casos d'estudi–, els loadings, esdevinguin directament la representació de cada dia en un dels seus components, en forma de coeficients de correlació.

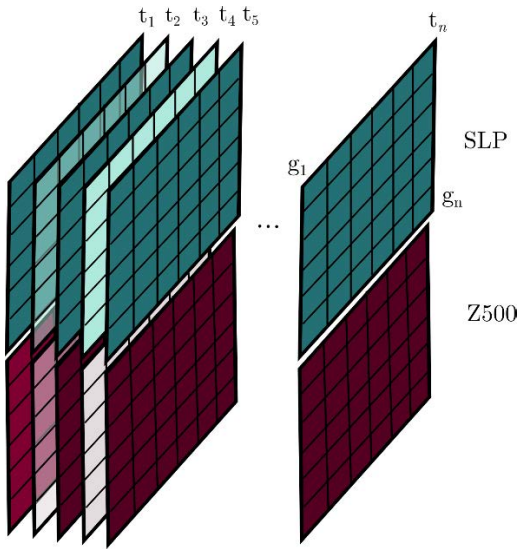

	t_1	t_2	t_3	t_n
g_1	SLP(g_1)	SLP(g_2)	SLP(g_3)	SLP(g_n)
g_2	SLP(g_1)	SLP(g_2)	SLP(g_3)	SLP(g_n)
g_3	SLP(g_1)	SLP(g_2)	SLP(g_3)	SLP(g_n)
g_n	...	...	...	...
g_1	Z500(g_1)	Z500(g_2)	Z500(g_3)	Z500(g_n)
g_2	Z500(g_1)	Z500(g_2)	Z500(g_3)	Z500(g_n)
g_3	Z500(g_1)	Z500(g_2)	Z500(g_3)	Z500(g_n)
g_n	...	...	...	...

Figura 8. A l'esquerra representació esquemàtica de la disposició d'un conjunt multidimensional de dades climàtiques a l'hora d'aplicar un ACP en mode T. Les matrius de color verd representen la pressió atmosfèrica en superfície (SLP) i les de color granat, l'altura geopotencial a 500 hPa (Z500). Cada variable te el mateix nombre de passos temporals (t_n) i de punts de retícula (g_n). A la dreta trobem la disposició de la matriu de dades emprada a l'hora de realitzar aquest ACP en mode T, la qual es concreta en què les variables, o caps de columna, són els casos a classificar (t_n), i les files són els punts de retícula. Per tant, per a cada cas o dia (variable) es desplega tota una fila que són tots els valors del mapa que configura aquell dia.

Queda palès que aquest tipus d'aplicació facilita molt la feina en el cas de voler aconseguir un catàleg sinòptic sense haver de realitzar processos de clustering. De fet, en aquesta metodologia es tracta de trobar la màxima correlació positiva o negativa que té cada dia amb cada component i realitzar-ne l'assignació (Taula 5). Per tant, en aquest cas també es poden assolir el doble de tipus de circulació que de components principals.

Taula 5. Exemple fictici de classificació dels loadings en el seu grup/CP més representatiu. Per a cada data es cerca el valor màxim absolut de correlació amb cada CP, preservant-ne el sentit de la correlació. Es tracta d'un procés iteratiu que finalitza quan s'han revisat tots els dies d'estudi.

Dies	PC1	PC2	PC3	PN
2000-01-01	0.7	0.3	-0.4	1+
2000-01-02	0.5	0.4	-0.6	3-
2000-01-03	0.2	0.5	-0.7	3-
2000-01-04	-0.3	0.5	-0.4	2+

Ara bé, vista la simplicitat d'aquest mètode, quin sentit té emprar la matriu en mode S per a l'aplicació de l'ACP? Una de les principals limitacions que té l'ACP en mode T és que el número de dies (variables) a classificar en cap cas pot ser superior a la retícula de punts (observacions). D'aquesta manera, si volem classificar una sèrie diària de 30 anys (>10000 dies), no podrem emprar aquest mètode, ja que encara que emprem una retícula d'alta resolució espacial, aquesta no tindrà tants punts de retícula com de número de dies. El motiu d'aquesta mancança és fàcilment

comprensible a través del següent exemple. A l'eq.4 es mostra una matriu de 2x3, és a dir, dos punts en un espai tridimensional:

$$X = \begin{bmatrix} 1 & 1 & 1 \\ 2 & 2 & 2 \end{bmatrix} \qquad \text{(eq.4)}$$

La seva representació en aquest espai tridimensional es mostra a la Figura 9:

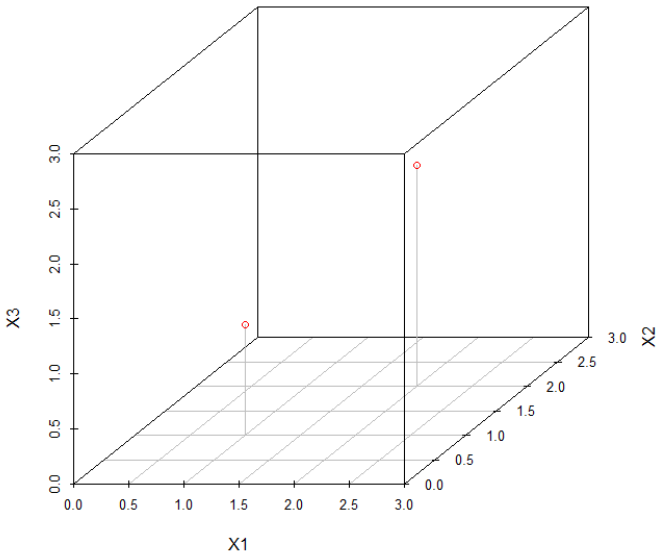

Figura 9. Representació tridimensional de les coordenades proporcionades en la matriu 2x3 de l'eq.4.

Amb la matriu esperada, que conté tres variables, hom esperaria obtenir tres components principals, però la limitació ve donada pel nombre d'observacions. La rotació dels eixos establerta per l'ACP procura cercar la màxima variabilitat del conjunt d'observacions des d'una geometria ortogonal. En l'exemple, amb dos punts d'observació, és factible traçar l'eix de la primera component, ja que podem unir aquests dos punts, ara bé, de quina manera podem generar el segon eix, si aquest ha de ser ortogonal al primer? Ja no hi ha més observacions que permetin aquesta ortogonalitat i, per tant, ja no hi ha més variabilitat a explicar ni més components principals possibles.

Fet aquest petit apunt, una altra de les limitacions d'aquesta aplicació és el temps de càlcul. Si el nombre de dies és relativament gran i la retícula de punts d'elevada resolució espacial, el procés de computació es pot demorar notablement.

2.2.3. Metodologies d'interpolació espacial

Relacions multivariades

Durant aquesta investigació s'ha fet ús de mètodes multivariants per a la predicció espacial de la precipitació diària vinculada a cada un dels tipus de circulació obtinguts. En aquest sentit, la regressió estadística és la metodologia que s'ha emprat majoritàriament per a establir les relacions entre variables amb l'assumpció de causa-efecte. L'equació matemàtica de la regressió, o bàsicament, de la recta, del pla o del hiperplà d'ajust, pot contenir una o més variables independents (x); el paràmetre d'intercepció (a); el pendent (β), i l'error intrínsec del model (ε). Tots aquests paràmetres

permetran explicar part de la variància de la variable dependent (y). La intercepció a representa el valor de y quan x val zero, en el cas d'una recta, mentre que el pendent indica el canvi, augment o disminució, en la variable dependent per cada augment unitari de la variable independent.

La regressió estadística es basa en el mètode de mínims quadrats, el qual consisteix a buscar la recta que minimitzi les distàncies quadrades entre els valors observats i la recta de predicció. En funció del nombre de variables independents, es distingeix entre regressió simple, només una variable independent (eq.5), i regressió múltiple, més d'una variable independent (eq.6):

$$y = a + \beta x + \varepsilon \qquad \text{(eq.5)}$$

$$y = a + \beta_1 x_1 + \beta_2 x_2 + ... + \beta_k x_k + \varepsilon \qquad \text{(eq.6)}$$

El contrast d'hipòtesis en el model de regressió lineal es realitza mitjançant el contrast de nul · litat (pendent $\beta = 0$) per als coeficients de la regressió, emprant en aquest cas la distribució de t-Student; per a avaluar el conjunt del model, s'empra la distribució de Fisher. Si el p-valor és inferior a 0.05 podem rebutjar la hipòtesi nul · la que indica que els coeficients de la regressió no posseeixen una pendent diferent a zero. Això indica que, si el p-valor < 0.05, la variable independent x_k està realitzant una contribució sobre la variable dependent. A més, per dur a terme el contrast d'hipòtesis en el model lineal de regressió, s'ha de complir que els residus tinguin una distribució normal, que aquests compleixin el principi d'homoscedasticitat, i que existeix independència entre variables independents; així com una relació lineal significativa entre variable dependent i independent. En un model de regressió lineal el coeficient de determinació (R^2) és el quadrat del coeficient de correlació de Pearson i informa sobre la qualitat del model, la seva capacitat predictiva i la proporció de variància dels resultats explicable pel model.

En el camp de la interpolació espacial, la regressió és una tècnica estadística que permet incorporar els efectes geogràfics en variables climàtiques, com la que ens depara en aquest estudi la precipitació. En aquest sentit, les variables independents poden ser variables geogràfiques tals com l'altitud, la latitud, la continentalitat o la radiació solar, entre d'altres (eq. 7):

$$y = \beta_0 + \beta_1(ALT) + \beta_2(LAT) + \beta_3(CON) + \beta_4(RAD) \qquad \text{(eq.7)}$$

En la propera secció es revisen les diverses variables independents que s'han emprat en els models de regressió aplicats en aquesta tesi.

Consideracions sobre les variables independents

Les variables independents són aquelles variables necessàries per ajustar el model, o, el que és el mateix, generar una predicció el més acurada possible de la variable dependent en aquelles zones on no hi ha observació pluviomètrica. D'aquesta manera durant els diferents treballs que empren mètodes d'interpolació espacial, s'utilitzen diferents variables explicatives per construir els mapes de precipitació mitjana diària basats en els tipus de circulació atmosfèrica. Com és àmpliament sabut, la topografia afecta directament la variabilitat espacial de la precipitació, pel que és crucial utilitzar

un model digital d'elevació (MDE) amb una resolució elevada per millorar la predicció espacial de la nostra variable de resposta. En aquests treballs, s'ha emprat un MDE de 90 × 90 m extret del Shuttle Radar Topography Mission (SRTM), el qual ha permès derivar la resta de variables explicatives utilitzades en els estudis implicats. A part de l'ús de l'elevació com a variable explicativa de la precipitació mitjana diària, s'ha emprat la latitud, calculada com la distància euclidiana des de la cel · la més meridional del ràster. De la mateixa manera es computa la longitud, però, en aquest cas, mitjançant la distància euclidiana des de la cel · la més occidental. També s'ha considerat com a variable explicativa la continentalitat, que permet avaluar la influència de la mar Mediterrània i de l'Oceà Atlàntic en la precipitació del Pirineu. Pel que respecta a la capa ràster de continentalitat, aquesta ha estat calculada a partir de la funció de cost de distància respecte la mar Mediterrània i l'oceà Atlàntic. El MDE s'ha usat com a superfície de fricció, a partir del qual s'han generat els valors acumulats de cost. L'algoritme que calcula aquest cost de distància acumulada funciona de la següent manera:

(1) Cost de cel · la = cost assignat (elevació)*resolució de la cel · la (90 m)

(2) Cost desplaçament de cel · la (a1) = cost 1 + (cost 2)/2

On cost 1 és el cost de la cel · la 1, cost 2 és el cost de la cel · la 2 i a1 és el cost de viatjar de la cel · la 1 a la 2.

(3) Cost acumulat = a1 + (cost 2 + cost 3)/2

On cost 2 és el cost de la cel · la 2, cost 3 és el cost de la cel · la 3. Per tant, la funció Cost acumulat indica el cost total de la cel · la 1 a la 3.

(4) Cost d'una diagonal (a1) = 1.4142*(cost 1 + cost 2)/2

El cost de realitzar un desplaçament en diagonal es valoritza com l'arrel quadrada de 2. El mapa de fricció resultant s'obté una vegada que l'algoritme ha assignat el valor de cost més baix a cada cel · la.

Seguint el mateix plantejament que amb la continentalitat, generem una variable que anomenem influència de nord, ja que s'ha comprovat que les adveccions de nord són molt efectives al vessant nord de la serralada en comparació amb les condicions més seques de la cara sud, produint en aquesta el conegut fenomen anomenat efecte Föhn (Queno et al., 2016). A mesura que ens desplacem cap al sud, aquest efecte disminueix, i no provoca problemes de multicol · linealitat amb la variable latitud. Una altra variable explicativa computada és la distància euclidiana als massissos muntanyosos superiors a 2000 m.s.n.m, per emfatitzar els fenòmens de tempestes orogràfiques i d'ombra pluviomètrica que es produeixen principalment a finals de primavera i durant l'estiu. Per últim, s'han generat mapes mensuals de radiació solar potencial (considerant unes condicions atmosfèriques constants) a partir del MDE i les equacions astronòmiques de la posició del sistema Terra-Sol (Pons i Ninyerola, 2008). D'aquesta última covariable i del MDE, se'n genera un duplicat però remostrejant-les a 20 km de mida de cel · la, amb l'objectiu de percebre els efectes espacials de la precipitació a una escala més general.

Un cop generades totes les variables independents, s'ha testat el grau de correlació entre elles, per tal de detectar problemes de multicol · linealitat. Com es fa visible a la Figura 10, inicialment

s'havia inclòs la distància euclidiana a la mar Mediterrània i a l'oceà Atlàntic, però, en generar el correlograma, s'han descartat per estar massa correlacionades amb les variables de continentalitat mediterrània i atlàntica ($r \geq 0.8$) i aportar menys informació que aquestes últimes.

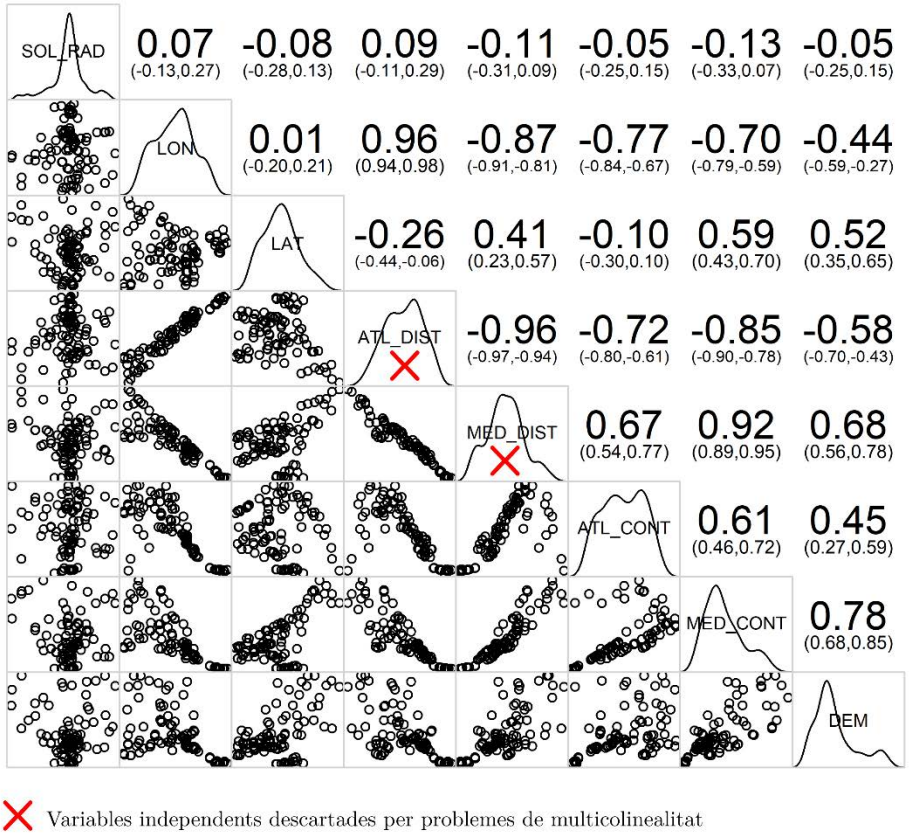

Figura 10. Correlograma per a la detecció de problemes de multicol · linealitat. Les variables de distància euclidiana a la mediterrània i de distància euclidiana a l'Atlàntic han estat excloses de l'anàlisi per aquest motiu

Mètodes de regressió estadística aplicats a la interpolació climàtica

Regressió lineal múltiple i posterior interpolació dels residus

La metodologia de base utilitzada és molt similar a la que es pot trobar a Ninyerola et al. (2000). Es tracta de relacionar la informació geogràfica (variables independents) amb la informació climàtica (variables dependents) mitjançant una anàlisi de regressió múltiple. Els coeficients de regressió poden ser utilitzats per a reproduir, mitjançant l'àlgebra de mapes, l'equació de la regressió lineal múltiple i, així, obtenir un mapa per a la corresponent variable dependent.

Lògicament, aquest procés passa per disposar d'una matriu ràster de les diferents variables independents: un MDE per l'altitud, un mapa de latitud, un mapa de continentalitat, etc, fet que ja s'ha introduït en l'apartat anterior. Fins aquest punt, el mètode és exactament idèntic a una regressió lineal múltiple (eq. 7). L'aspecte a destacar és el refinament posterior que es realitza sobre aquests mapes, utilitzant precisament els residus de la mateixa anàlisi de regressió lineal múltiple. D'aquesta manera obtenim, mitjançant una interpolació estrictament matemàtica (invers a la distància ponderada, Splines o Kriging), uns mapes de residus o anomalies que ens serveixen per corregir els mapes inicials.

Cal destacar que en el cas de la regressió lineal múltiple i la interpolació dels valors residuals mitjançant el mètode de Kriging –també anomenada regressió Kriging (Hengl et al., 2007)–, aquesta posseeix una major complexitat, ja que prèviament cal modelar la dependència entre la semivariància i la distància geogràfica entre les parelles de valors residuals. En el cas de la regressió lineal múltiple i posterior interpolació dels residuals mitjançant els mètodes d'invers a la distància ponderada i splines, s'empra el software Miramon (Pons, 2000). Pel cas de la interpolació dels residuals mitjançant el mètode geostadístic de Kriging es fa ús de la llibreria R gstat (Pebesma, 2004).

Generalized Linear Model (GLM)

Existeixen nombrosos mètodes per abordar el modelatge geoespacial de la precipitació per tal de caracteritzar millor la seva elevada variabilitat espacial. El model GLM (McCullagh i Nelder, 1989) representa una generalització de diversos mètodes de regressió (regressió lineal, regressió logística, regressió de Poisson, etc.) per tal de modelar la variable explicada o dependent. El principal avantatge que ofereix aquest model respecte al model de regressió lineal és que permet que la variable de resposta segueixi una distribució de dades diferent a la normal podent-se escollir entre una distribució gaussiana, binomial, gamma, Poisson, etc. A més, els GLM permeten diferents tipus d'enllaços entre les variables dependents i independents mitjançant funcions adaptades a la seva distribució (identitat, lògit, pròbit, etc.). Per tant, aquests models s'expressen de la següent manera (eq.8):

$$g(y) = \beta_0 + \beta_1 x_1 + \beta_2 x_2 + ... + \beta_k x_k \qquad \text{(eq.8)}$$

On g (y) és la funció d'enllaç, β_0 la intercepció, β_k el coeficient de regressió determinista estimat per a la variable explicativa, i x_k és la variable explicativa. Quan una variable climàtica està vinculada a un patró atmosfèric, la distribució de la variable de resposta es converteix habitualment en log-normal, com senyala l'estudi de Dayan i Levy (2005). Per a la resta d'aspectes metodològics, el GLM coincideix amb la regressió lineal, en què la variable dependent i la variable independent han de tenir una relació lineal.

Com ja s'ha comentat anteriorment, no totes les variables independents poden tenir pes explicatiu a l'hora de predir la variable dependent. Per aquest motiu la selecció de les variables geogràfiques explicatives de la precipitació s'ha realitzat a partir de la regressió lineal múltiple mitjançant un procés per passos iteratiu. Aquest mètode integra les covariables de manera iterativa ja que, en cada pas, avalua quin conjunt de variables independents s'han d'incloure en el model final. L'algoritme s'atura quan el model ja no millora, a l'incloure o excloure una nova variable. La qualitat relativa de l'ajust del model s'avalua mitjançant el criteri d'informació (AIC) d'Akaike. Com més baix sigui el valor AIC, millor serà l'ajust del model.

Generalized Additive Models (GAM)

El GAM (Hastie i Tibshirani, 1990) és un mètode de regressió semiparamètric, ja que utilitza funcions de suavitzat local per a cada variable independent (eq.9):

$$g(y) = \beta_0 + s_1(x_1) + s_2(x_2) + ... + s_k(x_k) \qquad \text{(eq.9)}$$

on S_k és el paràmetre de suavitzat que cal estimar. Aquest suavitzat permet una major flexibilitat pel que fa a estimar la relació entre variables dependents i variables independents. Aquest fet és important, ja que a la zona d'estudi no hi ha una relació lineal entre la precipitació i l'altitud. Per seleccionar les covariables més significatives també hem utilitzat la selecció progressiva cap enrere. La implementació d'aquests models es realitza mitjançant la llibreria R gam (Hastie, 2017).

Validació de les interpolacions

Per a cada interpolació, s'utilitza la tècnica de validació creuada per avaluar la bondat d'ajust dels models, mitjançant diferents mesures estadístiques. Aquestes mesures estadístiques són: el coeficient de determinació R^2, l'arrel de l'error quadràtic mitjà (en anglès, Root-Mean-Square Error, RMSE), el RMSE normalitzat (en anglès, Normalized Root Mean Square Error, NRMSE), i l'error mitjà absolut (en anglès, Mean Absolute Error, MAE). Wilmott (1982) suggereix que el RMSE i el MAE es troben entre els millors estimadors d'error globals, ja que resumeixen les diferències mitjanes en les unitats dels valors observats i predits. El RMSE és sensible als valors extrems i es pot utilitzar com a indicador de la magnitud dels errors extrems (eq.10):

$$\text{RMSE} = \sqrt{n^{-1}\sum_{i=1}^{n}(O_i - P_i)^2}, \qquad \text{(eq.10)}$$

On O_i és el valor observat i P_i el valor predit, essent n el número d'observatoris. En el cas del NRMSE, en ser un índex normalitzat, permet comparar models amb diferents escales, tal com es formula a continuació (eq.11):

$$NRMSE = \frac{RMSE}{O_{i,\max} - O_{i,\min}} \qquad \text{(eq.11)}$$

On $O_{i,max}$ i $O_{i,min}$ són el valor màxim i mínim observat de les estacions, respectivament. Finalment, el MAE és menys sensible als valors extrems que el RMSE i es defineix com (eq.12):

$$\text{MAE} = n^{-1}\sum_{i=1}^{n}|O_i - P_i|, \qquad \text{(eq.12)}$$

Els valors obtinguts de les mètriques d'error sols són representatius per a l'àrea d'interès, i no per aquelles estacions circumdants a l'àrea d'estudi. La validació creuada es realitza utilitzant l'entorn de programació estadística R mitjançant l'ús de la llibreria caret (Khun, 2008) pels models GLM i GAM i la llibreria gstat (Pebesma, 2004) per al modelatge de la regressió Kriging.

2.2.4. Metodologia de regionalització categòrica

La metodologia final presentada en aquest apartat és fruit dels tests realitzats prèviament en el treball de Lemus-Canovas et al. (2019a). En aquest primer treball es proposa l'ús del classificador no supervisat ISODATA (Duda i Hart, 1973) com a mètode per definir els règims de precipitació en una àrea geogràfica determinada, basat en una classificació sinòptica prèvia i en els patrons de precipitació associats a aquests tipus de circulació. En aquest cas, es treballa a escala del Pirineu català, ja que aquesta permet la comparació amb les regions nivoclimàtiques emprades en aquesta àrea per l'ICGC, mitjançant l'índex Kappa, el qual permet conèixer els errors d'omissió i comissió del clustering en aquestes regions nivoclimàtiques. Els resultats obtinguts mostren una gran dependència de l'altitud, el que fa pensar en la necessitat d'aplicar certs mètodes estadístics que permetin suavitzar la complexa topografia per tal d'obtenir regions espacialment homogènies i no tan dependents de l'altitud. En aquest sentit, i amb l'objectiu de crear una cartografia de les principals regions pluviomètriques per a tota l'àrea del Pirineu, a la Figura 11 es mostra el flux de treball amb la metodologia proposada a Lemus-Canovas et al. (2019b). Aquest procés consta de 5 passos que donen lloc a dos resultats: (1) generació d'un mapa de regions pluviomètriques, i (2) generació d'una sèrie de valors sintètics de precipitació anual per a cada regió de precipitació.

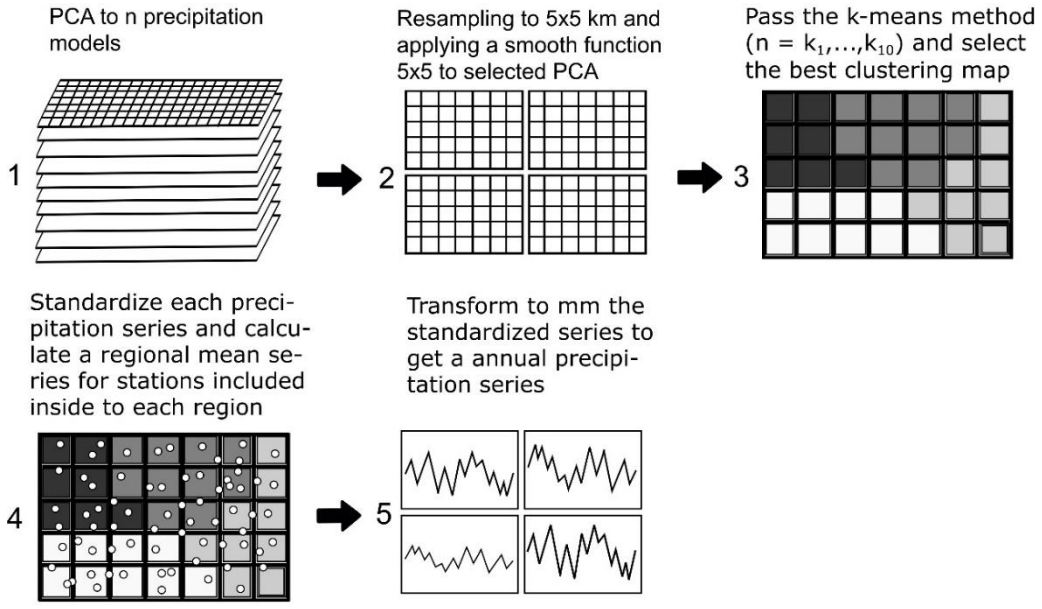

Figura 11. Diagrama de flux pas a pas que mostra el procediment dissenyat per obtenir els règims de precipitació i les sèries regionals de precipitació anual.

Per aconseguir aquests dos resultats principals, (1) primer s'aplica una ACP als n models de precipitació estandarditzats, obtinguts a partir dels models de precipitació condicionats a cada tipus de circulació atmosfèrica. Aquest procés permet eliminar informació redundant entre els diferents mapes de precipitació –pot haver dos tipus de circulació que impliquin una cartografia pluviomètrica molt similar– i capturar només la informació més significativa del conjunt de models. (2) Posteriorment, es remostregen els mapes sintètics obtinguts de l'ACP a una resolució espacial superior; en el cas dels Pirineus, traslladem la resolució espacial de 1x1 km a 5x5 km, per tal de

reduir els efectes locals, com l'efecte fons de vall. Per a emfatitzar encara més la continuïtat espacial de les regions, s'aplica un filtre de mitjana de 5x5 per evitar discontinuïtats acusades a les nostres regions. (3) En tercer lloc, s'aplica el mètode d'agrupació de k-mitjanes de manera iterativa per generar d'1 a 10 clústers, obtenint 10 classificacions. S'utilitza la distància euclidiana a l'hora de realitzar la cerca de distàncies entre grups. La selecció del nombre de clústers òptims es realitza mitjançant el proposat pseudo-MAE (eq.13):

$$\mathrm{MAE} = n^{-1}\sum_{i=1}^{n}|d_i - c_i|, \qquad \text{(eq.13)}$$

On d_i és la cel · la mitjana de la retícula resultant de la mitjana de cada PC seleccionat, i c_i és la mitjana dels respectius centroides de cada PC seleccionat. Com es menciona a Carro-Calvo et al. (2017), l'increment de la variància explicada en el procés d'agrupació estadística es pot explicar per l'increment del nombre de centroides. Tanmateix, l'increment del nombre de grups no sempre implica un augment de la variància explicada, fent que n grups expliquin un percentatge de variància pràcticament idèntic a n+1 grups. Per tant, la representació gràfica d'aquest índex pseudo-MAE permet visualitzar a partir de quin clúster no hi ha una disminució de l'error, ni un augment de la variància explicada pel procés d'agrupació. Aquesta mesura es proposa com a complement a la decisió basada en la inspecció visual. L'objectiu del procés d'agrupació és aconseguir un nombre reduït però suficient de clústers que capturin la diversitat dels règims de precipitació sense pèrdua de generalització. (4) Un cop ajustada la classificació final de les regions de precipitació, totes les estacions pluviomètriques incloses a l'àrea d'estudi es normalitzen i se'n realitza la mitjana per a cada regió classificada, proporcionant així una única sèrie estandarditzada per a cadascuna de les regions. Finalment, (5) la sèrie regional estandarditzada es transforma en valors reals de precipitació anual (eq.14) de la següent manera (Jones i Hulme, 1996):

$$X = \mu + z\sigma, \quad \text{(eq.14)}$$

On X és el valor real de precipitació en mm, z és el valor estandarditzat; μ és la mitjana de les mitjanes de les sèries de precipitació incloses a la regió i σ és la mitjana de les desviacions típiques de les sèries de precipitació incloses a la regió.

2.2.5. Construint una recerca repetible

Per què construir investigacions repetibles és necessari en la recerca científica?

La major part de la comunitat científica estarà d'acord que sovint és molt complicat intentar repetir les anàlisis conduïdes en la majoria de publicacions. Aquesta dificultat pot venir donada per l'obtenció de les dades de partida, o bé, perquè les anàlisis produïdes no estan prou ben detallades. Un treball científic és repetible si és possible replicar el mateix estudi (amb noves dades) a partir de la informació proporcionada en l'article (codi, programari lliure, etc.). El concepte és, per tant, diferent al de reproductibilitat, que es relaciona, principalment, amb la transparència, traçabilitat, i completesa del protocol seguit per arribar a uns resultats concrets a partir d'un conjunt de dades determinat (Rodríguez-Sanchez et al., 2016). Per tant, en la reproductibilitat, el text de l'article ve

acompanyat de codi (text interpretable per un ordinador) que permet recrear exactament a partir de les dades originals tots els resultats i figures inclosos en l'article (Peng, 2011; Marwick, 2017).

Un dels principals beneficis d'aquest esforç és que es permet l'automatització de la recerca i, per tant, executar tasques repetitives sense esforç. De la mateixa manera, en construir un flux de treball robust, es redueix notablement el risc de cometre errors per causa humana.

Disseny de la llibreria R synoptReg

Una llibreria R és una col · lecció de funcions que tenen un mateix objectiu comú. En el cas que ens ocupa, la llibreria synoptReg té per objectiu: 1) permetre un accés fluït i senzill a dades atmosfèriques de reanàlisi; 2) el còmput d'una classificació sinòptica objectiva; 3) l'especialització d'una variable climàtica o ambiental a partir dels patrons sinòptics classificats en el punt anterior; 4) finalment, obtenir una regionalització categòrica de tipus climàtic/ambiental mitjançant el punt anterior.

Una de les virtuts que té el llenguatge R és que es tracta de programari lliure, el que en facilita el seu accés i ús a gran escala, tal i com ho demostra l'augment de llibreries desenvolupades en aquest llenguatge durant els últims anys. Lògicament, la llibreria synoptReg no ha estat exempta d'actualitzacions durant el transcurs d'aquesta tesi doctoral. En aquest sentit, en la Figura 12 es mostra l'evolució que ha patit aquesta llibreria d'ençà que se'n publica l'article que presenta la llibreria (Lemus-Canovas et al., 2019c; versió 0.2.2), fins a l'aparició de l'última versió (1.2.1).

En general, els canvis introduïts han anat en la línia de facilitar-ne el seu ús, actuant com una caixa negra, en la qual l'usuari tan sols necessita llegir la documentació de la llibreria per a fer-ne ús, sense la necessitat de patir per l'adquisició de dades o la construcció del mètode, entre d'altres. L'únic aspecte que no cobreix la llibreria és el que fa referència a la visualització dels resultats. El motiu principal és que sovint l'usuari pot pretendre representar una composició sinòptica amb més d'una variable i amb una estètica particular. R disposa de multitud de llibreries que permeten realitzar visualitzacions de forma senzilla. No obstant això, al portal web dedicat a la llibreria synoptReg (https://lemuscanovas.github.io/synoptreg/), s'ofereixen diversos codis que permeten realitzar aquestes representacions.

Un dels canvis més significatius que ha patit la llibreria ha estat l'increment dels mètodes disponibles per a realitzar la classificació sinòptica. Inicialment, en la versió 0.2.2, tan sols hi havia la possibilitat de realitzar una classificació mitjançant l'ACP en una matriu mode S, amb la posterior conformació dels tipus de circulació mitjançant un clustering per k-mitjanes seguint el mètode de les puntuacions extremes d'Esteban et al. (2005). Actualment, també és possible realitzar l'ACP en una matriu T, la qual no precisa d'algoritmes de clustering per a la conformació dels tipus de circulació. També s'ha possibilitat l'opció de realitzar una classificació sinòptica mitjançant el mètode automàtic de Lamb -conegut també com a Jenkinson i Collison-. A banda de la funció que permet realitzar aquesta classificació com a tal, es disposa de dues funcions més, una per a l'obtenció de la malla de 16 punts per a computar la classificació, així com una altra per a realitzar-ne la seva visualització. Finalment, el mètode més recentment implementat és el dels mapes auto-organtizats (en anglès, Self-Organizing maps; SOM), el qual està basat en l'aprenentatge automàtic mitjançant xarxes neuronals.

	Version 0.2.2 (18-03-2019)	**Version 1.2.1 (22-04-2021**
Base de dades per a exemples reproduïbles	**mslp** - Pressió atmosfèrica en sup. - ERA-20C, 125x125 km - Diària, 2000-2009 - 60N-30N,30W-15E **precp_grid** - Precipitació - SPREAD, 5x5 km. - Diària, 2000-2009. - Illes Balears	**mslp** - Pressió atmosfèrica en sup. - NCEP-NCAR Rean., 250x250 km - Diària, 2000-2002 - 60N-30N,10W-30E **z500** - Alçada geopotencial a 500 hPa - NCEP-NCAR Rean., 250x250 km - Diària, 2000-2002 - 60N-30N,10W-30E **pcp** - Precipitació - SPREAD, 5x5 km. - Diària, 2000-2010 - Illes Balears
Descàrrega de dades de reanàlisi atmosfèric	innexistent	**download_ncep** Descàrrega de dades diàries de reanàlisi provinents del NCEP/NCAR Reanalysis
Lectura de dades	**read_nc** Lectura de fitxers NetCDF	innexistent, cobert per la funció ReadNetCDF (metR)
Preprocés dades d'entrada de la classificació	**tiddy_cuttime_nc** Conversió d'una matriu 3D en una matriu mode S.Possibilitat de delimitar el període temporal.	**tidy_nc** Estableix el període de temps i l'extensió geogràfica, així com calcula l'anomalia de la variable/s atmosfèrica. Permet realitzar els còmputs anteriors per diverses variables simultàniament.
Mètodes de classificació sinòptica	**pca_decision** Informació sobre el ACP, per a seleccionar el número de components principals **synoptclas** Classificació sinòptica basada en l'ACP sobre una matriu mode S + k-means (Esteban et al., 2005) - Limitat a una sola variable **raster_clas** transformació del resultat de la classificació (matriu 3D) a a un objecte de classe raster	*Basat en l'ACP* **pca_decision** Informació sobre el ACP, per a seleccionar en num. d'ACPs **synoptclas** Classificació sinòptica basada en: - ACP en mode S + k-means (Esteban et al., 2005) - ACP en mode T *Self-organizing maps* **som_clas** Classificació mitjançant Self-Organizing maps *Automàtic Lamb* **get_lamb_points** Obtenció coordenades oer al mètode objectiu de Lamb **plot_lamb_scheme** Visualització de l'esquema de Lamb **lamb_clas** Classificació automàtica de Lamb, amb dos variants: - Jones et al. 1993 - Trigo i DaCamara, 2000
Espacialització de la variable climàtica/ ambiental	**raster_ct2env** Espacialització de la variable ambiental/ climàtica en funció de cada patró sinòptic. Resultat en un objecte raster.	**ct2env** Espacialització de la variable ambiental/climàtica en funció de cada patró sinòptic. Resultat en un objecte data.frame o raster.
Regionalització climàtica/ambiental discreta	**raster_pca** ACP sobre una matriu de ràsters **regionalization** Regionalització discreta a partirdels mapes obtinguts amb raster_ct2env, o pels posteriors obtinguts amb raster_pca	**raster_pca** ACP sobre una matriu de ràsters **regionalization** Regionalització discreta a partirdels mapes obtinguts amb ct2env, o pels posteriors obtinguts amb raster_pca

Figura 12. Funcions disponibles en les versions 0.2.2 i 1.2.1 de la llibreria synoptReg. Cada caixa mostra un conjunt de funcions amb una mateixa finalitat. Dins de cada caixa, en negreta apareix el nom de la funció, i just a sota, se'n descriu la seva finalitat.

2.2.6. Definició estadística dels esdeveniments secs i càlids

Els esdeveniments secs i càlids es caracteritzen mitjançant les dimensions següents: durada (D), magnitud (M) i magnitud extrema (EM), pels als mesos de primavera –març, abril i maig (MAM)–, i pels mesos d'estiu, –juny, juliol i agost (JJA)–; ambdues estacions s'analitzen de forma independent. D es defineix com el nombre de dies consecutius en què les precipitacions són inferiors a 1 mm. Aquest llindar s'escull per ser coherent amb estudis previs (Orlowsky i Seneviratne, 2012; Donat et al., 2013; Manning et al., 2019), així com per evitar l'efecte plugim, que sistemàticament fa que els models climàtics sobreestimin la variable precipitació (Gutowski et al., 2003).

Per assegurar l'obtenció de ratxes seques independents i extremes, per a cada any (primavera i estiu, per separat) es calcula el percentil 95 de la durada de les ratxes seques, seleccionant posteriorment aquelles que presenten una durada superior a aquest llindar. La M és la distribució condicional de les temperatures màximes diàries (Tx) durant períodes secs de llarga durada (D), mentre que EM és la distribució condicional de la Tx durant els períodes secs de llarga durada i en què se supera el percentil 95 de Tx diària. Els valors de Tx superiors al percentil 95 que es produeixen fora d'aquests llargs períodes secs (D) no es consideren. La Figura 13 mostra el comportament d'aquestes tres variables en una sèrie temporal a l'extrem oriental dels Pirineus.

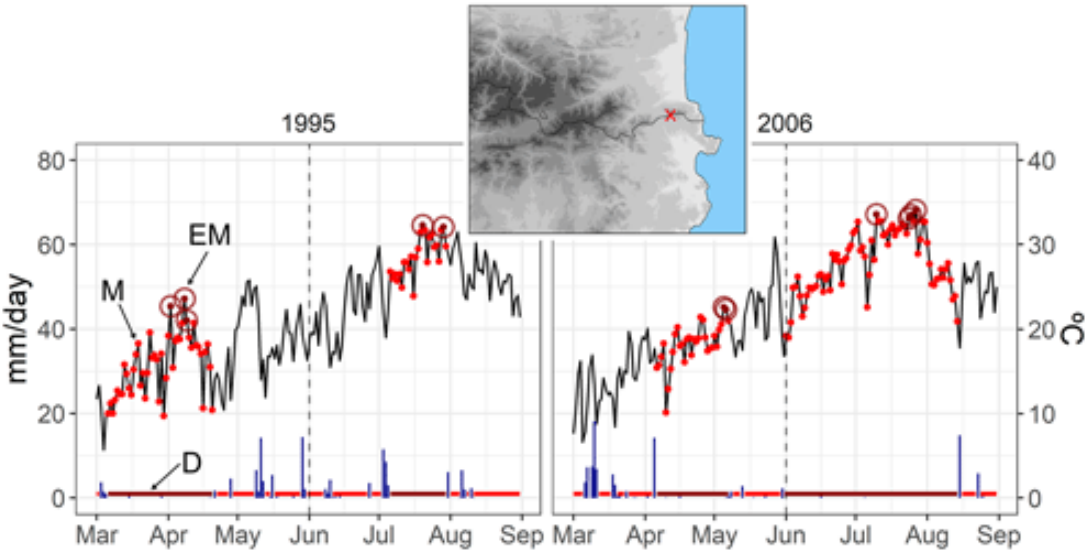

Figura 13. Sèrie temporal de precipitació diària (barres blaves verticals) i temperatura màxima diària (Tx) (línia negra) en un punt de la Serra de l'Albera (x = 2,9; y = 42,5). Les barres horitzontals de color vermell mostren la longitud de les ratxes seques, mentre que les barres horitzontals de color vermell fosc mostren les ratxes seques extremadament llargues (D). Els punts vermells (M) mostren els valors Tx durant un esdeveniment D. Els punts de color vermell fosc amb un cercle indiquen valors de Tx per sobre del percentil 95 durant un esdeveniment D. La línia vertical discontínua indica la separació entre les estacions de la primavera i l'estiu. La selecció d'anys destaca una primavera seca (1995; esquerra) i un estiu sec (2006; dreta) en aquesta zona.

L'anàlisi del subconjunt EM ens permet caracteritzar el major risc d'aparició simultània d'ambdues variables, D i EM, que a la vegada poden suposar un augment significatiu del risc d'incendis forestals.

2.2.7. Mètodes de correcció de biaix

Les tècniques de correcció de biaixos s'utilitzen per corregir les dades simulades pels models climàtics globals i regionals (GCM i RCM, respectivament) mitjançant dades observades. De fet, aquestes tècniques s'utilitzen amb més freqüència per corregir només una variable (Teutschbein i Seibert, 2012; Rajczak et al., 2016b). No obstant això, una correcció univariant pot afectar moderadament la dependència estructural mútua de diferents variables (Wilcke et al., 2013), per exemple, temperatura i precipitació, tot i que estudis recents han demostrat que els mètodes de correcció de biaix univariants poden ser prou robusts per a determinats estudis d'impacte regional (Casanueva et al., 2018). No obstant això, en el tractament d'esdeveniments compostos, l'ús de mètodes de correcció de biaixos multivariants pot proporcionar un valor afegit mitjançant una estimació òptima de la dependència multivariant (François et al., 2020).

Empirical Quantile Mapping (QM)

Una de les tècniques més populars i àmpliament utilitzades per a la correcció de biaix univariant és el quantile mapping (QM). La correcció de biaix mitjançant el QM s'utilitza freqüentment per a projectar les simulacions a escala d'estació meteorològica o a punts de retícula d'alta resolució espacial; tanmateix, aquest procediment indueix problemes d'inflació a les sèries corregides (Maraun, 2013) i és incapaç de generar variabilitat diària de subescala (Maraun et al., 2017). Les qüestions esmentades tendeixen a agreujar-se a les zones de muntanya, on molts processos locals poden no estar representats després del procés QM (Maraun i Widmann, 2018a). Com a alternativa a la correcció de biaixos univariants, i en un intent de corregir la correlació inter-variable, durant els darrers anys s'han proposat diferents mètodes de correcció de biaix mitjançant tècniques multivariants (Piani i Haerter, 2012; Vrac i Friederichs, 2015; Cannon, 2016, 2017).

En la present investigació, primer s'utilitza un enfocament de correcció de biaix univariant, mitjançant el mètode empirical quantile mapping (EQM), que estima els valors de la funció empírica de distribució acumulada (CDF) de la sèrie temporal observada i modelada per a cada quantil (Panofsky i Brier, 1968; Gudmundsson et al., 2012). Per tant, si X_o i X_m són els valors observats i modelats, respectivament, llavors (eq.15):

$$\hat{X}_m = F_o^{-1}\left(F_m\left(X_m\right)\right) \qquad \text{(eq.15)}$$

on F_m és la funció de distribució empírica acumulada de X_m i F_o^{-1} és la funció de distribució empírica inversa corresponent a X_o. L'EQM s'aplica a través de la llibreria R qmap (Gudmundsson, 2016), i mitjançant 100 quantils per tal d'obtenir el valor simulat corregit $\hat{X}_m$. L'efecte plugim (drizzle effect) es corregeix mitjançant un llindar de 1 mm/dia (Hay i Clark, 2003; Piani et al., 2010).

Multivariate Bias Correction with N-dimensional probability density function transform (MBCn)

En segon lloc, s'empra un mètode de correcció de biaix multivariant, proposat per Cannon (2017), i que du el nom de: correcció de biaix multivariant amb transformació de funció de densitat de probabilitat N-dimensional (MBCn). Aquest mètode es basa en una adaptació d'un algorisme de processament d'imatges utilitzat per transferir la informació del color de la imatge. El MBCn permet transferir les característiques estadístiques d'una distribució multivariant de referència a la distribució multivariant de variables del model climàtic. Abans d'abordar la relació de dependència entre variables, aquest mètode realitza una correcció univariada de les distribucions de les variables objectiu utilitzant el mètode quantil-delta mapping (QDM; Cannon et al., 2015), el qual preserva els canvis absoluts o relatius en els quantils, per exemple, per a variables, com ara la temperatura o la precipitació. Un cop es corregeixen les distribucions univariades, l'estructura de dependència s'ajusta mitjançant un procés iteratiu. En cada pas, les dades es multipliquen per matrius de rotació ortogonals aleatòries per a descorrelacionar parcialment les variables climàtiques a corregir. El QDM s'aplica de nou a les dades (parcialment) no correlacionades abans del pas de recorrelació amb les matrius aleatòries inverses. Aquest pas –és a dir, incloent la rotació, les correccions QDM i la rotació posterior– es repeteix de manera iterativa fins que s'arriba a la convergència entre les distribucions multivariants de referència i les simulacions climàtiques durant el període de calibratge, és a dir, durant el període històric. De fet, són aquestes iteracions les que permeten corregir l'estructura de dependència del model. A més, el MBCn permet que els canvis en l'estructura de dependència siguin d'acord amb els canvis del model.

Avaluació del comportament dels mètodes de correcció de biaix

Tots dos mètodes de correcció de biaix s'han avaluat mitjançant una validació creuada de 5 grups de 7 anys (4 grups per a l'ajust i 1 per a la validació). La validació creuada no és una metodologia recomanada a l'hora de validar les simulacions climàtiques contra sèries observades, ja que els models climàtics són temporalment estocàstics i realitzar aquesta validació creuada podria induir greus errors en l'avaluació de les sèries diàries (Maraun i Widmann, 2018b). Tanmateix, en aquesta ocasió es treballa a una escala estacional –primavera i estiu– sobre les variables D, M i EM (vegeu la secció 2.2.6.), on s'espera que el model climàtic sigui capaç de reflectir l'estacionalitat i la tendència general de les dades observades.

La dependència estructural entre la temperatura i la precipitació s'avalua mitjançant el coeficient de correlació de Pearson per a les sèries observades i les sèries de simulació històrica sense corregir i, per a les sèries de simulació històrica amb el biaix corregit. Previ a la correlació entre ambdues variables, es calcula la mitjana de la temperatura diària i de la precipitació diària per a cada dia julià i per a tota la sèrie (1981-2014), evitant així soroll en els resultats.

També es testen les diferències entre les distribucions simulades i observades de les ratxes seques de llarga duració, mitjançant la prova de Kolmogorov-Smirnov (KS). Aquesta prova estadística permet avaluar les possibles mancances dels mètodes de correcció del biaix a l'hora d'estimar amb precisió la longitud dels períodes secs, una problemàtica que ha estat mencionada en distintes recerques (Rajzak et al., 2016; Maraun et al., 2017). Finalment, s'ha estimat el biaix per a

la temperatura mitjançant dos llindars: el percentil 95 de distribució de temperatura i el percentil 95 de distribució de la temperatura durant el percentil 95 de la durada de les ratxes seques, amb la finalitat de discutir el rendiment de cada mètode de correcció de biaix en els extrems tèrmics.

2.2.8. Anàlisis de freqüència

Per estimar la quantitat de retorn de la precipitació donat un període de retorn específic (PR), s'ha emprat la distribució generalitzada de valors extrems (en anglès, Generalized Extreme Value Distribution; GEV). La funció de distribució acumulativa per a la GEV resulta de combinar les famílies de distribucions Fréchet, Gumbel i Weibull, en una única funció de distribució (eq.16):

$$F(x) = \exp\left\{-\left[1+\xi\left(\frac{x-\mu}{\sigma}\right)\right]^{-1/\xi}\right\} \qquad \text{(eq.16)}$$

on tres paràmetres (ξ, μ i σ) representen la forma, la localització i l'escala de la funció de distribució, respectivament. σ i $1 + \xi\ (x - \mu) / \sigma$ han de ser superiors a zero. L'especificació de ξ determinarà el comportament de la cua de la distribució de manera que, en funció del valor d'aquest paràmetre, es pot obtenir qualsevol de les distribucions següents:

- $\xi > 0$ Fréchet;
- $\xi = 0$ Gumbel. Per aquest cas (eq.17):

$$F(x) = \exp\left\{-\exp\left[-\left(\frac{x-\mu}{\sigma}\right)\right]\right\} \qquad \text{(eq.17)}$$

- $\xi < 0$ Weibull.

La família de distribucions GEV permet modelitzar la precipitació màxima diària anual amb l'ús de l'aproximació block maxima. Aquest procediment consisteix a agrupar les dades en blocs de la mateixa mida –valor màxim per any, per exemple–, i després ajustar la distribució GEV al conjunt de valors màxims corresponents a cadascun dels blocs. Existeix una altra aproximació possible –no contemplada en aquesta tesi–, basada en la superació de llindar, i que en el seu cas empra la distribució general de Pareto.

2.2.9. Anàlisi de tendència

En l'anàlisi de tendència, bàsicament, s'ha quantificat la taxa de canvi, així com la significació estadística de la mateixa. En aquest sentit, per avaluar aquesta taxa de canvi, s'ha utilitzat el mètode del pendent de Sen (Sen, 1968). Aquest mètode no paramètric permet quantificar la taxa de canvi en una sèrie univariant, indistintament de la distribució estadística de la sèrie de dades originals. Per tant, aquesta metodologia és una alternativa robusta a l'estimació de tendència mitjançant una regressió paramètrica per mínims quadrats. La formulació del pendent de Sen és molt senzilla (eq.18):

$$d_k = \frac{x_j - x_i}{j - i} \qquad \text{(eq.18)}$$

On x_j és el valor en la posició j, i x_i el valor en la posició i; j i i són l'índex de la posició, per exemple, l'any que correspongui. Per a comprovar la significació estadística de tals tendències, s'empra el test de Mann-Kendall (Mann, 1945). El test no paramètric consisteix, bàsicament, en la comparació entre els valors que componen una mateixa sèrie temporal en ordre seqüencial. En una sèrie temporal d'observacions x_1, x_2,..., x_n, Mann proposa que per acceptar la hipòtesi nul · la (H_0) les dades que composen la sèrie temporal han d'ésser aleatòries, independents i igualment distribuïdes. Per a la hipòtesi alternativa (H_1), les dades han de seguir una tendència monòtona. L'estadístic de Mann-Kendall s'obté com continua (eq19 i eq.20):

$$S = \sum_{i=1}^{n-1} \sum_{j=i+1}^{n} sgn\left(x_j - x_i\right) \qquad \text{(eq.19)}$$

$$sgn\left(x_j - x_i\right) = \begin{cases} 1 & si \quad \left(x_j - x_i\right) > 0 \\ 0 & si \quad \left(x_j - x_i\right) = 0 \\ -1 & si \quad \left(x_j - x_i\right) < 0 \end{cases} \qquad \text{(eq20)}$$

On x_j representen les dades estimades de la seqüència de valors i n és la mida de la sèrie temporal. En cas de H_0, S ha de presentar una distribució aproximadament normal, amb mitjana zero i la següent variància (Var(S)) (eq.21):

$$var(S) = \frac{1}{18}\left[n(n-1)(2n+5) - \sum_{p=1}^{q} t_p(t_p-1)(2t_p+5) \right] \qquad \text{(eq.21)}$$

El valor de S indica la possible existència de tendències en cas que sigui estadísticament i significativa diferent de zero. Sent S diferent de zero, la hipòtesi nul · la H_0 pot ser rebutjada, i la hipòtesi alternativa H_1 acceptada. El valor estadístic del test és representat a través de l'estadístic Z, el qual s'expressa en la següent equació (eq.22):

$$Z = \begin{cases} \dfrac{S-1}{\sqrt{var(S)}} & si \quad S > 0 \\ 0 & si \quad S = 0 \\ \dfrac{S+1}{\sqrt{var(S)}} & si \quad S < 0 \end{cases} \qquad \text{(eq.22)}$$

L'existència d'una tendència estadísticament significativa és avaluada mitjançant aquest valor Z. Un valor positiu d'aquest indica que hi ha una tendència positiva, mentre que el valor negatiu indica una tendència negativa. El valor Z és el paràmetre de sortida del test de Mann-Kendall. Per a un nivell de significació α, es rebutja la hipòtesi nul · la H_0 quan el valor absolut de Z és més gran que Z_1 - α/2

Capítol 3. Resultats

3.1. Una aplicació mixta d'una classificació sinòptica objectiva i models de regressió espacial per a la derivació de règims de precipitació hivernal als Pirineus orientals

3.1.1. Resum de l'article

La gestió dels recursos hídrics en els entorns de muntanya requereix del coneixement espacial de la precipitació com a variable de notable importància en l'estudi dels riscos hidrològics (allaus, esllavissades, inundacions, etc.), especialment, durant l'estació hivernal. D'aquesta manera, en aquest treball s'estudia la distribució espacial de la precipitació mitjana diària (MDP) i la probabilitat de precipitació diària (DPP) al Pirineu Oriental, a partir d'una classificació sinòptica objectiva prèvia que defineix els patrons atmosfèrics més freqüents durant la meitat freda de l'any (novembre-maig) entre 1990 i 2015. La classificació sinòptica ha proporcionat 12 patrons sintetitzadors de la circulació atmosfèrica d'aquest període. Per a cada un d'ells es genera un compendi de mapes de MDP, i de DPP d'igualació o superació dels llindars 2, 5, 10, 20 i 50 mm diaris, mitjançant mètodes de regressió estadística multivariant. El millor ajust dels models s'obté per a una DPP $\geq$ 2 mm, amb un R^2 ajustat al voltant de 0.8, seguit dels models de MDP i DPP $\geq$ 5 mm, amb un R^2 ajustat generalment entre 0.7 i 0.8. Finalment, es realitza una classificació no supervisada dels 12 models de MDP amb l'objectiu d'obtenir una cartografia categòrica i simplificada que expliqui els règims de precipitació dels mesos freds al Pirineu Oriental.

3.1.2. Article

Lemus-Canovas, M., Ninyerola, M., Lopez-Bustins, J. A., Manguan, S., & Garcia-Sellés, C. (2019a). A mixed application of an objective synoptic classification and spatial regression models for deriving winter precipitation regimes in the Eastern Pyrenees. International Journal of Climatology, 39(4), 2244–2259. https://doi.org/10.1002/joc.5948

Received: 15 May 2018 | Revised: 19 November 2018 | Accepted: 21 November 2018 | Published on: 25 December 2018

DOI: 10.1002/joc.5948

International Journal of Climatology RMetS

RESEARCH ARTICLE

A mixed application of an objective synoptic classification and spatial regression models for deriving winter precipitation regimes in the Eastern Pyrenees

Marc Lemus-Canovas[1] | Miquel Ninyerola[2] | Joan A. Lopez-Bustins[1] | Santiago Manguan[3] | Carles Garcia-Sellés[3]

[1]Climatology Group, Department of Geography, University of Barcelona, Barcelona, Catalonia, Spain

[2]Grumets Research Group, Department of Animal, Vegetal and Ecology Biology, Cerdanyola del Vallès, Catalonia, Spain

[3]Cartographic and Geological Institute of Catalonia (ICGC), Barcelona, Catalonia, Spain

Correspondence
Marc Lemus-Cánovas, Climatology Group, Department of Geography, University of Barcelona, 08001 Barcelona, Catalonia, Spain.
Email: mlemus@ub.edu

Funding information
Catalonia Regional Government, Grant/Award Number: 2017 SGR 1362; Spanish Government, Grant/Award Number: CLICES (CGL2017-83866-C3-2-R) WEMOTOR (CSO2014-55799-C2-1-R)

Management of hydric resources in alpine mountains requires spatial knowledge of precipitation as a variable of noteworthy importance in the study of hydrological hazards (avalanches, landslides, floods, etc.), especially during the winter season. We therefore study the spatial distribution of mean daily precipitation (MDP) and daily precipitation probability (DPP) in the Eastern Pyrenees, based on a previous objective synoptic classification defining the most frequent atmospheric patterns during the winter season (November–May) between 1990 and 2015. The synoptic classification provided 12 circulation weather types. For each of these, we obtained MDP maps and DPP maps possessing a threshold equal to, or greater than, 2, 5, 10, 20 and 50 mm. The best fit of the models was obtained in the DPP ≥ 2 mm, with an adjusted R^2 of around 0.8, followed by the models showing MDP and DPP ≥ 5 mm, with an adjusted R^2 generally between 0.7 and 0.8. Finally, we performed an unsupervised classification of the 12 MDP models in order to obtain a categorical and simplified cartography explaining the winter precipitation regimes in the Eastern Pyrenees.

KEYWORDS
ISODATA, PCA, precipitation modelling, precipitation regimes, spatial regression, synoptic classification

1 | INTRODUCTION

Knowledge of spatial precipitation amounts associated with the most frequent circulation types during the winter season (November–May) is essential with regard to developing strategies aimed at addressing avalanche risk, floods or any other hydrological hazard. The use of a synoptic classification in combination with spatial models might help us to understand the role of the spatial variability of the climatological elements. Such models would enable us to establish fine scale continuous fields as inputs to, for instance, distributed hydrological models allowing us to investigate the impacts of current and future climate change upon ecological and social systems (Tveito and Ustrnul, 2003). Several studies attempt to determine the climatic impacts driving atmospheric circulation. For example, in the study presented by Bissolli and Müller-Westermeier (2005), simple linear regression models of precipitation were performed with the use of a digital elevation model (DEM) as the independent variable to obtain precipitation maps for each circulation type defined in the objective synoptic classification conducted by the German Weather Service. Esteban *et al.* (2009) applied a multiple linear regression with residual interpolation in order to map temperature and precipitation over Andorra at fine spatial resolution (90 m). Fernández-Montes *et al.* (2013) analysed the relationship between weather types and days with extreme temperatures during the spring and summer seasons.

For climate modelling in mountainous areas it is appropriate to apply an interpolation method based upon in situ data from weather stations as well as geographical information. Along these lines, spatial modelling of climatic variables by means of linear multiple regression implies the possibility to include independent variables that adjust the climate models in topographically complex areas. Ninyerola *et al*. (2000, 2007) proposed a corrector based upon the residual value of the regression analysis, thus reducing the final error in the cartography. In the aforementioned studies the spatial availability of climatic data constitutes a recurring issue because the information is generally scattered throughout the territory. This is more evident in mountainous areas, where the lack of high-altitude weather data causes a poorer fit of the models (Vicente-Serrano *et al.,* 2003). Furthermore, the shortage of in situ data advises against the use of the geographically weighted regression methodology (Brunsdon *et al.,* 1996), due to the fact that this approach requires a dense observation network to adjust the model.

Although the strong point of spatial modelling based on multiple linear regression (MLR) involves the ability to analyse and visualize spatial complexity, the large number of output maps may not provide a summarizing view of the whole set of maps. It might therefore be useful to apply an unsupervised classification method to summarize the information as a whole. For instance, ISODATA (Duda and Hart, 1973), which stands for *Iterative Self-Organizing Data Analysis Technique,* is a nonsupervised classification method often used in the field of remote sensing in the exploratory stage. Few studies classify climatic variables by means of nonsupervised classifications. Thus, Zscheischler *et al*. (2012) attempts to use a k-means cluster (CL) method to perform a global climatic classification combining weather data and remote-sensing derived data. Another similar paper is presented by Carro-Calvo *et al*. (2017), in which the main goal involves regionalisation of summertime tropospheric ozone (O_3) in Europe. They applied the k-means clustering technique to the near-surface ozone average over Europe at a $1° \times 1°$ resolution for the summer periods of 1998–2012. The results show a spatial division of nine regions in which tropospheric ozone presents coherent spatiotemporal patterns.

In this study, we attempt to accomplish three objectives: (1) to establish an objective synoptic classification centred on Western Europe, and therefore valid for the Eastern Pyrenees; (2) to interpolate mean daily precipitation (MDP) and

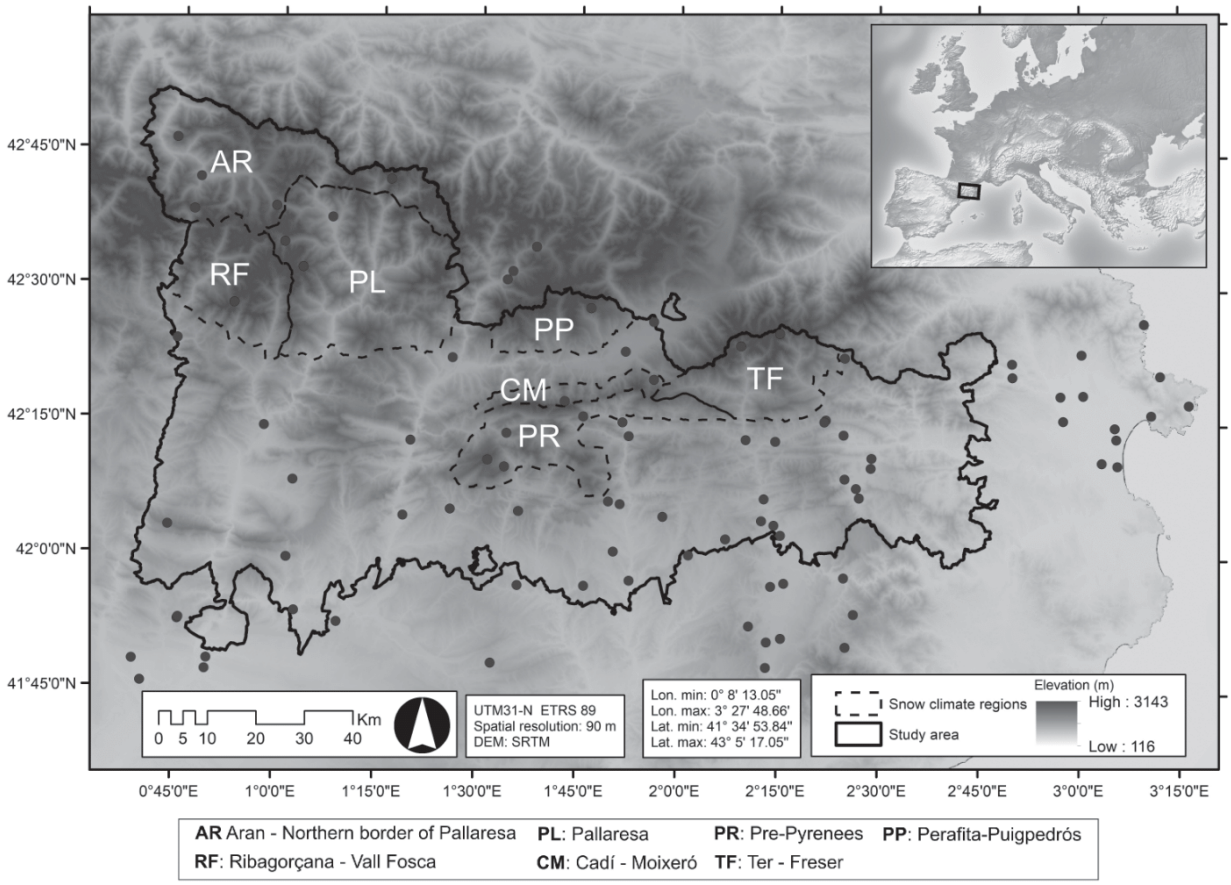

FIGURE 1 Location in the Eastern Pyrenees. The study area was subdivided into seven snow climate regions. In addition, the spatial distribution of the rain gauges used in our study is indicated in black points

daily precipitation probability (DPP) (exceeding a specific threshold) values for each circulation type; (3) finally, to put forward a proposal for semi-objective regionalisation of precipitation regimes in the Eastern Pyrenees by means of an unsupervised classifier. In Section 2, we present the study area. The data and methods employed in the present research are presented in Section 3; we subsequently set forth the results in Section 4. Finally, in Section 5 we provide a summary of the main results and the conclusions derived.

2 | STUDY AREA

The Pyrenees comprise a mountain range extending approximately 450 km from the Atlantic Ocean (west) to the Mediterranean Sea (east). They separate the Iberian Peninsula from the rest of the Euro Asiatic continent. The Eastern Pyrenees lie within Spanish territory and are 146 km long, with a width ranging from 19 to 52 km, diminishing toward the east. The elevation of the study area is mostly between 2,000 and 3,000 m a.s.l., although the highest elevations surpass 3,000 m a.s.l. (Figure 1).

Three climatic zones are defined for the Eastern Pyrenees (García *et al.,* 2007). The north-western zone presents a humid ocean climate. Precipitation is abundant and winter amounts (November–May) do not exhibit strong interannual variation. Precipitation associated with oceanic air masses diminishes rapidly toward the south. Therefore, in the central region climate takes on continental characteristics toward the south and east (Figure 2). In the easternmost part of the Eastern Pyrenees, oceanic influence disappears completely, and the effect of the Mediterranean Sea has a significant impact upon precipitation in this area.

Seven snow climate regions (SCR) are mapped in García *et al*. (2009); they pertain to the different behaviour patterns of the snow climate and avalanche activity (Figure 1). These differences in the conditions of snow climate and avalanche activity mainly result from certain characteristics of the terrain (Oller *et al.,* 2006). The seven regions of the Eastern Pyrenees on the Spanish side are, from west to east: the Aran-Northern border of Pallaresa (AR) presenting oceanic conditions; Ribagorçana-VallFosca (RF), Pallaresa (PL), Perafita-Puigpedrós (PP), CadíMoixeró (CM) exhibiting continental conditions; Pre-Pyrenees (PR) and Ter-Freser (TF) revealing a Mediterranean influence. This is the only previous climatic regionalisation of the area and it is therefore the only way our results can be compared.

3 | DATA AND METHODS

Figure 3 shows the workflow followed, which involves four procedures: classification of atmospheric circulation, quality control of daily precipitation data, spatial interpolation of these data, and finally, unsupervised classification of the data resulting from interpolation.

3.1 | Synoptic classification

We applied the methodology of Esteban *et al*. (2005) to classify the daily weather data in order to derive the principal

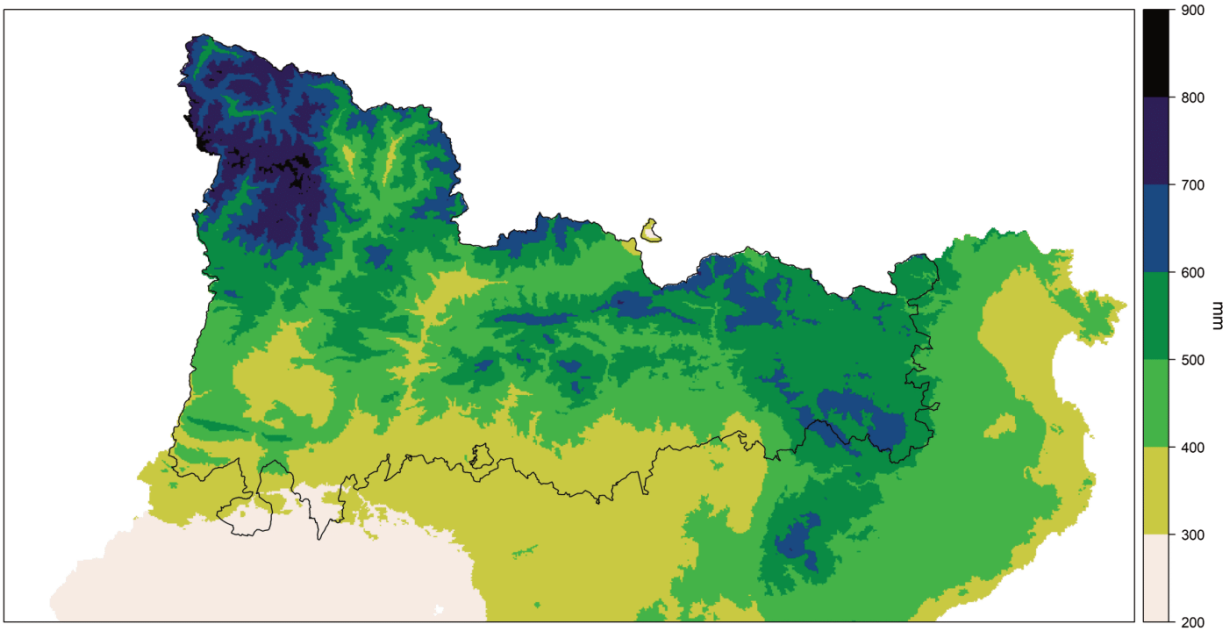

FIGURE 2 Average winter precipitation (November–May) over the study area during the 1951–1999 period (Ninyerola *et al.,* 2000). The highest amounts of precipitation are distributed throughout the highest massifs, particularly in the north and west of the region [Colour figure can be viewed at wileyonlinelibrary.com]

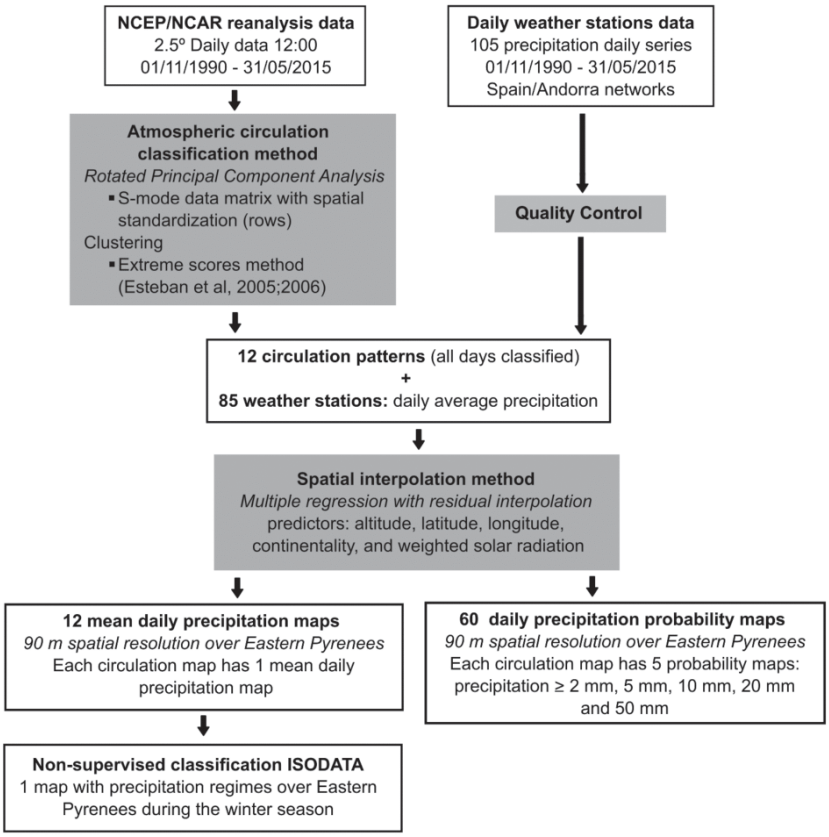

FIGURE 3 Flow chart showing the methodological steps followed to obtain the mean daily precipitation (MDP) and daily precipitation probability (DPP) maps. As a final step extended from the original figure (Esteban *et al.*, 2009), a nonsupervised classification is proposed to obtain the precipitation regimes of the study area

atmospheric circulation patterns. The details of this method are explained below.

A S-mode principal component analysis (PCA) was applied to reduce the dimension of the variables, in which the grid points are the variables and the days are the observations. The S-mode PCA enables a climate regionalization (Richman, 1986; Lopez-Bustins *et al.,* 2015) to be performed because it shows the representative degree of each day in each component. Nonetheless, with an S-mode PCA we cannot obtain a direct synoptic classification because we have not obtained a classification of circulation types, due to the fact that our real cases have not been allocated to a specific group and as a result, a clustering method must be performed to finalize the atmospheric circulation catalogue. As for the variables used, we standardized the matrix to maintain one single scale for the different variables, thus avoiding overrepresentation of any one of them. We employed the Scree test (Cattell, 1966) to retain the components explaining a significant portion of the total variance; these principal components were subsequently rotated by means of a varimax rotation (Esteban *et al.,* 2006).

Along with the rotated components, we used the scores to apply the extreme scores method (Esteban *et al.,* 2005). The scores show the degree of representativeness associated with the variation modes of each principal component, that is, the classification of each day to its most representative centroid. Thus, the extreme scores method uses the scores >2 and < -2, establishing a positive and negative phase for each principal component. The extreme scores procedure establishes the number of groups and their centroids for the K-means CL method (Esteban *et al.,* 2006). K-means is applied without iterations because the centroids are well established by the method of extreme scores.

We employed data on Daily Sea Level Pressure (slp) and Geopotential Height at 500 hPa (z500) provided by the NCEP/NCAR Reanalysis 2 (Kalnay *et al.,* 1996) enveloping the area 30°–60°N and 30°W–15°E, at a spatial resolution of 2.5° and for the 26 winters (November–May) between 1990 and 2015. We selected this study period due to the lack of weather data in the mountainous areas prior to 1990.

3.2 | Quality control of precipitation

Errors in rainfall series can occur for various reasons, such as metadata or data errors. This section is therefore of great importance. We extracted 105 daily precipitation series across the Eastern Pyrenees from the Meteorological Service of Catalonia (METEOCAT) and the Spanish National

Meteorology Agency (AEMET) for the Catalan series, and from the FEDA (*Forces Elèctriques d'Andorra*) for the Andorran series. The study period of the temporal series ranges from 1990 to 2015. Nonetheless, some series exhibit gaps or are incomplete. Series of less than 10 years were discarded. To check the quality of the daily rainfall data, we ran the extension ExtraQC (Aguilar and Prohom, 2011) from the RClimdex software (Zhang and Yang, 2004). The ExtraQC processes are described below.

We detected highly anomalous values (outliers) by adding five times the interquartile range (IQR) to the days on which precipitation exceeds the third quartile (values >3r quartile +5*IQR). Counting the days with decimal rainfall between 0.0 and 0.9 (discarding the days with registers of 0.0 mm) enabled us to test the precision quality of the series. Many series are rounded to 1 mm or to 0.5 mm, with fewer being rounded to 0.2 mm. The Gross errors procedure is intended to detect abnormally high and low values, such as daily precipitation above 200 mm, and negative values, often recorded to indicate inappreciable precipitation or summation of several days.

The False Zero method is unavailable in the ExtraQC extension and is based upon consideration of the series presenting a monthly value of 0 mm (candidate) and on one of the following conditions (Abaurrea *et al.,* 2004): at least 75% of the nearest series (auxiliary) must register a monthly precipitation >15 mm (minimum 4 series); the two closest series should exceed 10 mm per month. When at least one of the aforementioned conditions is met, the daily value for the whole month affected is replaced by a missing value.

Finally, to detect date displacements in daily rainfall values, we employed an index as the annual sum of the absolute differences between the candidate and the auxiliary series divided by the same differences when the candidate series is displaced 1 day forward (Equation (1)).

$$\sum|y_t - x_t| / \sum|y_{t+1} - x_t|, \quad (1)$$

where y_t is the daily value of the candidate series and x_t is the daily value of the auxiliary series. The same procedure was applied, but 1 day was subtracted from the candidate series (Equation (2)).

$$\sum|y_t - x_t| / \sum|y_{t-1} - x_t|. \quad (2)$$

3.3 | Spatial regression

We created interpolated maps based on MDP and DPP, both of these previously computed at station level, to exceed a specific threshold of precipitation amount ($p \geq 2$, ≥5, ≥10, ≥20, ≥50 mm) for each atmospheric circulation class. DPP

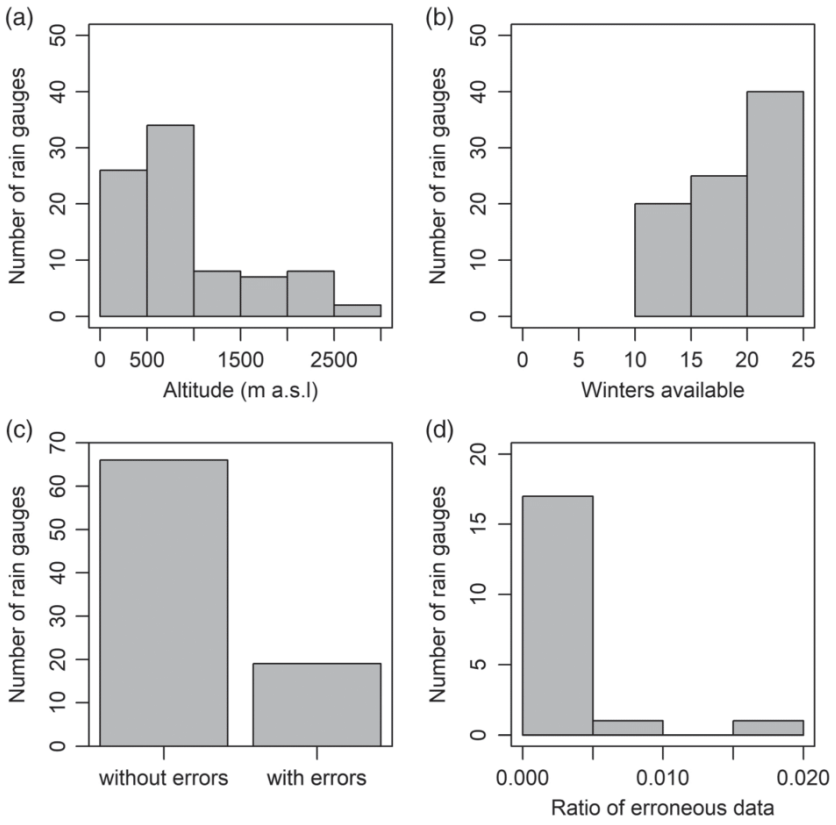

FIGURE 4 Distribution of stations used to apply the spatial interpolation (a), and the available winter seasons (b). Additionally, number of stations with and without erroneous data (c), and finally, number of erroneous stations showing the percentage of data affected (d)

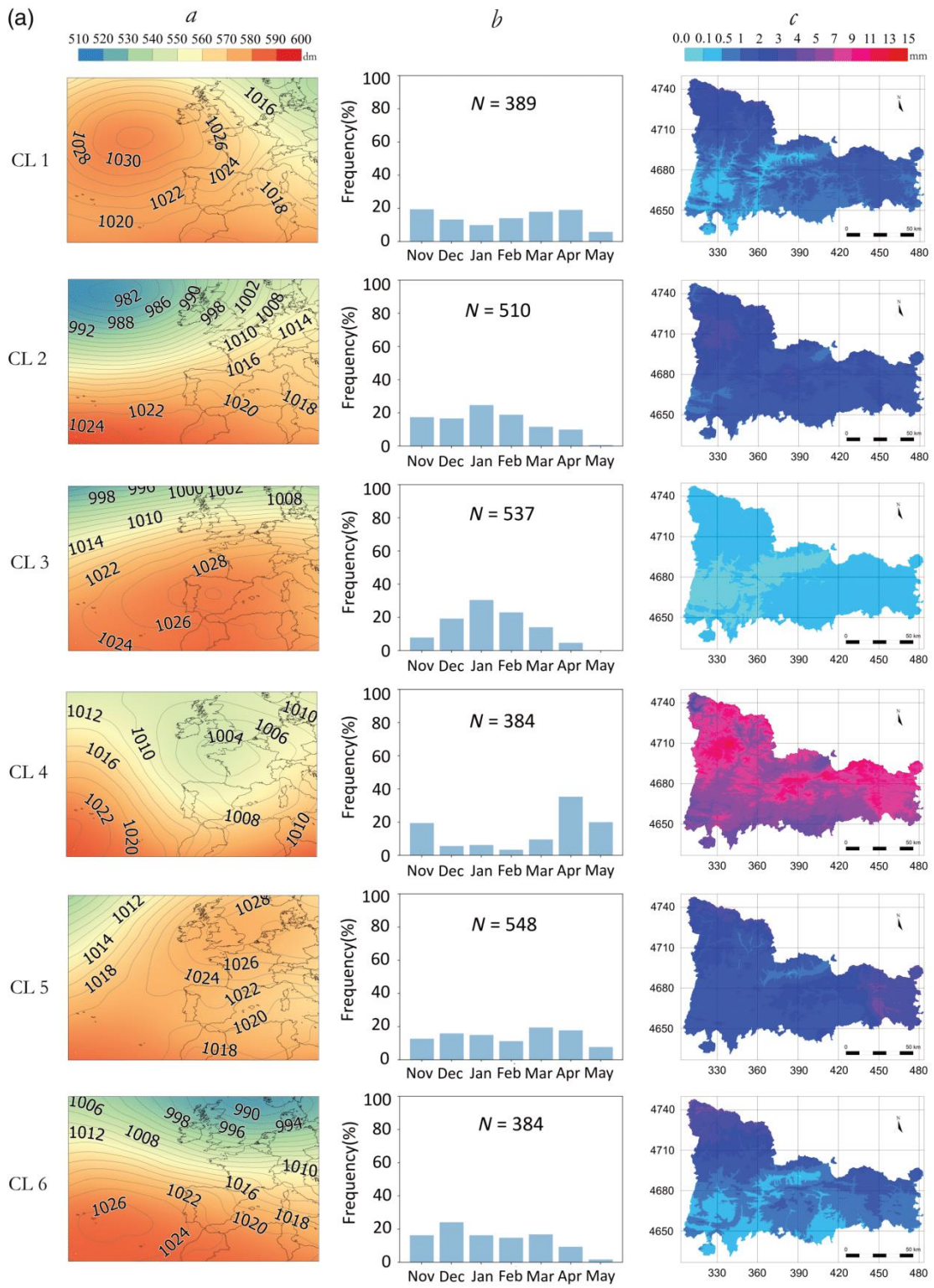

FIGURE 5 (a) Atmospheric circulation patterns and MDP related CLs 1 to 6. *a*) The colour palette shows geopotential height at 500 hPa while the isolines represent sea level pressure. *b*) Winter distribution of the days. *N* indicates the total number of days by CL. *c*) Mean daily precipitation maps. (b) Atmospheric circulation patterns and MDP related CLs 6 to 12. *a*) The colour palette shows geopotential height at 500 hPa while the isolines represent sea level pressure. *b*) Winter distribution of the days. *N* indicates the total number of days by CL. *c*) Mean daily precipitation maps [Colour figure can be viewed at wileyonlinelibrary.com]

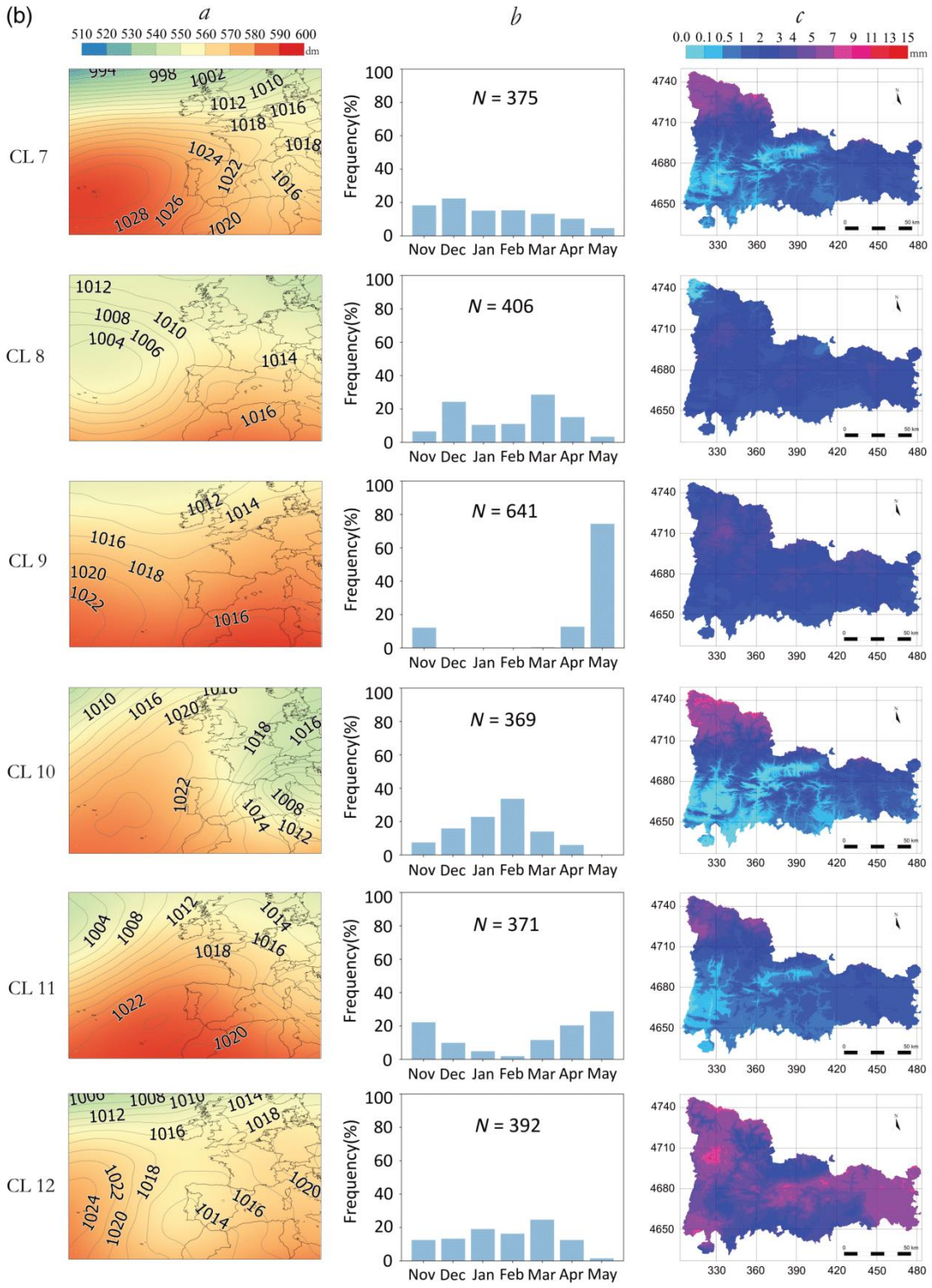

FIGURE 5 (Continues) [Colour figure can be viewed at wileyonlinelibrary.com]

was calculated as the quotient between the daily frequency of exceeding a certain threshold and the total number of days containing the weather type. To interpolate MDP and DPP values, we applied a MLR to adjust the models with greater certainty. A set of independent variables was taken into account for this adjustment; all of these were derived from a DEM at a 90-m spatial resolution and in the UTM—ETRS89 reference system. The first independent variable

used was latitude, which was computed as the Euclidean distance from the southern raster cell, that is, the Y min. Likewise, longitude was calculated through the Euclidean distance from the X min. We also took continentality into account, calculated as a function of cost distances from the sea to each target raster cell; to this end we employed a cost-push algorithm (Eastman, 1987–1997). It is first necessary to build a friction surface (obtained from the DEM) and a source feature indicating from where we want to model the air-mass motion. In this case, we used a single source feature indicating the Mediterranean as well as the Atlantic coasts. The resulting friction map is obtained once the algorithm has assigned the lower cost value to each cell.

Finally, we contemplated a monthly DEM-based potential solar radiation model considering astronomic data, geographical data and a uniform optical density (0.288) with clear conditions (Pons and Ninyerola, 2008). We implemented each of these solar radiation models in a weighted manner, considering the relative frequency of each month in the CL. Indeed, solar radiation constitutes a prioristically interesting variable because it integrates information on topography (slope, orientation and shading) influencing air temperature and precipitation, and establishes patterns in the formation of fog, clouds and local wind circulation.

Once all the independent variables were generated, the degree of correlation between them was tested to detect multicollinearity. Finally, we interpolated residual values (observed—predicted) employing the inverse distance weighted (IDW) and spline (SP) methods. Thus, local errors are resolved and exact values are obtained at the observation points.

We chose leave-one-out cross validation as a methodology for validating models inside the study area (Figure 1). The error (Equation (3)) is estimated by calculating the root mean square error (RMSE) to establish the error in units of the map (mm).

$$\mathrm{RMSE} = \sqrt{\frac{\sum_{i=1}^{n}\left(X_{\mathrm{obs},\,i} - X_{\mathrm{pred},\,i}\right)^2}{n}}, \tag{3}$$

where X_{obs} is the observed value and X_{pred} the predicted value, and n the number of observatories.

The normalized RMSE (NRMSE) is also used (Equation 4), which is defined as:

$$\mathrm{NRMSE} = \frac{\mathrm{RMSE}}{X_{\mathrm{obs},\,\max} - X_{\mathrm{obs},\,\min}}, \tag{4}$$

where $X_{\mathrm{obs,max}}$ is the observed maximum value of the observatories and $X_{\mathrm{obs,min}}$ the minimum observed value of the observatories.

Finally, we used the stepwise selection method in backward mode in order to choose the independent variables intended to fit our models.

3.4 | Unsupervised classification

ISODATA constitutes an iterative method for grouping observations in a multidimensional space. We employed this methodology to classify the models of the MDP. Thus, we attempt to obtain a regional image of the precipitation regimes in the Eastern Pyrenees during the winter season in order to provide a categorical cartography. When generating a classification of land uses from satellite images, the ISODATA method classifies the pixels into groups based on spectral similarities. The regression raster can be classified in the same way, but rather than employing spectral bands we use spatial variables resulting from an interpolation of data from weather stations. To initiate the automatic classification process, the ISODATA method requires selection of a

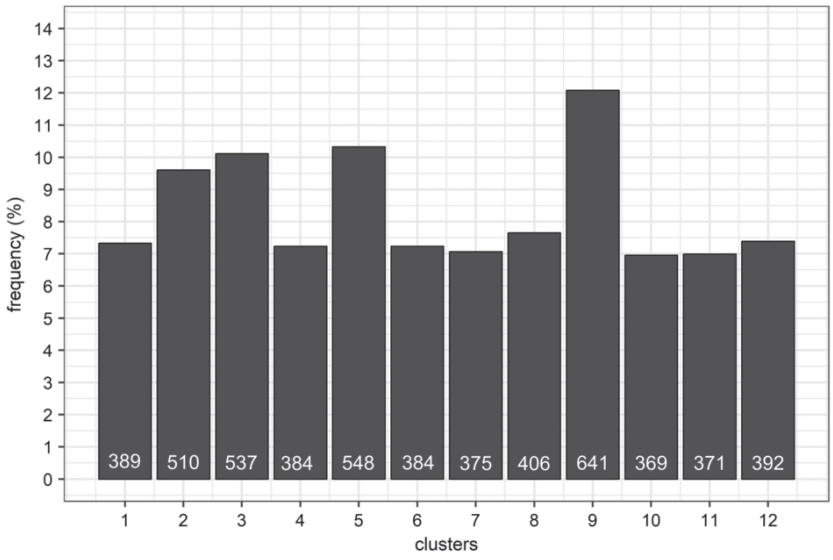

FIGURE 6 Percentage of days for each CL. Inside each bar the total number of days by CL is shown

maximum number of CLs, a minimum number of pixels conforming each CL, a convergence threshold and a certain percentage of pixels that is not expected to change CLs, among other factors. In our case, it was required that a maximum of 17 CLs be obtained from a systematic sampling of rasters, a criterion based on the previous knowledge of the area. A convergence threshold was established and a minimum similarity between classes of 1, and each CL contains a minimum of 1,000 pixels (90 km^2), sufficient to completely or partially cover a mountain massif in the study area. In addition, 40 iterations were established to solve the clustering if the convergence threshold was not reached beforehand. The number of iterations can be higher or lower depending on the study area. During this process, the distance between the CL centres is calculated and each pixel is assigned to its closest centroid based on the Euclidean distance (Pons, 2004). This process is given the sufficient number of times (iterations) until the convergence threshold is reached, at which moment the centroids become stabilized. To partially validate the cartography, we employed the SCR. As was explained in Section 2, we defined these regions availing of our expert knowledge of the region and of the snow and climate characteristics, which explains why the comparison was partial.

Therefore, the present paper proposes the use of the non-supervised classifier ISODATA as a method for defining the precipitation regimes in a given geographic area, based on a previous synoptic classification and on the associated precipitation patterns.

4 | RESULTS AND DISCUSSION

We obtained 12 atmospheric circulation types and 72 maps for MPD and DPP. Subsequently, we present an unsupervised classification that regionalises the precipitation regimes. We previously set forth the results of the quality control of precipitation data (Figure 4). The distribution of the final rain gauges used to interpolate the MDP and DPP shows an irregular frequency distribution in altitude due to an existing lack of stations at high altitudes, above 1,000 m a.s.l. (Figure 4a). In this respect, a substantial number of stations possess scarce data for the winter seasons (between 15 and 25—Figure 4b). In 20 rain gauges, we detected quality errors (Figure 4c); therefore, we removed these data, obtaining a small ratio of erroneous data, most of them lower than 0.005 (Figure 4d).

4.1 | Synoptic classification

The synoptic classification shows diverse patterns with low precipitation: CL1 (Figure 5), column *a*), which produces north-eastern advection with high pressures; CL2 (Figure 5a, column *a*), a zonal situation in which depressions tend to circulate to northern latitudes; CL3 (Figure 5a, column *a*), situation of a high centred on the Iberian Peninsula, very common in the central months of winter. In addition, the circulation patterns associated with instability are: CL4 (Figure 5a, column *a*), a 500 hPa trough situation along with a depression on the surface with a north-westerly flow; CL10 (Figure 5b, column *a*), a north-eastern advection with a depression in northern Italy, which gives rise to noteworthy precipitation in the northern area of the Pyrenees; CL12 (Figure 5a, column *b*), a situation of depression in the south-west of the Iberian Peninsula which generates an advection of wet south-easterly winds.

The Pyrenees and the Iberian Peninsula in general are highly influenced by high-pressures arising from the Azores anticyclone. The spatial representation of the atmospheric circulation types clearly shows that the winter season is generally dominated by stable weather (Figure 5a,b, column *a*).

If we analyse the absolute frequencies of each CL (Figure 6), the more stable ones (CL2, CL3 and CL5) can be seen to accumulate a large number of days (1,595 days, 30.1% of the total). It should be noted that the CL1, CL7 and CL11 types are very similar over the Pyrenees, since the variations occur at high latitudes between the three types (Figure 5a,b, column *a*). The sum of these three CLs results in 1135 days, that is, 21.4% of the total (n = 5,306 days). It should also be pointed out that CL9 presents the highest absolute frequency of days containing a CL. In May alone, it accumulates 477 days (0.74%) of the 641 conforming this CL (Figure 5b, CL9, column *b*), since in this situation, the regime of breezes and convective processes predominates as from midday, which hardly occurs in the rest of the studied months.

4.2 | Spatial regression

The cartography obtained with respect to the MDP (Figure 5a,b, column *c*) denotes the close relationship

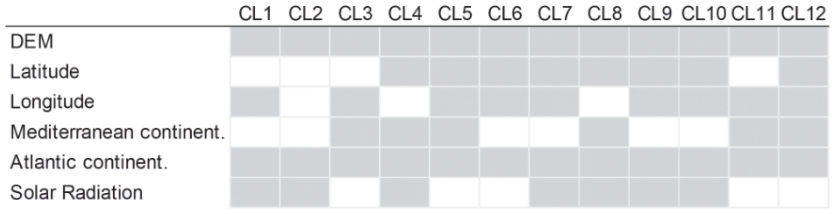

FIGURE 7 Independent variables participating in the multiple linear regression of the MDP models (in grey)

between altitude and precipitation in all CLs. In this sense, Figure 7 shows that all CLs use a DEM to interpolate the MDP. Another striking phenomenon refers to why the Atlantic continentality predictor has a much greater presence than the Mediterranean continentality on the MDP maps. The Atlantic continentality predictor better captures the spatial distribution because precipitation in the Eastern Pyrenees tends to present a relatively clear west–east gradient due to the bigger massifs in the western area. Analysis of the spatial distribution of precipitation values reveals that the northern

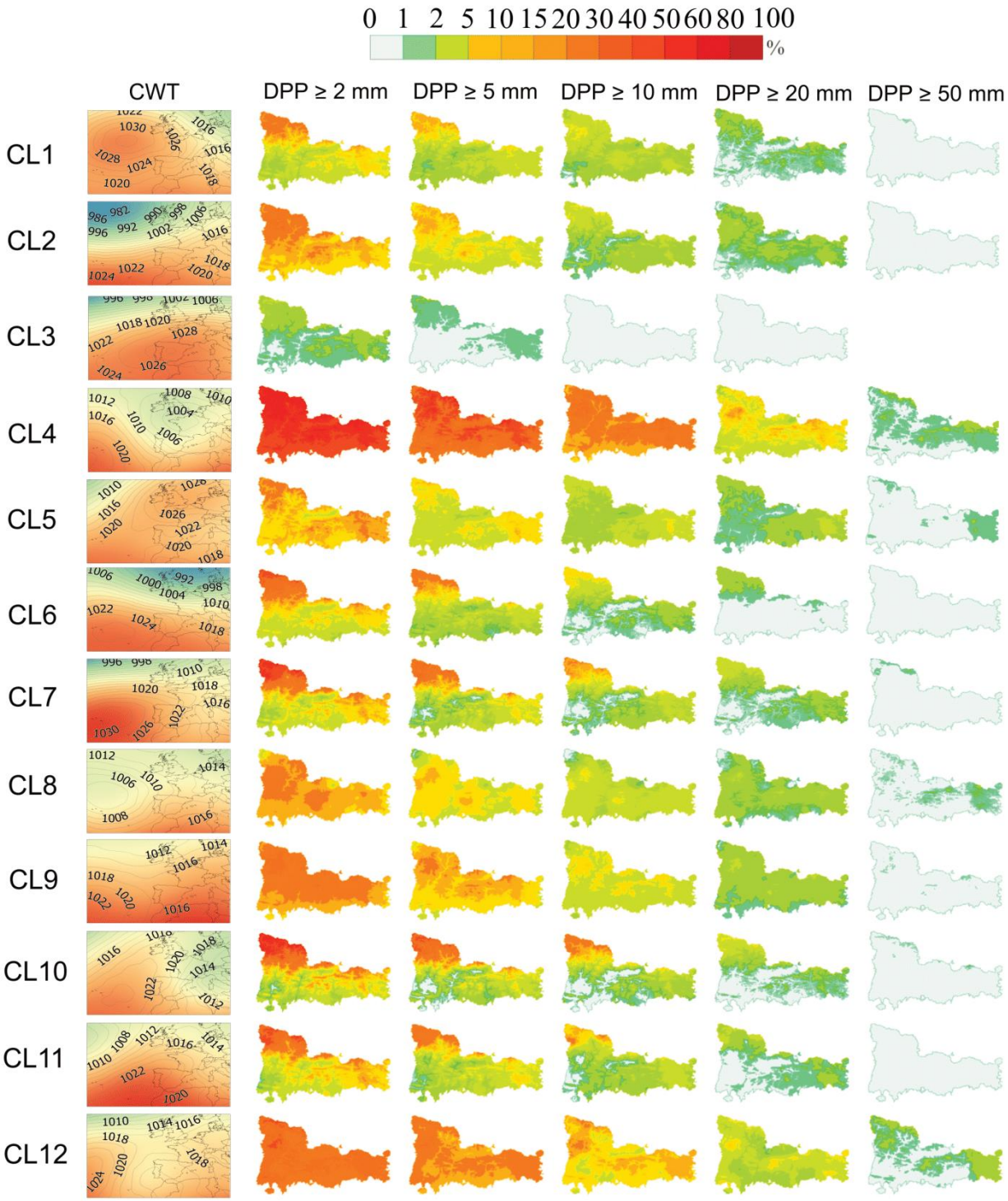

FIGURE 8 DPP maps for CLs (CL) from 1 to 12. The circulation weather types are also shown [Colour figure can be viewed at wileyonlinelibrary.com]

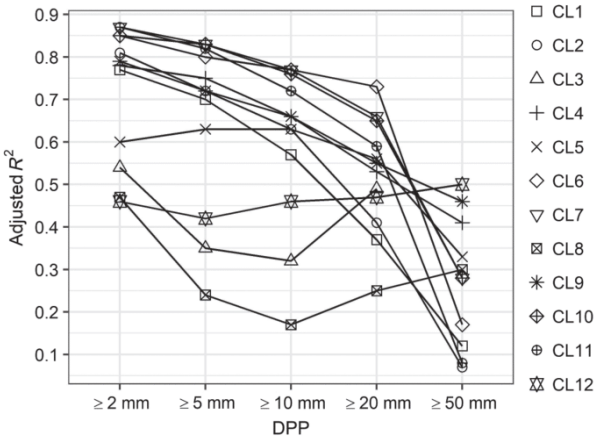

FIGURE 9 Graphical representation of DPP adjusted R^2 values for each CL

retention episodes (CL7, CL10 and CL11) are very well characterized, leaving extensive rainfall with moderate amounts in the AR region (Figure 1), from 5 to 9 mm. These northern advections also produce significant records in the northern part of the PP and TF sectors (regions Figure 1), with records from 4 to 7 mm/day, but located in the north of these sectors. Finally, it should be noted that in this type of situation, the PR and CM sectors (regions Figure 1) receive low precipitation, between 1 and 3 mm, in the same way that the valley area presents mostly negligible precipitation amounts (UP = 0.1 mm).

Another pattern to be considered is CL4, referring to a trough situation generating high instability both on the surface and at high altitude. This results in a high amount of DDP in the boundary area of the AR, RF and PL regions (Figure 1), and in the PR and TF sectors. In these sectors the records range from 9 to 13 mm of daily average precipitation, with maximums reaching 15 mm per day.

Finally, the MDP of CL12 refers to a situation of southeasterly winds, with records from 5 to 7 mm in the area closest to the northern coast. Within this same CL it should be noted that the orographic barrier effect of the CM and PR sectors in the PP sector is quantified between 7 and 9 mm in the former area, and between 3 and 5 mm in the latter one. Although the MDP maps clearly indicate the spatial precipitation patterns and their gradients, they do not define the intensity that any of the circulation types studied can reach. For this reason, the DPP maps are based on several thresholds to represent precipitation intensity (Figure 8). The graphical results show how the probability of each group decreases gradually with an increase in the precipitation threshold.

Based on the 5 mm threshold (Figure 8), situations with northern advection, CL7, CL10 and CL11, are seen to range from probabilities of 30–50%, mainly in AR. In any case, CL4 is the one presenting the highest potential risk of affecting a large area, with probabilities ranging from 30 to 50%, and locally reaching 60%. Indeed, there is still a 30–40% probability of surpassing the 10-mm threshold in all SCR.

The fit of the models varies significantly depending on the variable modelled (Figure 9). In the case of the models referring to MDP, the adjusted values of R^2 oscillate from 0.28 to 0.84. In this case, it is interesting to discuss the reason for the lack of fit in some CLs. The CL8 is defined by a western circulation pattern that is often accompanied by low, well distributed precipitation, thus avoiding a satisfactory fit due to the lack of gradients between precipitation observatories (Table 1). Similar problems can be observed in CL3 and CL12, where the low gradient between stations implies fits below 0.5 (adjusted R^2). On the other hand, the circulation types exhibiting a more contrasted precipitation topography, such as the different northern component situations (CL6, CL7, CL10, CL11), provide a satisfactory fit.

The DPP models reveal quite satisfactory results at the 2-mm threshold, since 8 of the 12 CLs obtain a value of adjusted R^2 above 0.77, with all the fits better than in the case of MDP, except for CL12. However, these good adjustments diminish in most cases, with an increase in the precipitation probability threshold, because the lowest values are at

TABLE 1 Adjusted R^2 values of MDP and DPP models for each CL

Adjusted R^2	MDP	DPP ≥ 2 mm	DPP ≥ 5 mm	DPP ≥ 10 mm	DPP ≥ 20 mm	DPP ≥ 50 mm
CL1	0.62	0.77	0.70	0.57	0.37	0.12
CL2	0.67	0.81	0.72	0.63	0.41	0.07
CL3	0.41	0.54	0.35	0.32	0.49	/
CL4	0.65	0.78	0.75	0.66	0.53	0.41
CL5	0.56	0.60	0.63	0.63	0.56	0.33
CL6	0.84	0.85	0.80	0.77	0.73	0.17
CL7	0.78	0.87	0.83	0.77	0.66	0.28
CL8	0.28	0.47	0.24	0.17	0.25	0.30
CL9	0.74	0.79	0.72	0.66	0.55	0.46
CL10	0.76	0.85	0.83	0.76	0.65	0.28
CL11	0.78	0.87	0.82	0.72	0.59	0.08
CL12	0.50	0.46	0.42	0.46	0.47	0.50

TABLE 2 Selection of the optimal residual interpolation IDW method and spline (SP) and its respective adjustment parameter, power or tension, for the MDP and DPP models

	MDP			DPP ≥ 2 mm			DPP ≥ 5 mm		
	Residuals method	**RMSE (mm)**	**NRMSE**	**Residuals method**	**RMSE (%)**	**NRMSE**	**Residuals method**	**RMSE (%)**	**NRMSE**
CL1	IDW 1	0.6	0.15	IDW 1	3.4	0.12	IDW 1	2.7	0.13
CL2	IDW 3.75	0.4	0.11	IDW 2.25	2.6	0.10	SP 800	2.0	0.11
CL3	IDW 1	0.1	0.16	IDW 1	1.1	0.13	IDW 1	0.6	0.16
CL4	IDW 3.75	1.0	0.13	IDW 1.75	4.1	0.11	IDW 2.25	3.4	0.10
CL5	IDW 3	0.4	0.11	SP 700	2.5	0.12	SP 800	1.6	0.13
CL6	IDW 1	0.4	0.10	IDW 1.25	3.7	0.08	SP 800	3.5	0.11
CL7	IDW 1.25	1.0	0.12	IDW 1.75	5.3	0.10	IDW 1.5	4.5	0.12
CL8	IDW 3.75	0.4	0.14	IDW 3.25	2.7	0.14	IDW 3.25	1.9	0.12
CL9	SP 400	0.4	0.10	SP800	2.6	0.10	SP 800	2.5	0.12
CL10	IDW 1	1.3	0.12	IDW 1.25	6.9	0.11	IDW 1	5.7	0.11
CL11	IDW 2	0.7	0.11	IDW 2.25	4.1	0.09	IDW 2.25	3.4	0.10
CL12	SP 75	0.9	0.12	SP 175	3.0	0.12	SP 200	2.6	0.12
Mean		0.6	0.12		3.5	0.11		2.9	0.12
	DPP ≥ 10 mm			**DPP ≥ 20 mm**			**DPP ≥ 50 mm**		
	Residuals method	**RMSE (%)**	**NRMSE**	**Residuals method**	**RMSE (%)**	**NRMSE**	**Residuals method**	**RMSE (%)**	**NRMSE**
CL1	IDW 1	2.1	0.15	IDW 1.25	1.6	0.20	IDW 4	0.1	0.28
CL2	SP 150	1.4	0.13	IDW 2.75	0.9	0.18	IDW 1	0.4	0.39
CL3	IDW 1	0.3	0.25	SP 800	0.1	0.15	/	/	/
CL4	SP 425	3.4	0.13	SP 200	2.5	0.14	IDW 1	0.9	0.21
CL5	SP 800	1.3	0.14	IDW 2.25	0.8	0.11	IDW 2.5	0.4	0.14
CL6	IDW 1	2.0	0.12	IDW1	0.6	0.13	IDW 1	0.2	0.35
CL7	IDW 1	3.2	0.12	IDW 1	1.7	0.14	IDW 1.5	0.4	0.17
CL8	IDW 3.5	1.5	0.12	IDW 3.25	0.9	0.15	IDW 2.5	0.5	0.22
CL9	SP 800	1.6	0.12	SP 800	1.0	0.18	IDW 1.5	0.3	0.32
CL10	IDW 1	4.4	0.12	IDW 1	2.3	0.13	IDW 1	0.5	0.16
CL11	IDW 2.5	2.6	0.10	IDW 2	1.1	0.13	IDW 1	0.2	0.21
CL12	IDW 4	1.8	0.10	SP75	1.8	0.13	SP 375	0.8	0.20
Mean		2.1	0.13		1.3	0.15		0.4	0.24

Note. In addition, the RMSE and NRMSE values are shown for the different models.

the 50-mm threshold, with the exception of some specific cases (Figure 9).

This lack of adjustment is due to the large number of precipitation observatories providing values of 0.0% and irregular distribution throughout the region. This value disables the linearity of the model, since an observatory at an altitude of 2,000 m in the AR sector can be seen to register a probability of 1.5%, but an observatory at the same altitude in the TF sector quantifies a probability of 0.0%. Despite the low adjusted R^2 values obtained, residual interpolation helps to provide a reasonably good interpolated surface. Thus, deficient predictions become evident when the database has a large number of 0 values. In this case, application of the GWR would not be preferable, since in areas where all observations are 0 the model cannot be adjusted. For instance, in CL3, in which all the observatories register a 0.0% probability of precipitation, there is no possible adjustment. In this situation, it would be advantageous to employ a Poisson regression inflated by 0 values (zero-inflated) (Arab, 2015), a technique that uses this distribution, which is readjusted by the appearance of many 0 values in the data. This methodology is applicable because the Poisson distribution usually adjusts to absolute frequencies.

Apart from the adjustment of the models, it is necessary to extract the error by means of some indicators of interpolation quality. Table 2 shows the errors extracted from the RMSE (absolute values) and the NRMSE (standardized values). In addition, the residual interpolation method used, SP or IDW, as well as the *tension* and *power* parameters used respectively, are indicated. The main function of this residual interpolation involves reducing the errors the global model is unable to adjust. In general, it becomes visible as the lowest RMSEs are achieved through IDW interpolation (Figure 10).

In the case of MDP, with one exception the RMSE does not exceed 1 mm of error, and the average error value for MDP is 0.6 mm. The absolute error in the DPP models is greater due to the higher data range; it is therefore useful to

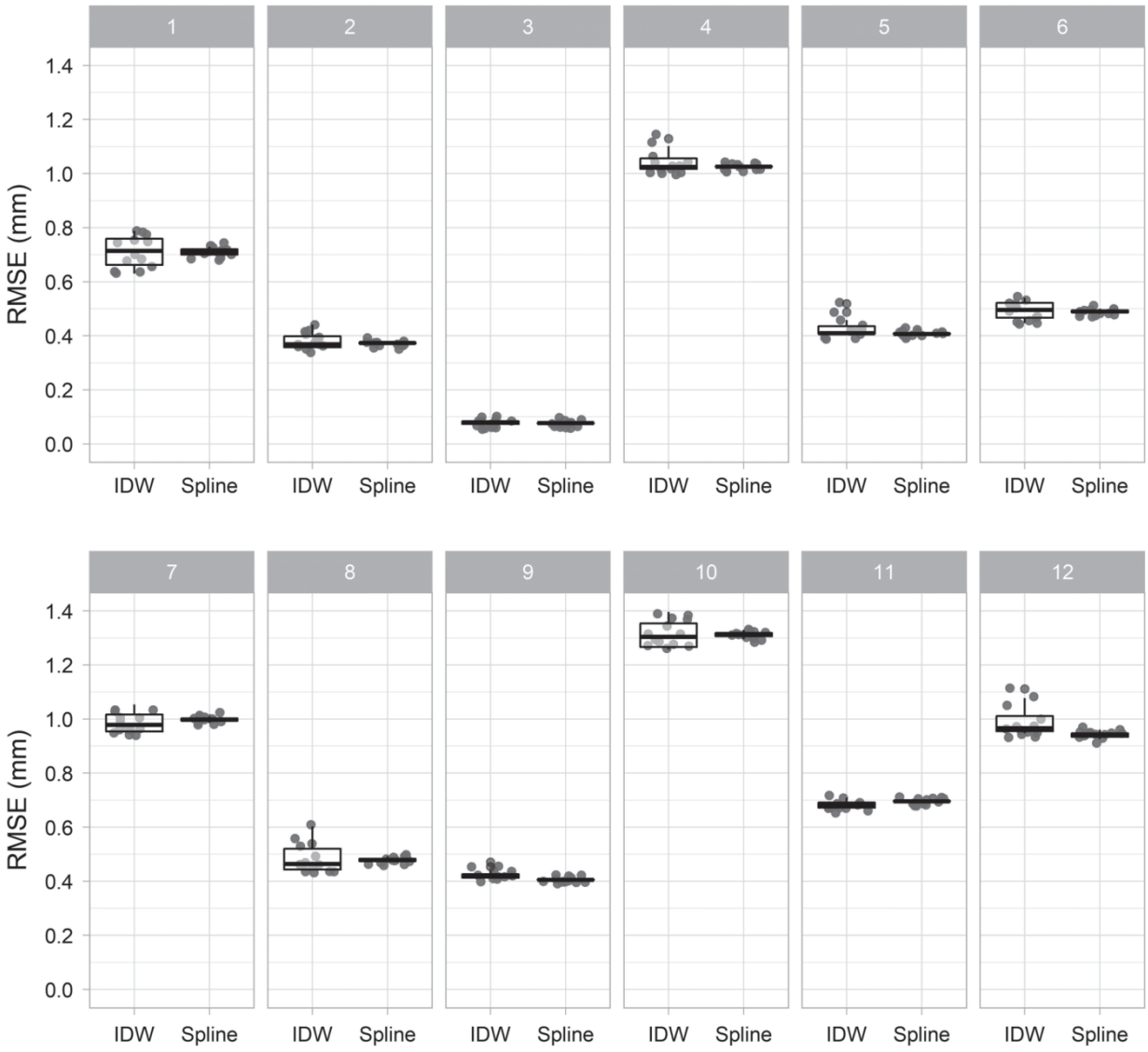

FIGURE 10 Boxplot representing the dispersion of the error of the different tests applied in the interpolation of the residues. For the IDW method, tests conducted with the parameter power between 1 and 4. In the case of the Spline method, the tests were performed with the parameter tension between 250 and 800. The IDW method was generally seen to present a higher accuracy than the Spline method in the residual interpolation

contrast the errors with the use of the NRMSE. This second indicator reflects how the errors referring to a DPP ≥ 50 mm are the most pronounced ones, although in absolute terms they are the lowest. The lowest error, comparatively, is found in the models referring to a DPP ≥ 2 mm, followed by that of MDP and DPP ≥ 5 mm. Thus, a constant increase in the relative error is evidenced with an increment in the threshold of DPP.

It is difficult to make comparisons with other interpolation studies due to the different study areas, evaluation of the error measurements and interpolation techniques involved. However, we put forward some results of similar studies. Hasenauer *et al*. (2003) obtained a mean absolute error (MAE) of 3 mm for MDP in Austria. Hunter and Meentemeyer (2005) achieved a MAE of 2.5 mm after modelling MDP for California. Finally, Esteban *et al*. (2009) obtained an averaged RMSE of 1.1 mm of the 20 MDP maps for each circulation weather type in Andorra.

4.3 | Unsupervised classification ISODATA

Unsupervised classification returns 6 classes defined from 12 MDP regression models (Figure 11). Visually, it can be observed how in the Western Pyrenees (AR, RF and PL), the classification categories show a remarkable fit with the SCR. For this reason, this region is used to validate the

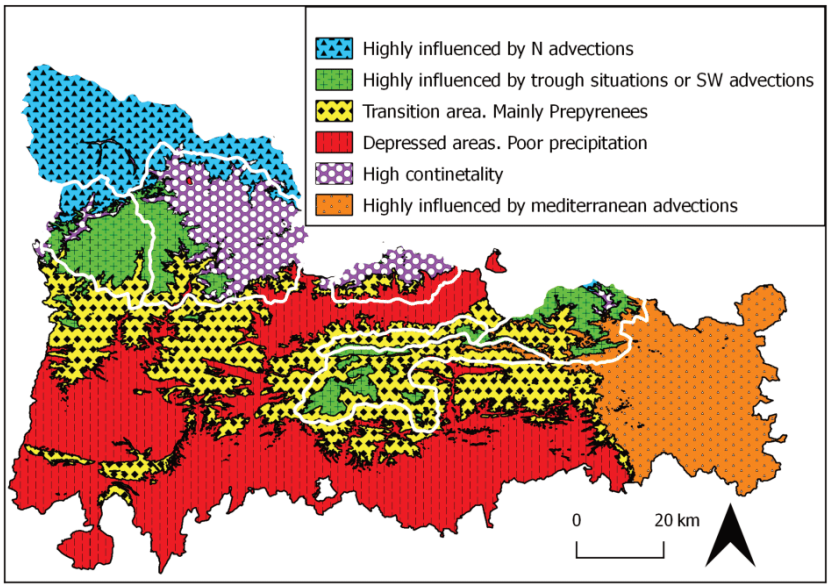

FIGURE 11 Result of the nonsupervised classification ISODATA of the 12 MDP maps. The figure contains diverse precipitation regimes described in the legend [Colour figure can be viewed at wileyonlinelibrary.com]

classification, since a different identifier is assigned to each of the three sectors. When a global inspection is performed, a very well-defined precipitation regime can be seen to fit with the AR region. In addition, we also detected a small extension of this precipitation regime in the TF sector, widely defined by northern component advections. Most of the PL and PF-PP sectors are defined as areas characterized by greater continentality, both the north and Mediterranean flows being leeward (foehn effect). The last well-characterized region is the one comprising much of the RF, CM, PR and TF sectors. The greater part of these 4 regions collects high precipitation in trough situations, as well as in western and south-western advections of Mediterranean origin. Situations of convection and orographic precipitation during the spring season are also significant, as these regions receive greater insolation and the phenomenon of convection is more marked than in other sectors.

Given the results of the classification, we prepared the western area of the eastern Pyrenees (AR, PL and RF) as a zone for partial comparison of the classification. This decision was taken because the three SCR possess three similar classified regions, which enables them to be compared (Figure 11). In the rest of the sectors in the eastern Pyrenees, the classification was more heterogeneous and therefore did not permit comparison between the SCR and the classified sectors.

In relation to the results of similarity between the SCR and the ISODATA classification (Table 3), the overall success is seen to be 71.8%, given that it shows some similarity between the two areas. The Kappa index is 0.6, indicating a similarity between moderate and good. On analysing the three regions individually, the precipitation region classified in the AR is seen to be very similar to the SCR one, with few inaccurate omission errors, but more accountable commission errors, which indicates that the influence of northern advections reaches further south than the SCR borders. The classification obtained for the PL sector displays a very low rate of commission error, since the area classified as PL falls within the proposed SCR. However, if the omission error is observed, it rises to almost 45%, given that much of this sector is also classified as RF and AR. Finally, the RF sector is the one presenting the lowest degree of similarity in relation to the classification. The errors of commission and omission are approximately 40% due to the greater influence of northern advections, and to the increase in size of the AR sector.

5 | CONCLUSIONS

The need to identify the different spatial distributions of winter precipitation over the Eastern Pyrenees has heretofore constituted an unresolved issue; this is of great interest due to their involvement in natural disasters (i.e., snow avalanches, floods, etc.). The synoptic classification performed has enabled 12 different types of atmospheric circulation to be defined, with a set of days assigned to each one of them.

TABLE 3 Results of the similarity between the western snow climate regions (A-FN, PALL and RB-VF) from Figure 1 and the nonsupervised classification ISODATA

	Error of commission (%)	Error of omission (%)	Global accuracy (%)	Kappa coefficient
A-FN	19.6	1.8	71.8	0.6
PALL	8.8	44.7		
RB-VF	40.8	38.8		

These 12 circulation types were directly related to daily precipitation records, by means of which the MDP and the DPP were modelled. The results obtained show a spatial coherence between the types of circulation obtained and the spatial modelling of precipitation. The precipitation models referring to anticyclonic situations and days exhibiting a low-barometric gradient are those that achieved a weaker fit. In this sense, interpolation of the residual values of the models has enabled a more realistic final cartography to be obtained. The northern advections, which involve a greater spatial gradient, were satisfactorily adjusted. Calculation of the NRMSE shows that the models presenting a lower relative error are those referring to a DPP $\geq$ 2 mm. The present research has generated an unsupervised ISODATA classification from 12 MDP models. The results obtained provide a robust definition of the winter precipitation regimes for the Eastern Pyrenees, as well as a mutual comparison with the regionalization performed by García *et al*. (2009). The validation, which was partial, due to the fact that only the western region of the study area could be validated, indicates a global similarity not very different from that of the SCR. The AR is the sector displaying the greatest similarity in relation to its SCR region. To conclude, the methodology proposed for classification of the precipitation regimes in the present paper constitutes one step further with regard to enhancing the climatic regionalisation of mountainous areas.

ACKNOWLEDGEMENTS

We wish to thank Pere Esteban for his advice in relation to the synoptic classification procedure. The present study was conducted within the framework of the Climatology Group of the University of Barcelona (2017 SGR 1362, Catalonia Regional Government) and the WEMOTOR (CSO2014-55799-C2-1-R) and CLICES (CGL2017-83866-C3-2-R) Spanish Government projects. M.L.-C. is granted with a pre-doctoral FPU grant (Spanish Ministry of Education, Culture and Sports).

CONFLICTS OF INTEREST

The authors declare that there is no conflict of interest regarding the publication of this article.

ORCID

Marc Lemus-Canovas https://orcid.org/0000-0002-0925-3827

Miquel Ninyerola https://orcid.org/0000-0002-1101-0453

Joan A. Lopez-Bustins https://orcid.org/0000-0003-3414-5577

REFERENCES

Abaurrea, J., Asín, J., Cebri, A.C. and Centelles, A. (2004) Metodología para el control de calidad y homogeneidad de una base de datos de precipitación diaria (in spanish). *Public Spanish Climatological Society*, 4, 431–440.

Aguilar, E. and Prohom, M. (2011) *RClimDex-extraQC (EXTRAQC Quality Control Software). User Manual*. Tarragona, Spain: Centre for Climate Change, University Rovira I Virgili.

Arab, A. (2015) Spatial and spatio-temporal models for modeling epidemiological data with excess zeros. *International Journal of Environmental Research and Public Health*, 12(9), 10536–10548. https://doi.org/10.3390/ijerph120910536.

Bissolli, P. and Müller-Westermeier, G. (2005, 2005) The spatial distribution of precipitation in Germany for different weather types. In: *Proceedings from the 5th Annual Meeting of the European Meteorological Society*. Utrecht, The Netherlands: Session AW8, Weather Types Classifications.

Brunsdon, C., Fotheringham, S. and Charlton, M. (1996) Geographically weighted regression—modelling spatial non-stationarity. *Geographical Analysis*, 28, 281–289.

Carro-Calvo, L., Ordóñez, C., García-Herrera, R. and Schnell, J.L. (2017) Spatial clustering and meteorological drivers of summer ozone in Europe. *Atmospheric Environment*, 167, 496–510. https://doi.org/10.1016/j.atmosenv.2017.08.050.

Cattell, R.B. (1966) The scree test for the number of factors. *Multivariate Behavioral Research*, 1(2), 245–276.

Duda, R. and Hart, P.E. (1973) *Pattern Classification and Scene Analysis*. New York: John Wiley & Sons.

Eastman, J.R. (1987–1997) *Idrisi. Users' Guide*. Worcester, MA: Clark University.

Esteban, P., Jones, P.D., Martín-Vide, J. and Mases, M. (2005) Atmospheric circulation patterns related to heavy snowfall days in Andorra, Pyrenees. *International Journal of Climatology*, 25(3), 319–329. https://doi.org/10.1002/joc.1103.

Esteban, P., Martin-Vide, J. and Mases, M. (2006) Daily atmospheric circulation catalogue for western Europe using multivariate techniques. *International Journal of Climatology.*, 26, 1501–1515. https://doi.org/10.1002/joc.1391.

Esteban, P., Ninyerola, M. and Prohom, M. (2009) Spatial modelling of air temperature and precipitation for Andorra (Pyrenees) from daily circulation patterns. *Theoretical and Applied Climatology*, 96(1–2), 43–56. https://doi.org/10.1007/s00704-008-0035-3.

Fernández-Montes, S., Rodrigo, F.S., Seubert, S. and Sousa, P.M. (2013) Spring and summer extreme temperatures in Iberia during last century in relation to circulation types. *Atmospheric Research*, 127(June 2013), 154–177. https://doi.org/10.1016/j.atmosres.2012.07.013.

García, C., Martí, G., García, A., Muntán, E., Oller, P. and Esteban, P. (2007) Weather and snow pack conditions of major avalanches in the Eastern Pyrenees. In: *Proceedings of the Alpine & Snow Workshop*, Forschungsbericht pp. 49–56.

García, C., Martí, G., Oller, P., Moner, I., Gavaldà, J., Martínez, P. and Peña, J. C. (2009) Major avalanches occurrence at regional scale and related atmospheric circulation patterns in the Eastern Pyrenees. *Cold Regions Science and Technology*, 59(2–3), 106–118. https://doi.org/10.1016/j.coldregions.2009.07.009.

Hasenauer, H., Merganicova, K., Petritsch, R., Pietsch, S. and Thornton, P.E. (2003) Validating daily climate interpolations of complex terrain in Austria. *Agricultural and Forest Meteorology*, 119, 87–107.

Hunter, R.D. and Meentemeyer, R.K. (2005) Climatologically aided mapping of daily precipitation and temperature. *Journal of Applied Meteorology.*, 44, 1501–1510. https://doi.org/10.1175/JAM2295.1.

Kalnay, E., Kanamitsu, M., Kistler, R., Collins, W., Deaven, D., Gandin, L., Iredell, M., Saha, S., White, G., Woollen, J., Zhu, Y., Chelliah, M., Ebisuzaki, W., Higgins, W., Janowiak, J., Mo, K.C., Ropelewski, C., Wang, J., Leetmaa, A., Reynolds, R., Jenne, R. and Jospeh, D. (1996) The NCEP/NCAR 40-year reanalysis project. *Bulletin American Meteorological Society*, 77, 437–472. https://doi.org/10.1175/1520-0477(1996)077<0437:TNYRP>2.0.CO;2.

Lopez-Bustins, J.A., Serrano, E., Ayarzagüena, B. and Sanchez-Lorenzo, A. (2015) Spatial and temporal temperature trends in the lower stratosphere during the extended boreal winter from reanalysis. *International Journal of Climatology.*, 35, 3888–3901. https://doi.org/10.1002/joc.4253.

Ninyerola, M., Pons, X. and Roure, J.M. (2000) A methodological approach of climatological modelling of air temperature and precipitation through GIS techniques. *International Journal of Climatology*, 20(14), 1823–1841. https://doi.org/10.1002/1097-0088(20001130)20:14<1823::AID-JOC566>3.0.CO;2-B.

Ninyerola, M., Pons, X. and Roure, J.M. (2007) Monthly precipitation mapping of the Iberian Peninsula using spatial interpolation tools implemented in a geographic information system. *Theoretical and Applied Climatology*, 89(3–4), 195–209. https://doi.org/10.1007/s00704-006-0264-2.

Oller, P., Marturià, J., González, J.C., and Martínez, P. (2006). The avalanche cartography of Catalonia. A preliminary evaluation of the spatial avalanche data. *5th European Congress on Regional Geoscientific Cartography and Information Systems. Barcelona, 13 to 16 June 2006*. PIETRI, C., 1993: Rénovation de la carte de localisation probable des avalanches. Revue de Géographie Alpine n°1., pp. 85–97.

Pons, X. (2004) *MiraMon. Geographic Information System and Remote Sensing Software*. Cerdanyola del Vallès, Bellaterra.

Pons, X. and Ninyerola, M. (2008) Mapping a topographic global solar radiation model implemented in a GIS and refined with ground data. *International Journal of Climatology*, 28(13), 1821–1834. https://doi.org/10.1002/joc.1676.

Richman, M.B. (1986) Rotation of principal components. *Journal of Climatology*, 6(3), 293–335. https://doi.org/10.1002/joc.3370060305.

Tveito, O.E.. and Ustrnul, Z. (2003) A review of the use of large-scale atmospheric circulation classification in spatial climatology, met. no. Report 10/03 KLIMA.

Vicente-Serrano, S.M., Saz-Sánchez, M.A. and Cuadrat, J.M. (2003) Comparative analysis of interpolation methods in the middle Ebro Valley (Spain): application to annual precipitation and temperature. *Climate Research*, 24(2), 161–180. https://doi.org/10.3354/cr024161.

Zhang, X. and Yang, F. (2004) *RClimDex*. Downsview, Canada: Climate Research Branch Environment Canada.

Zscheischler, J., Mahecha, M.D. and Harmeling, S. (2012) Climate classifications: the value of unsupervised clustering. *Procedia Computer Science*, 9, 897–906. https://doi.org/10.1016/j.procs.2012.04.096.

How to cite this article: Lemus-Canovas M, Ninyerola M, Lopez-Bustins JA, Manguan S, Garcia-Sellés C. A mixed application of an objective synoptic classification and spatial regression models for deriving winter precipitation regimes in the Eastern Pyrenees. *Int J Climatol*. 2019;39:2244–2259. https://doi.org/10.1002/joc.5948

3.2. Combinant els tipus meteorològics de circulació i el modelatge diari de precipitacions per obtenir regions de precipitació climàtica als Pirineus

3.2.1. Resum de l'article

Els Pirineus són un sistema muntanyós que presenta una diversitat climàtica molt àmplia, així com presenta una multitud de factors geogràfics que condicionen el comportament espacial de la precipitació en aquesta regió. El coneixement en profunditat del comportament espacial de la precipitació i, concretament, quan aquesta es veu condicionada per la circulació atmosfèrica a les regions de muntanya, és de gran importància per a la gestió de riscos naturals com les allaus o les inundacions. Per això, la present investigació treballa la relació entre l'escala sinòptica i el seu impacte en la precipitació a l'escala local. Mitjançant models lineals generalitzats (GLM), models additius Generalitzats (GAM) i la Regressió Kriging (RK), es modelitza la precipitació mitjana diària (MDP) vinculada als patrons sinòptics més freqüents a l'àrea d'estudi durant el període 1961-2010. Aquesta combinació d'escales permet realitzar una regionalització espacial de la precipitació al Pirineu mitjançant el flux de treball que es presenta en aquesta investigació. El primer resultat és un compendi de 20 tipus de circulació atmosfèrica. Per a cada un d'aquests tipus de circulació s'obtenen mapes de MDP per a cada un dels mètodes d'interpolació esmentats. L'ajust més satisfactori dels models el proporcionen els mètodes GAM i RK, amb un R^2 mitjà de tots els models de 0,58 i 0,61, respectivament. Mitjançant aquests mapes de MDP condicionats a cada un dels tipus de circulació atmosfèrica, s'estableix una regionalització categòrica de la precipitació al Pirineu formada per vuit regions diferenciades, dues de les quals revelen una tendència anual estadísticament significativa cap a una disminució de la precipitació.

3.2.2. Article

Lemus-Canovas, M., Lopez-Bustins, J. A., Trapero, L., & Martin-Vide, J. (2019b). Combining circulation weather types and daily precipitation modelling to derive climatic precipitation regions in the Pyrenees. Atmospheric Research, 220. doi: 10.1016/j.atmosres.2019.01.018

Atmospheric Research 220 (2019) 181–193

Contents lists available at ScienceDirect

Atmospheric Research

journal homepage: www.elsevier.com/locate/atmosres

Combining circulation weather types and daily precipitation modelling to derive climatic precipitation regions in the Pyrenees

Marc Lemus-Canovas[a,*], Joan A. Lopez-Bustins[a], Laura Trapero[b], Javier Martin-Vide[a]

[a] Climatology Group, Department of Geography, University of Barcelona, c/ Montalegre, 6, Barcelona 08001, Spain
[b] Snow and Mountain Research Center of Andorra (CENMA-IEA), Institut d'Estudis Andorrans, Av. Rocafort, 21-23, Sant Julià de Lòria AD600, Spain

ARTICLE INFO

Keywords:
Synoptic classification
Spatial interpolation
Clustering
Regionalization
Precipitation

ABSTRACT

The Pyrenees is a mountain range that presents a very broad range of climatic diversity, as well as a multitude of geographical factors conditioning precipitation in this region. In-depth knowledge of this precipitation, specifically of its association with atmospheric circulation types in mountain regions, is of great importance for the management of natural hazards such as avalanches or floods. Thus, the present research combines the synoptic scale with the local scale. We employed the regional scale of the Pyrenees to interpolate, by means of the General Linear Models (GLM), General Additive Models (GAM) and Regression Kriging (RK) methods, mean daily precipitation (MDP) based upon a classification of weather types at the synoptic scale; this procedure reflects the most frequent atmospheric patterns in the study area during the 1961–2010 period. This combination of scales makes it possible to perform a spatial precipitation regionalization of the Pyrenees by means of the work flow proposed in the present research. The result is a compendium of 20 atmospheric circulation types. For each of these circulation types, we obtained MDP maps for each of the aforementioned interpolation methods. The most satisfactory fit of the models was provided by the GAM and the RK methods, with an average R^2 of all models of 0.58 and 0.61, respectively. These models provided a precipitation regionalization of the Pyrenees involving eight differentiated regions, two of which reveal a statistically significant annual tendency towards a decrease in precipitation.

1. Introduction

The Pyrenees are characterized by constituting an area of high spatiotemporal precipitation variability due to their geographic location, on the border between the Mediterranean climate and the temperate oceanic mid-latitude climate, and as a result of their complex orography. Indeed, several studies analyze this variability in several areas of the Pyrenees (Beguería et al., 2009; Vicente-Serrano et al., 2009; Buisan et al., 2015). In addition, knowledge of precipitation associated with atmospheric circulation types is essential with regard to improving the management of water resources and to developing strategies aimed at reducing the impact of natural hazards in mountain areas such as avalanches, landslides, floods, among other hydrogeological hazards. However, there has been no previous research on the spatial modelling of precipitation or other climatic variables based on different synoptic situations for the Pyrenees area as a whole, a fact that highlights the interest of the study presented herein. On the contrary, numerous studies exist in this sense for the Iberian Peninsula (IP), such as Goodess and Jones (2002); Paredes et al. (2006); Muñoz-Díaz and Rodrigo (2006); Cortesi et al. (2013, 2014); Ramos et al. (2014). There exists a series of papers at regional scale within the IP, particularly in the southeast (Goodess and Palutikof, 1998), on the Mediterranean coastal fringe (Romero et al., 1999), Portugal (Trigo and Dacamara, 2000; Ramos et al., 2011), the northwest of Spain (Lorenzo et al., 2008, 2011), and the inland basins, such as the Duero catchment (Fernández-González et al., 2011), and the Ebro Basin in the north-east inland areas (Vicente-Serrano and López-Moreno, 2006).

For the Pyrenees, we highlight the research of Esteban et al., 2009, in which the method of extreme scores (Esteban et al., 2005) was applied to obtain an objective synoptic classification and to subsequently generate multiple linear regression models of mean daily precipitation values for each atmospheric circulation type in Andorra. Following the same approach, Lemus-Canovas et al. (submitted) provided a classification of precipitation regimes for the Eastern Pyrenees. The study performed a multiple linear regression using mean daily precipitation as a dependent variable, which serves to generate a cartography of the precipitation regimes in this area based on the ISODATA clustering method.

* Corresponding author at: Climatology Group, Department of Geography, University of Barcelona, c/ Montalegre, 6, Barcelona 08001, Spain.
E-mail address: mlemus@ub.edu (M. Lemus-Canovas).

https://doi.org/10.1016/j.atmosres.2019.01.018
Received 8 October 2018; Received in revised form 14 January 2019; Accepted 20 January 2019
Available online 21 January 2019

Note that several of the above mentioned studies made use of a pre-existing interpolated grid (Morata et al., 2006; Casado et al., 2010; Cortesi et al., 2014; Ramos et al., 2014), which means there is no need to use regression models of mean daily precipitation according to each circulation type. Despite this advantage, these grids possess a rough spatial resolution, usually over 10 km. In order to attenuate this limitation, in the present paper we reviewed some interpolation methods used for mapping topographically complex areas. Most interpolation studies work with multiple linear regressions, often with a subsequent interpolation of regression residuals by means of spline or inverse distance weighted interpolation (Ninyerola et al., 2000), due to the normal distribution of the monthly data generally used in this kind of climatic interpolation studies (Ninyerola et al., 2007; Brunetti et al., 2014; Batalla et al., 2016). Other authors, such as Peña-Angulo et al. (2016) or Crespi et al. (2018), adjusted the residuals by setting the semivariogram and interpolated them by means of simple Kriging (Hengl et al., 2007), in order to obtain monthly climatic surfaces of temperature and precipitation for mainland Spain and Italy, respectively. However, on occasion, natural processes cannot be explained by linear relationships and tend to have a curvilinear response, and a possible nonlinear response to our data can therefore be expected. The Generalized Additive Models (GAM) (Hastie and Tibshirani, 1990) are a semiparametric extension of the Generalized Linear Models (GLM), with the benefit of not representing a strict parametric form, thus enabling a more flexible response. Aalto et al. (2013) use GAM to adjust the monthly precipitation in Finland; Stauffer et al. (2017) adjust GAM to generate a daily precipitation grid for Austria.

Although one of the strengths of spatial modelling based on regression models involves the possibility to analyze and visualize the spatial complexity of environmental variables, the large number of output maps may make it difficult to provide a summarized view of the different patterns. This fact leads to the application of a clustering method intended to implement a classification of precipitation regimes, as proposed by Lemus-Canovas et al. (2018). The present research proposes the ISODATA method for classifying precipitation regimes in the Eastern Pyrenees by means of multiple linear regression precipitation models based on atmospheric circulation types as clustering inputs. In other atmospheric studies such as Zscheischler et al. (2012) and Carro-Calvo et al. (2017), the K-means clustering method using the Euclidean metric was used to establish a global climatic classification by means of meteorological and remote sensing data, and to regionalize the summertime tropospheric ozone (O_3), respectively. Not only is the Euclidean metric used in atmospheric studies that perform clustering methods, we can also find works using the Mahalanobis (1936) for detecting atmospheric circulation pathways (Makra et al., 2010).

The present study addresses three main objectives: (1) to perform an objective synoptic classification centred on Western Europe, and therefore valid for the Pyrenees; (2) to interpolate the mean daily precipitation values for each circulation type; (3) to present an improved-proposal for objective regionalization of precipitation regimes in the Pyrenees by means of the non-supervised clustering method. Finally, a secondary goal (4) involves generating a synthetic annual precipitation series for each region derived from the previous clustering. Thus, the present paper is structured as follows: in Section 2, the study area is described. We provide the data and methods used in the present research in Section 3; we subsequently present the results and the discussion in Section 4. Finally, in Section 5 we provide a summary of the main results and the derived conclusions.

2. Study area

The Pyrenees constitute the main orographic system of the IP, extending from the Cantabrian coast (Atlantic) to the Mediterranean (Lyon Gulf) and linking the IP with the rest of the European continent (Fig. 1). This mountain range lies between two depressed areas: the Ebro River basin (Spain) in the south and the Aquitania (France) in the North; the Pyrenees are approximately 425 km long and 150 km wide. Their altitude ranges mostly from 2000 to 3000 m a.s.l., although the highest elevations exceed 3000 m a.s.l (Aneto peak, 3404 m a.s.l.).

The climate of the Pyrenees is characterized by higher precipitation and lower temperatures than the surrounding territories. It also constitutes a climatic division between the prevailing Atlantic climate in the northwest, and the Mediterranean climate in the southeast (exhibiting continental characteristics in the south). Precipitation decreases from west to east and from north to south. In the easternmost area, precipitation increases once again due to its proximity to the Mediterranean sea. The oceanic influence is intense at the western end of the Pyrenees, with maximum rainfall amounts reaching 1500 to 2500 mm $year^{-1}$. This influence extends to most of the mountain range on its northern slope, but hardly affects the southern slope. On the southern slope, precipitation is less frequent but often more intense than on the northern slope, which explains the duration of sunshine hours despite the fact that both slopes present similar precipitation records (1000 to 1500 mm^{-1} year), except for the valley bottom (close to 600–700 mm $year^{-1}$).

3. Data and methods

3.1. Database

The database used in the present research was provided thanks to the international cooperative effort of 4 meteorological institutions within the framework of the Interreg Project POCTEFA CLIM'PY: AEMET (Spain), MeteoFrance (France), SMC (Catalonia, Spain) and CENMA-IEA (Andorra). The CLIM'PY project conducted several processes of homogenization and quality control of daily precipitation data to create a unique high-quality climatic database for the Pyrenees. The entire dataset includes 673 stations covering the 1950–2015 period with series of different longitudes, some of them involving < 10 years of daily data. In order to obtain the most robust possible results we considered the 1961–2010 period and series containing a minimum of 10 years of daily data, except in the case of stations at elevations exceeding 1500 m a.s.l., where rain gauges with a minimum of 7 years of data were considered due to the lower density of climatic information in high- altitude areas (Fig. 2a and c). Once the filtering was finalized, the final number of stations distributed throughout the study area, as well as in the surroundings, was 349 (Fig. 1), with most series (208) covering a period > 30 years (Fig. 2b).

3.2. Approach for circulation weather types

Daily mean sea level pressure (mslp) was provided by the ERA-20C reanalysis at 18 UT (Poli et al., 2016), enveloping the area 30°N-55°N and 12°W-15°E at a spatial resolution of 1° for the 1961–2010 period. We applied the methodology developed by Esteban et al. (2005), implemented in the COST733 software (Philipp et al., 2016), to classify the aforementioned daily mslp data in order to derive the principal atmospheric circulation patterns. To this end, we employed an S-mode matrix to reduce the dimension of the variables, in which the grid points are the variables and the days are the observations. The S-mode enables a climate regionalization (Richman, 1986; Lopez-Bustins et al., 2015) to be performed because it shows the representative degree of each day in each component. Nonetheless, with an S-mode matrix a direct synoptic classification cannot be obtained and as a result, a clustering method must be performed to finalize the atmospheric circulation catalogue. As for the variables used, we applied a standardization of the matrix to maintain one single scale for the different variables, thus avoiding overrepresentation of any one of them. The Scree test (Cattell, 1966) was used to retain the components explaining a significant portion of the total variance; these principal components were subsequently rotated by means of a varimax rotation (Esteban et al., 2006).

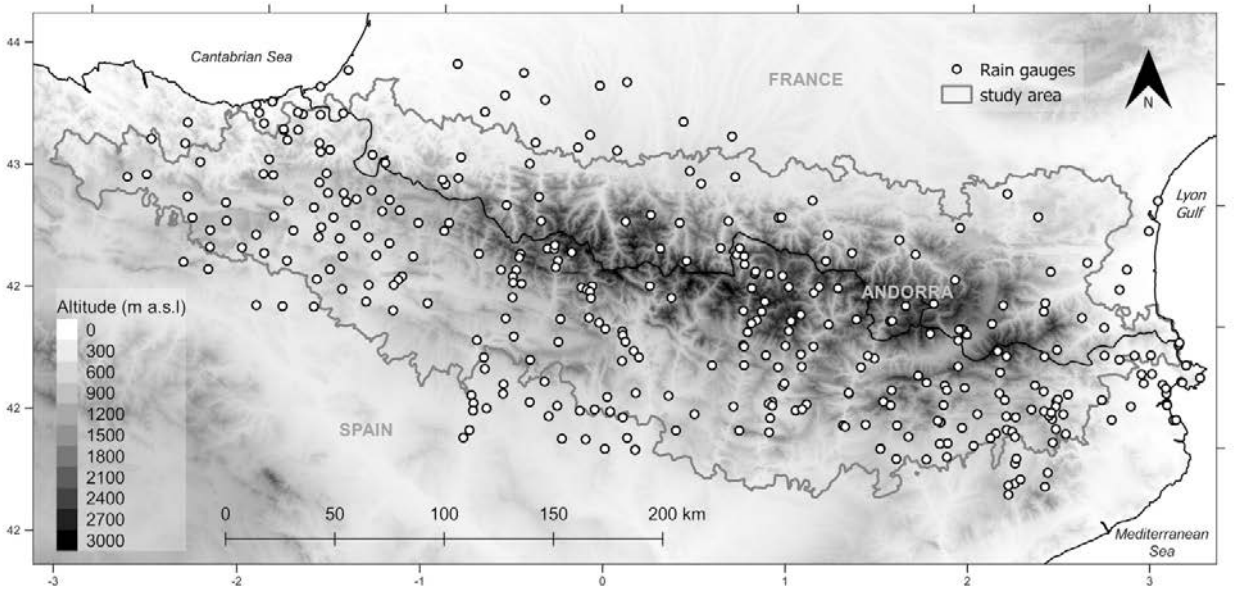

Fig. 1. Pyrenees location, orography and spatial distribution of the rain gauges (white dots) used in this study. The grey line shows the Pyrenees administrative border.

With the rotated components, we used the scores to apply the extreme scores method (Esteban et al., 2005). The scores show the degree of representativeness associated with the variation modes of each principal component, i.e., the classification of each day to its more representative centroid. Thus, the extreme scores method uses the scores > 2 and < -2, establishing a positive and negative phase for each principal component. The extreme scores procedure establishes the number of groups and their centroids for the K-means method (Esteban et al., 2006). K-means is applied without iterations because the centroids are well established by the method of extreme scores.

3.3. Spatial regression methods

3.3.1. Geospatial covariate data

Different explanatory variables were used to build the mean daily precipitation (MDP) grids based on circulation weather types (CWT). Due to the fact that topography directly affects the spatial variability of precipitation, it is crucial to use a digital elevation model (DEM) at a fine resolution to improve the spatial prediction of our response variable. In our case, we employed a 90 × 90 m DEM extracted from the Shuttle Radar Topography Mission (SRTM). With the use of this DEM we were able to derive the remaining explanatory variables used in this study. The first of these was latitude, computed as the Euclidean distance from the southernmost cell of the raster, i.e. the Y min. Likewise, longitude was calculated by means of the Euclidean distance from the

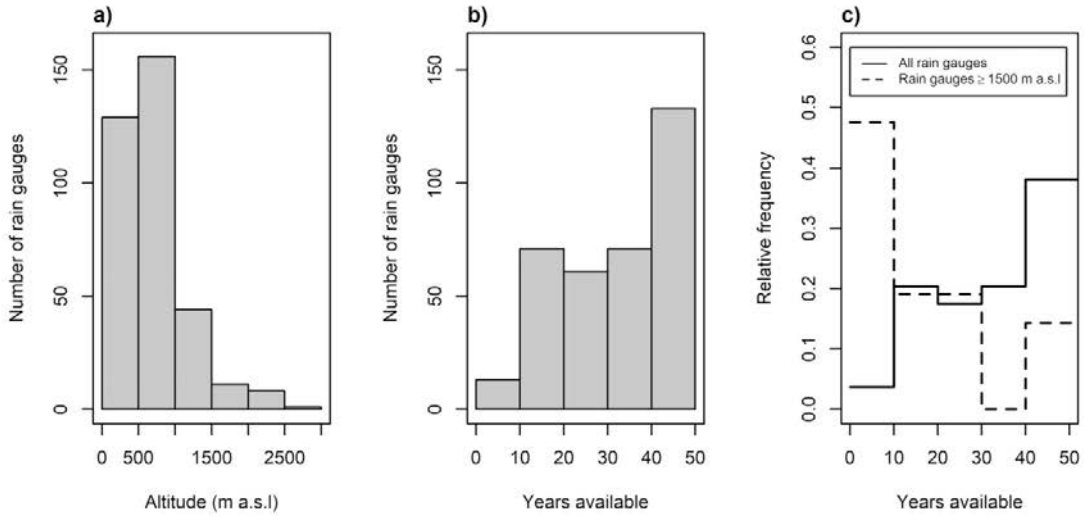

Fig. 2. Frequency distribution of the total available data (349 stations): (a) total number of rain gauges by ranges of 500 m altitude, (b) total number of rain gauges per yearly longevity of series, and (c) relative annual frequency distribution of rain gauges over 1500 m a.s.l and for all rain gauges.

westernmost cell (X min). We also considered the factor of continentality, the influence of both the Mediterranean sea and the Atlantic ocean, which is very important in the Pyrenees, with different characteristics clearly affecting the precipitation distribution over the region. We calculated this variable as a function of cost distances from the coast to each target raster cell using a cost-push algorithm (Eastman, 1987–1997). It was previously necessary to build a friction surface (obtained from the DEM) and a source feature indicating from where we wanted to model the air-mass motion. In this case, we used a single source feature indicating the Mediterranean and Atlantic coasts. The resulting friction map is obtained once the algorithm has assigned the lower cost value to each cell. Following the same approach as with continentality, we generated a variable which we called the northern influence since northern advections have been proven to be highly effective on the northern slope of the mountain range in comparison with the very dry conditions on the southern face, producing the well-known phenomenon named the Foehn effect (Quéno et al., 2016). As we move southwards, this effect diminishes, and does not cause multicollinearity problems with the latitude variable. We also computed the Euclidian distance from mountain massifs higher than 2000 m.a.s.l. to emphasize the phenomena of orographic storms that occur mainly at the end of spring and during the summer. Finally, we considered a DEM-based potential solar radiation model considering astronomical data, geographic data and a uniform optical density (0.288) with clear conditions (Pons and Ninyerola, 2008). The latter covariable and the DEM were resampled to 20 km in order to collect spatial effects of precipitation at a more general scale.

3.3.2. Generalized linear model (GLM)

Numerous methods exist for addressing geospatial modelling of precipitation in order to better characterize its high spatial variability. The performance of the GLM model (McCullagh and Nelder, 1989) represents a generalization of several methods of regression (linear regression, logistic regression, Poisson regression, etc.) in order to enable the response variable to be modelled. The major advantage provided by this model with respect to the linear regression model is that it allows the response variable to follow a data distribution different from the normal one (Gaussian, binomial, gamma, Poisson, etc.). In addition, GLM enables different types of links between the dependent and the independent variables through functions adapted to their distribution (identity, log, logit, etc.). Thus, these models are expressed as follows:

$$g(y) = \beta_0 + \beta_1 x_1 + \beta_2 x_2 + ... + \beta_k x_k \quad (1)$$

where g(y) is the link function, β_0 is the intercept, β_k is the estimated deterministic regression coefficient for the explanatory variable, x_k is the explanatory variable. When a climatic variable is linked to an atmospheric pattern, the response variable distribution habitually becomes log-normal, as in the study by Dayan and Levy (2005) who modelled the distribution of PM10. Only in some cases does this distribution tend to be normal.

For the remaining methodological aspects, GLM coincides with multiple linear regressions in which the response variable and the covariate must have a linear relationship. Independent variables must accomplish the assumption of independence to avoid the phenomenon of multicollinearity. In addition, the data must also accomplish the assumption of homoscedasticity, i.e. variance of the errors must be constant.

All seven explanatory variables described in Section 3.3.1. possess the same predictive capacity in each model. This fact highlights the need to use the stepwise selection method in backward mode in order to choose the independent variables that will be used to fit our models. This method integrates the covariates iteratively since, in each step, it evaluates which set of independent variables should be included in the model. The algorithm stops when the model no longer improves, although we include or extract variables. The relative quality of the model adjustment is evaluated by means of Akaike's information criterion (AIC). The lower the AIC value, the better the model adjustment.

3.3.3. Regression kriging (RK)

The RK (Hengl et al., 2007) is a spatial interpolation technique that combines ordinary least squares (OLS) with a Simple Kriging of the regression residuals (Tveito and European Cooperation in the Field of Scientific and Technical Research, 2008; Brunetti et al., 2014). The interpolation of residuals in the OLS equation is included as follows:

$$y = \sum_{k=0}^{p} \beta_k \cdot q_k(s_0) + \sum_{i=1}^{n} \lambda_i \cdot e(s_i) \quad (2)$$

where $q_k(s_0)$ are the values of the auxiliary variables at the target location, λ_i are kriging weights determined by the spatial dependence structure of the residuals and where $e(s_i)$ is the residual at the location s_i. Finally, p is the number of predictors or auxiliary variables and n the number of locations with residuals.

The variogram was used to adjust the residuals interpolation, which provides information on the spatial correlation of regression residuals. The variogram model selected to model the dependence between the semivariance and the distance was the exponential model, which provided the slightest error of the final model. The bin width of the variogram was set at 5 km and all the pairs of stations within a radius of 150 km were considered. As in the previous case, the stepwise selection method was used in backward mode to optimize the result of the regression. Regression Kriging interpolations were performed in the R statistical programming environment (R Core Team, 2018) with the gstat package (Pebesma, 2004).

3.3.4. Generalized additive models (GAM)

GAM was used (Hastie and Tibshirani, 1990) as semiparametric models, since individual local smoothing functions are used for each independent variable:

$$g(y) = \beta_0 + s_1(x_1) + s_2(x_2) + ... + s_k(x_k) \quad (3)$$

where S_k is the smoothing parameter to be estimated.

This smoothing allows greater flexibility with regard to representing the response of the data and enables the relationship between dependent variable and independent variables to be estimated. This fact is important, since in the study area there is no linear relationship between precipitation and altitude. To select the most significant covariates we also used the backward stepwise selection. GAMs were fitted using the R statistical programming environment with the gam package (Hastie, 2017).

3.3.5. Evaluation

For each precipitation map, n-1 stations were used following the leave-one-out cross-validation technique to evaluate the fitness of the models by means of different statistical measures. These statistical measures were: the coefficient of determination R^2, the root mean square error (RMSE), and the mean absolute error (MAE). The coefficient of determination R^2 was performed with the use of the observed and predicted values as the first calculation of fitness of the model. Willmott (1982) suggests that the RMSE and the MAE are among the best overall measures of model performance, as they summarize the average differences in units of the observed and predicted values. The RMSE is sensitive to the outliers and can be used as an indicator of the magnitude of the extreme errors, defined here as follows:

$$\mathrm{RMSE} = \sqrt{n^{-1} \sum_{i=1}^{n} \left(O_i - P_i \right)^2}, \quad (4)$$

where O_i is the observed and P_i the predicted value.

The MAE is less sensitive to extreme values and is defined as

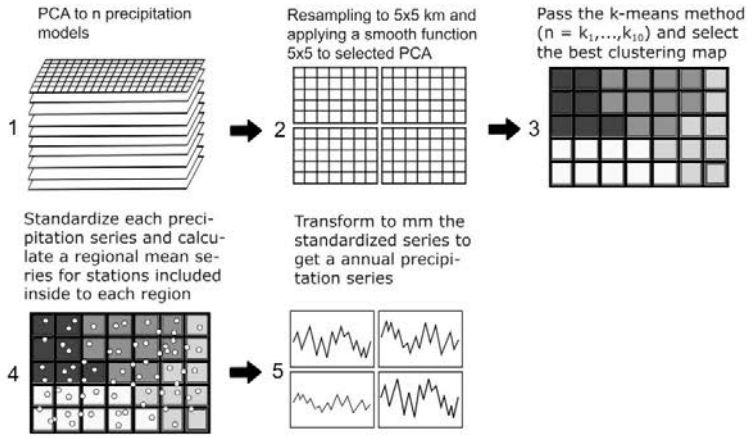

Fig. 3. Step-by-step flow chart showing the procedure designed to obtain the precipitation regimes (clustering map) and the annual precipitation regional series.

$$\mathrm{MAE} = n^{-1} \sum_{i=1}^{n} |O_i - P_i|, \tag{5}$$

The calculation of these indices was estimated for the stations inside the study area (Fig. 1). Cross-validation was performed using the R statistical programming environment with the caret package (Kuhn, 2008) for GLM and GAM and the gstat package for RK modelling.

3.4. Precipitation clustering and series regionalisation

With the aim of creating a cartography of the precipitation regimes in the Pyrenees, a workflow with the designed methodology is shown in Fig. 3. This process consists of 5 steps which give rise to two results: (1) generation of a map of precipitation regions, (2) and generation of a series of synthetic annual precipitation values between 1961 and 2010 for each precipitation region.

To achieve these two main results, (1) we first applied a principal component analysis (PCA) to the n standardized precipitation models which we obtained from the regression models for each CWT. This process enabled us to remove redundant information from correlated models and to capture only the most significant information from the set of models. (2) Subsequently, we resampled the selected principal components (PC) at 5 × 5 km spatial resolution to reduce local effects, such as the valley bottom effect. In addition, and to further emphasize the spatial continuity of the regions, we applied a 5 × 5 smooth filter function in order to avoid accused discontinuities in our regions. (3) We applied the K-means clustering method iteratively to generate from 1 to 10 clusters, obtaining 10 classifications. We used the Euclidean metric when performing the k-means clustering. The number of optimal clusters was chosen by means of a pseudo-MAE index:

$$\mathrm{MAE} = n^{-1} \sum_{i=1}^{n} |d_i - c_i|, \tag{6}$$

where d_i is the mean grid cell resulting from the average of PC selected, and c_i is the mean of respective centroids of the selected PC. As mentioned in Carro-Calvo et al. (2017), the increase in the explained variance by clustering can be explained by the increase in the number of centroids. However, the increase does not always imply increased variance, due to the fact that the n clusters explain practically the same variance as the $n + 1$ clusters. Thus, this graphically represented pseudo-MAE index enables us to visualize from which cluster there is no decrease in the error or increase in the variance. This measure is proposed as a complement to the decision based upon visual inspection. The purpose of the clustering process is to achieve a small but sufficient number of clusters that capture the diversity of precipitation regimes without a loss of generalization. (4) Once the final classification of precipitation regimes is adjusted, all stations included in the study area are normalized and then averaged by each classified region, thus providing a single standardized series for each of the regions of the classification. Finally, (5) the standardized regional series is transformed to real values of annual precipitation as follows (Jones and Hulme, 1996):

$$X = \mu + z\sigma, \tag{7}$$

where x is the real precipitation values in mm, z is the standardized value; x is the precipitation value; μ is the series mean, and σ is the standard deviation of the series. Thus, we obtained a regional and annual precipitation series that allows us to test their tendency and to verify their statistical significance with the use of the Mann-Kendall test.

4. Results and discussion

4.1. Synoptical classification

Based on the methodology described in Section 3.2, we obtained 20 CWT; Fig. 4 presents the spatial representation of the mean sea level pressure field for each atmospheric circulation type. The synoptic classification shows several patterns presenting a clear predominance of high pressures in the area of the Pyrenees, twelve out of the twenty CWT, although with a pronounced baric gradient over the study area: CWT 2 is defined by a blocking anticyclone in central Europe in which depressions tend to circulate southwards of the IP; CWT 4 and CWT 15 show an anticyclonic ridge extended to the northwest of the IP, forcing depressions to circulate to the north of the Pyrenees; CWT 7 and CWT 8 show two variants of blocks in central Europe with north-eastern advection over the Pyrenees area. Complementarily, we also detected five synoptic patterns presenting a situation of low pressure affecting the area of the Pyrenees: CWT 5, which shows a depression in the northwest of the IP with a distinct south-western advection over Iberia; CWT 11 shows a depression crossing the IP from west to east, blowing westerly winds over the study area; CWT 12 and CWT 17 both show northern advection over the IP with low pressures over the British Isles and Central Europe, respectively; finally, CWT 16 shows a depression over the western Mediterranean, advecting easterly and north-easterly winds over the entire region. As with the previous one, CWT 3 displays a north-eastern advection but in this case, the depression is moved to centre of Italy, driving winds that are more continental but relatively wet. In addition, we observed a series of synoptic patterns that are rather indefinite, since they do not exhibit a strong barometric gradient over the study area, a fact that indicates a predominant flow direction:

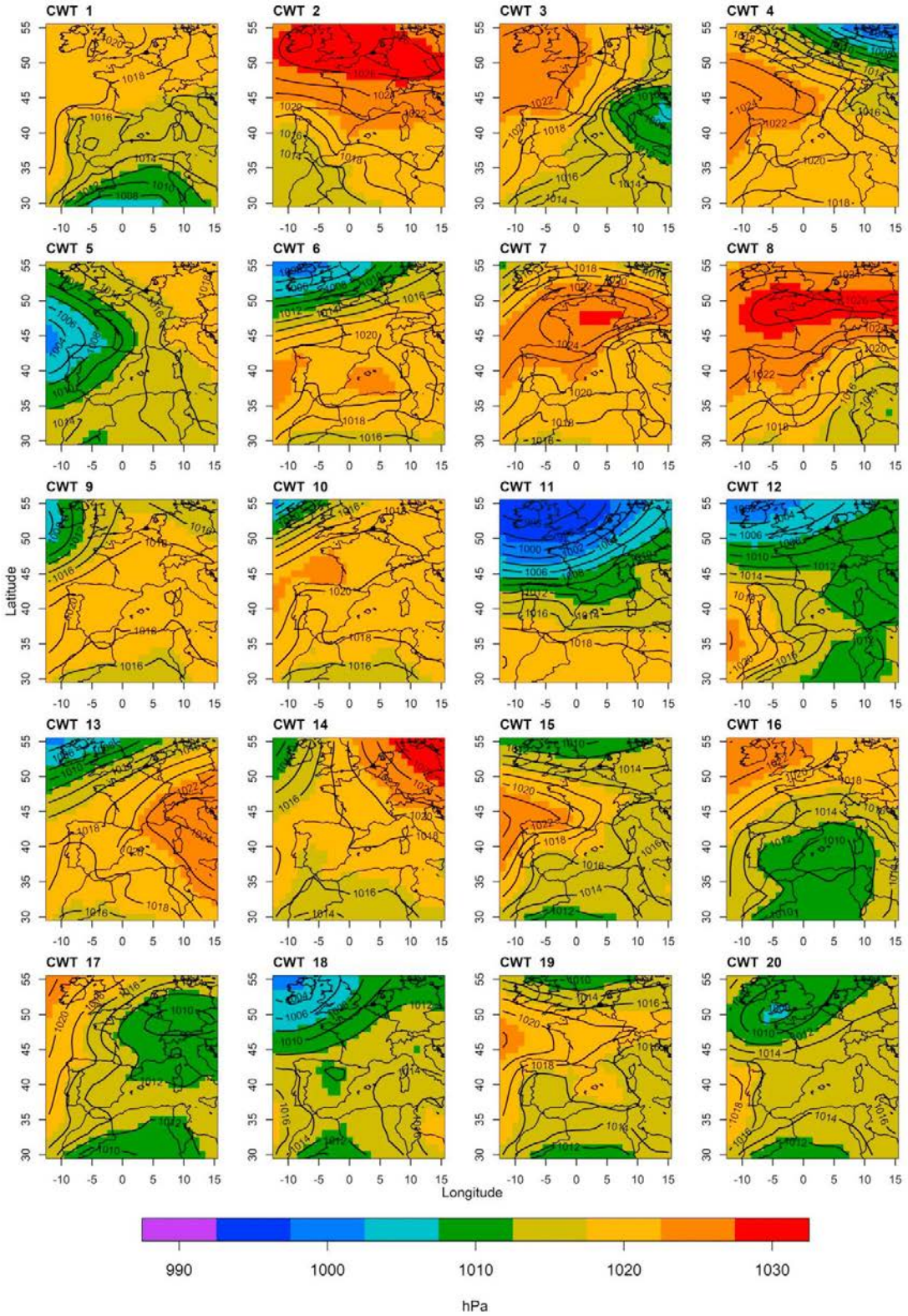

Fig. 4. Spatial representation of the mean sea level pressure field obtained for each circulation weather type (CWT) over the study area.

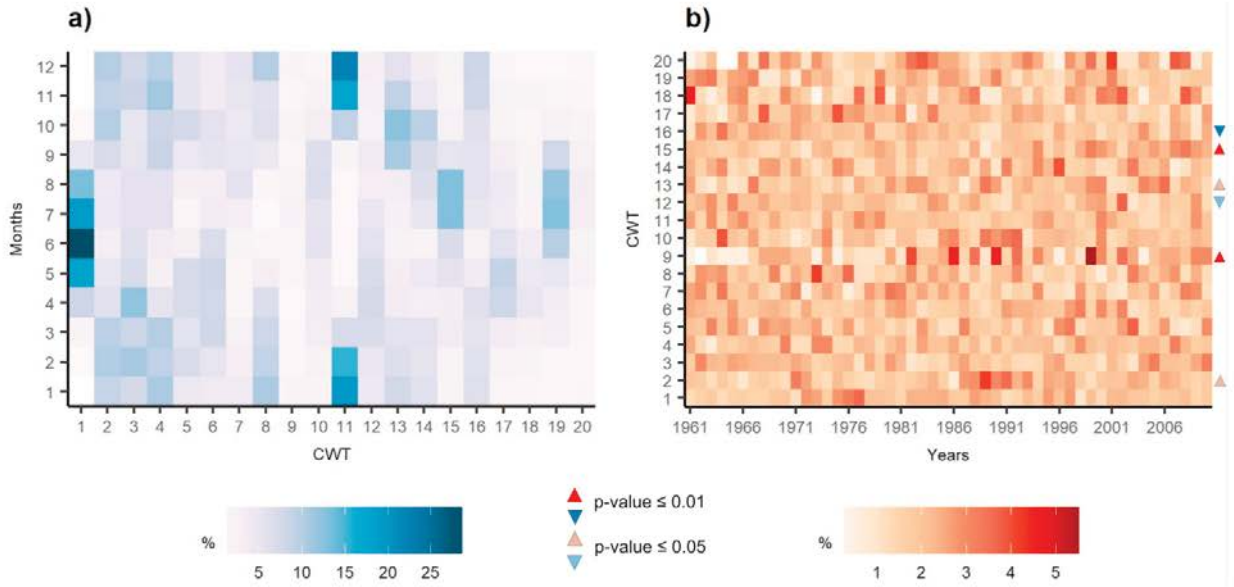

Fig. 5. Relative frequencies in percentage of each CWT by months (a) and annual relative frequency in percentages of each CWT during the 1961–2010 period (b). Statistically significant temporal trends are noted at 0.01 and 0.05 significance levels in (b).

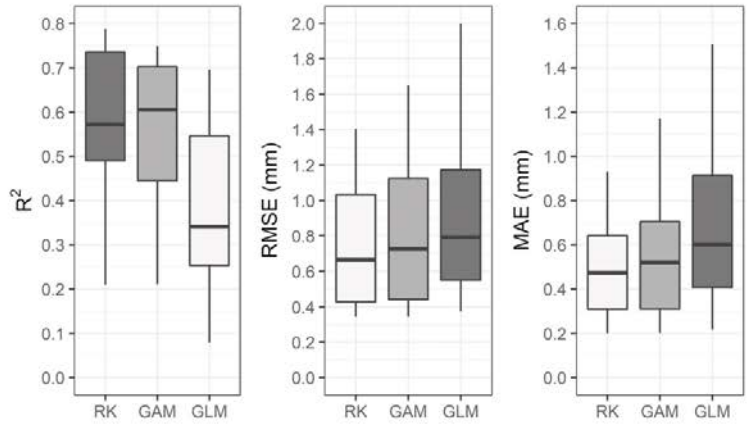

Fig. 6. Global fitness of regression models GLM, GAM and RK evaluated through R^2, RMSE and MAE indices.

CWT 1, CWT 6, CWT 9, CWT 10, CWT 14, CWT 18, CWT 19 and CWT 20.

For a more in-depth analysis, there is a need to establish the monthly frequency of these synoptic patterns. For this reason, we generated a matrix plot showing the percentage of days per month for each CWT (Fig. 5a). In this sense, we found that CWT 1 and CWT 11 present the highest daily concentrations in specific months. In the case of CWT 1, this concentration mostly occurs between May and August because of a common atmospheric circulation type during summer in which a thermic low originates in the southern half of the IP as a result of the intense heating during this season, a fact that reflects clear but limited convection. CWT 19 follows a similar synoptic structure to CWT 1 and is also very frequent during the summer months. As for CWT 11, this is an eminent cyclonic winter circulation type (November to February). In addition, we identified other circulation types that also reveal marked seasonality, such as CWT 2, CWT 4, CWT 8 and CWT 16 (cold semester: October to March), and CWT 10, CWT 12, CWT 15 and CWT 17 (warm semester: April to September). Finally, we identified a series of atmospheric circulation types that present quite regular distribution throughout the year: CWT 9 and CWT 20.

We also analysed the trend of these atmospheric circulation types annually between 1961 and 2010 (Fig. 5b). The results show that CWT 9 and CWT 15 reveal a statistically significant tendency (*p*-value ≤.01) towards an increase in the number of days per year of these patterns. CWT 2 and CWT 13 also show a statistically significant increase (p-value ≤.05). The CWTs that tend to undergo an increase in their daily frequency per year are all affected by high pressures. On the other hand, two CWT present a statistically significant trend, indicating a decrease in their number of days per year: CWT 16 (p-value ≤.01) and CWT 12 (p-value ≤.05), and in this case, low pressures prevail for both types.

4.2. Spatial regression results

This section is of great interest due to the results provided in Section 4.1., since establishing the spatial distribution of precipitation based on

Table 1
R^2, RMSE and MAE values obtained from leave-one-out cross-validation for the GLM, GAM and RK interpolation methods for each circulation weather type.

CWT	R^2			RMSE			MAE		
	GLM	GAM	RK	GLM	GAM	RK	GLM	GAM	RK
1	0.22	0.60	0.58	0.71	0.51	0.52	0.57	0.39	0.39
2	0.35	0.61	0.57	0.46	0.36	0.37	0.34	0.25	0.26
3	0.68	0.73	0.77	1.25	1.11	1.03	0.79	0.65	0.61
4	0.70	0.73	0.80	0.79	0.67	0.58	0.49	0.40	0.36
5	0.30	0.65	0.74	1.68	1.18	1.04	1.28	0.87	0.73
6	0.34	0.45	0.49	0.42	0.39	0.37	0.29	0.28	0.25
7	0.08	0.21	0.21	0.37	0.34	0.34	0.22	0.20	0.20
8	0.57	0.70	0.74	0.67	0.55	0.51	0.45	0.35	0.33
9	0.28	0.38	0.36	0.79	0.74	0.74	0.59	0.54	0.56
10	0.26	0.54	0.57	0.57	0.44	0.43	0.41	0.31	0.31
11	0.54	0.70	0.81	2.08	1.65	1.32	1.51	1.17	0.83
12	0.62	0.75	0.79	1.69	1.36	1.25	1.18	0.87	0.84
13	0.10	0.42	0.46	0.95	0.76	0.74	0.72	0.56	0.52
14	0.12	0.33	0.42	0.46	0.41	0.37	0.38	0.31	0.29
15	0.43	0.75	0.77	1.09	0.72	0.70	0.83	0.50	0.47
16	0.38	0.64	0.63	1.69	1.28	1.31	1.32	0.93	0.93
17	0.69	0.81	0.83	2.00	1.50	1.41	1.38	0.94	0.84
18	0.44	0.61	0.66	0.93	0.78	0.73	0.71	0.58	0.55
19	0.19	0.44	0.49	0.53	0.44	0.42	0.40	0.31	0.30
20	0.32	0.45	0.57	0.80	0.73	0.63	0.62	0.55	0.48
Mean average	0.38	0.58	0.61	1.00	0.80	0.74	0.72	0.55	0.50
Standard deviation	0.20	0.16	0.17	0.55	0.41	0.36	0.40	0.28	0.23

the different synoptic patterns identifies the areas most affected by the decline or the increase in days displaying a specific CWT.

4.2.1. Assessing the uncertainty of each interpolation method

The results of the comparison between the estimated and observed values are shown in Fig. 6, where the fitting of each method (GLM, RK, and GAM) is displayed in a box plot based on R^2, RMSE, and MAE scores. The variability shown in the values of R^2 for all methods was very high, which means that we found models with a correct fit and others with a very weak adjustment. The RK and GAM methods obtained higher R^2 values than the GLM, because of the linear dependence between the dependent and independent variables, which is very limited when the covariate response is unknown. Furthermore, the RK models, due to the subsequent interpolation of the residual values, enhance the initial linear regression. The use of smooth function in the GAM allows a greater goodness of fit, although it only performs the adjustment better than the RK in four CWT models (Table 1). With regard to the RMSE, the RK results show a slightly lower error range (0.34–1.41 mm) than the GAM (0.34–1.65 mm), while the GLM denotes higher errors than the previous ones, offering a greater disparity of error values (0.37–2.08 mm).

MAE follows the same pattern as in the case of RMSE, giving a high amplitude error in the GLM and a rather low error in all CWT models of RK, which in no case exceeds 1 mm. the GAM provided slightly higher errors than the RK, which quantifies the extreme error as 1.17 mm. In summary, as a global performance of the interpolation methods, the RK is seen to be the most accurate, with an averaged R^2 value of 0.61 versus 0.58 R^2 for the GAM and 0.38 R^2 for the GLM (Table 1).

4.2.2. Individual analysis of the CWT model errors and interpretation of the associated mean daily precipitation cartography

In addition to estimating the overall adjustment of each spatial interpolation technique, it becomes important to emphasize the degree of the individual adjustment presented by each CWT model obtained from their respective regression methods. In this section, we perform a joint analysis of the errors together with the climatic interpretation of the CWT models, since in many cases there is a clear relationship between the degree of adjustment of the model and the model's climatic base.

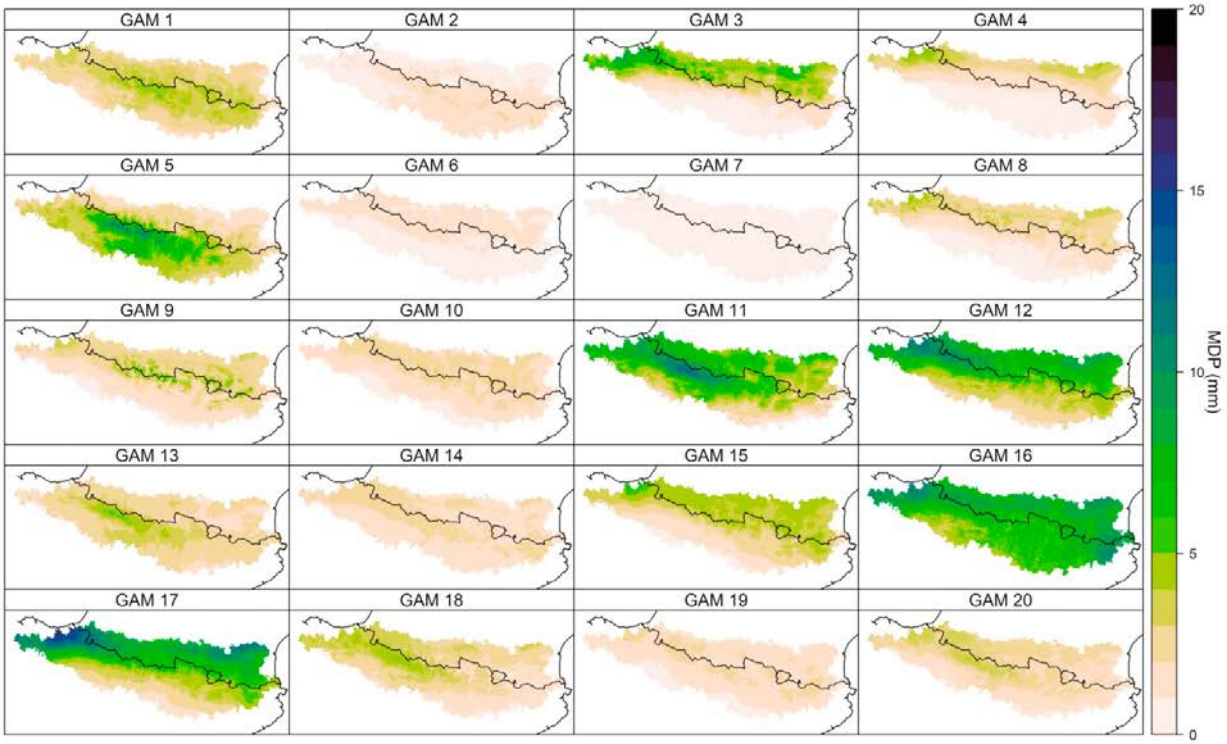

Fig. 7. Results of the GAM interpolation method for each model related to each CWT.

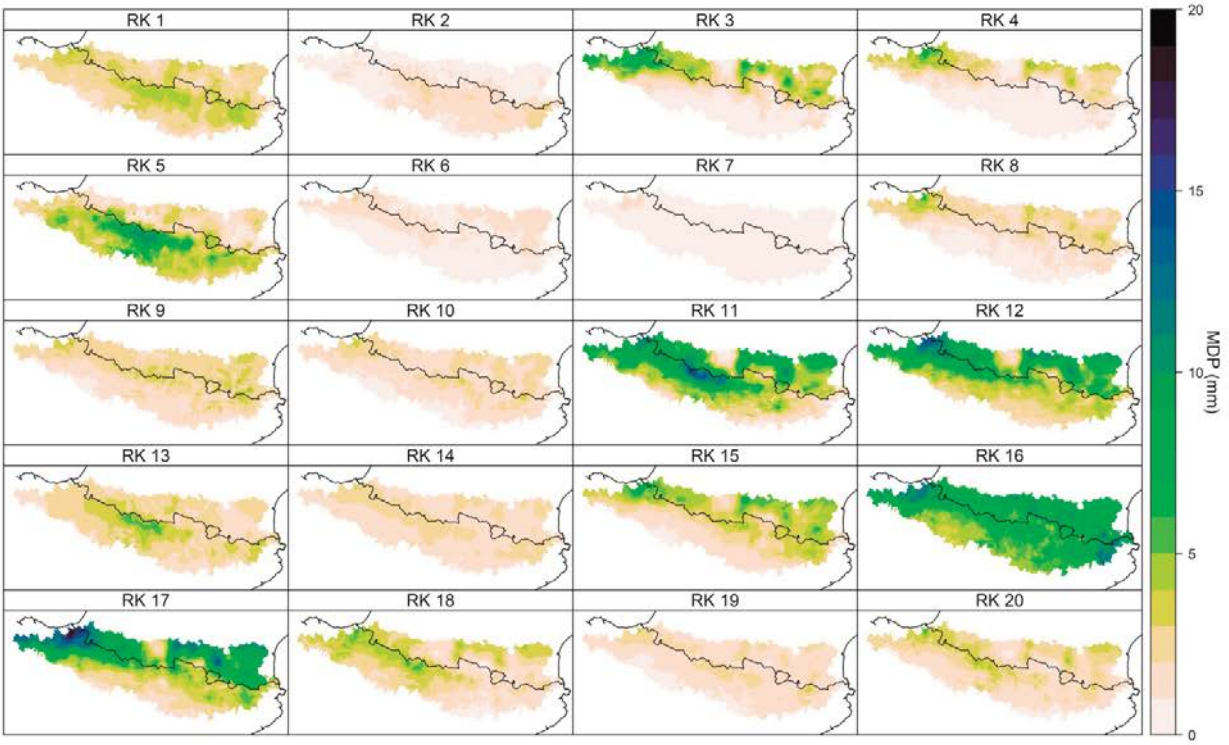

Fig. 8. Same as Fig. 7, but for the RK interpolation method.

The resulting cartography of mean precipitation for each CWT obtained with the GAM and RK methods is illustrated in Figs. 7 and 8, respectively. GLM interpolation results can be inspected in the supplement to this paper (Fig. S1).

If we take the RK models (Fig. 8) as a reference, we have 8 models with an $R^2 > 0.7$, which indicates a satisfactory fit. These models are: RK 3, which reveals a marked north-south gradient, obtaining the highest values in the northern half of the study area, as it corresponds to a cyclonic advection from the Northeast, which causes precipitation retention in the northern area; RK 4 and RK 8 show the same scenario as in the previous case, but with lower precipitation over the study area, since they constitute an anticyclonic northern advection; RK 15 also reflects a gradual distribution of precipitation from north to south, but in this case there is an increase in precipitation on the southern slope of the Pyrenees resulting from summer storms, since this pattern occurs mostly during this season (Fig. 5a); RK 5 denotes a high MDP on the southern slope of the Pyrenees, specifically in its central area, where mean accumulations are > 10 mm; RK 11 denotes a west-east gradient, with highest precipitation values registered in the same area as the RK 5, since in this case, the synoptic pattern is characterized by cyclonic western advection. Note that, RK detects maximum values of MDP quantified at 15 mm, whereas the GAM quantifies the maximum value at 13 mm. Finally, we point out that RK 12 and RK 17 present a marked north-south gradient, because the predominant synoptic situation is a cyclonic northern advection. This CWT favours higher records than a situation characterized by northern anticyclonic advection due to its inherent instability and the orographic lifting over the Pyrenees. In all cases with northern advection, the gradient is much more evident in the GAM than in the RK since interpolation of residuals in the latter method can generate a certain spatial discontinuity favouring a more accurate prediction between the observed and the predicted values.

Regarding the cases in which the adjustment was very weak ($R2 \leq 0.5$), these are dominated by situations with very low precipitation in the study area, because they are linked to an anticyclonic or indefinite CWT, but with little noticeable advection (Fig. 4). For example, the cases of RK 6 and RK 7 are precisely those that have the lowest precipitation throughout the study area, with a practically homogeneous spatial distribution, which gives rise to a poor adjustment skill ($R^2 = 0.21$). Mention should also be made of some precipitation peculiarities occurring in the study area according to some models. For instance, RK 16 is the only one that makes the highest contribution to the easternmost part of the study region, due to a synoptic situation defined by a Mediterranean low driving easterly wet winds to the eastern Pyrenees. In RK 18, and especially in GAM 18, an inverse relationship gradient between precipitation and altitude is clearly observed. This occurs during the beginning of spring when the snow still remains at levels exceeding 2000 m a.s.l. and is sufficiently abundant to play a role in inhibiting convective storms (Pascual et al., 2009); these convective precipitations are consequently produced to a greater extent on the south face and below 2000 m a.s.l.; Finally, note that GAM 1, which shows greater accuracy than RK 1, denotes the phenomenon of convective precipitation, highly concentrated during the summer months (Fig. 5a) where precipitation can be affected by orographic enhancement.

It is difficult to compare our results with those of other authors because few studies have combined atmospheric circulation with precipitation modelling by means of regression models. The paper by Lemus-Canovas et al. (submitted) focuses upon the southern slope of the Eastern Pyrenees, thus avoiding many non-linear effects between the covariates and the response variable, as described in Section 1, and implying a mean R^2 of 12 mean daily precipitation maps quantified in 0.63. Esteban et al. (2009) obtained an averaged RMSE of 1.1 mm of the 20 MDP maps for each circulation weather type in Andorra.

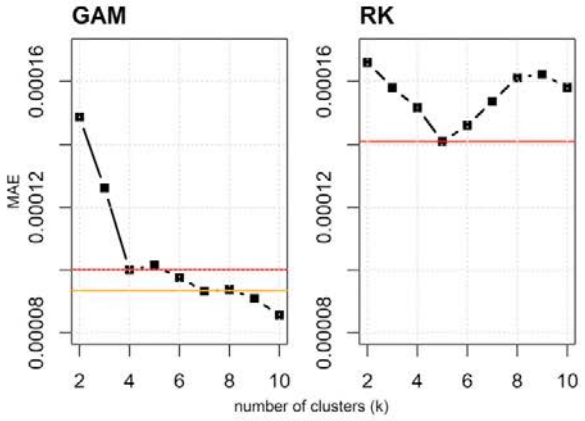

Fig. 9. Representation of the pseudo mean absolute error for each number of clusters. Horizontal lines help to decide the number of clusters to be selected.

4.3. Regionalisation result: clustering and regional series

The iterative clustering described in Section 3.4, was performed twice: with the GAM as well as the RK precipitation models since the goodness of fit between them was not very acute. The results obtained from this clustering denoted an obvious difference between the two methods. Fig. S2 clearly shows that the GAM clusters present greater continuity and spatial cohesion than the clusters derived from the RK models, which demonstrate a certain degree of heterogeneity and difficulty in distinguishing the precipitation regions of the Pyrenees by means of visual inspection. This phenomenon is also visible in the line plot, a fact that serves to evaluate the pseudo-MAE corresponding to each clustering (Fig.9). In the case of the clustering performed with the GAM, the error tends to decline steadily, which indicates that in general terms, as the number of clusters (k) increases, a low error is provided and the explained variance for each cluster shows an increase. Only in some points is this decrease halted, and an increase in the number of clusters does not necessarily involve a decrease in the MAE, as in the sequence of k = 4 to k = 5 and in k = 7 to k = 8. On the other hand, in the case of the RK, since it involves such a heterogeneous surface, we find a minimum value for the MAE when k = 5. The error increases from k = 5 to k = 9, which indicates that a greater number of clusters does not provide a better regionalization of the area. In addition, as in the case of the clustering of the GAM models, the intracluster error evaluated by means of MAE is observed to be lower than in the case of the RK models; consequently, we selected the GAM interpolations to apply the clustering algorithm.

Once the k-means method was implemented with the GAM models, the number of clusters or regions was decided. Fig. 9 shows that the number of optimal clusters should be: first, 4 regions, or second, 7 regions, since successive clusters do not cause a decrease in the MAE. However, we decided to use 8 clusters because the authors are very familiar with the study area. The criterion adopted results from the fact that the 8th cluster highlights the division between the northern and the southern slopes of the Pyrenees (Fig. S2), an area exhibiting clear differences in precipitation amounts and variability (García et al., 2007).

Fig. 10 presents the results of the regionalization and highlights the influence of each GAM in the various regions, providing a synthesis map of the 20 models. With regard to its general aspects: (1) there is a

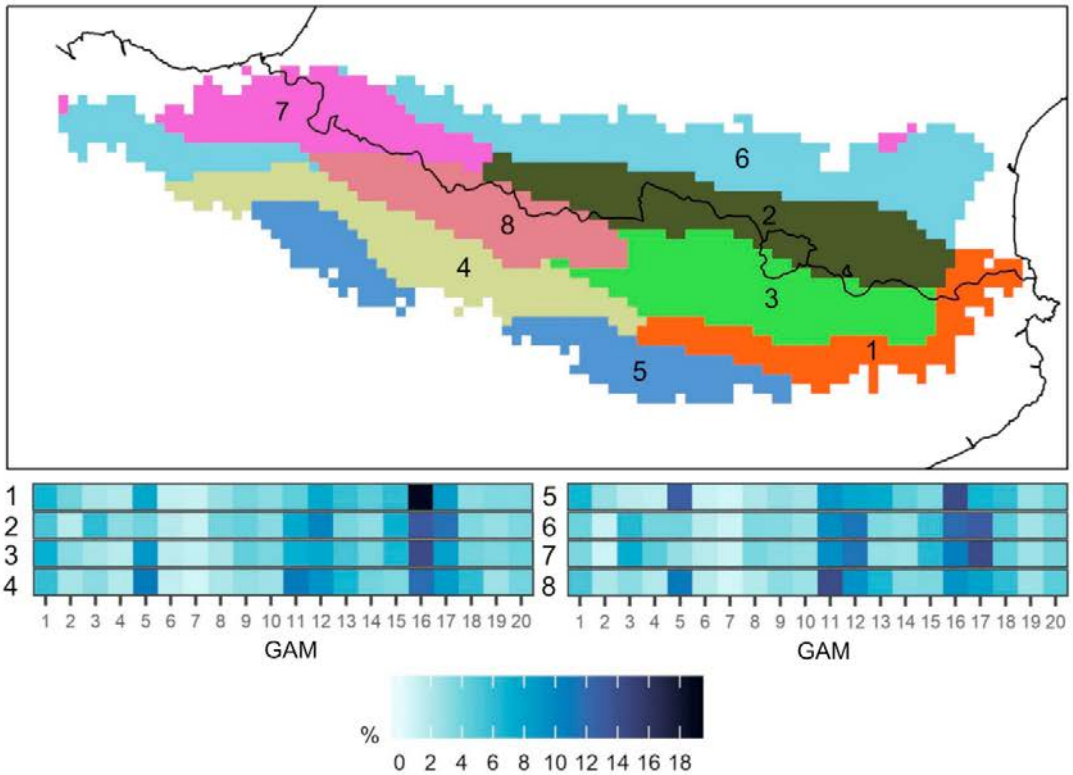

Fig. 10. Result of the clustering procedure finalized with a k-means unsupervised method of the 20 GAMs of MDP. The daily precipitation efficiency of each CWT model is calculated for each region and shown below the map.

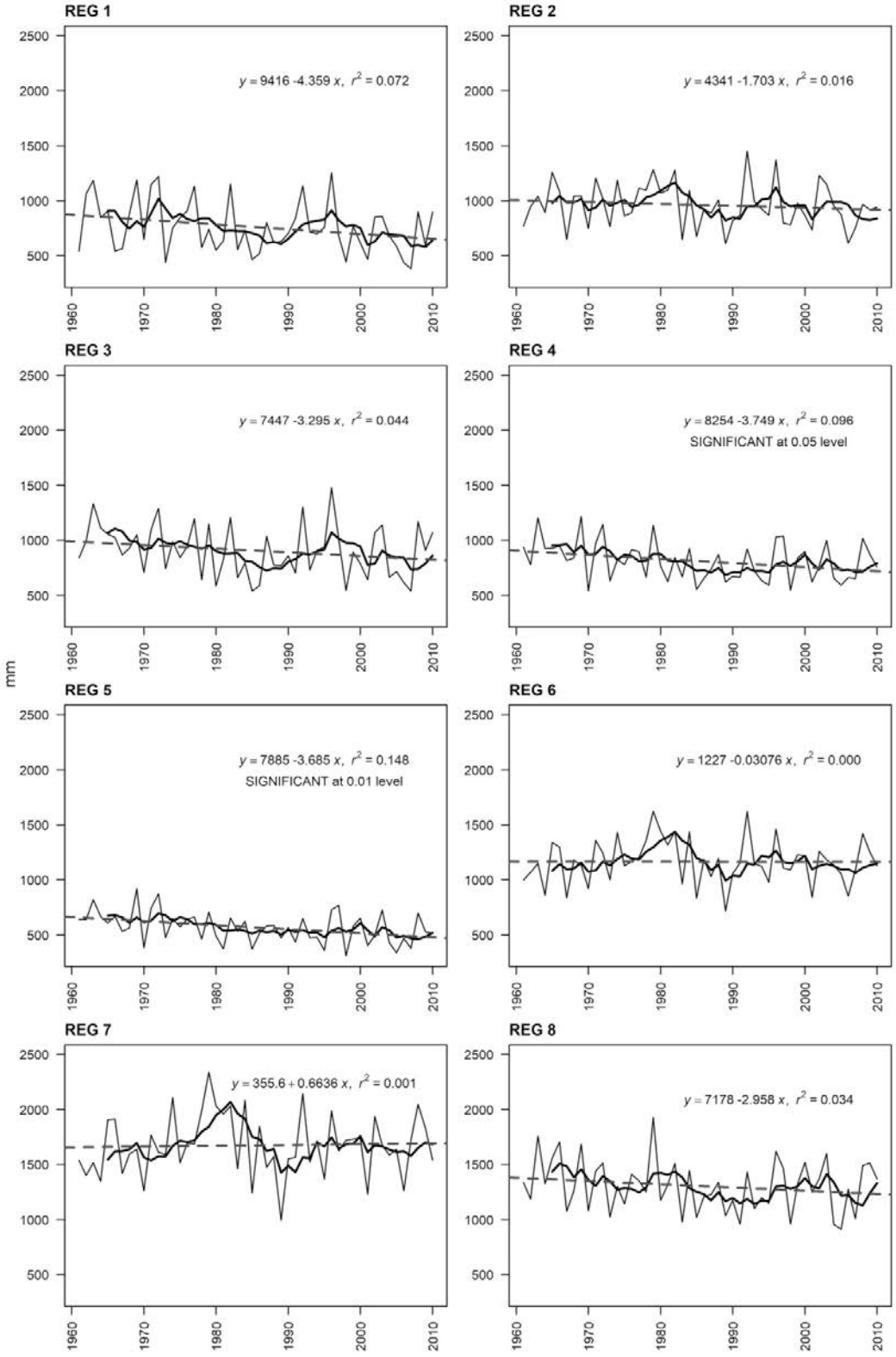

Fig. 11. Annual temporal evolution of precipitation (mm) over each cluster region. Linear regression (dashed line) and 5-year moving average (continuous line) are shown for each precipitation region.

zonal or subzonal arrangement of the regions obtained, in accordance with the layout of the mountain range; (2) there is a certain distribution between regions of Mediterranean filiation (1 and 3) and Atlantic regions (7 and 8), which is consistent with the influence of the two large bodies of water; and (3) the northern regions and those of Atlantic influence receive more precipitation than the eastern ones or those subjected to Mediterranean influence, although the MDP may be high in these. By order, region 1 constitutes a clear definition of Mediterranean precipitation, since it is strongly influenced by GAM 16, which accounts for 18.7% of the region's rainfall efficiency. In other words, the episodes defined by GAM 16 are those that contribute with the highest daily precipitation in this area. Region 2 shows the influence of the northern and north-eastern component advection (GAM 12, GAM 16 and GAM 17), as these retain all precipitation on the northern slope of the Pyrenees, accounting for 35% of precipitation efficiency. Region 3 is located in the south of the previous region, which implies a loss of efficiency of the GAM associated with northern advection. In this sense, GAM 16 takes first place (14.2%) and GAM 5 comes second (8.9%), and the latter model is characterized by a cyclonic south-western advection; these constitute the most effective episodes. Regions 4 and 5 have the most effective GAM in common, which in this case are GAM 5, GAM 11 and GAM 16. The basic difference between these two regions is that the former is wetter than the latter. Region 6 is located mainly in the north and northeast of the study area; this region reproduces the same distribution of percentages as in region 2, but in this case, the efficiency of GAM 11 (9.6%), GAM 12 (11.2%) and GAM 17 (13.0%) is higher. Moreover, GAM 16 is very productive (12.1%). Region 7, the wettest one, receives a high contribution from GAM 17 (14.2%), because of the strong influence of northern advection. GAM 12 is the second most effective (11.4%) in region 7. In addition, the location of region 7 close to the Atlantic Ocean causes western cyclonic advection to be highly productive (GAM 11: 9.4%). Lastly, region 8 is characterized by very efficient precipitation, under GAM 5 and GAM 11 i.e., western and south-western advection. Under these advections, region 8 is windward to the western mass of air, thus generating abundant precipitation in this sector. In comparison to previous studies, the final map produced herein (Fig. 10) contains a more comprehensive and continuous spatial regionalisation than the classification provided in Lemus-Canovas et al. (submitted), in which the fine spatial resolution employed to perform the classification implied more discontinuous and heterogeneous regions. Baeriswyl and Rebetez (1997) presented a clearly stratified regionalization of yearly precipitation for Switzerland, obtaining a total of 13 stratified regions for the 1981–1993 period, which were divided into a set of central regions and other more peripheral ones.

In relation to the annual precipitation tendencies of each region (Fig. 11), most series do not show a statistically significant trend, apart from regions 4 and 5, which exhibit a statistically significant decrease in precipitation. These are, at the same time, two of the driest regions in the Pyrenees area and both are located on the southern slope.

5. Conclusions

Heretofore the spatial distribution of mean daily precipitation values based on different circulation weather types (CWT) in the Pyrenees has not been established due to the difficulty involved in providing a dense climatic dataset for this area, and because of the difficulty of working with areas presenting complex orography and a high spatial variability of precipitation. The synoptic classification generated 20 different atmospheric circulation types, with a set of days from the 1961–2010 period assigned to each one. Concretely, we obtained 7 CWT associated with anticyclonic types (41.7% of total days) and 5 CWT were linked to cyclonic types (26.8%). Finally, the remaining 8 CWT (31.5%) were classified as types presenting a weak pressure gradient.

These 20 types of circulation were directly related to the mean daily precipitation (MDP) values, which were spatially interpolated by means of different parametric regression methods (GLM and RK) and semi-parametric (GAM) methods. Finally, a clustering process was performed to regionalise precipitation regions in the study area; we also generated annual precipitation series to estimate precipitation trends.

The results obtained from the annual trend of the daily frequency of the CWTs indicated a statistically significant decrease in CWTs dominated by low pressures, i.e. types that denote high MDP records. On the other hand, 4 circulation types with a predominance of high pressures and low MDP values tended to show a significant increase during the study period (1961–2010). As for the accuracy of the MDP models, the RK method is generally the one that provided the greater goodness of fit (16 of 20 models), followed by the GAM method (4 of 20), although both methods produced very similar errors in relation to the averaged error of all models, with a RMSE of 0.74 mm and 0.80 mm, respectively. Individually, the best-adjusted models were those that present a clear spatial gradation of MDP values; these models are usually associated with cyclonic circulation types and with a clear advection, and therefore with high MDP values. On the other hand, the models that produced the highest error were the ones linked to a CWT with high pressures and generally exhibiting a weak barometric gradient and a low MDP.

We used the classification of precipitation models proposed in this paper to obtain 8 regions exhibiting differentiated precipitation characteristics. It should be pointed out that two regions present a statistically significant annual tendency towards a decrease in precipitation; both regions are located in the south of the study region. To conclude, the results contributed by our research constitute an important advance with regard to characterising precipitation in the Pyrenees, a task that heretofore had not been performed. In addition, our paper presents a methodological proposal for the climatic regionalization of precipitation regimes in mountain areas.

Acknowledgments

The present study was funded by CENMA-IEA (FBIG309591), by the Water Research Institute of the University of Barcelona, and by the WEMOTOR Project (CSO2014 -55799-C2-1-R) of the Spanish Ministry of Science, Innovation and Universities. The present research was conducted within the framework of the Climatology Group of the University of Barcelona (2017 SGR 1362, Catalonia Regional Govt.), the CLICES project (CGL2017-83866-C3-2-R) of the Spanish Ministry of Science, Innovation and Universities. This study was benefited from the daily data base generated in the CLIM'PY project: 'Characterization of the evolution of climate and provision of information for adaptation in the Pyrenees' (EFA081/015), funded by INTERREG V-A Spain-France-Andorra Program (POCTEFA 2014-2020). CENMA-IEA also acknowledges the Government of the Principality of Andorra for the 2015 complementary grant to the European POCTEFA 2014-2020 Program, Ref. AUEP002-AND/2015. M.L-C is granted with a pre-doctoral FPU Grant (Spanish Ministry of Education, Culture and Sports).

Appendix A. Supplementary data

Supplementary data to this article can be found online at https://doi.org/10.1016/j.atmosres.2019.01.018.

References

Aalto, J., Pirinen, P., Heikkinen, J., Venäläinen, A., 2013. Spatial interpolation of monthly climate data for Finland: comparing the performance of kriging and generalized additive models. Theor. Appl. Climatol. 112, 99–111. https://doi.org/10.1007/s00704-012-0716-9.

Baeriswyl, P.-A., Rebetez, M., 1997. Regionalization of precipitation in Switzerland by means of principal component analysis. Theor. Appl. Climatol. 58, 31–41. https://doi.org/10.1007/BF00867430.

Batalla, M., Ninyerola, M., Trapero, L., Esteban, P., 2016. ACDA: andorran climate digital atlas (period 1981-2010). Map server. Institut d'Estudis Andorrans (IEA), Universitat Autònoma de Barcelona (UAB). http://www.acda.ad.

Beguería, S., Vicente-Serrano, S.M., López-Moreno, J.I., García-Ruiz, J.M., 2009. Annual and seasonal mapping of peak intensity, magnitude and duration of extreme precipitation events across a climatic gradient, Northeast Spain. Int. J. Climatol. 29, 1759–1779. https://doi.org/10.1002/joc.1808.

Brunetti, M., Maugeri, M., Nanni, T., Simolo, C., Spinoni, J., 2014. High-resolution temperature climatology for Italy: interpolation method intercomparison. Int. J. Climatol. 34, 1278–1296. https://doi.org/10.1002/joc.3764.

Buisan, S.T., Saz, M.A., López-Moreno, J.I., 2015. Spatial and temporal variability of winter snow and precipitation days in the western and central Spanish Pyrenees. Int. J. Climatol. 35, 259–274. https://doi.org/10.1002/joc.3978.

Carro-Calvo, L., Ordóñez, C., García-Herrera, R., Schnell, J.L., 2017. Spatial clustering and meteorological drivers of summer ozone in Europe. Atmos. Environ. 167, 496–510. https://doi.org/10.1016/j.atmosenv.2017.08.050.

Casado, M.J., Pastor, M.A., Doblas-Reyes, F.J., 2010. Links between circulation types and precipitation over Spain. Phys. Chem. Earth Parts A/B/C 35, 437–447. https://doi.org/10.1016/j.pce.2009.12.007.

Cattell, R.B., 1966. The scree test for the number of factors. Multivariate Behav. Res. 1, 245–276. https://doi.org/10.1207/s15327906mbr0102_10.

R Core Team, 2018. R: A Language and Environment for Statistical Computing. R Foundation for Statistical Computing, Vienna. https://www.R-project.org/.

Cortesi, N., Trigo, R.M., Gonzalez-Hidalgo, J.C., Ramos, A.M., 2013. Modelling monthly precipitation with circulation weather types for a dense network of stations over Iberia. Hydrol. Earth Syst. Sci. 17, 665–678. https://doi.org/10.5194/hess-17-665-2013.

Cortesi, N., Gonzalez-Hidalgo, J.C., Trigo, R.M., Ramos, A.M., 2014. Weather types and spatial variability of precipitation in the Iberian Peninsula. Int. J. Climatol. 34, 2661–2677. https://doi.org/10.1002/joc.3866.

Crespi, A., Brunetti, M., Lentini, G., Maugeri, M., 2018. 1961–1990 high-resolution monthly precipitation climatologies for Italy. Int. J. Climatol. 38, 878–895. https://doi.org/10.1002/joc.5217.

Dayan, U., Levy, I., 2005. The influence of meteorological conditions and atmospheric circulation types on PM $_{10}$ and visibility in tel aviv. J. Appl. Meteorol. 44, 606–619. https://doi.org/10.1175/JAM2232.1.

Eastman, J.R., 1987–1997. Idrisi. Users' Guide. Clark University, Worcester, MA.

Esteban, P., Jones, P.D., Martín-Vide, J., Mases, M., 2005. Atmospheric circulation patterns related to heavy snowfall days in Andorra, Pyrenees. Int. J. Climatol. 25, 319–329. https://doi.org/10.1002/joc.1103.

Esteban, P., Martin-Vide, J., Mases, M., 2006. Daily atmospheric circulation catalogue for western Europe using multivariate techniques. Int. J. Climatol. 26, 1501–1515. https://doi.org/10.1002/joc.1391.

Esteban, P., Ninyerola, M., Prohom, M., 2009. Spatial modelling of air temperature and precipitation for Andorra (Pyrenees) from daily circulation patterns. In: Theoretical and Applied Climatology, pp. 43–56. https://doi.org/10.1007/s00704-008-0035-3.

Fernández-González, S., del Río, S., Castro, A., Penas, A., Fernández-Raga, M., Calvo, A.I., Fraile, R., 2011. Connection between NAO, weather types and precipitation in León, Spain (1948–2008). Int. J. Climatol. 32https://doi.org/10.1002/joc.2431. n/a-n/a.

García, C., Martí, G., García, A., Muntán, E., Oller, P., Esteban, P., 2007. Weather and snow pack conditions of major avalanches in the Eastern Pyrenees. In: Proceedings of the Alpine & Snow Workshop, pp. 49–56.

Goodess, C.M., Jones, P.D., 2002. Links between circulation and changes in the characteristics of Iberian rainfall. Int. J. Climatol. 22, 1593–1615. https://doi.org/10.1002/joc.810.

Goodess, C.M., Palutikof, J.P., 1998. Development of daily rainfall scenarios for Southeast Spain using a circulation-type approach to downscaling. Int. J. Climatol. 18, 1051–1083. https://doi.org/10.1002/(SICI)1097-0088(199808)18:10<1051::AID-JOC304>3.0.CO;2-1.

Hastie, Trevor, 2017. gam: Generalized Additive Models. R Packageversion 1.14-4. https://CRAN.R-project.org/package=gam.

Hastie, T., Tibshirani, R., 1990. Generalized Additive Models. Chapman and Hall.

Hengl, T., Heuvelink, G.B.M., Rossiter, D.G., 2007. About regression-kriging: from equations to case studies. Comput. Geosci. 33, 1301–1315. https://doi.org/10.1016/J.CAGEO.2007.05.001.

Jones, P.D., Hulme, M., 1996. Calculating regional climatic time series for temperature and precipitation: methods and illustrations. Int. J. Climatol. 16, 361–377.

Kuhn, M., 2008. Caret package. J. Stat. Softw. 28 (5).

Lemus-Canovas, M., Ninyerola, M., Lopez-Bustins, J.A., Manguan, S., Garcia-Sellés, C., 2018. A mixed application of an objective synoptic classification and spatial regression models for deriving winter precipitation regimes in the Eastern Pyrenees. Int. J. Climatol. https://doi.org/10.1002/joc.5948.

Lopez-Bustins, J.A., Serrano, E., Ayarzagüena, B., Sanchez-Lorenzo, A., 2015. Spatial and temporal temperature trends in the lower stratosphere during the extended boreal winter from reanalyses. Int. J. Climatol. 35, 3888–3901. https://doi.org/10.1002/joc.4253.

Lorenzo, M.N., Taboada, J.J., Gimeno, L., 2008. Links between circulation weather types and teleconnection patterns and their influence on precipitation patterns in Galicia (NW Spain). Int. J. Climatol. 28, 1493–1505. https://doi.org/10.1002/joc.1646.

Lorenzo, M.N., Ramos, A.M., Taboada, J.J., Gimeno, L., 2011. Changes in present and future circulation types frequency in northwest iberian peninsula. PLoS One 6, e16201. https://doi.org/10.1371/journal.pone.0016201.

Mahalanobis, P.C., 1936. On the generalized distance in statistics. In: Proceedings of the National Institute of Sciences of India. 2. pp. 49–55.

Makra, L., Sánta, T., Matyasovszky, I., Damialis, A., Karatzas, K., Bergmann, K.C., Vokou, D., 2010. Airborne pollen in three European cities: Detection of atmospheric circulation pathways by applying three-dimensional clustering of backward trajectories. J. Geophys. Res.-Atmos. 115, D24220. https://doi.org/10.1029/2010JD014743.

McCullagh, P., Nelder, J.A., 1989. Generalized Linear Models. Chapman and Hall.

Morata, A., Martín, M.L., Luna, M.Y., Valero, F., 2006. Self-similarity patterns of precipitation in the Iberian Peninsula. Theor. Appl. Climatol. 85, 41–59. https://doi.org/10.1007/s00704-005-0175-7.

Muñoz-Díaz, D., Rodrigo, F.S., 2006. Seasonal rainfall variations in Spain (1912–2000) and their links to atmospheric circulation. Atmos. Res. 81, 94–110. https://doi.org/10.1016/j.atmosres.2005.11.005.

Ninyerola, M., Pons, X., Roure, J.M., 2000. A methodological approach of climatological modelling of air temperature and precipitation through GIS techniques. Int. J. Climatol. 20, 1823–1841. https://doi.org/10.1002/1097-0088(20001130)20:14<1823::AID-JOC566>3.0.CO;2-B.

Ninyerola, M., Pons, X., Roure, J.M., 2007. Monthly precipitation mapping of the Iberian Peninsula using spatial interpolation tools implemented in a Geographic Information System. Theor. Appl. Climatol. 89, 195–209. https://doi.org/10.1007/s00704-006-0264-2.

Paredes, D., Trigo, R.M., Garcia-Herrera, R., Trigo, I.F., 2006. Understanding precipitation changes in iberia in early spring: weather typing and storm-tracking approaches. J. Hydrometeorol. 7, 101–113. https://doi.org/10.1175/JHM472.1.

Pascual, R., Callado, A., Terradelles, E., Téllez, B., 2009. Influence of spring snowpack melting on thunderstorm activity in the Catalan Pyrenees. In: Plinius Conference Abstracts. 11th Plinius Conference on Mediterranean Storms.11, Plinius11-124, 2009.

Pebesma, E.J., 2004. Multivariable geostatistics in S: the gstat package. Comput. Geosci. 30, 683–691. https://doi.org/10.1016/J.CAGEO.2004.03.012.

Peña-Angulo, D., Brunetti, M., Cortesi, N., Gonzalez-Hidalgo, J.C., 2016. A new climatology of maximum and minimum temperature (1951–2010) in the Spanish mainland: a comparison between three different interpolation methods. Int. J. Geogr. Inf. Sci. 30, 2109–2132. https://doi.org/10.1080/13658816.2016.1155712.

Philipp, A., Beck, C., Huth, R., Jacobeit, J., 2016. Development and comparison of circulation type classifications using the COST 733 dataset and software. Int. J. Climatol. 36, 2673–2691. https://doi.org/10.1002/joc.3920.

Poli, P., Hersbach, H., Dee, D.P., Berrisford, P., Simmons, A.J., Vitart, F., Laloyaux, P., Tan, D.G., Peubey, C., Thépaut, J., Trémolet, Y., Hólm, E.V., Bonavita, M., Isaksen, L., Fisher, M., 2016. ERA-20C: an atmospheric reanalysis of the twentieth century. J. Climate 29, 4083–4097. https://doi.org/10.1175/JCLI-D-15-0556.1.

Pons, X., Ninyerola, M., 2008. Mapping a topographic global solar radiation model implemented in a GIS and refined with ground data. Int. J. Climatol. 28, 1821–1834. https://doi.org/10.1002/joc.1676.

Quéno, L., Vionnet, V., Dombrowski-Etchevers, I., Lafaysse, M., Dumont, M., Karbou, F., 2016. Snowpack modelling in the Pyrenees driven by kilometric-resolution meteorological forecasts. Cryosphere 10, 1571–1589. https://doi.org/10.5194/tc-10-1571-2016.

Ramos, A.M., Ramos, R., Sousa, P., Trigo, R.M., Janeira, M., Prior, V., 2011. Cloud to ground lightning activity over Portugal and its association with circulation weather types. Atmos. Res. 101, 84–101. https://doi.org/10.1016/J.ATMOSRES.2011.01.014.

Ramos, A.M., Cortesi, N., Trigo, R.M., 2014. Circulation weather types and spatial variability of daily precipitation in the Iberian Peninsula. Front. Earth Sci. 2, 25. https://doi.org/10.3389/feart.2014.00025.

Richman, M.B., 1986. Rotation of principal components. J. Climatol. 6, 293–335. https://doi.org/10.1002/joc.3370060305.

Romero, R., Ramis, C., Guijarro, J.A., 1999. Daily rainfall patterns in the Spanish Mediterranean area: an objective classification. Int. J. Climatol. 19, 95–112. https://doi.org/10.1002/(SICI)1097-0088(199901)19:1<95::AID-JOC344>3.0.CO;2-S.

Stauffer, R., Mayr, G.J., Messner, J.W., Umlauf, N., Zeileis, A., 2017. Spatio-temporal precipitation climatology over complex terrain using a censored additive regression model. Int. J. Climatol. 37, 3264–3275. https://doi.org/10.1002/joc.4913.

Trigo, R.M., Dacamara, C.C., 2000. Circulation weather types and their influence on the precipitation regime in Portugal. Int. J. Climatol. Int. J. Clim. 20, 1559–1581.

Tveito, O.E., European Cooperation in the Field of Scientific and Technical Research, 2008. The Use of Geographic Information Systems in Climatology and Meteorology: COST Action 719 : Final Report. Office for Official Publications of the European Communities.

Vicente-Serrano, S.M., López-Moreno, J.I., 2006. The influence of atmospheric circulation at different spatial scales on winter drought variability through a semi-arid climatic gradient in Northeast Spain. Int. J. Climatol. 26, 1427–1453. https://doi.org/10.1002/joc.1387.

Vicente-Serrano, S.M., Beguería, S., López-Moreno, J.I., El Kenawy, A.M., Angulo-Martínez, M., 2009. Daily atmospheric circulation events and extreme precipitation risk in Northeast Spain: Role of the North Atlantic Oscillation, the Western Mediterranean Oscillation, and the Mediterranean Oscillation. J. Geophys. Res. 114, D08106. https://doi.org/10.1029/2008JD011492.

Willmott, C.J., 1982. Some comments on the Evaluation of Model Performance. Bull. Am. Meteorol. Soc. 63, 1309–1313. https://doi.org/10.1175/1520-0477(1982)063<1309:SCOTEO>2.0.CO;2.

Zscheischler, J., Mahecha, M.D., Harmeling, S., 2012. Climate classifications: the value of unsupervised clustering. Proc. Comput. Sci. 9, 897–906. https://doi.org/10.1016/J.PROCS.2012.04.096.

3.3. Caracterització d'esdeveniments de precipitació extrema als Pirineus. De l'escala local a l'escala sinòptica

3.3.1. Resum de l'article

Els sistemes muntanyosos de la regió mediterrània, per exemple, els Pirineus, són molt sensibles al canvi climàtic. En el present estudi es quantifica la magnitud dels esdeveniments de precipitació extrema i el nombre de dies amb precipitació torrencial (precipitació diària ≥ 100 mm) en tots els pluviòmetres oficials disponibles al Pirineu per al període 1981-2015, analitzant la contribució de l'escala sinòptica en aquest tipus d'esdeveniments. Les zones més orientals –sota influència mediterrània– i nord-occidentals –sota influència atlàntica– dels Pirineus registren el major nombre d'esdeveniments torrencials. Els esdeveniments diaris més intensos s'esperen a la part oriental, assolint els 400 mm per a un període de retorn de 200 anys. Les adveccions de nord sobre la Península Ibèrica, que presenten un índex zonal baix donen lloc a esdeveniments torrencials sobre el Pirineu occidental; i les adveccions de l'est afavoreixen les precipitacions extremes a l'àrea més oriental de la serralada. En el primer cas, la massa d'aire és de llarg recorregut, amb origen a la costa est d'Amèrica de Nord, promovent d'aquesta manera situacions de precipitació abundant al Pirineu occidental. En el cas dels esdeveniments torrencials a l'àrea oriental del Pirineu, la trajectòria de la massa d'aire que provoca els esdeveniments en aquestes zones és molt curta i s'origina, habitualment, a la conca de la Mediterrània occidental. L'índex de l'Oscil · lació de l'Atlàntic Nord (NAO) no influeix en l'ocurrència d'esdeveniments torrencials als Pirineus, ja que aquests esdeveniments estan estretament relacionats amb certes teleconnexions mediterrànies com l'Oscil · lació de la Mediterrània Occidental (WeMO).

3.3.2. Article

Lemus-Canovas, M., Lopez-Bustins, J. A., Martín-Vide, J., Halifa-Marin, A., Insua-Costa, D., Martinez-Artigas, J., Trapero, L., Serrano-Notivoli, R., & Cuadrat, J. M. (2021a). Characterisation of Extreme Precipitation Events in the Pyrenees: From the Local to the Synoptic Scale. Atmosphere, 12(6), 665. https://doi.org/10.3390/atmos12060665

atmosphere

MDPI

Article

Characterisation of Extreme Precipitation Events in the Pyrenees: From the Local to the Synoptic Scale

Marc Lemus-Canovas [1,*], Joan Albert Lopez-Bustins [1], Javier Martín-Vide [1], Amar Halifa-Marin [2], Damián Insua-Costa [3], Joan Martinez-Artigas [1], Laura Trapero [4], Roberto Serrano-Notivoli [5] and José María Cuadrat [6]

1 Climatology Group, Department of Geography, University of Barcelona, c/Montalegre, 6, 08001 Barcelona, Spain; jlopezbustins@ub.edu (J.A.L.-B.); jmartinvide@ub.edu (J.M.-V.); joan.martinez.ar@gmail.com (J.M.-A.)
2 Regional Atmospheric Modelling (MAR) Group, Department of Physics, Regional Campus of International Excellence Campus Mare Nostrum (CEIR), University of Murcia, 30100 Murcia, Spain; amar.halifa@um.es
3 CRETUS, Non-Linear Physics Group, University of Santiago de Compostela, 15705 Santiago de Compostela, Spain; damian.insua@usc.es
4 Snow and Mountain Research Center of Andorra (CENMA-IEA), Av. Rocafort 21-23, AD600 Sant Julià de Lòria, Spain; ltrapero@iea.ad
5 Department of Geography, Autonomous University of Madrid, 28049 Madrid, Spain; roberto.serrano@uam.es
6 Department of Geography and Regional Planning, University of Zaragoza, 50009 Zaragoza, Spain; cuadrat@unizar.es
* Correspondence: mlemus@ub.edu

Citation: Lemus-Canovas, M.; Lopez-Bustins, J.A.; Martín-Vide, J.; Halifa-Marin, A.; Insua-Costa, D.; Martinez-Artigas, J.; Trapero, L.; Serrano-Notivoli, R.; Cuadrat, J.M. Characterisation of Extreme Precipitation Events in the Pyrenees: From the Local to the Synoptic Scale. *Atmosphere* **2021**, *12*, 665. https://doi.org/10.3390/atmos12060665

Academic Editor: Alexandre M. Ramos

Received: 26 April 2021
Accepted: 19 May 2021
Published: 22 May 2021

Publisher's Note: MDPI stays neutral with regard to jurisdictional claims in published maps and institutional affiliations.

Abstract: Mountain systems within the Mediterranean region, e.g., the Pyrenees, are very sensitive to climate change. In the present study, we quantified the magnitude of extreme precipitation events and the number of days with torrential precipitation (daily precipitation $\geq$ 100 mm) in all the rain gauges available in the Pyrenees for the 1981–2015 period, analyzing the contribution of the synoptic scale in this type of event. The easternmost (under Mediterranean influence) and north-westernmost (under Atlantic influence) areas of the Pyrenees registered the highest number of torrential events. The heaviest events are expected in the eastern part, i.e., 400 mm day^{-1} for a return period of 200 years. Northerly advections over the Iberian Peninsula, which present a low zonal index, i.e., implying a stronger meridional component, give rise to torrential events over the western Pyrenees; and easterly advections favour extreme precipitation over the eastern Pyrenees. The air mass travels a long way, from the east coast of North America, bringing heavy rainfall to the western Pyrenees. In the case of the torrential events over the eastern Pyrenees, the trajectory of the air mass causing the events in these areas is very short and originates in the Mediterranean Basin. The North Atlantic Oscillation (NAO) index has no influence upon the occurrence of torrential events in the Pyrenees, but these events are closely related to certain Mediterranean teleconnections such as the Western Mediterranean Oscillation (WeMO).

Keywords: backward trajectory; extreme precipitation; Mediterranean region; Pyrenees; return period; teleconnection indices; weather type

1. Introduction

The climate of the Pyrenees, in southwestern Europe, is especially diverse, due to the orographic complexity of the sector. The Pyrenees are located in the geographical transition between the wet mild domain of the mid-latitudes and the arid area of the subtropical anticyclone belt. Both its marked topography and its location between two climatically differentiated basins, the Mediterranean and Atlantic basins, mean that this mountain area presents a highly variable climate. The precipitation variability in this area has been extensively studied [1–3] since it is clearly associated with different natural hazards in the

Pyrenees, such as avalanches [4–6], heavy snowfall [7–9], or flood events [10–12], among many others.

These natural hazards, particularly floods, can be triggered by torrential rainfall [13,14]. Insua-Costa et al. [14] were able to precisely characterise 1991 hazardous precipitation events into four main weather types and an extra one for low gradient pressure situations. This highlights the need to study atmospheric patterns involving this type of torrential event. However, most studies that characterize atmospheric patterns are based upon a "Circulation-to-Environment" approach; this means that the atmospheric circulation in a particular area is previously characterized and its implications for a given atmospheric/environmental variable at local scale are subsequently monitored [15,16]. Examples of this approach are widespread in the Pyrenees area. For example, Esteban et al. [17] modelled daily mean precipitation and temperature in Andorra for different circulation types, the latter obtained through principal component analysis (PCA) applied to an S-mode matrix [7] and subsequent clustering with k-means; similarly, Lemus-Canovas [18] employed statistical regression techniques to perform a synoptic classification focused on SW Europe aimed at mapping the daily mean precipitation of each weather type over the whole Pyrenees. Other examples of this type of approach can be found in different parts of the Iberian Peninsula [19–23], frequently using the objective Lamb approach [19,24]. However, another approach for characterising atmospheric patterns related to torrential events is known as "Environment-to-Circulation". It involves selecting days of interest (e.g., days with precipitation $\geq$100 mm) and creating a synoptic classification with these torrential days [14], or simply averaging the synoptic variable of interest on the days in which a given threshold is surpassed at the surface in order to finally perform a synoptic composite [25]. This type of approach has been applied to NE Iberia [26], Iberia [27], Southern Europe [14,28] and to other areas of the world, such as Japan [29] and Northern Chile [30], among others. In the abovementioned studies [14,26,27], the most commonly used approach to classify these extreme events is a PCA applied to a T-mode matrix. However, it has never been applied to the whole Pyrenees sector, a fact that constitutes a knowledge gap in relation to the synoptic characterization of torrential events in this region. Precisely, heavy precipitation is the product of two significant factors: a large amount of water vapour in the atmosphere and the upward flow of air, which generates the condensation of water vapour and subsequent precipitation. The Clausius–Clapeyron equation [31] provides a strong thermodynamic relationship between temperature and water vapour. Future climate projections indicate a greater increase in extreme precipitation than in the mean annual total precipitation [32].

In this sense, the main objective of this study involves describing in detail the spatial and temporal behavior of torrential rainfall in the Pyrenees, in order to subsequently synoptically characterize such events and to establish the origin of the air masses driving such episodes. The specific objectives are: (i) to compute the annual maximum daily precipitation values from different return periods, and to quantify the number of days with torrential precipitation (daily precipitation $\geq$ 100 mm) and establish its temporality; (ii) to characterize the large-scale atmospheric patterns causing such torrential events ($\geq$100 mm); and (iii) to employ a backward trajectory analysis in order to determine the main trajectories of the air masses giving rise to the occurrence of torrential events.

2. Data and Methods

2.1. Data

Daily precipitation was extracted from the database of the CLIMPY Project (Characterisation of evolution of climate and provision of information for adaptation in the Pyrenees), a transboundary project intended to establish a detailed analysis of recent trends in temperature, precipitation, and snow cover in the Pyrenees [33]. Only the weather stations containing at least 90% of the data in the 1981–2015 period (158 in total) were considered when counting the torrential events (Figure 1). For the computation of return periods, we only used observatories providing a complete record in their data series. All series were

subjected to a previous quality control process described in Serrano-Notivoli et al. [34]. The spatial and altitudinal distribution of weather stations is generally homogeneous, except for the central Pyrenees, for which no historical records meet the criterion for data availability.

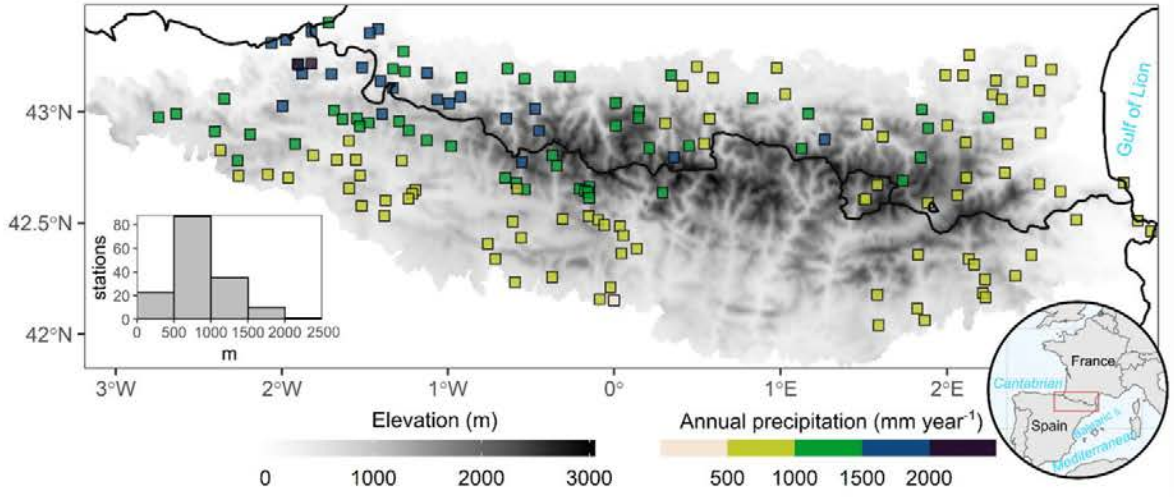

Figure 1. Pyrenees location (**bottom right**), elevation (**greyscale legend**) and spatial distribution of the rain gauges in the Pyrenees area and annual amounts of precipitation (**coloured squares**). At bottom left, a histogram shows the frequency of rain gauges per range of elevation. The black line shows the national boundaries.

We used mean sea level pressure (mslp), temperature at 850 hPa (t850) and geopotential height at 500 hPa (z500) to compute the synoptic classification. These gridded variables were supplied by the ERA-5 reanalysis [35] by means of daily mean values, encompassing the area 30° N–60° N and 20° W–20° E at a horizontal resolution of 0.25° for the 1981–2015 period. Finally, backward trajectories were computed by means of the Hysplit model [36], fed by the NCEP/NCAR reanalysis database [37] at a horizontal spatial resolution of 2.5°.

Additionally, we analysed the Western Mediterranean Oscillation (WeMO) [38], the Mediterranean Oscillation (MO) [39], the Upper-Level Mediterranean Oscillation (ULMO) [40] and the North Atlantic Oscillation (NAO) [41]. They are all at daily resolution and for the 1981–2015 period. The MO, NAO and WeMO indices were provided by the Climatic Research Unit (https://crudata.uea.ac.uk/cru/data/pci.htm, accessed on 16 May 2021), whilst the ULMO was furnished by the authors.

2.2. *Analysis of Extreme Events and Definition of Torrential Events*

To estimate the return level of precipitation given a specific return period (RP), we employed the generalized extreme value (GEV) distribution for extreme events. The cumulative distribution function of the GEV results from combining the Frechet, Gumbel and Weibull families of distributions in one single distribution function:

$$F(x) = \exp\left\{-\left[1+\xi\left(\frac{x-\mu}{\sigma}\right)\right]^{-1/\xi}\right\} \quad (1)$$

where three parameters (ξ, μ and σ) represent the shape, location and scale of the distribution function, respectively. The σ and $1 + \xi(x - \mu)/\sigma$ must be greater than zero. The specification of ξ will determine the behavior of the tail of the distribution so that, depending on the value of this parameter, any of the following distributions might be obtained:

- $\xi > 0$ giving the heavy-tailed (Frechet) case;
- $\xi = 0$ giving the light-tailed (Gumbel) case. For this case:

$$F(x) = \exp\left\{-\exp\left[-\left(\frac{x-\mu}{\sigma}\right)\right]\right\} \quad (2)$$

- $\xi < 0$ giving the bounded-tailed (Weibull) case.

The GEV family of distributions enables the annual daily maximum precipitation to be modelled with the use of the block maxima approach. This procedure consists of grouping the data into blocks of equal size—one for each year—and then fitting the GEV distribution to the set of maxima corresponding to each of the blocks.

Apart from the modeling of extremes by means of GEV analysis, torrential events were defined as days when daily accumulated precipitation ≥100 mm. A precipitation equal to or greater than 100 mm day^{-1} was the threshold used to identify heavy rainfall events in Catalonia (NE Iberia) [26,42,43], associated with an increase in soil erosion processes [44]. In addition, the precipitation threshold equal or greater than 100 mm day^{-1} could be considered equivalent to the 95th percentile or above across all precipitation series of the study area (Figure S1 of the Supplementary Material).

2.3. Synoptic Classification Approach and Circulation Composites

We applied a PCA to a T-mode (temporal) matrix of mslp, t850 and z500, where the variables (columns) were the 220 days displaying torrential precipitation and the cases (rows) were the grid points of ERA-5. Once the PCA was applied to the standardized data matrix, new variables were obtained, the principal components (PCs), which are linear combinations of the original variables. Subsequently, the PCs explaining most of the variance of the original data needed to be retained by conducting a Scree Test [45]. Once the PCs were retained, the components were rotated with a Varimax rotation in order to readjust the orthogonal combination of each PC to obtain a greater variance, which was explained by those PCs of lesser rank [46]. From the rotated PCs, we obtained the loading, i.e., the correlation matrix, which indicates the degree of correlation of each day with respect to each PC. In this sense, the assignment of each day to each of the PCs is based on the value of maximum positive correlation and minimum negative correlation. For example, day 1 is assigned to the highest absolute correlation, but subsequently retains the correlation symbol. For this reason, PC1 may be split into two groups, one for the days with the highest positive maximum correlation, and one for the days presenting the lowest negative correlation. This means that, if we retain 5 PCs, up to 10 weather types can be obtained. We used the R package synoptReg [15] to develop the synoptic classification.

To complement the explanation of the synoptic mechanisms that lead to such torrential events, we computed the vertically integrated water vapor transport (IVT) between the 1000 and 300 hPa levels, following the methodology proposed by Lavers et al. [47]:

$$IVT = \sqrt{\left(\frac{1}{g}\int_{1000hPa}^{300hPa} q \cdot u \cdot dp\right)^2 + \left(\frac{1}{g}\int_{1000hPa}^{300hPa} q \cdot v \cdot dp\right)^2} \quad (3)$$

where q is the specific humidity (kg kg^{-1}); u and v are the layer-averaged zonal and meridional winds (m s^{-1}), respectively; g is the acceleration due to gravity (m s^{-2}); and p is the pressure difference between two adjacent pressure levels (Pa).

Furthermore, the meridional and zonal components of the wind at 300 hPa were used to identify the positions of the polar jet during these torrential events.

2.4. Hysplit Model

The Hybrid Single Particle Lagrangian Integrated Trajectory (HYSPLIT) model enables trajectories of simple air particles to be computed, and their transport, dispersion, and deposition [36] to be simulated. It is one of the most widely used models in the atmospheric sciences to determine the origin of air masses and to define the source–receptor relationship [48,49]. The use of gridded climate data permits the HYSPLIT model to define the trajectory air parcel arriving at a specific location at a specific time on a specific date.

We used the NOAA Hysplit model to determine the backward trajectories of episodes equal to or greater than 100 mm at Darnius (easternmost Pyrenees) and Artikutza (westernmost Pyrenees); both of these locations possess the highest number of records above this threshold and in opposite geographical locations within the study area.

Meteorological data were obtained from the NCEP/NCAR Reanalysis database [37] with 2.5° resolution. The set-up of the model was based on mean sea level pressure, 850 hPa, and 500 hPa. With these settings, we obtained the back trajectories for 96 h, departing at 00, 06, 12 and 18 h for each of the torrential days during the 1981–2015 period.

3. Results and Discussion

3.1. Maximum Daily Precipitation for Different Return Periods

The GEV analysis provided the return levels for six RPs: 5, 10, 20, 50, 100 and 200 years (Figure 2). For a 5-year RP, maximum daily precipitation was generally estimated to be below 100 mm, except in the extreme east, where values of 150 mm day^{-1} were reached. The eastern Pyrenees is one of the areas receiving the most torrential episodes on the Iberian Peninsula [14,43]. For a 10-year RP, 100 mm day^{-1} was generally reached throughout the region, with over 150 mm per day in the northeastern Pyrenees. The same spatial pattern was repeated for a 20-year RP, with the northeastern region exceeding 200 mm day^{-1}. Interestingly, values of 150 mm day^{-1} were recorded in different observatories in the northwest of the study area. For the most extreme RPs (RP 100 and RP 200), 300 mm day^{-1} was easily exceeded on the eastern slope of the Pyrenees. Even in the extreme northeast, over 400 mm day^{-1} was recorded for a RP of 200 years. In the rest of the study area, several observatories in the west and south stand out, providing 200–300 mm day^{-1} for a 200-year RP. Intense NW wind circulation over the Iberian Peninsula can lead to heavy rainfall in non-typical Mediterranean climates such as that of the Western Pyrenees [39]. The areas presenting the lowest extremes were the central part of the northern slopes of the Pyrenees, where different observatories did not reach 150 mm day^{-1} for the highest RP (200 years).

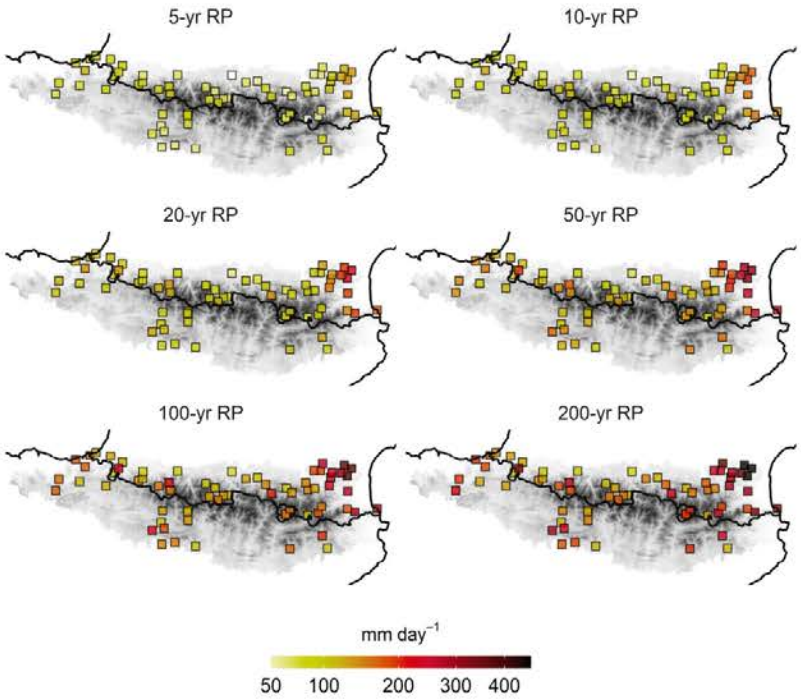

Figure 2. Return levels of maximum daily precipitation per year for 6 different return periods (RPs): 5, 10, 20, 50, 100 and 200 years. Only the stations with the complete series were used.

3.2. Characterisation of Torrential Events: Spatial Distribution and Seasonality

The frequency of torrential events exhibits certain well-defined spatial patterns. Figure 3a clearly shows the dependence on distance to the sea of the days with amounts equal to or greater than 100 mm in the eastern part of the study area [50]. Moreover, in the extreme west, the maximum was located slightly southward of the axis of the mountain range (Artikutza), whereas in the extreme east the torrential episodes spread over a wider strip, both north and south of the axis of the mountain range, with a maximum in Darnius (Figure 3a). The latter phenomenon might be caused by the N–S direction of the coast, which is at a right angle to the mountain range's W–E axis [51]. The remaining rain gauges depend, to a certain degree, upon altitude. The observatories situated at higher elevations also present a higher number of torrential days as a result of convective precipitation in summer.

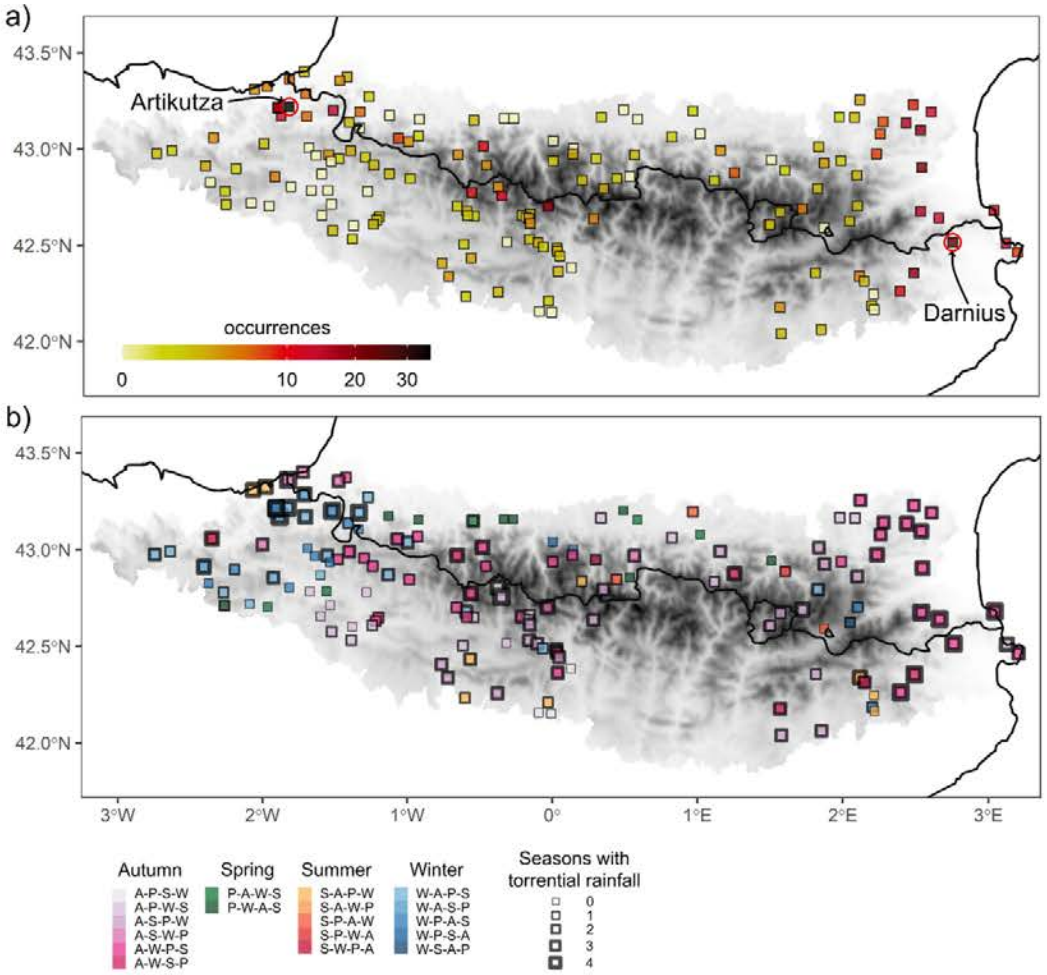

Figure 3. (**a**) Number of days with torrential rainfall for the 1981–2015 period. Location of Artikutza and Darnius rain gauges, which present the greatest number of torrential events (they are, therefore, used to calculate the backward trajectories with the Hysplit model in Section 3.4). (**b**) Seasonal torrential regimes in the Pyrenees: A (autumn), P (spring), S (summer), and W (winter). The border thickness of the box indicates the number of seasons with torrential rainfall, and the boxes with the thickest line, therefore, correspond to weather stations that recorded at least one event in winter as well as in spring, summer and autumn.

Figure 3b shows a great variety of days with seasonally distributed torrential precipitation in the Pyrenees, a fact that reinforces the pluviometric complexity of the study area. In addition, episodes are observed to be prevalent in winter in the westernmost extreme, when NW advections are frequent [18], and in autumn in the extreme east, when easterly flows are more intense [50]. On the Mediterranean coast, all seasons are perceived to present at least one episode of torrential rain. Moreover, the colour purple symbolises the season of the year with the most torrential events, autumn, followed by winter in most of rain gauges located in the area closest to the coastline. At the opposite end (west) of the study area, a large number of observatories indicate that the torrential event occurs mainly in winter, with a transition to the autumn months towards the centre and south of the study area. Spring and summer, however, have a lesser impact, only affecting the northernmost central part of the region and presenting no torrential episodes. Furthermore, the springtime precipitation regime has become less predominant over the Iberian Peninsula during the last few decades (1976–2005) due to an increase in autumn rainfall, with respect to the 1946–1975 period [52].

3.3. Large-Scale Attribution of Torrential Events

Based on the methodology described in Section 2.3, we obtained nine weather types (WT), since five PCs were retained, accounting for 80 % of the variance of the original data (Figure S2 of the Supplementary Material). Figure 4 presents the spatial representation of the mslp, t850 and z500 of the WTs. All of the synoptic patterns presented resulted in days with 100 mm or greater in a rain gauge. The high number of synoptic patterns (nine) is due to the geographical and pluviometric diversity of the study area, already seen in the previous maps (Figures 2 and 3), and the synoptic variety, which for this kind of event is already known in areas of the northeast of the Iberian Peninsula [26].

The most frequent synoptic pattern in the occurrence of torrential events is WT1, which is associated with 19.1% of the cases, and with an unequivocal seasonality in the cold half of the year (Figure S3 of the Supplementary Material). This WT is characterized by a low-pressure system near the surface in the Balearic Sea, which drives moist maritime winds to the easternmost area of the Pyrenees (Figure 5). In addition, this evident surface low is also accompanied by a low at 500 hPa and a below-average temperature at 850 hPa over the Iberian Peninsula. This WT1 is very well characterized by the negative phase of the WeMO (Figure 6) due to the combination of low surface pressure on the south of the Iberian Peninsula with high pressure in northern Italy in this type of situation [26]. Moreover, the MO presents clearly negative values when such a situation occurs. Figure 5 shows that for WT1 there is evidence of moisture advection in the extreme east of the Pyrenees, which increases the potential of these torrential events [53], whilst a meridional position of the jet stream with a north direction can be observed. Precisely, this WT1 is at its most effective in the eastern Pyrenees (Figure 7b), as well as in other areas of the western façade of the Iberian Peninsula [54], causing a large number of torrential events (Figure 7a). Due to its winter seasonality and negative temperature anomalies, the WT1 causes a significant fraction of these episodes to occur as snowfall [55]. WT2 (Figure 4) is characterized by a trough located at the northwest of the Iberian Peninsula and an increase in pressure towards eastern Europe, a situation which is very well characterized by both the WeMO and MO. The location of the low favours warm and moist air advection from the Mediterranean over the study area, with an increase in IVT intensity (Figure 5), giving rise to prefrontal precipitation [53]. This pattern can appear throughout the year, but its maximum frequency is in mid-autumn (Figure S3). Torrential rainfall during this synoptic situation is concentrated on the southern slope, as shown in Figure 7, as a result of this important moisture that was advected from subtropical origin. In fact, Insua-Costa et al. [56] recently showed that moisture advected via an atmospheric river from the tropical and subtropical Atlantic played a major role in a well-known case of this type, the November 1982 flood event. In addition, this type of episode has aroused interest in studying the physical mechanisms of high precipitation events related to this

synoptic pattern in the eastern Pyrenees [10,11]. WT3 and WT4 exhibit similar surface characteristics, although the former occurs in late summer and during autumn, and the latter mainly during the winter months (Figure S3). In both cases, north-northwesterly winds over the Pyrenees are involved. However, in WT4 the main action centres driving the northerly advection are more clearly defined: the Azores anticyclone in the west of the Iberian Peninsula and a depression in Italy, favouring positive values of the WeMO index (Figure 6). This indicates a stronger advection in WT4 than in WT3. The aforementioned phenomenon can also be observed depending on the intensity and direction of the IVT (Figure 5) and with a wind trajectory at 300 hPa (Figure S4), which is perpendicular to the Pyrenees, mainly in WT4. This brings abundant precipitation to most of the northern façade of the region (see Figure 7). Precisely, WT3 displays low pressure gradient over the Pyrenees, a common occurrence in summertime in this area when convective activity in the whole area is dominant [17]. Because of that, torrential situations under this weather type might not be persistent but rather stormy, a situation also defined in Pineda et al. [57].

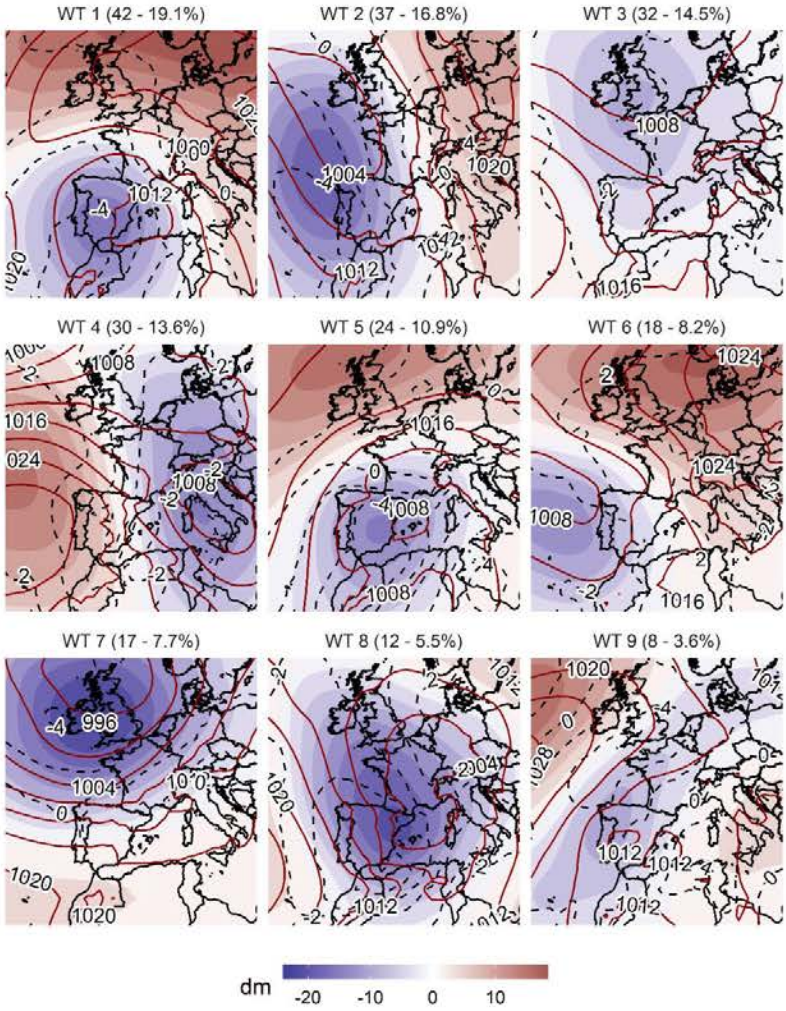

Figure 4. Mean sea level pressure (dark red contours, hPa), 500 hPa geopotential height anomalies (shaded colours, dam) and 850 hPa temperature anomalies (dashed contours) of the nine most frequent weather types associated with torrential precipitation in the western Mediterranean region. Above each map, the number of days assigned to each synoptic pattern and their percentages with respect to the total are shown in parentheses.

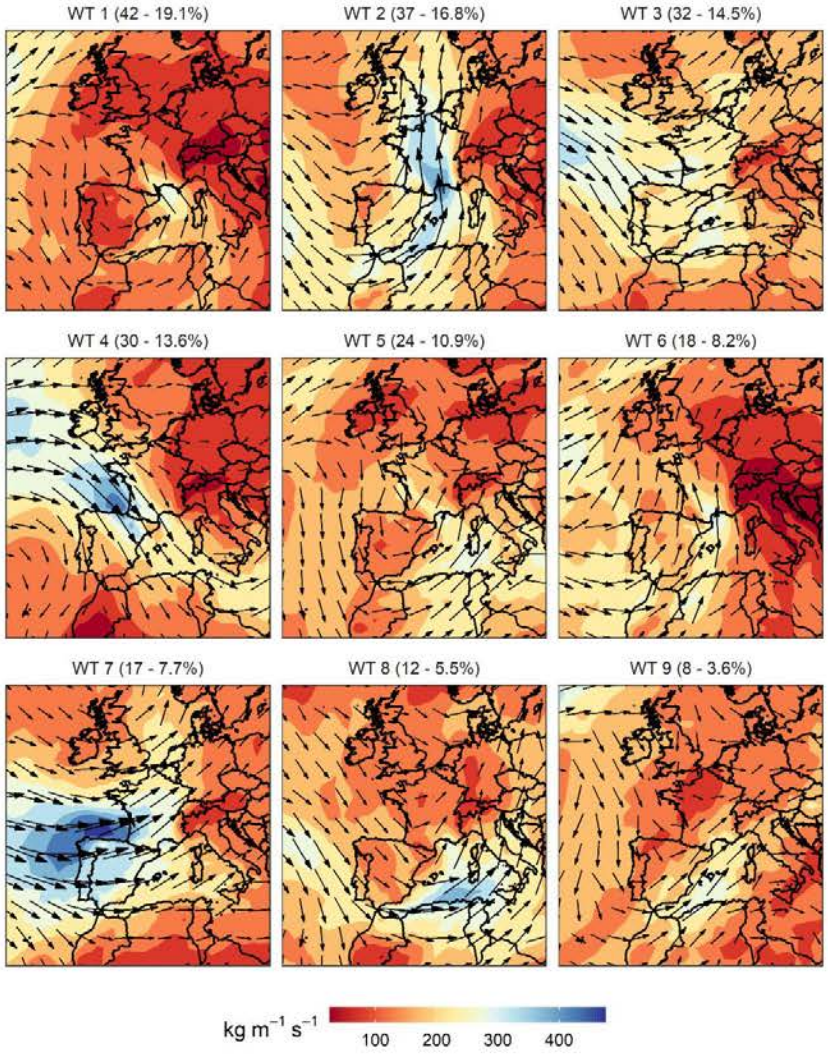

Figure 5. Vertically integrated water vapor transport (IVT) intensity (shaded colours, kg m^{-1} s^{-1}) and direction (vectors) of the 9 most frequent atmospheric patterns associated with torrential precipitation in the western Mediterranean region. Above each map, the number of days assigned to each synoptic pattern and their percentages with respect to the total are shown in parentheses.

As opposed to WT1, WT5 occurs more frequently in late spring and early autumn (Figure S3). This pattern reveals a surface depression over the Balearic Sea driving an east-northeasterly advection in the eastern area of the Pyrenees and a north-northeasterly advection in the westernmost area, favoring two poles of precipitation maxima in both areas (map 5, Figure 7b). Such a situation is captured very well by the ULMO teleconnection pattern, which represents the MO dipole, but at 500 hPa (Figure 5). WT6, with a depression to the northwest of the peninsula and an anticyclone in central Europe, favours a warm air advection from the south-southeast with a significant moisture content (Figure 5) that favors abundant precipitation in the eastern coastal area (Figure 7b), and also in the southernmost mountainous sector of the study area. This is one of the situations that is captured well by the negative phase of the WeMO (Figure 6), and it concisely explains the occurrence of torrential-type events in the extreme northeast of the Iberian Peninsula [49], and their pluviometric variability in general [51,58]. WT7 presents a high zonal gradi-

ent that favours westerly flows over the Iberian Peninsula with a long-lasting advection over the ocean, which causes significant moist advection over the Atlantic façade; this exhibits a temporal frequency centred in the months of October, November and December (Figure S3). This situation promotes notable precipitation in the western half of the Pyrenees, whereas, in the eastern half, this contribution is truncated because the advection loses all its moisture due to an adiabatic process of leeward compression. For this situation, no teleconnection pattern clearly defines the aforementioned atmospheric pattern, a fact also reported in Merino et al. [53]. WT8 exemplifies a widespread depressional situation centred over France, both on the surface and at 500 hPa, driving a northerly advection over the whole Pyrenees range; this advection is reinforced by a southward shift of the jet stream (Figure S4), and, by default, a displacement of the polar vortex from the Arctic region. The MO and ULMO provide the best definition of such a situation: a large depression over the western Mediterranean and an anticyclonic centre over the eastern Mediterranean. This kind of configuration causes widespread precipitation along the northern slope of the Pyrenees (Figure 7b), and, in some rain gauges in this northernmost part of the Pyrenees, this is the WT that causes the most torrential episodes (Figure 7a). Finally, WT9 presents a more residual frequency, and is characterised by a weak depression in the southeast of the peninsula that drives southeasterly surface winds transporting significant moisture and distributes the highest amount of precipitation over the southeastern extreme of the Pyrenees (Figure 7b).

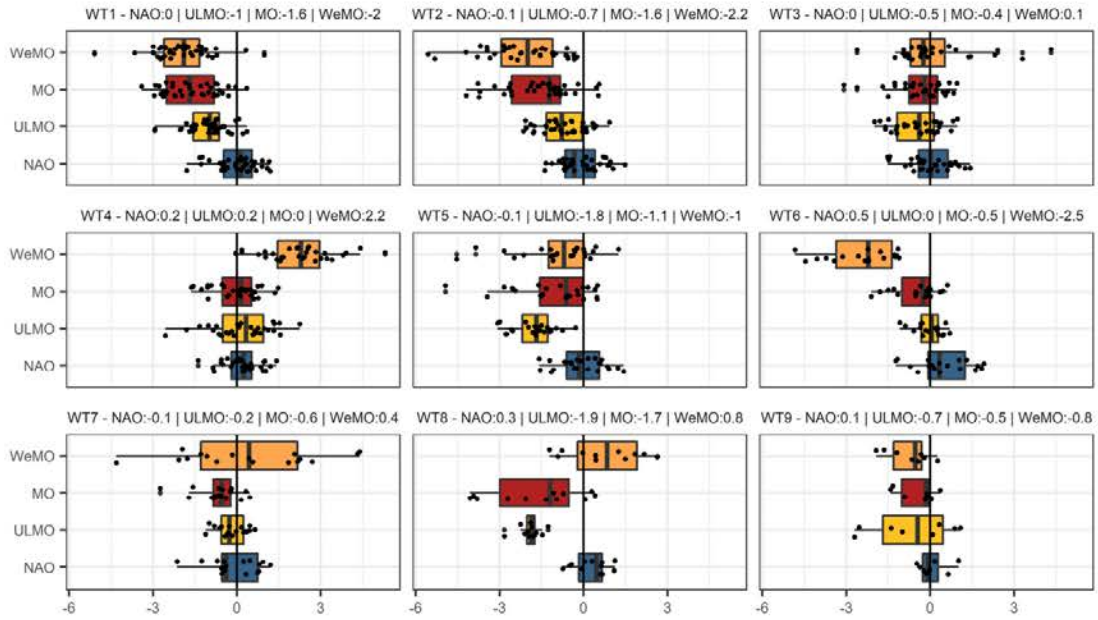

Figure 6. Distribution of daily values of the teleconnection indices for each weather type (WT). The mean value of each teleconnection index for each WT is shown in the header of each plot.

These results hardly reveal any influence of the NAO in any of the situations causing torrential precipitation events in the Pyrenees. Extreme precipitation events in northeastern Spain are not associated with the NAO index values [50]. The main influence of the NAO on rainfall over the Iberian Peninsula is observed in the central and southwestern parts [27,59]. Esteban et al. [60] found that winter rainfall over the southern central Pyrenees comes under the influence of the negative phase of the NAO, which is associated with southerly and southwesterly synoptic circulation (WT2 in Figure 7a). This can also be seen in the highest values of mean daily precipitation (25–50 mm) in WT2 (Figure 7b), which are mostly concentrated over the central area of the southern slope of the Pyrenees. The

amount reached for a 200-yr RP over the central-south slope of the Pyrenees is rather low (about 200 mm) in comparison with that amount over the extreme east (about 400 mm). This fact denotes a climate typically under Atlantic influence (NAO) in the central-south Pyrenees and a highly variable climate under Mediterranean influence (WeMO) in the easternmost Pyrenees. Esteban et al. [60] found no statistically significant correlation between precipitation over the north slope of the Pyrenees and the NAO index, a fact that is likely a result of the orography barrier.

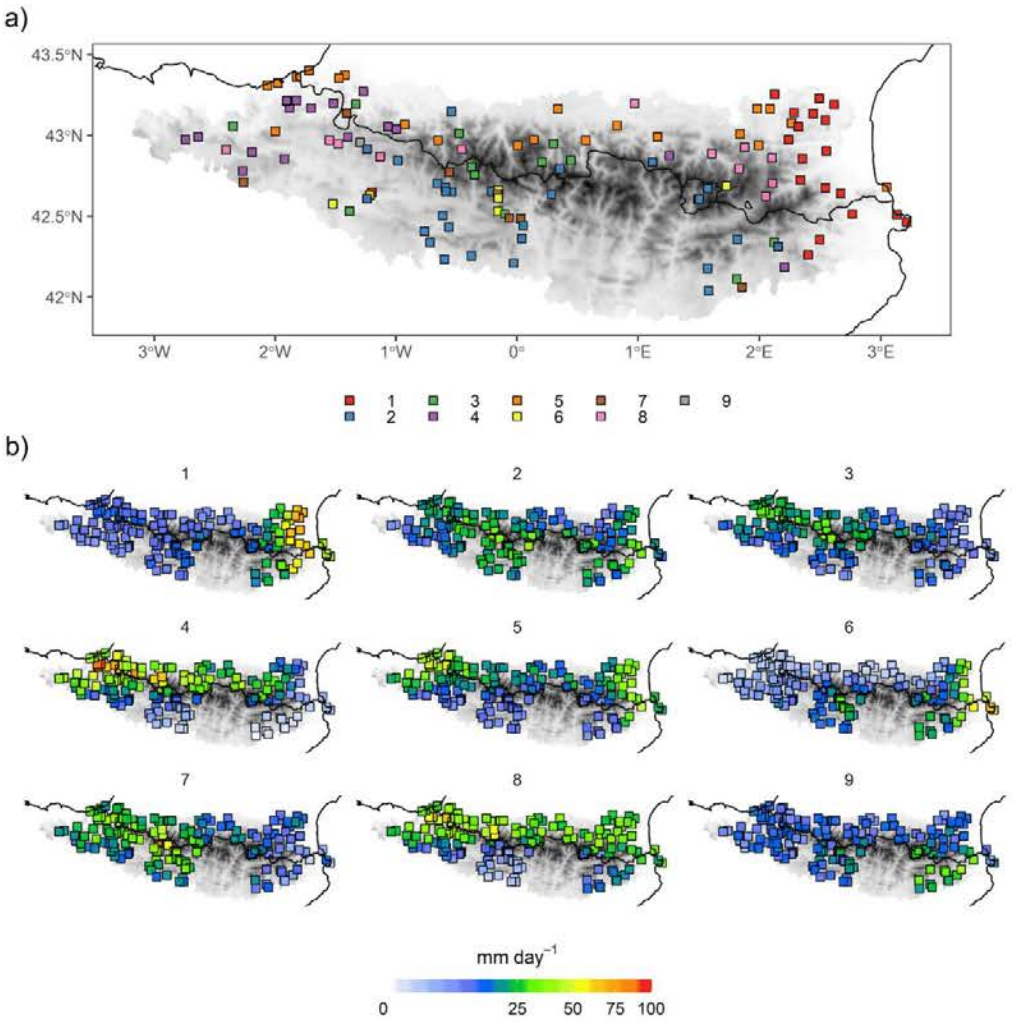

Figure 7. (**a**) Weather type (WT) with the maximum frequency in each rain gauge (each colour represents one of the nine WTs); (**b**) mean daily precipitation for each of the WTs.

3.4. Backward Trajectory Analysis

There is an unequivocal contrast between the backward trajectories of Artikutza and Darnius for the three altitudinal layers: 500 hPa (Figure 8a), 850 hPa (Figure 8b), and surface (Figure 8c). The first rain gauge is located at the northwestern end of the Pyrenees (Figure 3a), very close to the Atlantic coast, which implies a clear influence of the westerlies and the rapid westerly circulation. The second rain gauge is at the opposite (eastern) end of the Pyrenees, very close to the mediterranean coast (Figure 3a); it is in the lee side of the westerly flows and is clearly characterized by the Mediterranean climate. Most of

the trajectories at 500 hPa (Figure 8a) for Artikutza originate in the North Atlantic Ocean, implying a long maritime trajectory of the air particles, which come to favour synoptic patterns related to intense rainfall. Darnius is clearly different from the Artikutza, because at a height of 500 hPa a long trajectory is to be expected, but results reveal that most of the trajectories at that height are short, mainly of Mediterranean and subtropical Atlantic origins. In general, for the case of Darnius, the trajectory is short, but quite variable with regard to its origin, as noted in Pastor et al. [61], but for the Valencia region (Spain). The trajectories at 850 hPa (Figure 8b) do not reveal significant differences with respect to those at 500 hPa. They are shorter than those at 500 hPa as a result of atmospheric dynamics and surface friction. In the case of Darnius, it is worth noting that almost all the trajectories at 850 hPa are of Mediterranean origin (see WT1, WT5, and WT9 in Figure 4) or come from North Africa (see WT2 and WT6 in Figure 4). Finally, at the surface level (Figure 8c), the shortest trajectories are detected; these are clearly of North Atlantic origin in the case of Artikutza, which are clearly related to WT4 and WT7, although different situations exist which are characterized by trajectories of northern and even northeastern origin travelling over the Cantabrian Sea. In the case of Darnius, practically all the trajectories originate between the Balearic Sea, the Gulf of Lion and the Italian Peninsula; very occasionally, some trajectories originate in the North Atlantic. The surface trajectories for Darnius reveal a strong dependence on the local and mesoscale environments in the Mediterranean basin, as opposed to the rapid surface air circulation over Artikutza coming from a distant location, such as western Canada. Another remarkable fact involves the greater homogeneity in Artikutza than in Darnius at all levels with regard to the direction of the backward trajectories; these are mostly zonal and present very diverse origins.

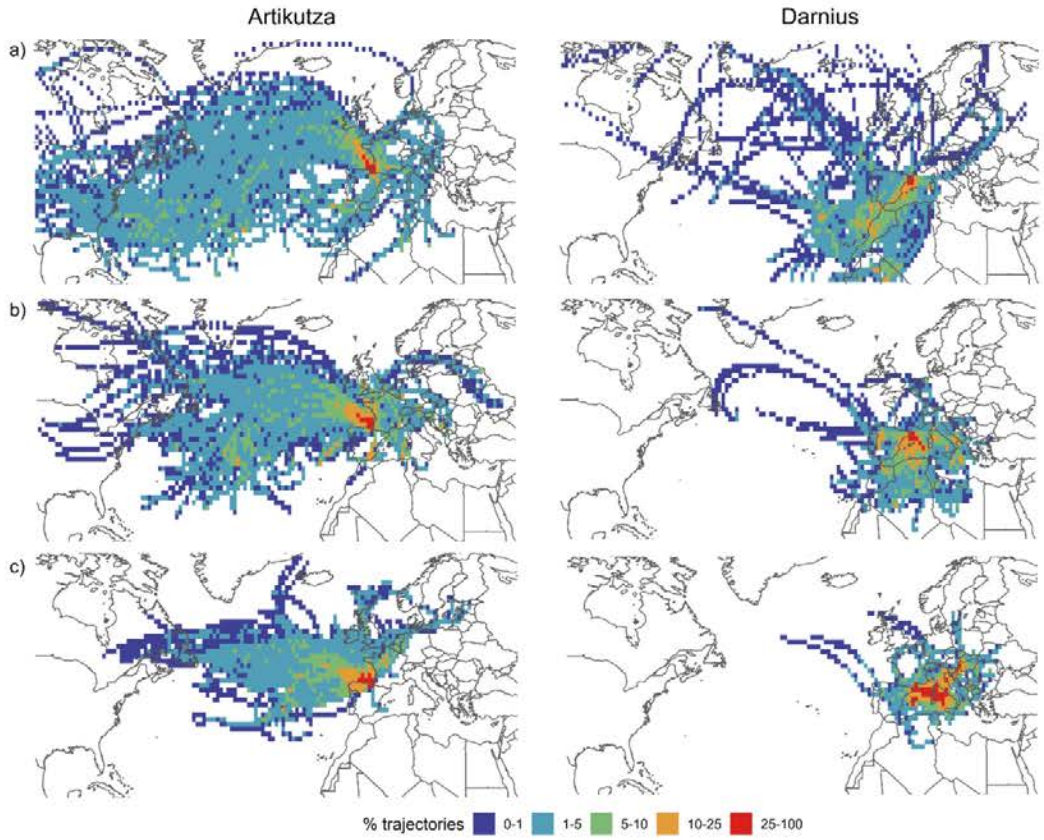

Figure 8. Backward trajectories for Artikutza (NW of the study area) and Darnius (E of the study area) for their respective days with torrential rainfall. The trajectories were computed for three different altitudinal layers: (**a**) 500 hPa, (**b**) 850 hPa and (**c**) surface.

4. Conclusions

Estimation of return periods revealed that, in the easternmost area of the Pyrenees, there is a high risk of events greater than 150 mm day^{-1} for return periods of only 5 years. For extreme return periods (200 years), the amounts are extremely high in this eastern area, reaching 400 mm day^{-1}. It is specifically this eastern area and the extreme northwest area that provide the most records equal to or greater than 100 mm, i.e., torrential rainfall.

Together with the climatic and geographic complexity of this region, a wide range of synoptic patterns accounts for these torrential events. Thus, in the northern and western areas of the Pyrenees, the main situations causing torrential events are characterized by advection from the north and northeast at surface level and a meridional circulation of the jet stream over the study area, usually accompanied by significant moisture content. The westerlies can also cause torrential events when a deep depression is located over the north of the Iberian Peninsula. This WT has a large air circulation over the North Atlantic, as shown by the analysis of the backward trajectories. In the central-southern sector of the study area, torrential rainfall is dominated by the second most recurrent WT, which is characterised by a low-pressure system in the northwest of the Iberian Peninsula, and which drives very moist southerly winds. On the other hand, the Mediterranean is subjected to the highest number of torrential events with low pressures over the western Mediterranean, which drive easterly and southeasterly winds over the Iberian Peninsula. Only one situation presented a significant number of torrential events; this was weakly defined at surface level due to cold air at high altitude during the summer season. In the easternmost area of the Pyrenees, the air masses that generate torrential rainfall present a short trajectory, coming from subtropical latitudes, in contrast with what happens in the westernmost area, where the path of the air masses is much longer and usually originates on the east coasts of North America and Canada. The heaviest precipitation in the Pyrenees is mainly monitored by the WeMO index: the eastern and northwestern areas come under the influence of the negative and positive phases of the WeMO, respectively (WT1 and WT4 in Figures 4 and 6). The NAO index has no effect upon the occurrence of torrential events in the Pyrenees, except for isolated areas on the southern façade of this mountain range.

Further research is required on these extreme precipitation events in Mediterranean mountain ranges such as the Pyrenees. This sector could be directly affected by climate change, with the risk of several associated natural hazards becoming more frequent.

Supplementary Materials: The following are available online at https://www.mdpi.com/article/10.3390/atmos12060665/s1, Figure S1: Scree test for the first 30 principal components (PCs). The red dots show the explained variance (%) for each principal component, while the black bars show the cumulative explained variance. Figure S2: Relative monthly frequencies in percentages of each weather type (WT) for the 1981–2015 period. Figure S3: Daily mean 300 hPa wind direction and speed (m s^{-1}) of the 9 most frequent weather types associated with torrential precipitation in the western Mediterranean region. Above each map, the number of days assigned to each synoptic pattern and their percentages with respect to the total are shown in parentheses.

Author Contributions: Conceptualization, M.L.-C., J.A.L.-B. and J.M.-V.; methodology, M.L.-C., J.A.L.-B. and J.M.-V.; validation, A.H.-M., D.I.-C., J.M.-A., L.T., R.S.-N. and J.M.C.; formal analysis, M.L.-C. and J.A.L.-B.; investigation, M.L.-C., J.A.L.-B. and J.M.-V.; data curation, M.L.-C. and R.S.-N.; writing—original draft preparation, M.L.-C., J.A.L.-B. and J.M.-V.; writing—review and editing, M.L.-C., J.A.L.-B., J.M.-V., D.I.-C., A.H.-M., J.M.-A., L.T., R.S.-N. and J.M.C.; supervision, L.T., D.I.-C., A.H.-M., J.M.-A. and J.M.C. All authors have read the manuscript and agreed to the published version of the manuscript.

Funding: The present study was conducted within the framework of the Climatology Group of the University of Barcelona (2017 SGR 1362, Catalan Government) and the Spanish CLICES project (CGL2017-83866-C3-2-R, AEI/FEDER, UE). M.L.-C. was awarded a pre-doctoral FPU Grant (FPU2017/02166) from the Spanish Ministry of Science, Innovation and Universities. R.S.-N. and J.M.C. are partially supported by the Government of Aragón through the "Program of research groups" (group H38, "Clima, Agua, Cambio Global, y Sistemas Naturales").

Institutional Review Board Statement: Not applicable.

Informed Consent Statement: Not applicable.

Data Availability Statement: Not applicable.

Acknowledgments: The daily precipitation data were provided by the CLIMPY Project (Characterisation of evolution of climate and provision of information for adaptation in Pyrenees) (2014–2020 INTERREG V-A Spain–France–Andorra, POCTEFA).

Conflicts of Interest: The authors declare that no conflict of interest exists.

References

1. Beguería, S.; Vicente-Serrano, S.M.; López-Moreno, J.I.; García-Ruiz, J.M. Annual and seasonal mapping of peak intensity, magnitude and duration of extreme precipitation events across a climatic gradient, northeast Spain. *Int. J. Clim.* **2009**, *29*, 1759–1779. [CrossRef]
2. Vicente-Serrano, S.M.; Beguería, S.; López-Moreno, J.I.; El Kenawy, A.M.; Angulo-Martínez, M. Daily atmospheric circulation events and extreme precipitation risk in northeast Spain: Role of the North Atlantic Oscillation, the Western Mediterranean Oscillation, and the Mediterranean Oscillation. *J. Geophys. Res.* **2009**, *114*, D08106. [CrossRef]
3. Buisan, S.T.; Saz, M.A.; López-Moreno, J.I. Spatial and temporal variability of winter snow and precipitation days in the western and central Spanish Pyrenees. *Int. J. Clim.* **2015**, *35*, 259–274. [CrossRef]
4. García-Sellés, C.; Peña, J.C.; Martí, G.; Oller, P.; Martínez, P. WeMOI and NAOi influence on major avalanche activity in the Eastern Pyrenees. *Cold Reg. Sci. Technol.* **2010**, *64*, 137–145. [CrossRef]
5. Oller, P.; Muntán, E.; García-Sellés, C.; Furdada, G.; Baeza, C.; Angulo, C. Characterizing major avalanche episodes in space and time in the twentieth and early twenty-first centuries in the Catalan Pyrenees. *Cold Reg. Sci. Technol.* **2015**, *110*, 129–148. [CrossRef]
6. Furdada, G.; Margalef, A.; Trapero, L.; Pons, M.; Areny, F.; Baró, M.; Reyes, A.; Guinau, M. The Avalanche of Les Fonts d'Arinsal (Andorra): An Example of a Pure Powder, Dry Snow Avalanche. *Geosciences* **2020**, *10*, 126. [CrossRef]
7. Esteban, P.; Jones, P.D.; Martín-Vide, J.; Mases, M. Atmospheric circulation patterns related to heavy snowfall days in Andorra, Pyrenees. *Int. J. Clim.* **2005**, *25*, 319–329. [CrossRef]
8. Buisan, S.; López-Moreno, J.; Saz, M.; Kochendorfer, J. Impact of weather type variability on winter precipitation, temperature and annual snowpack in the Spanish Pyrenees. *Clim. Res.* **2016**, *69*, 79–92. [CrossRef]
9. Navarro-Serrano, F.; López-Moreno, J.I. Spatio-temporal analysis of snowfall events in the spanish Pyrenees and their relationship to atmospheric circulation. *Cuadernos Investig. Geográf.* **2017**, *43*, 233–254. [CrossRef]
10. Trapero, L.; Bech, J.; Lorente, J. Numerical modelling of heavy precipitation events over Eastern Pyrenees: Analysis of orographic effects. *Atmos. Res.* **2013**, *123*, 368–383. [CrossRef]
11. Trapero, L.; Bech, J.; Duffourg, F.; Esteban, P.; Lorente, J. Mesoscale numerical analysis of the historical November 1982 heavy precipitation event over Andorra (Eastern Pyrenees). *Nat. Hazards Earth Syst. Sci.* **2013**, *13*, 2969–2990. [CrossRef]
12. Vicente-Serrano, S.M.; Zabalza-Martínez, J.; Borràs, G.; López-Moreno, J.I.; Pla, E.; Pascual, D.; Savé, R.; Biel, C.; Funes, I.; Azorin-Molina, C.; et al. Extreme hydrological events and the influence of reservoirs in a highly regulated river basin of northeastern Spain. *J. Hydrol. Reg. Stud.* **2017**, *12*, 13–32. [CrossRef]
13. Madsen, H.; Lawrence, D.; Lang, M.; Martinkova, M.; Kjeldsen, T.R. Review of trend analysis and climate change projections of extreme precipitation and floods in Europe. *J. Hydrol.* **2014**, *519*, 3634–3650. [CrossRef]
14. Insua-Costa, D.; Lemus-Cánovas, M.; Miguez-Macho, G.; Llasat, M.C. Climatology and ranking of hazardous precipitation events in the western Mediterranean area. *Atmos. Res.* **2021**, *255*, 105521. [CrossRef]
15. Lemus-Canovas, M.; Lopez-Bustins, J.A.; Martin-Vide, J.; Royé, D. synoptReg: An R package for computing a synoptic climate classification and a spatial regionalization of environmental data. *Environ. Model. Softw.* **2019**, *118*, 114–119. [CrossRef]
16. Lagouvardos, K.; Dafis, S.; Giannaros, C.; Karagiannidis, A.; Kotroni, V. Investigating the Role of Extreme Synoptic Patterns and Complex Topography During Two Heavy Rainfall Events in Crete in February 2019. *Climate* **2020**, *8*, 87. [CrossRef]
17. Esteban, P.; Ninyerola, M.; Prohom, M. Spatial modelling of air temperature and precipitation for Andorra (Pyrenees) from daily circulation patterns. In *Proceedings of the Theoretical and Applied Climatology*; Springer: Wien, Austria, 2009; Volume 96, pp. 43–56.
18. Lemus-Canovas, M.; Lopez-Bustins, J.A.; Trapero, L.; Martin-Vide, J. Combining circulation weather types and daily precipitation modelling to derive climatic precipitation regions in the Pyrenees. *Atmos. Res.* **2019**, *220*, 181–193. [CrossRef]
19. Trigo, R.M.; DaCamara, C.C. Circulation weather types and their influence on the precipitation regime in Portugal. *Int. J. Clim.* **2000**, *20*, 1559–1581. [CrossRef]
20. Lorenzo, M.N.; Taboada, J.J.; Gimeno, L. Links between circulation weather types and teleconnection patterns and their influence on precipitation patterns in Galicia (NW Spain). *Int. J. Clim.* **2008**, *28*, 1493–1505. [CrossRef]
21. Cortesi, N.; Gonzalez-Hidalgo, J.C.; Trigo, R.M.; Ramos, A.M. Weather types and spatial variability of precipitation in the Iberian Peninsula. *Int. J. Clim.* **2014**, *34*, 2661–2677. [CrossRef]
22. Ramos, A.M.; Cortesi, N.; Trigo, R.M. Circulation weather types and spatial variability of daily precipitation in the Iberian Peninsula. *Front. Earth Sci.* **2014**, *2*, 25. [CrossRef]

23. Lemus-Canovas, M.; Ninyerola, M.; Lopez-Bustins, J.A.; Manguan, S.; Garcia-Sellés, C. A mixed application of an objective synoptic classification and spatial regression models for deriving winter precipitation regimes in the Eastern Pyrenees. *Int. J. Clim.* **2019**, *39*, 2244–2259. [CrossRef]
24. Jones, P.D.; Hulme, M.; Briffa, K.R. A comparison of Lamb circulation types with an objective classification scheme. *Int. J. Clim.* **1993**, *13*, 655–663. [CrossRef]
25. Carro-Calvo, L.; Ordóñez, C.; García-Herrera, R.; Schnell, J.L. Spatial clustering and meteorological drivers of summer ozone in Europe. *Atmos. Environ.* **2017**, *167*, 496–510. [CrossRef]
26. Martin-Vide, J.; Sanchez-Lorenzo, A.; Lopez-Bustins, J.A.; Cordobilla, M.J.; Garcia-Manuel, A.; Raso, J.M. Torrential rainfall in northeast of the Iberian Peninsula: Synoptic patterns and WeMO influence. *Adv. Sci. Res.* **2008**, *2*, 99–105. [CrossRef]
27. Lopez-Bustins, J.A.; Martin-Vide, J.; Sanchez-Lorenzo, A. Iberia winter rainfall trends based upon changes in teleconnection and circulation patterns. *Glob. Planet. Chang.* **2008**, *63*, 171–176. [CrossRef]
28. Sanchez-Lorenzo, A.; Calbó, J.; Martin-Vide, J.; Garcia-Manuel, A.; García-Soriano, G.; Beck, C. Winter "weekend effect" in southern Europe and its connections with periodicities in atmospheric dynamics. *Geophys. Res. Lett.* **2008**, *35*, L15711. [CrossRef]
29. Nishiyama, K.; Endo, S.; Jinno, K.; Bertacchi Uvo, C.; Olsson, J.; Berndtsson, R. Identification of typical synoptic patterns causing heavy rainfall in the rainy season in Japan by a Self-Organizing Map. *Atmos. Res.* **2007**, *83*, 185–200. [CrossRef]
30. Meseguer-Ruiz, O.; Ponce-Philimon, P.I.; Baltazar, A.; Guijarro, J.A.; Serrano-Notivoli, R.; Olcina Cantos, J.; Martin-Vide, J.; Sarricolea, P. Synoptic attributions of extreme precipitation in the Atacama Desert (Chile). *Clim. Dyn.* **2020**, *55*, 3431–3444. [CrossRef]
31. Kunkel, K.E.; Stevens, S.E.; Stevens, L.E.; Karl, T.R. Observed Climatological Relationships of Extreme Daily Precipitation Events With Precipitable Water and Vertical Velocity in the Contiguous United States. *Geophys. Res. Lett.* **2020**, *47*, e2019GL086721. [CrossRef]
32. Sillmann, J.; Kharin, V.V.; Zwiers, F.W.; Zhang, X.; Bronaugh, D. Climate extremes indices in the CMIP5 multimodel ensemble: Part 2. Future climate projections. *J. Geophys. Res. Atmos.* **2013**, *118*, 2473–2493. [CrossRef]
33. Cuadrat, J.M.; Serrano-Notivoli, R.; Tejedor, E.; Saz, M.Á.; Prohom, M.; Cunillera, J.; Llabrés, A.; Trapero, L.; Pons, M.; López-Moreno, J.I.; et al. CLIMPY: Climate of the Pyrenees. *Zenodo* **2020**. [CrossRef]
34. Serrano-Notivoli, R.; Beguería, S.; Saz, M.Á.; Longares, L.A.; De Luis, M. SPREAD: A high-resolution daily gridded precipitation dataset for Spain—An extreme events frequency and intensity overview. *Earth Syst. Sci. Data* **2017**, *9*, 721–738. [CrossRef]
35. Hersbach, H.; Bell, B.; Berrisford, P.; Hirahara, S.; Horányi, A.; Muñoz-Sabater, J.; Nicolas, J.; Peubey, C.; Radu, R.; Schepers, D.; et al. The ERA5 global reanalysis. *Q. J. R. Meteorol. Soc.* **2020**, *146*, 1999–2049. [CrossRef]
36. Stein, A.F.; Draxler, R.R.; Rolph, G.D.; Stunder, B.J.B.; Cohen, M.D.; Ngan, F. Noaa's hysplit atmospheric transport and dispersion modeling system. *Bull. Am. Meteorol. Soc.* **2015**, *96*, 2059–2077. [CrossRef]
37. Kalnay, E.; Kanamitsu, M.; Kistler, R.; Collins, W.; Deaven, D.; Gandin, L.; Iredell, M.; Saha, S.; White, G.; Woollen, J.; et al. The NCEP/NCAR 40-Year Reanalysis Project. *Bull. Am. Meteorol. Soc.* **1996**, *77*, 437–472. [CrossRef]
38. Martin-Vide, J.; Lopez-Bustins, J.-A. The Western Mediterranean Oscillation and rainfall in the Iberian Peninsula. *Int. J. Clim.* **2006**, *26*, 1455–1475. [CrossRef]
39. Conte, M.; Giuffrida, A.; Tedesco, S. Mediterranean Oscillation: Impact on Precipitation and Hydrology in Italy. *Conf. Clim. Water* **1989**, *9*, 121–137.
40. Redolat, D.; Monjo, R.; Lopez-Bustins, J.A.; Martin-Vide, J. Upper-Level Mediterranean Oscillation index and seasonal variability of rainfall and temperature. *Theor. Appl. Clim.* **2019**, *135*, 1059–1077. [CrossRef]
41. Hurrell, J.W. Decadal trends in the North Atlantic oscillation: Regional temperatures and precipitation. *Science* **1995**, *269*, 676–679. [CrossRef]
42. Llasat, M.-C. An objective classification of rainfall events on the basis of their convective features: Application to rainfall intensity in the northeast of Spain. *Int. J. Clim.* **2001**, *21*, 1385–1400. [CrossRef]
43. Lopez-Bustins, J.; Arbiol-Roca, L.; Martin-Vide, J.; Barrera-Escoda, A.; Prohom, M. Intra-annual variability of the Western Mediterranean Oscillation (WeMO) and occurrence of extreme torrential precipitation in Catalonia (NE Iberia). *Nat. Hazards Earth Syst. Sci.* **2020**, *20*, 2483–2501. [CrossRef]
44. De Luis, M.; González-Hidalgo, J.C.; Raventós, J. Effects of fire and torrential rainfall on erosion in a Mediterranean gorse community. *Land Degrad. Dev.* **2003**, *14*, 203–213. [CrossRef]
45. Cattell, R.B. The scree test for the number of factors. *Multivar. Behav. Res.* **1966**. [CrossRef]
46. Richman, M.B. Rotation of principal components. *J. Clim.* **1986**, *6*, 293–335. [CrossRef]
47. Lavers, D.A.; Villarini, G.; Allan, R.P.; Wood, E.F.; Wade, A.J. The detection of atmospheric rivers in atmospheric reanalyses and their links to British winter floods and the large-scale climatic circulation. *J. Geophys. Res. Atmos.* **2012**, *117*, 117. [CrossRef]
48. Gustafsson, M.; Rayner, D.; Chen, D. Extreme rainfall events in southern Sweden: Where does the moisture come from? *Tellus A Dyn. Meteorol. Oceanogr.* **2010**, *62*, 605–616. [CrossRef]
49. Fleming, Z.L.; Monks, P.S.; Manning, A.J. Review: Untangling the influence of air-mass history in interpreting observed atmospheric composition. *Atmos. Res.* **2012**, *104–105*, 1–39. [CrossRef]
50. Martin-Vide, J. Spatial distribution of a daily precipitation concentration index in peninsular Spain. *Int. J. Clim.* **2004**, *24*, 959–971. [CrossRef]

51. Lopez-Bustins, J.A.; Lemus-Canovas, M. The influence of the Western Mediterranean Oscillation upon the spatio-temporal variability of precipitation over Catalonia (northeastern of the Iberian Peninsula). *Atmos. Res.* **2020**, *236*, 104819. [CrossRef]
52. de Luis, M.; Brunetti, M.; Gonzalez-Hidalgo, J.C.; Longares, L.A.; Martin-Vide, J. Changes in seasonal precipitation in the Iberian Peninsula during 1946-2005. *Glob. Planet. Chang.* **2010**, *74*, 27–33. [CrossRef]
53. Merino, A.; Fernández-Vaquero, M.; López, L.; Fernández-González, S.; Hermida, L.; Sánchez, J.L.; García-Ortega, E.; Gascón, E. Large-scale patterns of daily precipitation extremes on the Iberian Peninsula. *Int. J. Clim.* **2016**, *36*, 3873–3891. [CrossRef]
54. Pérez-Zanón, N.; Casas-Castillo, M.C.; Peña, J.C.; Aran, M.; Rodríguez-Solà, R.; Redaño, A.; Solé, G. Analysis of synoptic patterns in relationship with severe rainfall events in the Ebre Observatory (Catalonia). *Acta Geophys.* **2018**, *66*, 405–414. [CrossRef]
55. Bonsoms, J.; Gonzalez, S.; Prohom, M.; Esteban, P.; Salvador-Franch, F.; López-Moreno, J.I.; Oliva, M. Spatio-temporal patterns of snow in the Catalan Pyrenees (NE Iberia). *Int. J. Clim.* **2021**. Under review. [CrossRef]
56. Insua-Costa, D.; Miguez-Macho, G.; Llasat, C. Local and remote moisture sources for extreme precipitation: A study of the two catastrophic 1982 western Mediterranean episodes. *Hydrol. Earth Syst. Sci.* **2019**, *23*, 3885–3900. [CrossRef]
57. Pineda, N.; Esteban, P.; Trapero, L.; Soler, X.; Beck, C. Circulation types related to lightning activity over Catalonia and the Principality of Andorra. *Phys. Chem. Earth* **2010**, *35*, 469–476. [CrossRef]
58. Martinez-Artigas, J.; Lemus-Canovas, M.; Lopez-Bustins, J.A. Precipitation in peninsular Spain: Influence of teleconnection indices and spatial regionalisation. *Int. J. Clim.* **2021**, *41*, E1320–E1335. [CrossRef]
59. Rodó, X.; Baert, E.; Comin, F.A. Variations in seasonal rainfall in Southern Europe during the present century: Relationships with the North Atlantic Oscillation and the El Niño-Southern Oscillation. *Clim. Dyn.* **1997**, *13*, 275–284. [CrossRef]
60. Esteban, P.; Soler, X.; Prohom, M.; Planchon, O. *La Distribución de la Precipitación a Través del Índice NAO. El Efecto del Relieve a Escala Local: El Pirineo Oriental*; Publicaciones de la Sociedad Española de Climatología: Palma de Mallorca, Spain, 2002; pp. 25–34.
61. Pastor, F.; Valiente, J.A.; Estrela, M.J. Sea surface temperature and torrential rains in the Valencia region: Modelling the role of recharge areas. *Hazards Earth Syst. Sci.* **2015**, *15*, 1677–1693. [CrossRef]

3.4. synoptReg: un paquet R per calcular una classificació climàtica sinòptica i una regionalització espacial de dades ambientals

3.4.1. Resum de l'article

El coneixement espacial de les variables climàtiques o ambientals associades als tipus de circulació més freqüents és essencial per al desenvolupament d'estratègies per afrontar el risc d'allaus, inundacions, erosió del sòl, contaminació atmosfèrica o altres riscos naturals. En aquest article, es presenta una llibreria R de codi obert anomenada synoptReg, que s'encarrega de realitzar l'espacialització d'una variable ambiental en funció dels tipus de circulació atmosfèrica computats mitjançant mètodes estadístics multivariants. La llibreria synoptReg conté un conjunt de funcions que s'empren per a: (1) realitzar una classificació sinòptica basada en l'anàlisi de components principals; (2) cartografiar la distribució espacial de la variable ambiental seleccionada en base als tipus de circulació; (3) desenvolupar una regionalització ambiental categòrica basada en els resultats anteriors. En aquest treball, s'il · lustra la utilitat de la llibreria per a un cas d'estudi a l'àrea dels Alps.

3.4.2. Article

Lemus-Canovas, M., Lopez-Bustins, J. A., Martin-Vide, J., & Royé, D. (2019c). synoptReg: An R package for computing a synoptic climate classification and a spatial regionalization of environmental data. Environmental Modelling and Software, 118, 114–119. https://doi.org/10.1016/j.envsoft.2019.04.006

Environmental Modelling and Software 118 (2019) 114–119

Contents lists available at ScienceDirect

Environmental Modelling & Software

journal homepage: www.elsevier.com/locate/envsoft

synoptReg: An R package for computing a synoptic climate classification and a spatial regionalization of environmental data

Marc Lemus-Canovas[a,*], Joan A. Lopez-Bustins[a], Javier Martin-Vide[a], Dominic Royé[b,c]

[a] Climatology Group, Department of Geography, University of Barcelona, Catalonia, Spain
[b] Department of Geography, University of Santiago de Compostela, Spain
[c] Department of Geography, University of Porto, Portugal

ARTICLE INFO

Keywords:
Alps
Environmental regionalization
R package
synoptReg
Synoptic classification

ABSTRACT

Spatial knowledge of the climatic or environmental variables associated with the most frequent circulation types is essential with regard to developing strategies to address the risk of avalanches, floods, soil erosion, air pollution or other natural hazards. In order to derive an environmental regionalization, we present an Open Source R package known as synoptReg, which combines the spatialization of environmental variables based on the atmospheric circulation types. The synoptReg package contains a set of functions which we will employ (1) to perform a PCA-based synoptic classification using an atmospheric variable; (2) to map the spatial distribution of the selected environmental variable based upon the circulation types; (3) to develop a spatial environmental regionalization based on the previous results. We illustrate the usefulness of the package for a case study in the Alps area.

1. Introduction

The use of a synoptic classification (a branch of climatology focusing on the spatial and temporal characterization of large weather systems) in combination with environmental spatial variables could help us to understand the role played by the spatial variability of environmental elements. Such models would enable us to establish fine-scale continuous fields as inputs to, for instance, distributed hydrological models, allowing us to investigate the impacts of climate change upon ecological and social systems (Tveito and Ustrnul, 2003; Yalew et al., 2018). Several studies have attempted to determine the climatic or environmental impacts of atmospheric circulation. For example, Bissolli and Westermeier (2005) performed simple linear regression models of precipitation using a digital elevation model (DEM) as the independent variable to obtain daily mean precipitation maps for each circulation type; these were based on the objective synoptic classification conducted by the German Weather Service. Fernández-Montes et al. (2013) analyzed the relationship between weather types and days with extreme temperatures during the spring and summer seasons. Garrido-Perez et al. (2017) determined the impact of high-latitude blocks and subtropical ridges on daily PM10 (particulate matter ≤ 10 μm) observations. Finally, Duane et al. (2016) suggested that associating synoptic patterns with observed fire spread patterns may help to understand the factors causing fires to spread over the landscape.

One way to summarize environmental spatial grids involves the use of multivariate statistical methods such as the Principal Component Analysis (PCA) or the Cluster Analysis. Numerous studies attempt to stratify environmental variables in a given number of regions. For instance, Zscheischler et al. (2012) employ a k-means method to perform a global climatic classification combining weather data and remote-sensing derived data. Another similar study is presented by Carro-Calvo et al. (2017), the main goal of which involves regionalization of summertime tropospheric ozone (O_3) in Europe. They applied the k-means clustering technique to the near-surface O_3 average over Europe at a $1^\circ \times 1^\circ$ resolution for the summer season during the 1998–2012 period. The results reveal a spatial division of nine regions in which tropospheric O_3 displays coherent spatio-temporal patterns.

As for computer software for performing synoptic classifications, the most important development in this field involves the software package cost733class for development, comparison and evaluation of classifications (Philipp et al., 2016), created by the COST733 Action, within the framework of the European Cooperation in the field of Scientific and Technical Research (COST). This software, developed on Unix/Linux operating systems, enables computation of up to 27 basic automatic classification methods describing atmospheric circulation. Apart from the COST Action, the authors are only aware of the existence of the R package JCEXT (Otero, 2018b), which enables the circulation

* Corresponding author.
E-mail address: mlemus@ub.edu (M. Lemus-Canovas).

https://doi.org/10.1016/j.envsoft.2019.04.006
Received 3 January 2019; Received in revised form 29 March 2019; Accepted 10 April 2019
Available online 13 April 2019
1364-8152/

types of Jenkinson & Collison to be computed. One of its applications can be found in Otero et al. (2018a). However, no R package has been found to compute a synoptic classification based upon a PCA approach, a fact that gives greater relevance to the package presented herein.

Our paper presents the implementation of a new methodology for regionalizing environmental variables through thesynoptReg R package (https://CRAN.R-project.org/package=synoptReg). Users will be able to obtain a synoptic classification of any atmospheric variable (mean sea level pressure, geopotential height, etc.), a spatialization of the environmental variable of interest based on the weather types obtained from the synoptic classification and finally, a regionalization of this environmental variable. This package constitutes a step forward in the regionalization of climatic and environmental variables, because it links the synoptic-atmospheric scale with the regional-environmental one, thus providing a categorical regionalization of the environmental variable of interest considering characteristics other than the statistical ones.

The present study is structured as follows: in section 2, the methods of the entire procedure are described. In section 3, we provide user details referring to the internal features of the functions and their sequence of use for achieving results. Finally, in section 4, we provide a short summary of the main results. In addition, we describe some potential improvements of the package as well as projected future developments. The code of the figures produced in this article can be found in Appendix A.

2. Methodological basis

The methodology applied in this package mainly involves establishing an objective weather type classification, which assigns each of the days to a specific circulation type (CT) by means of multivariate statistical techniques. Furthermore, once the spatialization of the environmental or climatic variable has been conducted, a spatial regionalization is executed by means of a cluster analysis. Therefore, the procedure for establishing regionalization is as follows: 1) execution of an atmospheric synoptic classification;2) spatialization of the mean daily amounts of gridded environmental or climatic variable based on the various CTs; 3) synthesis of the different spatial patterns of the environmental variable by means of the PCA technique as well as mean filters and resampling of cell sizes; 4) clustering of the selected principal components (PC) to obtain an environmental spatial stratification.

2.1. Synoptic classification method

We applied a PCA to a spatial mode (S-mode) matrix to reduce the dimension of the variables. In this matrix, the grid points are the variables and the days are the observations. The S-mode PCA enables a climate regionalization (Richman, 1986; Lopez-Bustins et al., 2015) because it shows the representative degree of each day in each component. Nonetheless, an S-mode PCA does not provide a direct synoptic classification because a classification of circulation types has not been achieved. Hence, our cases need to be allocated to a specific group and as a result, a clustering method must be performed in order to categorize the atmospheric circulation types. As for the variables used, we standardized the matrix to maintain one single scale when using different variables, thus avoiding overrepresentation of any one of them. We employed the Scree test (Cattell, 1966) to retain the components explaining a significant portion of the total variance; these principal components were subsequently rotated by means of a Varimax rotation (Esteban et al., 2006).

Along with the rotated components, we made use of the scores to apply the extreme scores method (Esteban et al., 2005). The scores show the degree of representativeness associated with the variation modes of each principal component, i.e., classification of each day to its most representative centroid. The extreme scores method uses the scores > 2 and < -2, thus establishing a positive and negative phase for each principal component. The extreme scores establish the number of groups and their centroids for the K-means method (Esteban et al., 2006). K-means is applied without iterations because the centroids are well established by the method of extreme scores.

2.2. Regionalization

The regionalization process consists of the following four steps: 1) Establishing the spatialization of the gridded environmental variable based on the weather types. 2) Applying a PCA to n environmental maps in raster format and selecting the ones that present a greater variance. This process enabled us to reduce redundant information on the models and to extract only the most significant information from the set of maps. 3) Other options involve resampling of the previous environmental rasters to a coarse spatial resolution, and use of a filter based upon a weight matrix for the neighboring cells of the focal cell. This step is important with regard to reducing local effects, such as the valley bottom effect. In addition, applying the spatial filter avoids notable discontinuities in the final regionalization. 4) Finally, the K-means algorithm is applied to the rasters obtained in step 3. This final step must be applied iteratively in order to decide the correct number of regions. To facilitate this decision, a pseudo-MAE index is proposed (1):

$$\mathrm{MAE} = n^{-1} \sum_{i=1}^{n} |d_i - c_i|, \tag{1}$$

Where d_i is the mean grid cell resulting from the average of the PC selected, and c_i is the mean of the respective centroids of the selected PC. As mentioned in Carro-Calvo et al. (2017), the increase in the explained variance by means of clustering can be explained by the increase in the number of centroids. However, this increase does not always imply greater variance, since the n clusters explain practically the same variance as the $n+1$ clusters. This graphically represented pseudo-MAE index enables us to visualize which cluster shows no decrease in the error or increase in the variance. This measure is proposed as a complement to the decision based upon visual inspection. The purpose of the clustering process is to provide a small but sufficient number of clusters that capture the diversity of the environmental variable with no loss of generalization.

3. The synoptReg package

The use of the package functions provides 1) an objective synoptic classification that determines the most frequent weather types for a given study area; 2) a spatialization of the gridded environmental or climatic study variable based on the CT; 3) a discrete regionalization of the target variable. To this end, the package includes 8 functions that must be applied sequentially (although some of them can be applied separately).

3.1. Input data requirements

The synoptReg package contains a function for reading input data in NetCDF format, which is the most widespread format for storing large volumes of climate information, containing at least the spatial and temporal dimensions. The read_nc function enables us to read these files, as long as they are continuous and present no internal gaps. This function extracts the variable data, the latitude and the longitude

Table 1
Format of the data in spatial mode (S-mode). The heading indicates the grid points. The rows are the daily observations of mean sea level pressure (mslp).

	Col. 1lon = −20, lat = 60	Col. 2 lon = −20, lat = 59.25	Col. 3 lon = −20, lat = 58.5
t = 1	mslp (−20,60,1)	mslp (−20,59.25,1)	mslp (−20,58.5,1)
t = 2	mslp (−20,60,2)	mslp (−20, 59.25,2)	mslp (−20, 58.5,2)
t = n	mslp (−20,60,n)	mslp (−20, 59.25,n)	mslp (−20, 58.5,n)

vector, and the date sequence. These are stored in a list object which is subsequently used to conduct the rest of the methodological procedure. Although read_nc is used to read the file in NetCDF format, the tidy_cuttime_nc function must be used to format the data and transform them into an S-mode data frame (Table 1), in which the variables (columns) are the grid points (lat-lon) and the observations (rows) represent the dates of the dataset. Furthermore, we can select the range of years to be used in the synoptic classification (year_range), thus deciding whether we want to work with a concrete climatological season (winter, spring, summer, fall), using the season parameter. Importantly, the read_nc and tidy_cuttime_nc functions need to be used both for the synoptic classification to be computed by means of the reanalysis data and for the environmental variable to be regionalized.

The package includes a dataset of mean sea level pressure (mslp) from the ERA-Inerim project (Dee et al., 2011) at a spatial resolution of 2.5°, centered on Western Europe (60°N - 30°N, 30°W - 15°E) and used to perform the synoptic classification, and another dataset of daily precipitation for the Balearic Islands (Spain), provided by the SPREAD project (Serrano-notivoli et al., 2017)at a spatial resolution of 5 km. Herein, however, the ERA-Interim grid from the European Centre for Medium-Range Weather Forecasts (ECMWF) for mslp was focused upon Central Europe (60°N - 30°N, 10°W - 30°E). The spatial resolution of the dataset was 0.75° with a daily temporal resolution (12 h UT) between 1979 and 2017. Moreover, we chose the Alps mountain range (Fig. 1) for the climatic study (49°N - 43°N, 4°E - 16.5°E). For this purpose, we employed the E-OBS grid of daily precipitation (Haylock et al., 2008) at a spatial resolution of 0.25°. This gridded dataset can be downloaded from the European Climate Assessment & Dataset website (https://www.ecad.eu/).

3.2. Computing the synoptic classification

As was pointed out in the methodology section, the synoptic classification is computed by means of a PCA-based approach. For this reason, prior to the classification process, it is advisable to use the function pca_decision, which extracts a report on the proportion of variance explained by each of the PCs, as well as a plot of the Scree Test (Catell, 1966)(Fig. S1). Based upon the scree test information, we can decide the number of PCs to be retained, which was 6 in the example.

Once the number of components to be retained in the synoptic classification has been decided, the synoptclas function can be used. This function requires as input data: the data frame resulting from the use of the function tidy_cuttime_nc (smode_data) and the number of components (ncomp). We can then perform the classification with these two parameters. Consequently, the following results are obtained:

- A data frame containing the mslp data grouped by CT.
- Statistics on the number of days assigned to each CT for the whole period. We also obtain the frequency of each one of the CTs per month and per year. All these statistics enable us to perform a trend analysis for different circulation types (Fig. S2) or simply to calculate the frequency of each of the seCTs per month (Fig. S3), among other possibilities.
- In addition, the rotated loadings, the scores and the multivariate coordinates of these scores can be consulted; the latter ones are used to perform the classification with the k-means algorithm.

In order to obtain the maps of the synoptic classification we will first use the function raster_clas, which only requires the vector of longitudes and latitudes and the data frame result of the synoptclas application. By applying this function, we will obtain a RasterStack object that can be easily plotted using any of the existing visualization libraries (Fig. 2).

3.3. Spatial distribution of precipitation and regionalization

To obtain the final regionalization, we first mapped the mean daily precipitation over the study area based on each of the previous CTs (Fig. 3). To this end, we used the function raster_ct2env, obtaining raster maps of mean daily precipitation (MDP) for each weather type.

With the MDP maps, different spatial distributions of precipitation linked to the CTs can be observed, but with the use of theraster_pca function we obtained the most frequent spatial patterns of precipitation in the study area. This function applies an R-mode PCA to the precipitation RasterStack. Although in this demonstration a coarse resolution grid is used, the application of a mean filter to the raster cells of the PCA result can favour greater continuity of the spatial patterns, thus facilitating the final regionalization. (Fig. S4). Application of a 5 × 5 cell filter (Fig. S4) reveals the raster_pca result.

As can be seen in Table 2, PC1 obtains a higher percentage of explained variance than PC2, PC2 is higher than PC 3 in this sense, and so forth. As in the case of the Scree Test, the most relevant components expressing the main spatial patterns must be selected. This selection can

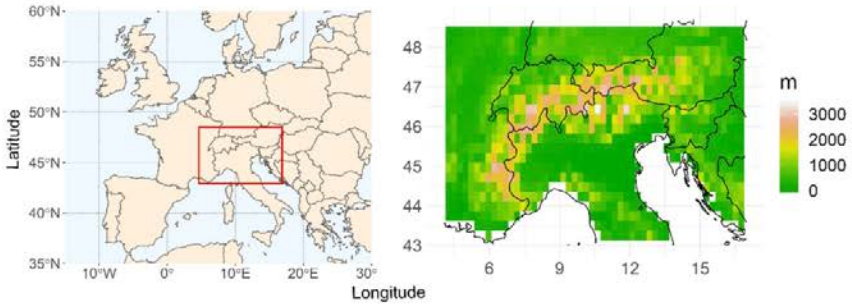

Fig. 1. Alps location and topography at 0.25° spatial resolution.

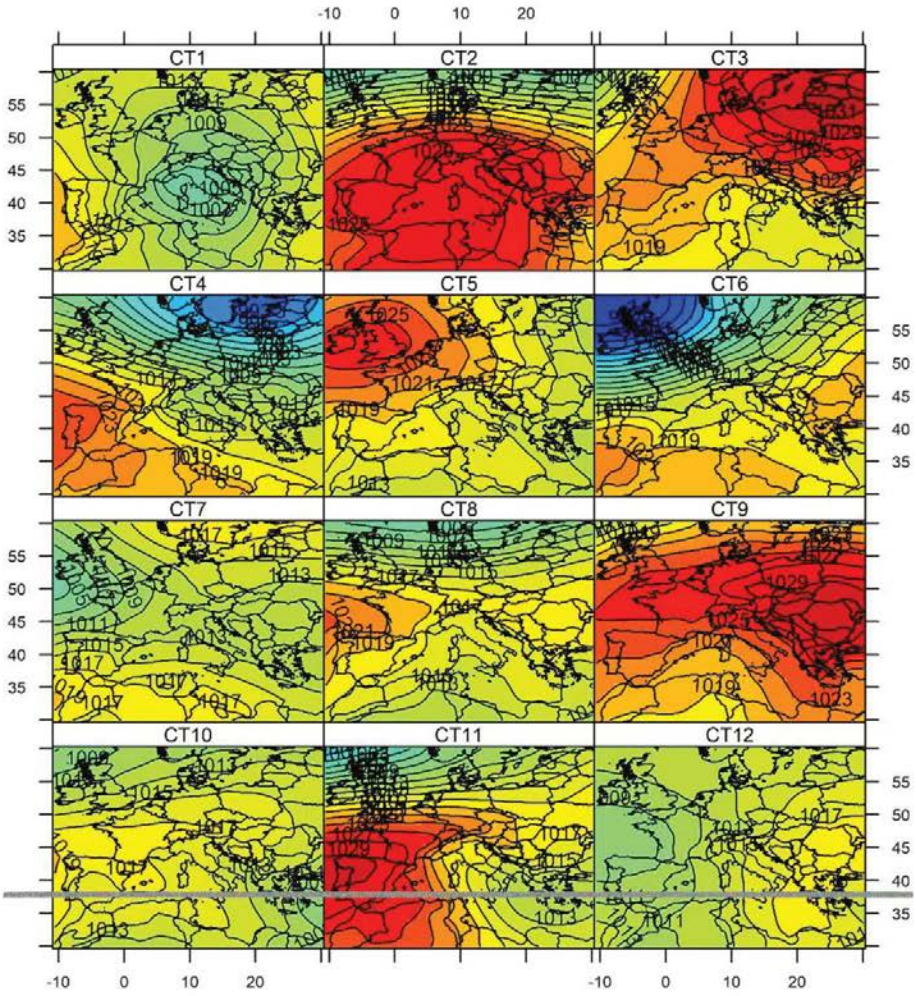

Fig. 2. Result of the synoptic classification by means of the synoptclas function. 12 circulation types (CT) are represented after the result obtained from the function raster_clas is plotted.

be made through visual inspection of Fig. S4 and the summary returned by the raster_pca function, where the percentages of variance explained by each of the PCs are noted (Table 2).

We used the above data to select the first 4 PCs in order to perform the cluster analysis using the regionalization function, which requires a RasterStack object and the number of cluster centers we desire, i.e. the number of regions. To use the regionalization function, performing an iterative process is recommended, which involves dividing the study area into k clusters. For example, Fig. 4 shows the result of regionalizing the Alps area from $k = 2$ to $k = 10$. Thus, it is possible to visually inspect the regionalization that appears to be the most appropriate. However, the pseudo-MAE value returned by the function, which measures the intracluster error, can be used to take the final decision.

To comment briefly upon the regionalization results, for $k = 2$ the two basic precipitation regions in the Alps area are displayed; these are based on maximums in the cold half of the year (blue), west and south, and maximums in the warm half of the year (red), centre and north. For $k = 3$, the three basic climates are shown: temperate (green) maritime influence, west; Mediterranean (red), south; and continental (blue), north. For $k \geq 5$ the spatial complexity of precipitation in a widely contrasted Alpine region is shown.

Graphing of the pseudo-MAE error reveals that adding a region does not always cause a clear decrease in the error, and it might therefore not be worth adding a new region if this does not cause a decrease in the pseudo-MAE value. Fig. 5 shows that, in the transition from $k = 3$ to $k = 4$, there is hardly any variation in the error; consequently, adding another region does not provide too much information, and the regionalization $k = 3$ could therefore be retained. The same occurs with an increase from $k = 8$ to $k = 9$, and $k = 8$ would therefore be the recommended option. In any case, the final decision depends upon the research objectives and on the geographical scale of the study area.

4. Further developments, limitations and conclusions

The synoptReg package contains a set of functions that provide an

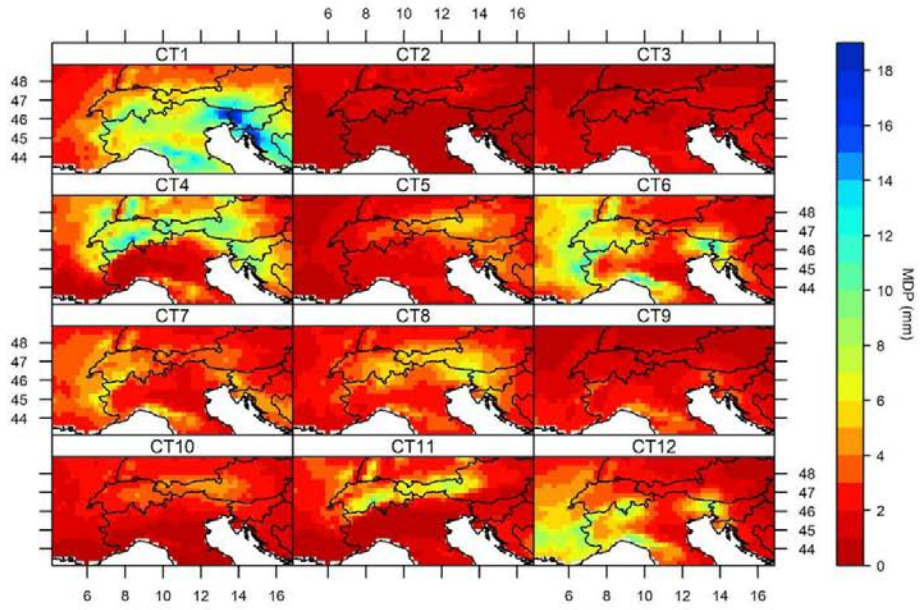

Fig. 3. Result of the spatialization of mean daily precipitation (MDP), by means of the function raster_ct2env, based on the 12 CTs.

Table 2
Information on the application of the PCA to the RasterStack object containing the mean daily precipitation (MDP) raster maps.

	PC1	PC2	PC3	PC4	PC5	PC6
Standard deviation	2.11	1.94	1.53	0.79	0.59	0.46
Proportion of variance	0.37	0.31	0.19	0.05	0.03	0.02
Cumulative variance	0.37	0.68	0.88	0.93	0.96	0.98

	PC7	PC8	PC9	PC10	PC11	PC12
Standard deviation	0.33	0.25	0.19	0.16	0.13	0.09
Proportion of variance	0.01	0.01	0.00	0.00	0.00	0.00
Cumulative variance	0.99	0.99	1.00	1.00	1.00	1.00

automatic synoptic classification and a regionalization of the climatic or environmental variable of interest. The functions integrated in this package have been tested in the present research, and have provided highly satisfactory results. Nonetheless, the package presents some limitations. For instance, it is not adapted to working with temporarily discontinuous data, or with series containing few observations (days) because the application of the PCA in S-mode means that the number of observations must be greater than the number of variables. This requires an extensive temporal series of observations (daily time-scale, for example). For this reason, we are working on a new function that applies the temporal mode (T-mode) matrix, which allows a synoptic classification when using short series of data, and the T-mode, unlike the S-mode, does not require a clustering process. Furthermore, we are also working to introduce a second variable in the synoptclas function,

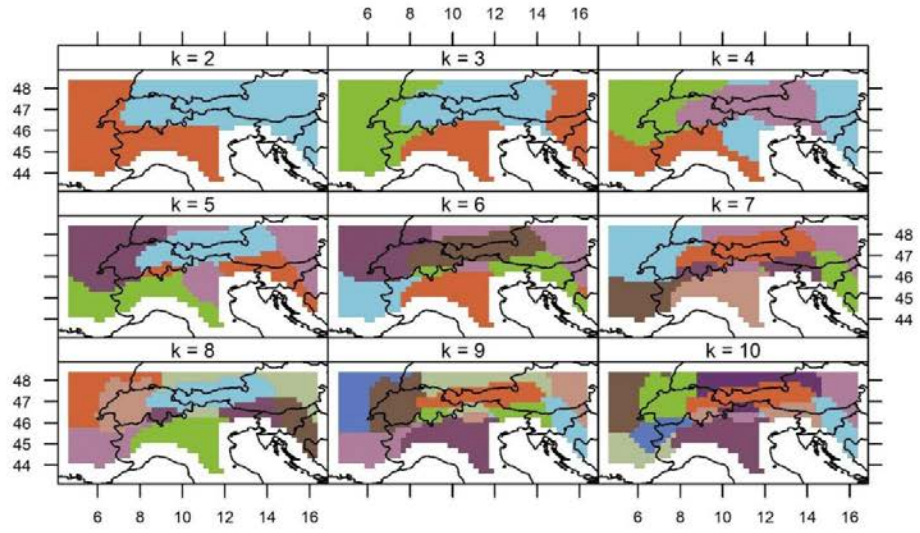

Fig. 4. Spatial regionalization of the MDP. The result of the iteration is shown from $k = 2$ to $k = 10$. k is the number of regions.

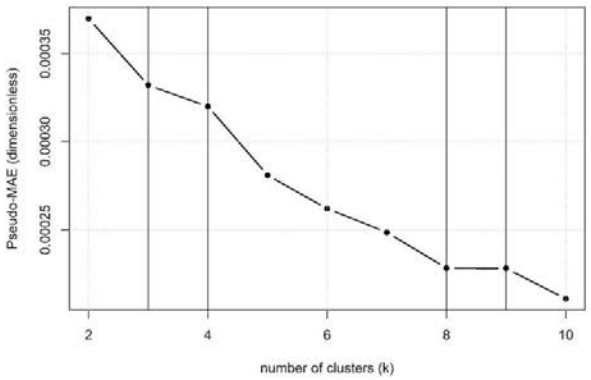

Fig. 5. Graph of the pseudo-MAE for the sequence from k = 2 to k = 10. The error tends to decrease with an increase in k, although this does not always occur (k = 4 or k = 9).

i.e. that the PCA can be applied to a data grid of two variables (e.g. mslp and geopotential height at 500 hPa). All these improvements will be implemented in future versions of the synoptReg package.

Acknowledgments

The present study was funded by the WEMOTOR project (CSO2014 -55799-C2-1-R) and the CLICES project (CGL2017-83866-C3-2-R) of the Spanish Ministry of Science, Innovation and Universities. This research was conducted within the framework of the Climatology Group of the University of Barcelona (2017 SGR 1362, Catalonia Regional Govt.) and the Water Research Institute of the University of Barcelona. We also wish to acknowledge the E-OBS dataset from the EU-FP6 project ENSEMBLES (http://ensembles-eu.metoffice.com; last accessed 21 December 2018) and the data providers in the ECA&D project (http://www.ecad.eu; last accessed 21 December 2018). M.L.-C has been granted a pre-doctoral FPU scholarship (Spanish Ministry of Education, Culture and Sports).

Appendix A. Supplementary data

Supplementary data to this article can be found online at https://doi.org/10.1016/j.envsoft.2019.04.006.

References

Bissolli, P., Müller-Westermeier, G., 2005. The spatial distribution of precipitation in Germany for different weather types. In: Proceedings from the 5th Annual Meeting of the European Meteorological Society, Session AW8, Weather Types Classifications. Utrecht, The Netherlands, 12–16 September 2005.

Carro-Calvo, L., Ordóñez, C., García-Herrera, R., Schnell, J.L., 2017. Spatial clustering and meteorological drivers of summer ozone in Europe. Atmos. Environ. 167, 496–510. https://doi.org/10.1016/j.atmosenv.2017.08.050.

Cattell, R.B., 1966. The scree test for the number of factors. Multivariate Behav. Res. 1, 245–276. https://doi.org/10.1207/s15327906mbr0102_10.

Dee, D.P., Uppala, S.M., Simmons, A.J., Berrisford, P., Poli, P., Kobayashi, S., Andrae, U., Balmaseda, M.A., Balsamo, G., Bauer, P., Bechtold, P., Beljaars, A.C.M., van de Berg, L., Bidlot, J., Bormann, N., Delsol, C., Dragani, R., Fuentes, M., Geer, A.J., Haimberger, L., Healy, S.B., Hersbach, H., Hólm, E.V., Isaksen, L., Kållberg, P., Köhler, M., Matricardi, M., McNally, A.P., Monge-Sanz, B.M., Morcrette, J.-J., Park, B.-K., Peubey, C., de Rosnay, P., Tavolato, C., Thépaut, J.-N., Vitart, F., 2011. The ERA-Interim reanalysis: configuration and performance of the data assimilation system. Q. J. R. Meteorol. Soc. 137, 553–597. https://doi.org/10.1002/qj.828.

Duane, A., Aquilué, N., Gil-Tena, A., Brotons, L., 2016. Integrating fire spread patterns in fire modelling at landscape scale. Environ. Model. Softw 86, 219–231. https://doi.org/10.1016/j.envsoft.2016.10.001.

Esteban, P., Jones, P.D., Martín-Vide, J., Mases, M., 2005. Atmospheric circulation patterns related to heavy snowfall days in Andorra, Pyrenees. Int. J. Climatol. 25, 319–329. https://doi.org/10.1002/joc.1103.

Esteban, P., Martin-Vide, J., Mases, M., 2006. Daily atmospheric circulation catalogue for western Europe using multivariate techniques. Int. J. Climatol. 26, 1501–1515. https://doi.org/10.1002/joc.1391.

Fernández-Montes, S., Rodrigo, F.S., Seubert, S., Sousa, P.M., 2013. Spring and summer extreme temperatures in Iberia during last century in relation to circulation types. Atmos. Res. 127, 154–177. https://doi.org/10.1016/j.atmosres.2012.07.013.

Garrido-Perez, J.M., Ordóñez, C., García-Herrera, R., 2017. Strong signatures of high-latitude blocks and subtropical ridges in winter PM10 over Europe. Atmos. Environ. 167, 49–60. https://doi.org/10.1016/j.atmosenv.2017.08.004.

Haylock, M.R., Hofstra, N., Klein Tank, A.M.G., Klok, E.J., Jones, P.D., New, M., 2008. A European daily high-resolution gridded dataset of surface temperature and precipitation. J. Geophys. Res. 113, D20119. https://doi.org/10.1029/2008JD10201.

Lopez-Bustins, J.A., Serrano, E., Ayarzagüena, B., Sanchez-Lorenzo, A., 2015. Spatial and temporal temperature trends in the lower stratosphere during the extended boreal winter from reanalyses. Int. J. Climatol. 35, 3888–3901. https://doi.org/10.1002/joc.4253.

Otero, N., Sillmann, J., Butler, T., 2018a. Assessment of an extended version of the Jenkinson–Collison classification on CMIP5 models over Europe. Clim. Dyn. 50, 1559–1579. https://doi.org/10.1007/s00382-017-3705-y.

Otero, N., 2018b. Jcext: Extended Classification of Weather Types. R Package Version 0.1.1. https://cran.r-project.org/package=jcext.

Philipp, A., Beck, C., Huth, R., Jacobeit, J., 2016. Development and comparison of circulation type classifications using the COST 733 dataset and software. Int. J. Climatol. 36, 2673–2691. https://doi.org/10.1002/joc.3920.

Richman, M.B., 1986. Rotation of principal components. J. Climatol. 6, 293–335. https://doi.org/10.1002/joc.3370060305.

Serrano-notivoli, R., Luis, M. De, Beguería, S., 2017. Environmental Modelling & Software an R package for daily precipitation climate series reconstruction. Environ. Model. Softw 89, 190–195. https://doi.org/10.1016/j.envsoft.2016.11.005.

Tveito, O.E., Ustrnul, Z., 2003. A Review of the Use of Large-Scale Atmospheric Circulation Classification in Spatial Climatology, Met. No. Report 10/03 KLIMA.

Yalew, S.G., Pilz, T., Schweitzer, C., Liersch, S., Kwast, J. Van Der, Griensven, A. Van, 2018. Environmental Modelling & Software Coupling land-use change and hydrologic models for quanti fi cation of catchment ecosystem services. Environ. Model. Softw 109, 315–328. https://doi.org/10.1016/j.envsoft.2018.08.029.

Zscheischler, J., Mahecha, M.D., Harmeling, S., 2012. Climate classifications: the value of unsupervised clustering. Procedia Comput. Sci. 9, 897–906. https://doi.org/10.1016/J.PROCS.2012.04.096.

3.5. Avaluació dels canvis interns en l'estructura futura dels esdeveniments conjunts secs-càlids: el cas dels Pirineus

3.5.1. Resum de l'article

Els impactes sobre zones vulnerables com les àrees de muntanya poden ser majors en un escenari futur amb unes condicions climàtiques adverses. En aquest sentit, la concurrència de llargs períodes de sequera i de temperatures extremadament càlides poden induir riscos ambientals com incendis forestals, pèrdues de rendiment de les collites o altres problemes, produint conseqüències molt més greus que si aquests fenòmens ocorren individualment –per exemple, només llargs períodes de sequera–. El present estudi tracta d'abordar els canvis recents i futurs en les següents dimensions: la durada (D), la magnitud (M) i la magnitud extrema (EM) dels esdeveniments compostos secs-càlids als Pirineus. L'anàlisi se centra en els canvis en els períodes secs extremadament llargs i en les temperatures extremadament altes que es produeixen dins d'aquests períodes secs amb la finalitat d'estimar si l'estructura interna d'aquests esdeveniments compostos ha patit canvis en el període observat (1981-2015), o si canviarà en el futur (2006-2100) sota escenaris d'emissions intermèdies (RCP4.5) i elevades (RCP8.5). D'aquesta manera, quantifiquem els canvis en les tendències temporals d'aquests esdeveniments, així com els canvis en les funcions de densitat de probabilitat bivariades per a les principals regions pirinenques. Els resultats mostren que, fins ara, el risc induït per aquests esdeveniments compostos només s'ha incrementat per l'augment de la temperatura interna d'aquests períodes secs. En relació amb el futur, s'ha comprovat que l'augment del risc estarà associat a un increment tant de la temperatura extrema en el si d'aquestes ratxes seques, com en l'allargament de la durada d'aquests períodes secs a tot el Pirineu, principalment, durant la primavera i per a un escenari RCP8.5. La part més septentrional d'aquesta serralada també patirà un increment en les dues dimensions durant l'estiu sota aquest mateix escenari més pessimista.

3.5.2. Article

Lemus-Canovas, M., & Lopez-Bustins, J. A. (2021). Assessing internal changes in the future structure of dry–hot compound events: the case of the Pyrenees. Natural Hazards and Earth System Sciences, 21(6), 1721–1738. https://doi.org/10.5194/nhess-21-1721-2021

Nat. Hazards Earth Syst. Sci., 21, 1721–1738, 2021
https://doi.org/10.5194/nhess-21-1721-2021

Natural Hazards and Earth System Sciences
Open Access
EGU

Assessing internal changes in the future structure of dry–hot compound events: the case of the Pyrenees

Marc Lemus-Canovas and Joan Albert Lopez-Bustins

Climatology Group, Department of Geography, University of Barcelona, Barcelona, 08001, Spain

Correspondence: Marc Lemus-Canovas (mlemus@ub.edu)

Received: 5 January 2021 – Discussion started: 14 January 2021
Revised: 1 May 2021 – Accepted: 4 May 2021 – Published: 2 June 2021

Abstract. Impacts upon vulnerable areas such as mountain ranges may become greater under a future scenario of adverse climatic conditions. In this sense, the concurrence of long dry spells and extremely hot temperatures can induce environmental risks such as wildfires, crop yield losses or other problems, the consequences of which could be much more serious than if these events were to occur separately in time (e.g. only long dry spells). The present study attempts to address recent and future changes in the following dimensions: duration (D), magnitude (M) and extreme magnitude (EM) of compound dry–hot events in the Pyrenees. The analysis focuses upon changes in the extremely long dry spells and extremely high temperatures that occur within these dry periods in order to estimate whether the internal structure of the compound event underwent a change in the observed period (1981–2015) and whether it will change in the future (2006–2100) under intermediate (RCP4.5, where RCP is representative concentration pathway) and high (RCP8.5) emission scenarios. To this end, we quantified the changes in the temporal trends of such events, as well as changes in the bivariate probability density functions for the main Pyrenean regions. The results showed that to date the risk of the compound event has increased by only one dimension – magnitude (including extreme magnitude) – during the last few decades. In relation to the future, increase in risk was found to be associated with an increase in both the magnitude and the duration (extremely long dry spells) of the compound event throughout the Pyrenees during the spring under RCP8.5 and in the northernmost part of this mountain range during summer under this same scenario.

1 Introduction

Research on dry spells or droughts, as well as on extreme heat events (i.e. heat waves), is habitually based upon an individual focus, and the compound nature of such events is often neglected. In this sense, in the case of spells (whether dry or wet), several studies have examined the duration thereof and have quantified the trends of such events in different regions of the world (Martin-Vide and Gomez, 1999; Zolina et al., 2013; Singh et al., 2014); however, the thermal component of these episodes has not been addressed therein. Similarly, we found different studies on temperature extremes that did not evaluate the effect of the duration of such extremes (Diffenbaugh and Ashfaq, 2010; Fonseca et al., 2016; Salameh et al., 2019). In general terms, the indices proposed by the Expert Team on Climate Change Detection and Indices (ETCCDI) do not involve analysing events in a compound manner, a shortcoming that can result in underestimation of risk (Zscheischler et al., 2018).

As mentioned above, compound analysis of events enables us to estimate the real risk induced by the simultaneous occurrence of several climatic variables; this is of particular interest in fragile and vulnerable areas, such as mountain ranges, in a context of anthropogenic climate change. In this sense, the area of the Pyrenees (Fig. 1), a transboundary area between three countries (Andorra, France and Spain), possesses a great wealth of natural resources and a high level of biodiversity. However, some studies have already addressed the initial impacts of the warming observed in this region, particularly in relation to the decline in mountain forests (Camarero, 2017). In addition, more frequent dry periods and droughts have also led to the defoliation of silver fir (*Abies alba*) forests in this region (Gazol et al., 2020). There is therefore an urgent need for a compound analysis of ex-

Published by Copernicus Publications on behalf of the European Geosciences Union.

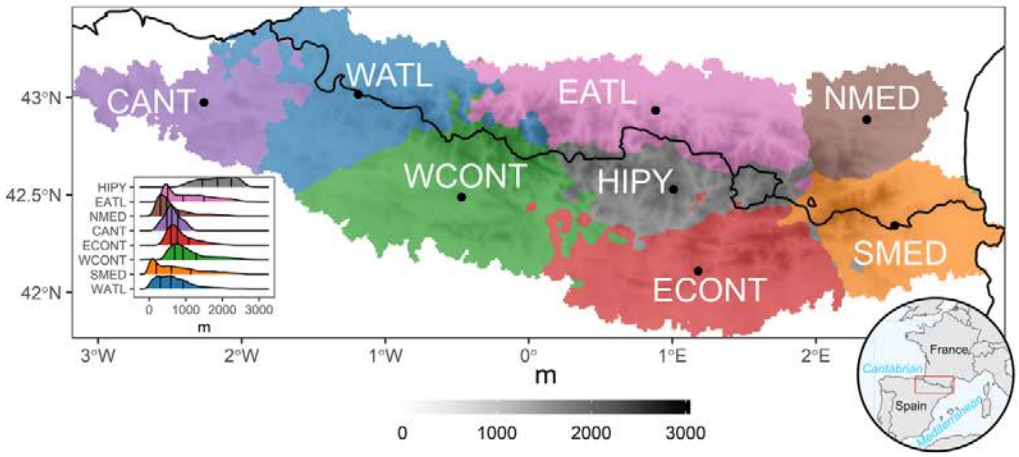

Figure 1. Regionalization obtained with the *k*-means method. From left to right: CANT – Cantabrian; WATL – West Atlantic; WCONT – West Continental; EATL – East Atlantic; HIPY – High Pyrenees; ECONT – East Continental; NMED – North Mediterranean; SMED – South Mediterranean. In the bottom left-hand corner, the elevation probability density curves (m) are shown for each region. The vertical lines indicate the 25th, 50th and 75th quantiles. The elevation base map was generated using the data provided by the Shuttle Radar Topography Mission (SRTM).

treme dry spells and extreme warm temperature events, i.e. the combination of duration (D) and magnitude (M), as conceptualized in Manning et al. (2019), in order to ascertain whether these compound events will be more widespread in the future and whether they pose other risks such as wildfires or crop yield losses.

As for the compound analysis of dry–hot events, previous studies have highlighted an increase in the frequency and spatial scope of such events in recent years in several areas such as the USA (Mazdiyasni and AghaKouchak, 2015), India (Sharma and Mujumdar, 2017) or China (Wu et al., 2019), although in Europe the magnitude (temperature) of these events was revealed to have greater weight than their duration (dry spells) as indicated by Manning et al. (2019). Several recently published studies focus mainly on the changes observed in these compound events (Wu et al., 2019; Hao et al., 2019; Manning et al., 2019). However, fewer analyses have employed future projections to assess the risk posed by the occurrence of compound events (Zscheischler and Seneviratne, 2017; Lu et al., 2018; Wu et al., 2020). Zscheischler and Seneviratne (2017) used a copula method to evaluate changes in the probability of future dry–hot compound events; they employed the Coupled Model Intercomparison Project (CMIP5) simulations to show an increase in the probability of these events in most regions of the world. Previous research has therefore highlighted a general increase in these kinds of events, but they have neglected to separately address the importance of the variables contributing to such compound events. Thus, the present study will attempt to account for the influence of the variables giving rise to dry–hot compound events. Herein we analyse the observed and projected changes in dry–hot compound events, understanding these as the combination of extremely long dry periods and extremely high temperatures within these periods.

Bias correction techniques are used to correct the data simulated by global and regional climate models (GCMs and RCMs, respectively) by means of observed data. Indeed, these techniques are most commonly employed to correct for only one variable at a time (Teutschbein and Seibert, 2012; Rajczak et al., 2016). Nonetheless, a univariate correction can moderately affect the mutual structural dependence of different variables (Wilcke et al., 2013), e.g. temperature vs. precipitation, although recent studies have shown that univariate bias correction methods can be sufficiently robust for certain specific regional impact studies (Casanueva et al., 2018). However, in the treatment of compound events, the use of multivariate bias correction methods can provide an added value (François et al., 2020) by optimally estimating multivariate dependence.

The main objectives of our paper are (1) to characterize the duration (D), magnitude (M) and extreme magnitude (EM) of events; (2) to estimate the observed regional trends of the variables at play in the compound event; and (3) to project the future trends of such compound events, under different representative concentration pathways (RCPs), in order to determine future changes in the weights of each variable involved in the compound event. As an intermediate and essential step between tasks 2 and 3, we will apply and evaluate a bias correction in relation to the historical simulations.

Section 2 describes the data collection method used in our study, including the observed and simulated data; the

Table 1. EURO-CORDEX climatic models used and their characteristics. Source: Copernicus Climate Change Service (https://cds.climate.copernicus.eu/cdsapp#!/home, last access: 30 April 2021).

Model	Institute	GCM	RCM
1	CNRM	CNRM-CM5	ALADIN63
2	CNRM	CNRM-CM5	RACMO22E
3	DMI	NCC-NorESM1-M	DMI-HIRHAM5
4	KNMI	EC-EARTH	RACMO22E
5	SMHI	IPSL-CM5A-MR	RCA4
6	SMHI	MPI-ESM-LR	RCA4

methodology employed to obtain the regionalized series of the Pyrenees; the criteria used to define each event; and the bias correction method and the assessment thereof. In Sect. 3, we present the exploratory analysis of the variables constituting the compound event, as well as the observed trends in the main regions of the study area defined in Sect. 2. In Sect. 4, we perform an exhaustive evaluation of the effects of the bias correction methods applied to the series simulated by the climate models. Subsequently, in Sect. 5, we analyse the results of the projection of the variables described in Sect. 2 with the use of different RCPs, in order to estimate changes in the internal structure of the hot–dry compound event. Finally, Sect. 6 presents the discussion of the results, and Sect. 7 presents some brief conclusions.

2 Data and methods

2.1 Observed and projected data

The accumulated daily precipitation and maximum daily temperature of the spring and summer seasons (MAM and JJA) were extracted from the database of the CLIMPY project (Characterization of the evolution of climate and provision of information for adaptation in the Pyrenees); this is a transboundary initiative whose objective is to perform a detailed analysis of recent trends in temperature, precipitation and snow cover in the Pyrenees, as well as the future projection thereof (Cuadrat et al., 2020). These two variables were provided in a 1 km × 1 km high-resolution grid, for the 1981–2015 period, and fed by 1343 weather stations located in Andorra, France and Spain; the grid was built following the quality control, reconstruction and gridding processes according to Serrano-Notivoli et al. (2017, 2019). We focused on spring and summer, as spring can constitute the precursor of summer wildfires (Turco et al., 2017) and is a season prone to crop yield losses (Zscheischler et al., 2017). We also centred our attention on summer, as this is the hottest and driest time of year in the area and is the most critical period for the occurrence of the above-mentioned environmental risks.

We used the 850 hPa temperature (T850) and the 500 hPa daily geopotential height (Z500) from ERA-Interim (Dee et al., 2011) at a spatial resolution of 0.75° to synoptically characterize these compound dry–hot events. For the climate simulation projections, six climate models were obtained from different regional climate models (RCMs), which were nested in different general circulation models (GCMs) and computed over Europe (Table 1), within the framework of the Coordinated Regional Climate Downscaling Experiment (EURO-CORDEX) (Jacob et al., 2014). These gridded projections cover all of Europe with a spatial resolution of 0.11° in latitude and longitude (∼ 12 km) for the 1981–2005 (historical experiment) and 2006–2100 (RCP scenarios) periods. We selected the climate models that provided sufficient data for such a study and which had been used in previous research (Jacob et al., 2014). Additionally, the RCPs used were RCP4.5 – stabilization without overshoot pathway to 4.5 $W m^{-2}$ (∼ 650 ppm CO_2) stabilization after 2100 (Wise et al., 2009) – and RCP8.5 – rising radiative forcing pathway leading to 8.5 $W m^{-2}$ (∼ 1370 ppm CO_2) by 2100 (Riahi et al., 2011). Herein we did not employ the gridded data but rather the cell closest to the centroid of each region (Fig. 1) in order to avoid inflation issues and misrepresentation of subgrid variability when bias correction methods (Maraun, 2013; Maraun et al., 2017) were used.

2.2 Regionalization

The Pyrenees constitute a mountainous system presenting high climatic variability, which can be summarized quite easily in order to explain the major part of the compound behaviour of dry–hot events. In this sense, the authors consider that to divide the Pyrenees into many different regions is of no particular interest for the present analysis because situations of long dry spells and extremely hot temperatures, for instance, display a practically identical synoptic behaviour pattern throughout the region. For example, a subtropical ridge produces a dry environment and above-average temperatures throughout southern Europe (Sousa et al., 2018) and hence in the Pyrenees (Lemus-Canovas et al., 2019a). This does not occur when spatial patterns of precipitation are investigated because spatial variability is much greater. Interestingly, with northern advection in this area, precipitation can be abundant on the Atlantic and northern slopes but scarce or non-existent on the southern slopes (Lemus-Canovas et al., 2018). This variability therefore differs depending on the variables analysed.

Although the synoptic driver of these dry–hot compound situations is broadly the same for the whole Pyrenees region, several geographical factors such as altitude, latitude or distance from the sea endow these events with different degrees of intensity in different areas of the Pyrenees. This subtropical ridge will have a greater impact in the southern area of the Pyrenees than in the northern sector, simply because of its proximity to the origin of the subtropical air mass. It is

therefore of great interest to divide the Pyrenees into a series of basic regions exhibiting relatively different behaviour patterns.

The use of clustering techniques is very common in the creation of regions of climate variables. For example, Carvalho et al. (2016) regionalized temperature and precipitation in Europe; Carro-Calvo et al. (2017) performed similar tasks for tropospheric ozone; and more recently, Lemus-Canovas et al. (2019b) employed these techniques by combining precipitation with circulation types to establish rainfall regions in the Alps. In the present paper we conducted a combined regionalization of temperature and precipitation, (as both variables constitute the basis of dry–hot events) by applying the k-means algorithm to the daily series of temperature and rainfall (normalized) of spring and summer. In order to obtain robust regionalization, we established a maximum of 100 iterations and 300 repetitions. As the algorithm converges, the spatiotemporal patterns of temperature and precipitation for all cells are observed to be consistent within a given region (i.e. close to the centroid), and each grid cell is seen to be better represented by its cluster centroid than by any other centre of cluster. To decide the optimal number of clusters, we performed an iteration from $k = 2$ to $k = 15$, obtaining 14 different classifications (see Fig. S1 in the Supplement). In order to establish the explained variance (EV) for each new created region (Eq. 1), we computed the mean of squared distances between cluster centres (betweenss) and the total sum of squares (totss). The highest possible values are expected, since the aim involves achieving a clear separation between clusters. Totss is the sum of betweenss and total withinss. Withinss is the within cluster sum of squares. It results in a vector with a value for each cluster. The lowest possible values are expected, since homogeneity within the clusters is sought.

$$\mathrm{EV} = \frac{\text{betweenss}}{\text{totss}} \cdot 100 \quad (1)$$

The percentage of explained variance can be explained by the increase in k clusters, as shown in the scree test (Cattell, 1966) in Fig. S2 in the Supplement. Such a representation shows two points – $k = 5$ (40 %) and $k = 8$ (48 %) – which could be considered a "slope change" and therefore possible delimiters of the number of regions. Despite the use of the scree test, the decision is subjective, and a compromise is therefore needed between the degree of complexity and the descriptive capacity of the regionalization (Carro-Calvo et al., 2017). Consequently, we decided to use eight clusters, which explain 48 % of the variance (Fig. S2).

For the construction of the regionalized series, the daily values of all cells were averaged in order to work with a series that is smoother than if the centroids were used. The main reason for working with averaged regional series was to avoid the downscaling process in the application of the bias correction method. Thus, inflation and modification of the trend represented by the climate model (Maraun, 2013) were avoided, among other undesirable effects. This and other aspects relating to the application of the bias correction are explained in Sect. 2.4.

2.3 Event definition

As previously stated, the dry–hot events are characterized by means of the following dimensions: duration (D), magnitude (M) and extreme magnitude (EM), corresponding to the spring months, March, April and May (MAM), and to the summer months, June, July and August (JJA); both seasons are analysed independently. D is defined as the number of consecutive days on which precipitation is below 1 mm (Fig. 2). This threshold was chosen to be consistent with previous studies (Orlowsky and Seneviratne, 2012; Donat et al., 2013; Lehtonen et al., 2014; Manning et al., 2019), as well as to avoid the drizzle effect, which systematically causes climate models to overestimate precipitation (Gutowski et al., 2003).

To ensure that independent and extreme spells are obtained, for each year (spring and summer, separately) we computed the duration of the 95th percentile of dry spells, subsequently selecting the ones displaying a duration longer than this threshold. We performed a sensitivity test in order to select an appropriate threshold capable of detecting sufficiently long and robust dry spells, especially in wet areas with few dry spells. Additionally, M is the conditional distribution of daily maximum temperatures (T_x) during long dry spells (D) while EM is the conditional distribution of temperature during dry spells that exceed the 95th percentile of daily T_x. T_x values above the 95th percentile occurring outside of these long dry spells (D) are not considered. Figure 2 shows the performance of these three variables in a grid cell time series in the easternmost part of the Pyrenees.

Analysing the EM subset enables us to characterize the greater risk of the simultaneous occurrence of both variables, D and EM, which in turn may significantly increase the risk of wildfires, for example. To estimate the trend of the events and to assess the statistical significance of these trends we employed Sen's slope (Sen, 1968) and Mann–Kendall's nonparametric test (Mann, 1945). We also computed the annual temperature anomalies of M and EM with respect to the daily T_x mean (spring and summer) over the1981–2015 period in an attempt to quantify temperature anomaly differences between these two types of variables.

2.4 Bias correction and evaluation

In the present study (1) we calculated the mean of daily T_x and daily precipitation from the observed grid cells belonging to each of the regions of the study area (Fig. 1); (2) we extracted the time series from the cell closest to the centroid of each region for each RCM (Table 1); (3) we applied a univariate and a multivariate bias correction method for correcting daily T_x and daily precipitation from the RCMs;

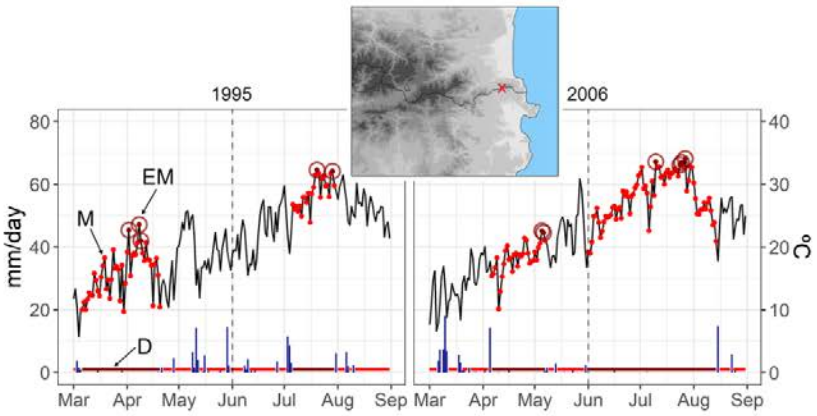

Figure 2. Time series of daily precipitation (vertical blue bars) and daily maximum temperature (T_x) (black line) at a mountainous location in the easternmost part of the Pyrenees ($x = 2.9$; $y = 42.5$). The horizontal red bars at the bottom end of the plot show the length of dry spells, while the dark red bars show the extremely long dry spells (D). The red dots (M) show the T_x values during a D event. The dark red dots with a circle indicate T_x values above the 95th percentile during a D event. The dashed vertical line indicates the separation between the spring and summer seasons. The selection of years highlights a dry spring (1995) and a dry summer (2006) in this area.

and (4) we aggregated to D, M and EM indices the RCM-corrected daily T_x and daily precipitation.

One of the most popular and widely used techniques for the univariate bias correction is quantile mapping (QM). Bias correction by QM is frequently used to downscale simulations at the station level or in high-resolution grid boxes; however, it induces inflation problems in the corrected series (Maraun, 2013) and is unable to generate daily subgrid variability (Maraun et al., 2017). The above-mentioned issues tend to be exacerbated in mountain areas, where many local processes may not be represented following the QM process (Maraun and Widmann, 2018b). As an alternative to univariate bias correction, and in an attempt to correct the inter-variable correlation, different multivariate bias correction methods have been proposed over the last few years (Piani and Haerter, 2012; Vrac and Friederichs, 2015; Cannon, 2016, 2018a).

In the present research we first employ a univariate bias correction approach, the empirical quantile mapping (EQM) method, which estimates the values of the empirical cumulative distribution function (ECDF) of the observed and modelled time series for each quantile (Panofsky and Brier, 1968; Gudmundsson et al., 2012). Hence, if X_o and X_m are the observed and modelled values, respectively, then

$$\hat{X}_m = F_o^{-1}(F_m(X_m)), \tag{2}$$

where F_m is the empirical cumulative distribution function of X_m and F_o^{-1} is the inverse empirical distribution function (or quantile function) corresponding to X_o. We apply univariate QM with the R package qmap (Gudmundsson, 2014) using 100 quantiles. The drizzle effect was corrected using a wet-day threshold of $1\,\mathrm{mm\,d^{-1}}$ for the observations (Hay and Clark, 2003; Piani et al., 2010)

Second, the multivariate bias correction method used is the one proposed by Cannon (2018a): the multivariate bias correction with N-dimensional probability density function transform (MBCn). This method is based on an adaptation of an image processing algorithm used to transfer colour information; MBCn enables the statistical characteristics of a reference multivariate distribution to be transferred to the multivariate distribution of climate model variables. The MBCn method can be summarized in four steps with regard to how it corrects climate simulations. In step (a), MBCn uses the quantile-delta mapping method (QDM; Cannon et al., 2015), which preserves absolute or relative changes in quantiles, e.g. for variables such as temperature or ratio variables like precipitation. In step (b), once univariate distributions have been corrected, the dependence structure is adjusted by means of an iterative process j. In each step, data are multiplied by random orthogonal rotation matrices to partially decorrelate the climate variables to be corrected.

$$\begin{aligned}\tilde{X}_m^{[j]} &= X_m^{[j]} R^{[j]},\\ \tilde{X}_p^{[j]} &= X_p^{[j]} R^{[j]},\\ \tilde{X}_o^{[j]} &= X_o^{[j]} R^{[j]}.\end{aligned} \tag{3}$$

In step (c), we apply the absolute change form of QDM to each variable in $\tilde{X}_m^{[j]}$ and $\tilde{X}_p^{[j]}$, using the corresponding variable in $\tilde{X}_o^{[j]}$ as the target, yielding $\hat{X}_m^{[j]}$ and $\hat{X}_p^{[j]}$. In step (d), we rotate back:

$$\begin{aligned}X_m^{[j+1]} &= \hat{X}_m^{[j]} R^{[j]-1},\\ X_p^{[j+1]} &= \hat{X}_p^{[j]} R^{[j]-1},\\ X_o^{[j+1]} &= X_o^{[j]}.\end{aligned} \tag{4}$$

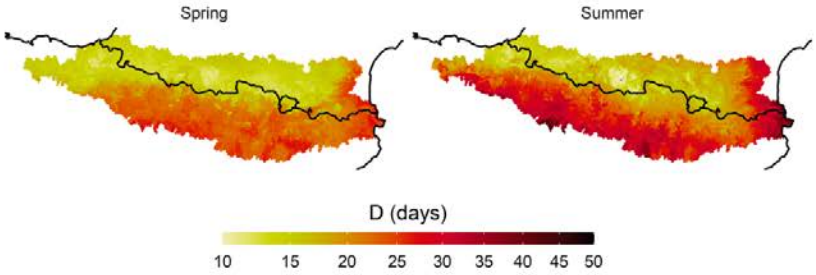

Figure 3. Annually averaged extremely long dry spells (> 95th percentile) for spring and summer during 1981–2015 period.

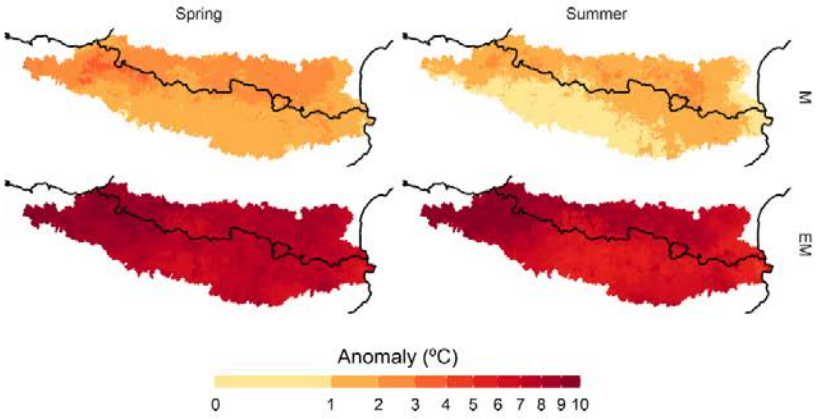

Figure 4. Annually averaged maximum temperature (T_X) anomaly for M and EM variables and for spring and summer with respect to daily means over the 1981–2015 period.

The steps (b)–(d) are repeated until the multivariate distribution of $X_m^{[j+1]}$ matches X_o. We applied MBCn with the R package MBC (Cannon, 2018b)

Both bias correction methods were evaluated by means of a 7-year 5-fold cross validation of (4 folds for adjustment and 1 fold for validation). Cross validation should not be applied to validating free-running climate simulations against observed series, as the climate models are temporarily stochastic and could induce serious errors in the assessment of the daily series (Maraun and Widmann, 2018a). However, herein we work on a seasonal scale – spring and summer – on the variables D, M and EM (see Sect. 2.3), where the RCM is expected to be able to reflect the seasonality component and trend.

We assessed the structural dependence between temperature and precipitation, which was bias-corrected, by means of Pearson's correlation coefficient between the observed series and the historical simulation (uncorrected) series and between the observed series and the bias-corrected historical simulation (corrected). Prior to the correlation, we averaged daily temperature and daily precipitation to each Julian day for the whole series (1981–2014) in order to avoid noise in the results.

In addition, we tested the differences between the simulated and observed distributions of extreme long dry spells, using the Kolmogorov–Smirnov (KS) test. This test serves to evaluate the weaknesses of bias correction methods in order to accurately estimate the length of dry spells, which have been noted in previous research (Rajzak et al., 2016; Maraun et al., 2017). Furthermore, we tested the bias estimation for temperature using two thresholds, the 95th percentile of temperature distribution and the 95th percentile of temperature distribution during the 95th percentile of extremely long dry spells, in order to discuss the performance of each bias correction method in these extreme temperature situations.

3 Characterization of the variables underlying the compound event and of the role they play in potential risks

Extremely long dry spells (D) have a main north–south pattern in which the northernmost areas present extreme D values of less than 15 d in spring and summer and the southernmost areas provide values that can exceed 30 d, mainly in summer (Fig. 3). A second spatial pattern enabled the Atlantic and Mediterranean coastal areas to be differentiated.

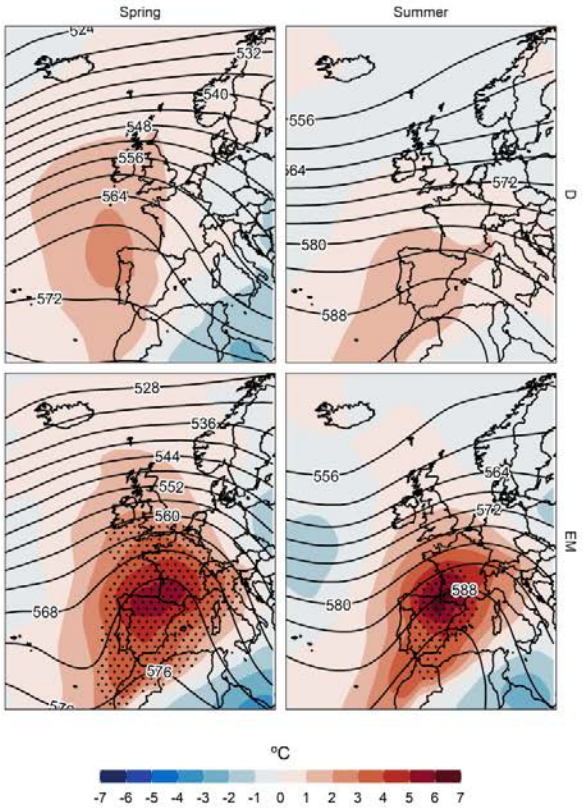

Figure 5. Daily anomalies of temperature at 850 hPa (°C, shading) and absolute geopotential height at 500 hPa (dm, contours), with contour interval of 4 dm for the days comprising *D* and EM variables in spring (1322 and 104, respectively) and summer (1396 and 111, respectively), in the HIPY region (most centred region of the Pyrenees). Dots identify regions under flash heating conditions (T850 daily mean above the local daily 99th percentile (with respect to 1981–2015), computed with a 31 d centred window).

The former area presented the lowest number of extreme spells throughout the study area in spring and summer. On the other hand, the Mediterranean area showed a very high number of extreme dry spells, especially in summer, when these lasted on average up to 50 d. These spatial patterns showed that, despite the small size of the study area, the *D* patterns are very diverse.

However, not only did the present paper focus upon variable *D*, but we also examined the combination of this variable and extremely high near-surface temperature. In this sense, it is important to emphasize the difference between analysing only the T_x values of the days comprising *D*, which we called *M*, and analysing the T_x values > 95th percentile (EM). This difference is illustrated in the T_x anomalies of both periods (Fig. 4).

Extremely long dry spells (*D*) are inherently characterized by warmer-than-normal periods (*M*). The long dry spells give rise to temperatures between 1 and 4 °C above the mean temperature in spring and between 0 and 3 °C above the mean temperature in summer. Although these anomalous temperatures are not extremely high in the dry periods, especially in summer, if we analyse the thermal extremes (EM) occurring within the *D* events, in spring and summer the thermal anomaly with respect to the normal values of these two seasons is observed to reach up to 10 °C above the average in the northern half of the study area and in the area of Atlantic influence of the study area. In the southernmost region, these anomalies are also accentuated, being between 6 and 8 °C above average. The reason why the thermal anomalies are slightly higher in the northern and Atlantic region of the study area is mainly due to the fact that in these areas the number of days with precipitation (and therefore with a moderate T_x) is very high by default (Lemus-Canovas et al., 2019a). Consequently, although the spells are short, they give rise to an extremely positive thermal anomaly, mainly on the hottest days of the spell (see EM for summer in Fig. 4). In contrast, in the south of the Pyrenees, most days present hardly any precipitation, especially in summer, and dry spells and a positive thermal anomaly are therefore not synonymous (see *M* for summer in Fig. 4). A similar explanation can be found in the seasonal differences: summer is the dry season in most of the study area, which usually presents high thermal values and no precipitation; consequently, thermal anomalies of *M* and EM are generally lower than those observed in spring. These surface conditions are also reflected in the upper layers (Fig. 5). Precisely, the mean thermal anomalies at 850 hPa during *D* events are slightly greater than normal, between 0 and 2 °C above the mean. However, when analysing the set of extreme thermal days (EM) in the *D* events, the anomalies at 500 hPa are also seen to reach very high values, between 5 and 7 °C, just above the study area. It also confirms a greater enhancement of the subtropical ridge in the EM than in the *D* events.

Before analysing the future projection of the variables *D*, *M* and EM, we reviewed the observed trends of such variables for each region and season. In the case of *D* (Fig. 6a), a non-significant trend was observed (p value ≤ 0.05) at the 95 % confidence level. A high interannual variability in the duration of extreme dry spells was detected.

This did not occur when assessing the EM and *M* trends (Fig. 6c and b, respectively), as both variables displayed a tendency to increase. This trend presented a higher slope in the spring and in the case of the EM. Indeed, the annual values of EM for spring and summer were almost all positive, whilst this was not the case for evaluating only *M*. At an intra-regional level, the main differences were observed in summer for EM, when the Mediterranean regions NMED and SMED accounted for a higher slope than the other regions. On the contrary, in spring growth was practically the same for all regions for EM and *M*. Remarkably, the HIPY

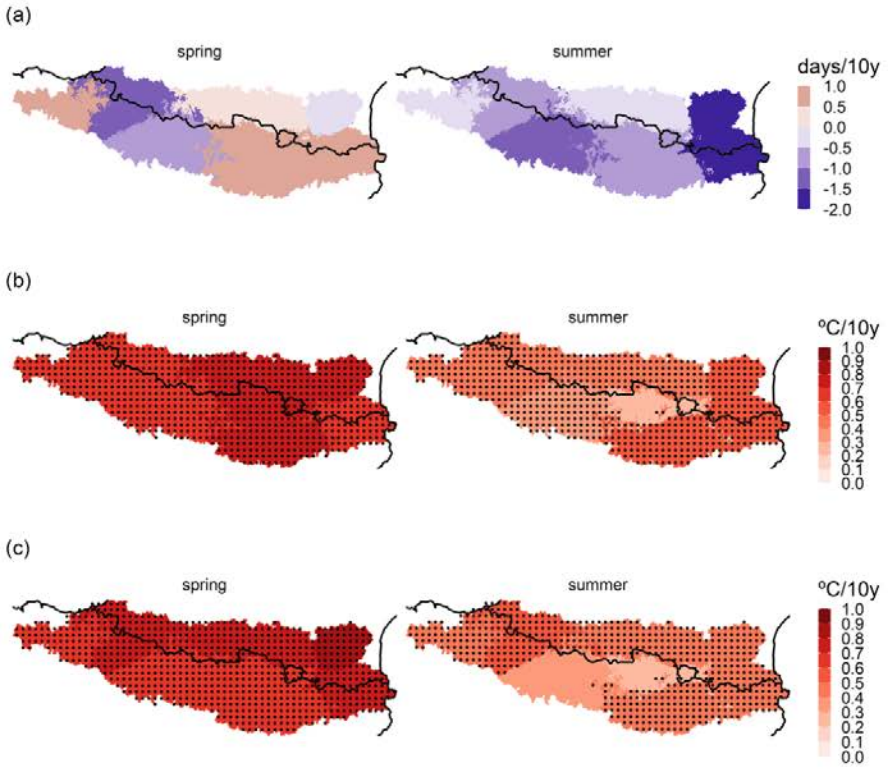

Figure 6. The 10-year trend (Sen's slope) for **(a)** extreme dry spell events per year (D), **(b)** mean maximum temperature events within the dry event per year (M) and **(c)** mean extreme maximum temperature events within the dry event per year (EM), for the spring and summer seasons and for all regions of the study area. The stippling shows statistically significant regions at the 95 % confidence level.

region did not show a significant increase in summer for EM and M for a p value ≤ 0.05.

4 Assessing the reliability of the bias-corrected projections

We evaluated the bias correction (BC) methods in order to estimate (1) how they are able to represent the dependence structure between temperature and precipitation (Figs. 7 and 8); (2) how well extremely long dry spells are simulated by RCMs, as well as to ascertain the contribution of the bias correction methods (Fig. 9); and (3) the degree of bias of daily maximum temperatures conditioned to extremely long dry spells (Fig. 10).

Regarding the structural dependence between temperature and precipitation, in the case of the CANT region (Fig. 7) a better correlation was observed in the simulation corrected with the MBCn method (Fig. 7b) in comparison with the univariate bias correction (UBC) method (Fig. 7a). Both methods adjust the bias of the marginal distributions, but MBCn can reproduce the dependence relationship between precipitation and temperature more closely to the observed values than UBC. A similar situation occurs in the dipole area of the NMED study area (Fig. S3 in the Supplement), where MBCn (Fig. S3b) tends to cause an increase in the correlation coefficient between temperature and precipitation, even above the correlation value estimated in the data observed.

The performance of the bias correction methods in reproducing the distribution of the extremely long dry spells is generally irregular and unable to reproduce the observed distribution in some cases, a phenomenon already pointed out by Maraun and Widmann (2018b) and François et al. (2020). On analysing the ECDFs (Fig. 8) generated for the CANT region and for the two bias correction methods, MBCn is seen to provide values of the D statistic of the KS test closer to zero than the UBC method for all models except for IPSL-RCA4. Furthermore, the ECDF of MBCn is also observed to fit the observed distribution better than the ECDF of the uncorrected model, with the exception of the CNRM-ALADIN63 model. For the two bias correction methods and for the CANT region, only the CNRM-ALADIN63 model and the NorESM1-HIRHAM5 model showed statistically significant KS test values at the 95 % confidence level; this indicates that only for these two cases, the duration of the

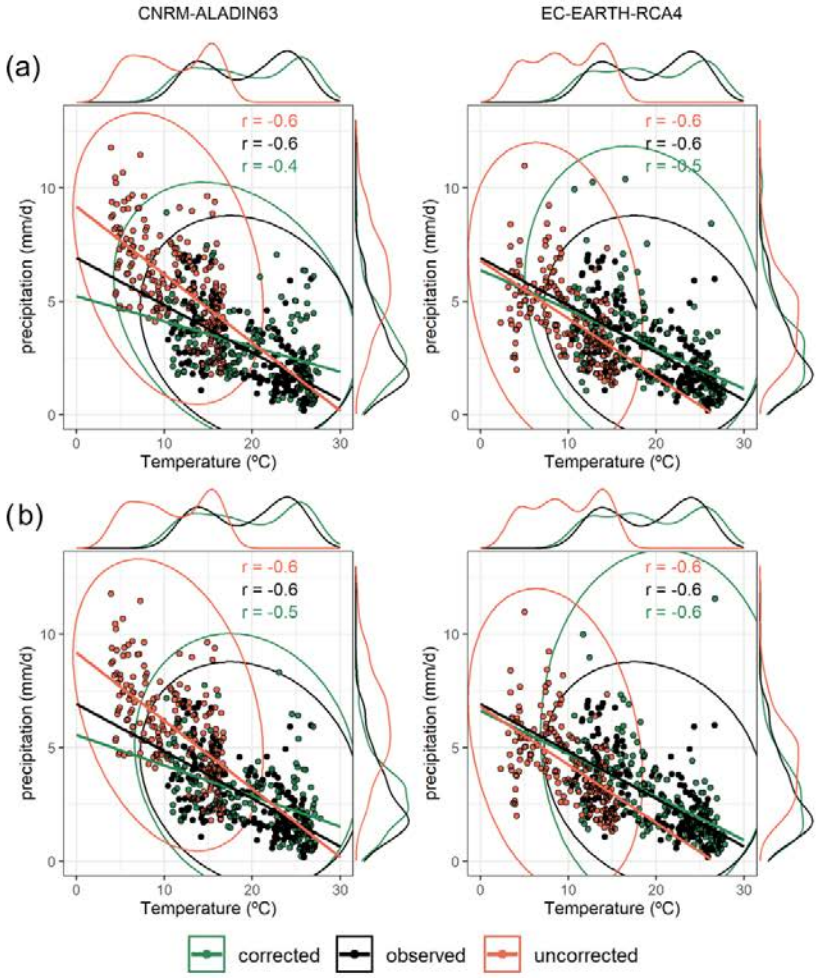

Figure 7. Distribution of mean daily temperature vs. mean daily precipitation from March to August (1981–2005) for the CANT region and for two RCMs: CNRM-ALADIN63 and EC-EARTH-RCA4. UBC method **(a)**; MBC method **(b)**. Fitted lines, areas of distribution and density distributions are shown; green refers to the bias-corrected model, black indicates the observed data, and red shows the raw/uncorrected model. Pearson correlation values (r) are also shown.

BC extreme dry spells differs from the observed values. The NMED region presents very different results from those provided for the previous region. Neither of the bias correction methods can be seen to outperform the other. In both methods the bias correction fails to reproduce the observed ECDF (p value < 0.05 in all models and bias correction methods). In the ECDFs there is clearly an underestimation of the length of the extreme dry spells both for the uncorrected model and for the model after correction by the two BC methods. Thus, we observe that although the results for the CANT region are quite accurate, there exists a high degree of uncertainty in the estimation of dry spells in the NMED dipole region, which implies that the results to be projected in subsequent analyses should be considered with caution.

In the case of temperature extremes, both bias correction methods perform well at extreme percentile daily temperature (95th percentile, p95) for the CANT and NMED dipole regions, with no apparent bias in performance (Fig. 9). On reaching more extreme values, such as the temperature extremes (p95) occurring within periods of extremely long dry spells (p95), which we call EM, the MBCn-corrected models are generally seen to reproduce these very extreme temperature values much better than the UBC-corrected ones. These differences are more noteworthy in the CANT region than in the NMED region. The patterns detected for these two re-

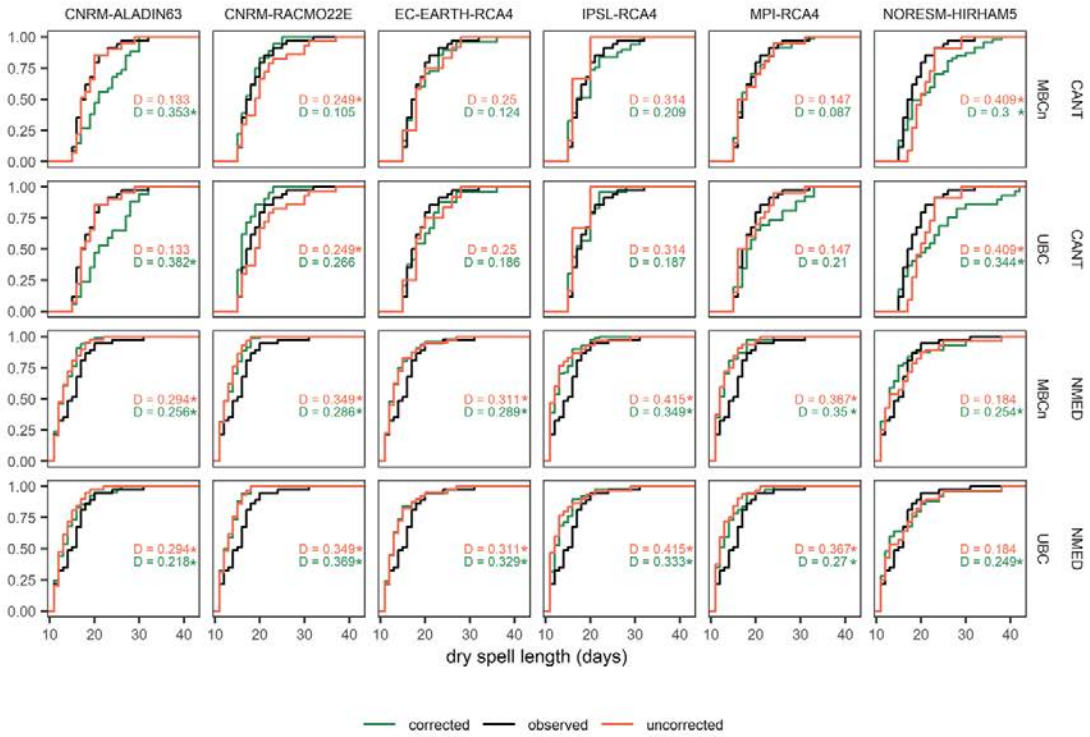

Figure 8. Empirical cumulative density function of the extreme dry spell length (p95) according to the CANT and NMED regions, UBC and MBCn bias correction methods, and the six historical RCMs used in this study for the 1981–2005 period. The Kolmogorov–Smirnov statistic is annotated in each plot as D. The asterisk indicates that the null hypothesis of the KS test is rejected. Green shows the corrected distribution; red shows the uncorrected distribution, and black indicates the observed distribution.

gions are very similar to the remaining regions of the study area (Fig. S4 in the Supplement).

5 Future changes in the variables underlying the compound event

After evaluating the bias correction methods, in this section we present the results of the bias-corrected projections using the MBCn method. The regional projections showed an increase in the duration of D events (Fig. 10a); these were only abundant in the case of the scenario of high greenhouse emissions (RCP8.5) and were consistent across all regions during spring. On the other hand, in summer substantial increases are only detected in the EATL, HIPY and NMED regions, which are all located in the northern half of the Pyrenees. However, the scenario projected by the RCP4.5 contrasts greatly with the previous one. In this moderate RCP4.5 scenario, with the exception of the WCONT and ECONT continental regions, no region showed any statistical significance in the duration of D events during spring. In summer and under the latter scenario, no statistically significant trend towards an increase in D events was detected in any of the regions.

In the case of the hot extremes (EM), the previously detected increase was evident under both scenarios (Fig. 10b). However, special attention should be paid to the greater increase in EM in relation to M (Fig. 11).

Moreover, the rate of warming during the hot extremes was variable albeit more consistent in a high emission scenario (RCP8.5) (Fig. 11). Interestingly, under this scenario and during the spring, the EM trend was above M throughout the study area, with particular incidence in the CANT, EATL and ECONT regions, at about 0.10 °C per 10 years. In summer, the increase in EM was faster than that in M in the southern regions, especially in WCONT, ECONT and SMED, at up to 0.15 °C per 10 years more than in M trends. In the intermediate scenario, there was greater equilibrium between the EM and M trends, but in all regions, there is a trend towards a faster increase in EM than in M.

It is of particular interest to analyse these D and EM events jointly to ascertain whether the compound risk of these two variables will be equally distributed or whether each of the two variables will have a different weighting in the joint event. This evaluation is shown in Fig. 12 for the CANT

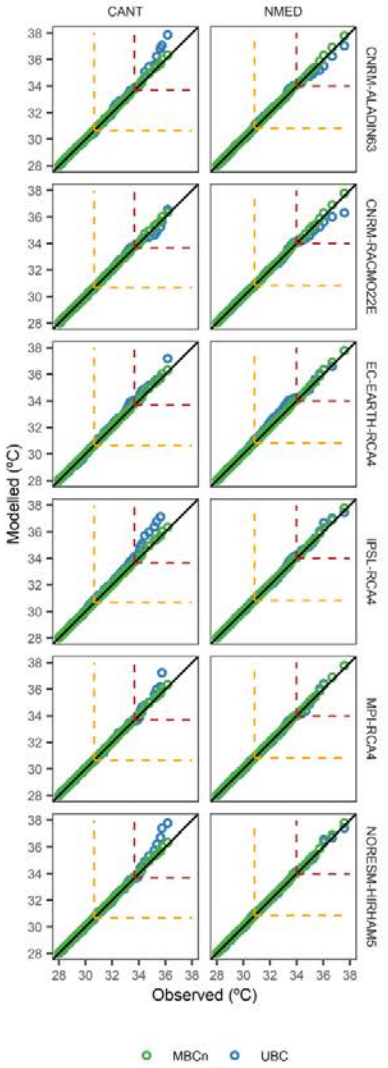

Figure 9. Quantile–quantile plot of observed vs. modelled values for temperatures in the CANT and NMED regions and all RCMs; green and blue circles indicate MBCn and the UBC method, respectively. The dashed yellow box at top right shows the 95th percentile of observed daily temperature, while the dashed dark red box at top right shows the 95th percentile of observed daily temperature during the occurrence of dry spells of extreme length (95th percentile).

and NMED dipole regions, where the multivariate coordinates of the anomalies of events D and EM are shown; these are divided into three periods, 2016–2035, 2046–2065 and 2081–2100, which are consistent with the periods selected in the *IPCC Fifth Assessment Report* (Stocker, 2014), for both seasons and both emission scenarios. On the one hand, the displacement along the y axis enabled the increase in the duration dimension (D) in the compound event to be evaluated. On the other hand, the displacement along the x axis indicated an increase in the thermal anomaly and, consequently, greater risk posed by the magnitude dimension (EM). In the case of the CANT region, the average value of the bivariate distribution of each spring and summer period projected by RCP4.5 clearly indicated that the increase in the compound risk was caused by an increase in extreme magnitude (EM), i.e. by the thermal increase, as opposed to an increase in the duration of such events (D). The same assessment can be extrapolated to the NMED region for the spring in an RCP4.5 scenario. A very similar pattern is observed in the case of summer for this intermediate scenario. In the RCP8.5 scenario, a very considerable increase in risk was perceived as a result of the increased weight of the magnitude, especially in the last two periods in both seasons and regions. The increase in the D dimension continued to be very weak for the CANT region, regardless of the season analysed. On the other hand, in the NMED region, there was a remarkable increase in dimension D, which rose by an average of 5 d (summer, 2081–2100) with respect to the historical average (1981–2005). In this case, we detected that a statistically significant increase (p value < 0.05) in the compound risk occurred in both dimensions (up to 6 °C in summer), thus implying a much higher risk than in the CANT dipole region.

With regard to the other regions, several patterns are observed across the study area. (i) For RCP4.5, in all regions and in both seasons, there is a noteworthy increase in the EM dimension, while no changes occur in the D dimension. (ii) However, in the RCP8.5 scenario for spring, all regions show an increase in the compound risk as a result of an increase in the duration of both D and EM events. (iii) For this extreme scenario in summer, only the EATL, HIPY and NMED regions, and to a lesser extent the WATL region, all located in the northern half of the Pyrenees, show an increase in both dimensions (D and EM). The rest only exhibit an increase in the thermal dimension (EM); see Figs. S5–S9 in the Supplement for details.

Of particular interest is the HIPY region, which presents the highest average elevation in the study area, with several glaciers and a multitude of snow-capped mountains. Precisely, this region in an RCP8.5 scenario will present a marked statistically significant increase (p value < 0.05) in both dimensions (Fig. 13). This will occur gradually both in spring and summer during this century.

These results are summarized in Fig. 14, which shows the future patterns of dry–hot compound events according to the D and EM variables for the whole Pyrenees area. Each season and emission scenario present a different pattern, summarized below:

- *Spring, RCP4.5.* This gives an increase in the one-dimensional compound risk based on (extreme) magnitude.
- *Summer, RCP4.5.* This gives an increase in the one-dimensional compound risk based mainly on (extreme)

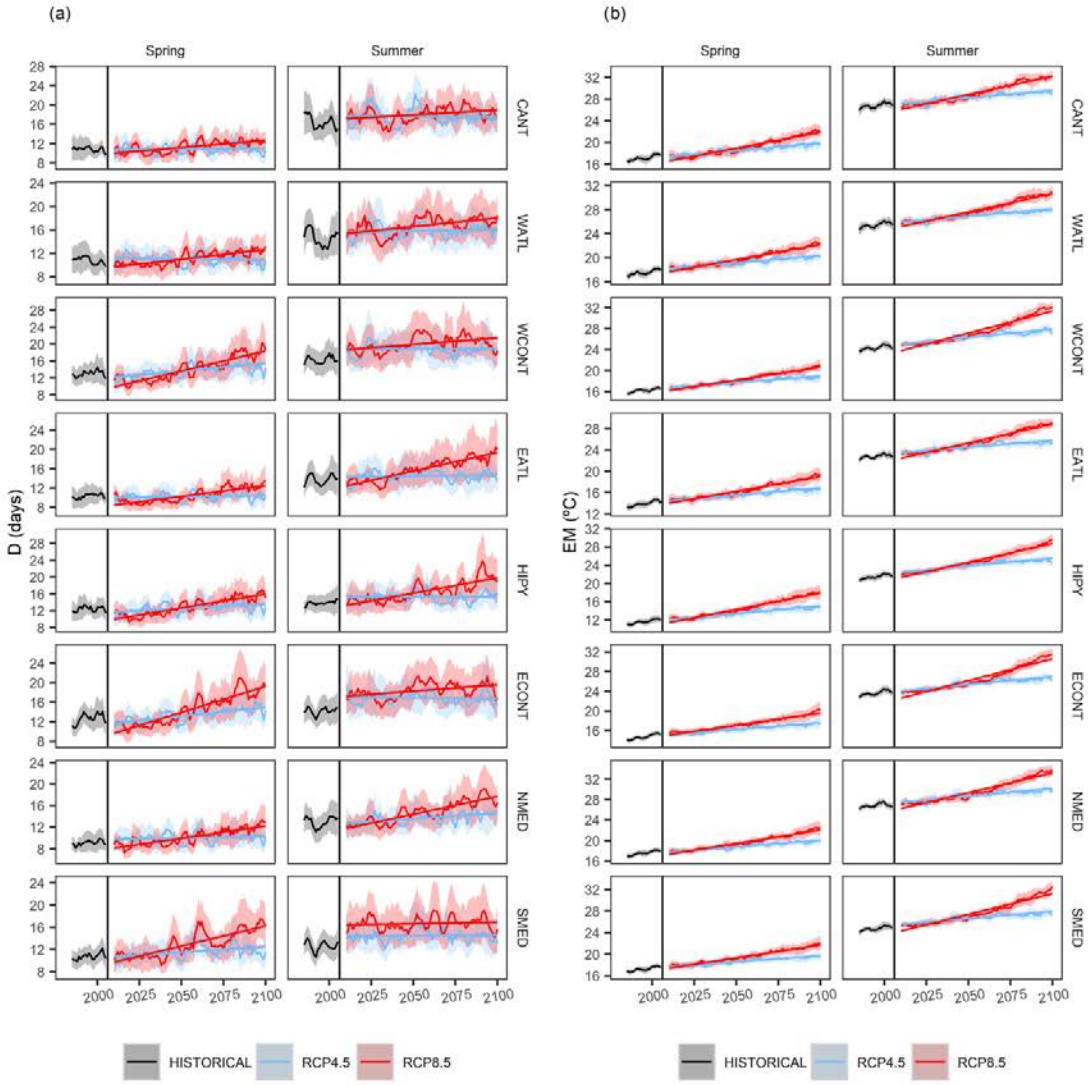

Figure 10. Observed period and historical (1981–2005) and future (2006–2100) projections (5-year moving average) of the events of **(a)** *D* and **(b)** EM for intermediate (RCP4.5) and extreme (RCP8.5) scenarios for all regions and for the spring and summer seasons. The curves show the average value of all models, while the shaded areas indicate the standard deviation of the models for each year.

magnitude. Although a greater increase in EM is observed in all regions (see Figs. 12 and 13 for CANT, NMED and HIPY regions), no increase in the second dimension (extreme length of dry spells) is detected.

– *Spring, RCP8.5.* This gives an increased risk resulting from a two-dimensional component in all regions of the Pyrenees. The increase in extreme magnitude is slightly greater in the Mediterranean (NMED and SMED) and continental regions (ECONT and WCONT). A sharp increase is observed in the second dimension (*D*) in all regions, except for the westernmost regions (CANT and WATL) (moderate increase).

– *Summer, RCP8.5.* This gives an increase in the two-dimensional compound risk in the northern façade of the Pyrenees (NMED; EATL; HIPY; and, to a lesser degree, WATL). The increase in the other regions mainly refers to the EM dimension. The increase in EM in the final period in all regions is the highest of the four patterns described.

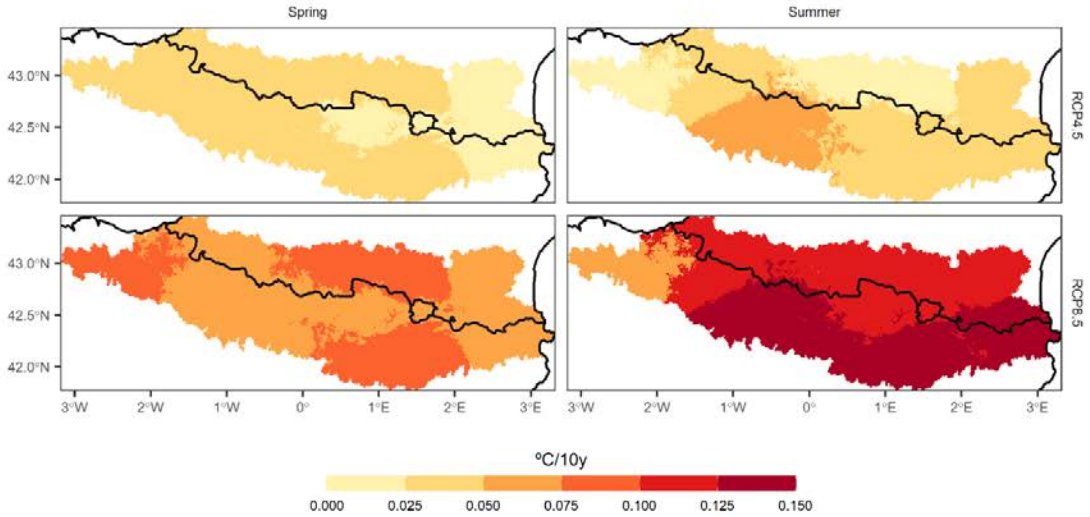

Figure 11. Multi-model mean projected change between the trends of M and of EM variables. Positive values indicate a higher positive trend in EM values than in M values.

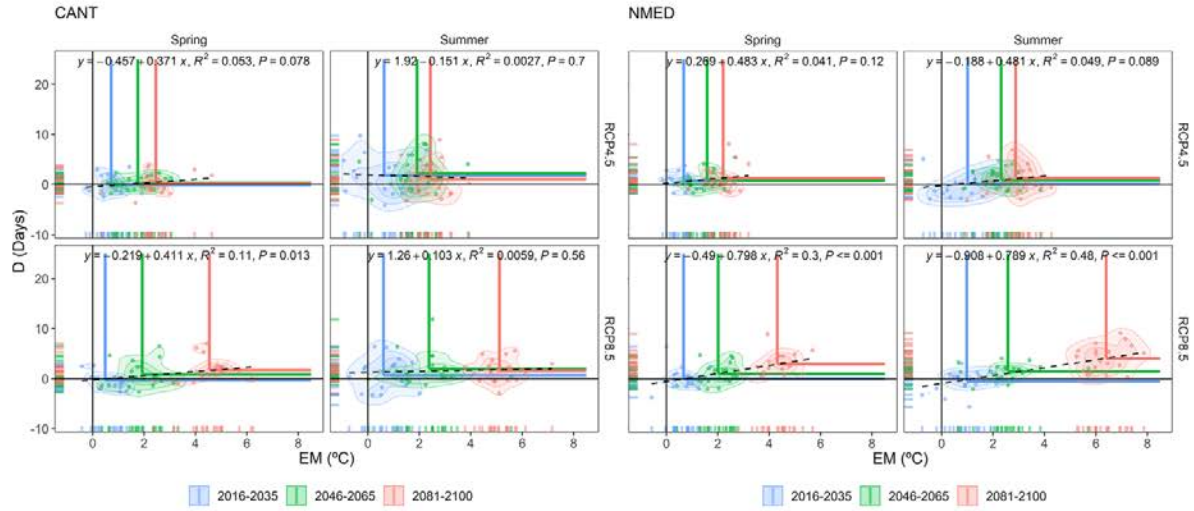

Figure 12. Bivariate probability density functions of D and EM anomalies for the three future periods (2016–2035, 2046–2065 and 2081–2100) and for the two emission and seasonal scenarios with respect to the historical period (1981–2005) for the CANT and NMED regions. Each point in the scatter plot represents the multi-model annual mean of D and EM in a given year. The intersections of the horizontal and vertical blue, green and red lines indicate the mean anomaly value of the bivariate distribution for each period. The linear fit regression was computed using the annual mean anomalies of EM and D for the 2016–2100 period. Each plot possesses a regression equation and its statistical significance (P, p value). The figure is generated using the ensemble of all RCMs.

The remaining regions shown in the supplementary document were at the intermediate stages of those described herein (Figs. S5–S9). However, the WATL region, which is adjacent to the CANT region, was influenced by both climates (Atlantic and Mediterranean) and therefore did not reflect a similar behaviour pattern to that of the CANT region (see Fig. 1 to verify the heterogeneity of this region).

6 Discussion

The use of bias correction methods to correct the distribution of dry spells indicated the inability to robustly resolve these types of bias. The bias correction only resolves the bias resulting from the drizzle effect but not the biases resulting from topographic issues or the underestimation of the persis-

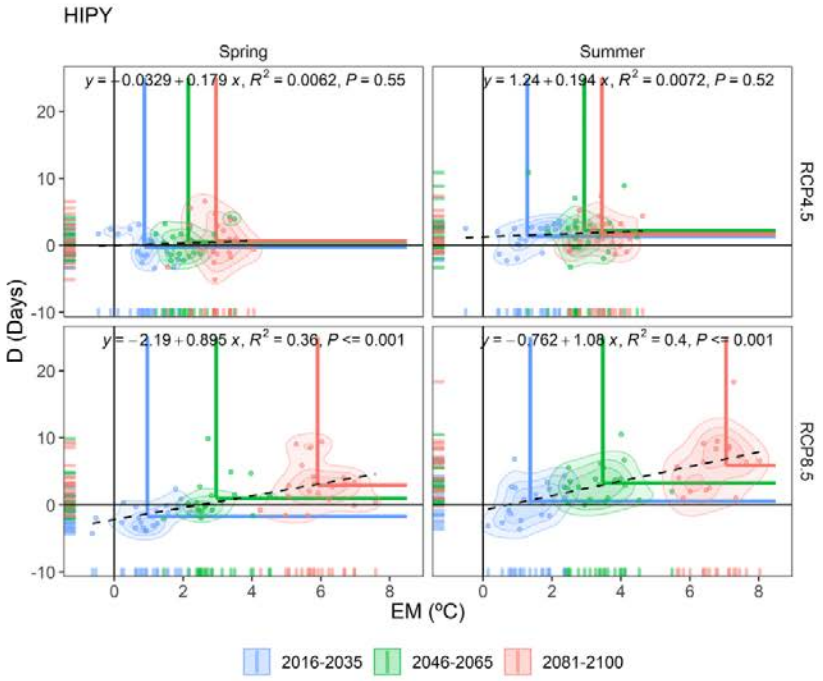

Figure 13. Same as Fig. 12 but for HIPY region.

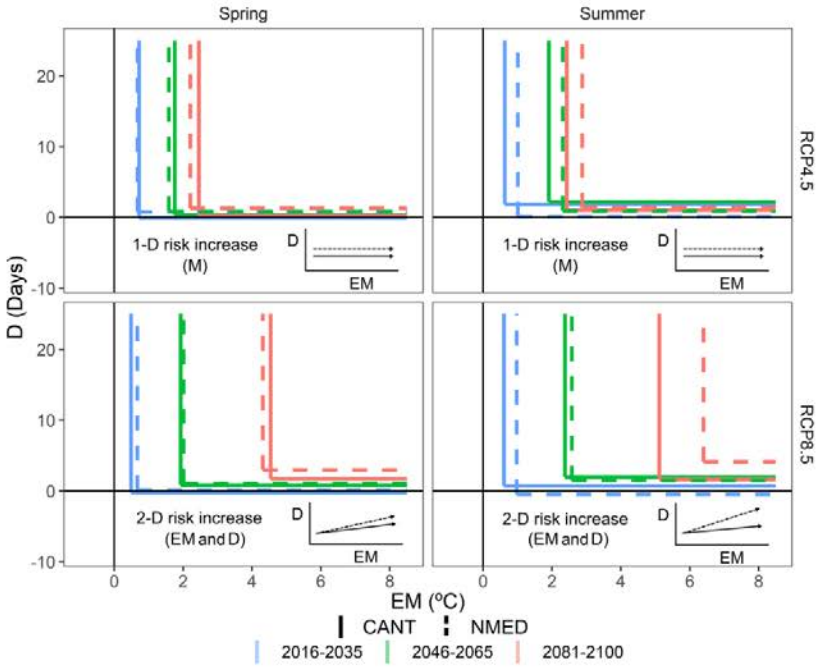

Figure 14. Diagram of the drivers of the three future periods (2016–2035, 2046–2065 and 2081–2100) of the compound event for D and EM in the CANT (solid line) and NMED (dashed line) regions, which acted as a dipole in the study area.

tence of anticyclonic conditions (Maraun et al., 2017). For future studies, as suggested by Maraun et al. (2021), before applying bias correction methods, a prior evaluation of the performance of GCMs in simulating the persistence of dry events is needed mainly to transfer the minimum bias in the temporal dependence when applying the bias correction.

On the other hand, the results of the present research reveal that up to the present there has been a general increase in the compound risk of dry–hot events due to an increase in the thermal component; thus, the duration dimension is excluded, as pointed out in various recent studies (Hao et al., 2018; Manning et al., 2019). A significant finding of our study refers to a significant increase throughout the Pyrenees and to the compound risk in relation both to the magnitude dimension (extreme temperature) and to the duration dimension (duration of extreme dry event), for spring under the RCP8.5 scenario. A sharp increase was also detected in both dimensions for the northernmost regions of the study area during summer under the RCP8.5 scenario. Therefore, it was estimated that in the future the compound event will exhibit a more balanced distribution between the two dimensions, with the D dimension gaining prominence. Polade et al. (2014) showed that the areas in which a greater increase in dry days is expected under an RCP8.5 scenario are the western Mediterranean and the eastern Atlantic, at approximately latitudes 35 and 55° N, in accordance with the findings of the present study.

Nonetheless, there are conflicting opinions regarding whether the observed warming is inducing an increase in the length of dry spells, as noted by Ye and Fetzer (2019) in Russia, or whether, as observed by Trenberth et al. (2014), the warming does not prolong the dry event but the warming itself may augment the intensity of the episode due to the effect of thermal magnitude. The authors consider that the observed warming has not caused longer-lasting droughts in the area of the Pyrenees, which does not correspond with the findings of Ye and Fetzer (2019). Furthermore, even under an intermediate emission scenario (RCP4.5), there is no evidence of increasingly longer dry spells, despite a significant rise in temperature. Consequently, the authors do not support the idea that a thermal increase is directly related to longer dry periods. This greater duration of dry spells in the most extreme emission scenarios may be due to northward shifting of the subtropical anticyclone belt (Gillett and Stott, 2009) as a consequence of the expansion of the Hadley cell in response to global warming (Lu et al., 2007). There is a need for further research in order to understand the future role of the subtropical anticyclone belt and variations therein and how these affect increases or decreases in compound events, considering the fact that subtropical ridges are the main drivers of these extreme events (Fig. 5).

7 Conclusions

The risk posed by the simultaneous occurrence of extremely dry and hot events is analysed for the first time in the Pyrenees, which is a very fragile area as a result of its altitude and transition latitude between the temperate and subtropical climates. Moreover, 59 % of its area is covered by forests, which will become susceptible to severe wildfires if climatic conditions are unfavourable during the coming years. We extracted the following main findings from the present study:

- The results for the observed period (1981–2015) showed a generalized increase in the thermal extremes (EM) within the extreme dry spells (D), with no increase in the duration of these spells. This showed that to date the compound risk has only augmented in one dimension, extreme magnitude (EM), and, by default, magnitude (M).

- As regards the results obtained from future projections, it is essential that an intermediate emission scenario (RCP4.5) is not exceeded, as this serves to prevent the D dimension (duration) of such events from increasing. The compound risk keeps rising but only because of the even more pronounced thermal increase.

- In a high emission scenario (RCP8.5), the increased risk of the compound event would be a consequence of an increase in both the extreme magnitude (EM) and the duration (D) dimensions. In addition and within this context, the thermal increase in extremely hot days (EM) during the dry event (D) is greater than the thermal increase in the set of days (M) comprising the dry event (D).

Finally and by way of a general conclusion, the present study reveals a potential increase in environmental risks in the Pyrenees (fires, crop yield losses, effects on biodiversity, water resources, etc.) resulting from more frequent compound events involving long dry periods and extreme temperatures. The high-altitude and northernmost regions could be affected to a greater extent, regardless of the season (spring or summer) during the high emission scenario. There also exists a need to study whether other natural hazards such as wildfires are observed during such extremely hot intervals within these very long dry periods in order to prepare this area for tackling large wildfires.

Data availability. The CLIMPY database is available from https://doi.org/10.5281/zenodo.3611127 (Cuadrat et al., 2020).

Supplement. The supplement related to this article is available online at: https://doi.org/10.5194/nhess-21-1721-2021-supplement.

Author contributions. MLC and JALB conceptualized the study. MLC was responsible for methodology, data curation, and writing the original draft. JALB was responsible for supervision.

Competing interests. The authors declare that they have no conflict of interest.

Special issue statement. This article is part of the special issue "Understanding compound weather and climate events and related impacts (BG/ESD/HESS/NHESS inter-journal SI)". It is not associated with a conference.

Acknowledgements. We wish to thank Jose Maria Cuadrat and Roberto Serrano-Notivoli for the CLIMPY project database.

Financial support. This research has been supported by the Ministerio de Ciencia, Innovación y Universidades (grant nos. CGL2017-83866-C3-2-R, AEI/FEDER, UE and FPU2017/02166) and the Agència de Gestió d'Ajuts Universitaris i de Recerca (grant no. 2017 SGR 1362).

Review statement. This paper was edited by Jakob Zscheischler and reviewed by three anonymous referees.

References

Camarero, J. J.: The Multiple Factors Explaining Decline in Mountain Forests: Historical Logging and Warming-Related Drought Stress is Causing Silver-Fir Dieback in the Aragón Pyrenees, in: High Mountain Conservation in a Changing World, edited by: Catalan, J., Ninot, J., and Aniz, M., Advances in Global Change Research, vol 62, Springer, Cham, https://doi.org/10.1007/978-3-319-55982-7_6, 2017.

Cannon, A. J.: Multivariate Bias Correction of Climate Model Output: Matching Marginal Distributions and Intervariable Dependence Structure, J. Climate, 29, 7045–7064, https://doi.org/10.1175/jcli-d-15-0679.1, 2016.

Cannon, A. J.: Multivariate quantile mapping bias correction: an N-dimensional probability density function transform for climate model simulations of multiple variables, Clim. Dynam., 50, 31–49, https://doi.org/10.1007/s00382-017-3580-6, 2018a.

Cannon, A. J.: Multivariate Bias Correction of Climate Model Outputs, available at: https://CRAN.R-project.org/package=MBC (last access: 30 April 2021), 2018b.

Cannon, A. J., Sobie, S. R., and Murdock, T. Q.: Bias correction of GCM precipitation by quantile mapping: How well do methods preserve changes in quantiles and extremes?, J. Climate, 28, 6938–6959, https://doi.org/10.1175/JCLI-D-14-00754.1, 2015.

Carro-Calvo, L., Ordóñez, C., García-Herrera, R., and Schnell, J. L.: Spatial clustering and meteorological drivers of summer ozone in Europe, Atmos. Environ., 167, 496–510, https://doi.org/10.1016/j.atmosenv.2017.08.050, 2017.

Carvalho, M. J., Melo-Gonçalves, P., Teixeira, J. C., and Rocha, A.: Regionalization of Europe based on a K-Means Cluster Analysis of the climate change of temperatures and precipitation, Phys. Chem. Earth, 94, 22–28, https://doi.org/10.1016/j.pce.2016.05.001, 2016.

Casanueva, A., Bedia, J., Herrera, S., Fernández, J., and Gutiérrez, J. M.: Direct and component-wise bias correction of multi-variate climate indices: the percentile adjustment function diagnostic tool, Climatic Change, 147, 411–425, https://doi.org/10.1007/s10584-018-2167-5, 2018.

Cattell, R. B.: The scree test for the number of factors, Multivar. Behav. Res., 1, 245–276, https://doi.org/10.1207/s15327906mbr0102_10, 1966.

Cuadrat, J. M., Serrano-Notivoli, R., Tejedor, E., Saz, M. Á., Prohom, M., Cunillera, J., Llabrés, A., Trapero, L., Pons, M., López-Moreno, J. I., Copons, R., Gascoin, S., Luna, Y., Rodríguez, E., Ramos, P., Amblar, P., and Soubeyroux, J.-M.: CLIMPY: Climate of the Pyrenees, Zenodo, https://doi.org/10.5281/ZENODO.3611127, 2020.

Dee, D. P., Uppala, S. M., Simmons, A. J., Berrisford, P., Poli, P., Kobayashi, S., Andrae, U., Balmaseda, M. A., Balsamo, G., Bauer, P., Bechtold, P., Beljaars, A. C. M., van de Berg, L., Bidlot, J., Bormann, N., Delsol, C., Dragani, R., Fuentes, M., Geer, A. J., Haimberger, L., Healy, S. B., Hersbach, H., Hólm, E. V., Isaksen, L., Kållberg, P., Köhler, M., Matricardi, M., McNally, A. P., Monge-Sanz, B. M., Morcrette, J.-J., Park, B.-K., Peubey, C., de Rosnay, P., Tavolato, C., Thépaut, J.-N., and Vitart, F.: The ERA-Interim reanalysis: configuration and performance of the data assimilation system. Q. J. Roy. Meteor. Soc., 137, 553–597. https://doi.org/10.1002/qj.828, 2011.

Diffenbaugh, N. S. and Ashfaq, M.: Intensification of hot extremes in the United States, Geophys. Res. Lett., 37, 1–5, https://doi.org/10.1029/2010GL043888, 2010.

Donat, M. G., Alexander, L. V., Yang, H., Durre, I., Vose, R., Dunn, R. J. H., Willett, K. M., Aguilar, E., Brunet, M., Caesar, J., Hewitson, B., Jack, C., Klein Tank, A. M. G., Kruger, A. C., Marengo, J., Peterson, T. C., Renom, M., Oria Rojas, C., Rusticucci, M., Salinger, J., Elrayah, A. S., Sekele, S. S., Srivastava, A. K., Trewin, B., Villarroel, C., Vincent, L. A., Zhai, P., Zhang, X., and Kitching, S.: Updated analyses of temperature and precipitation extreme indices since the beginning of the twentieth century: The HadEX2 dataset, J. Geophys. Res.-Atmos., 118, 2098–2118, https://doi.org/10.1002/jgrd.50150, 2013.

Fonseca, D., Carvalho, M. J., Marta-Almeida, M., Melo-Gonçalves, P., and Rocha, A.: Recent trends of extreme temperature indices for the Iberian Peninsula, Phys. Chem. Earth Pt. A/B/C, 94, 66–76, https://doi.org/10.1016/j.pce.2015.12.005, 2016.

François, B., Vrac, M., Cannon, A. J., Robin, Y., and Allard, D.: Multivariate bias corrections of climate simulations: which benefits for which losses?, Earth Syst. Dynam., 11, 537–562, https://doi.org/10.5194/esd-11-537-2020, 2020.

Gazol, A., Sangüesa-Barreda, G., and Camarero, J. J.: Forecasting Forest Vulnerability to Drought in Pyrenean Silver Fir Forests Showing Dieback, Frontiers in Forests and Global Change, 36, 1–13, https://doi.org/10.3389/ffgc.2020.00036, 2020.

Gillett, N. P. and Stott, P. A.: Attribution of anthropogenic influence on seasonal sea level pressure, Geophys. Res. Lett., 36, 1:5, https://doi.org/10.1029/2009GL041269, 2009.

Gudmundsson, L.: qmap: Statistical transformations for postprocessing climate model output, R package version 1.0-2, 2014.

Gudmundsson, L., Bremnes, J. B., Haugen, J. E., and Engen-Skaugen, T.: Technical Note: Downscaling RCM precipitation to the station scale using statistical transformations – a comparison of methods, Hydrol. Earth Syst. Sci., 16, 3383–3390, https://doi.org/10.5194/hess-16-3383-2012, 2012.

Gutowski, W. J., Decker, S. G., Donavon, R. A., Pan, Z., Arritt, R. W., and Takle, E. S.: Temporal-spatial scales of observed and simulated precipitation in Central U.S. climate, J. Climate, 16, 3841–3847, https://doi.org/10.1175/1520-0442(2003)016<3841:TSOOAS>2.0.CO;2, 2003.

Hao, Z., Singh, V. P., and Hao, F.: Compound extremes in hydroclimatology: A review, Water (Switzerland), 10, 1–24, https://doi.org/10.3390/w10060718, 2018.

Hao, Z., Hao, F., Xia, Y., Singh, V. P., and Zhang, X.: A monitoring and prediction system for compound dry and hot events, Environ. Res. Lett., 14, 1–10, https://doi.org/10.1088/1748-9326/ab4df5, 2019.

Hay, L. E. and Clark, M. P.: Use of statistically and dynamically downscaled atmospheric model output for hydrologic simulations in three mountainous basins in the western United States, J. Hydrol., 282, 56–75., 2003.

Jacob, D., Petersen, J., Eggert, B., Alias, A., Christensen, O. B., Bouwer, L. M., Braun, A., Colette, A., Déqué, M., Georgievski, G., Georgopoulou, E., Gobiet, A., Menut, L., Nikulin, G., Haensler, A., Hempelmann, N., Jones, C., Keuler, K., Kovats, S., Kröner, N., Kotlarski, S., Kriegsmann, A., Martin, E., van Meijgaard, E., Moseley, C., Pfeifer, S., Preuschmann, S., Radermacher, C., Radtke, K., Rechid, D., Rounsevell, M., Samuelsson, P., Somot, S., Soussana, J. F., Teichmann, C., Valentini, R., Vautard, R., Weber, B., and Yiou, P.: EURO-CORDEX: New high-resolution climate change projections for European impact research, Reg. Environ. Change, 14, 563–578, https://doi.org/10.1007/s10113-013-0499-2, 2014.

Lehtonen, I., Ruosteenoja, K., and Jylhä, K.: Projected changes in European extreme precipitation indices on the basis of global and regional climate model ensembles, Int. J. Climatol., 34, 1208–1222, https://doi.org/10.1002/joc.3758, 2014.

Lemus-Cánovas, M., Ninyerola, M., Lopez-Bustins, J. A., Manguan, S., and Garcia-Sellés, C.: A mixed application of an objective synoptic classification and spatial regression models for deriving winter precipitation regimes in the Eastern Pyrenees, Int. J. Climatol., 39, 2244–2259, https://doi.org/10.1002/joc.5948, 2018.

Lemus-Canovas, M., Lopez-Bustins, J. A., Trapero, L., and Martin-Vide, J.: Combining circulation weather types and daily precipitation modelling to derive climatic precipitation regions in the Pyrenees, Atmos. Res., 220, 181–193, https://doi.org/10.1016/j.atmosres.2019.01.018, 2019a.

Lemus-Canovas, M., Lopez-Bustins, J. A., Martin-Vide, J., and Royé, D.: synoptReg: An R package for computing a synoptic climate classification and a spatial regionalization of environmental data, Environ. Model. Softw., 118, 114–119, https://doi.org/10.1016/J.ENVSOFT.2019.04.006, 2019b.

Lu, J., Vecchi, G. A., and Reichler, T.: Expansion of the Hadley cell under global warming, Geophys. Res. Lett., 34, 1–5, https://doi.org/10.1029/2006GL028443, 2007.

Lu, Y., Hu, H., Li, C., and Tian, F.: Increasing compound events of extreme hot and dry days during growing seasons of wheat and maize in China, Sci. Rep., 8, 1–8, https://doi.org/10.1038/s41598-018-34215-y, 2018.

Mann, H. B.: Nonparametric Tests Against Trend, Econometrica, 13, 245–259, https://doi.org/10.2307/1907187, 1945.

Manning, C., Widmann, M., Bevacqua, E., Van Loon, A. F., Maraun, D., and Vrac, M.: Increased probability of compound long-duration dry and hot events in Europe during summer (1950–2013), Environ. Res. Lett., 14, 1–16, https://doi.org/10.1088/1748-9326/ab23bf, 2019.

Maraun, D.: Bias correction, quantile mapping, and downscaling: Revisiting the inflation issue, J. Climate, 26, 2137–2143, https://doi.org/10.1175/JCLI-D-12-00821.1, 2013.

Maraun, D. and Widmann, M.: Cross-validation of bias-corrected climate simulations is misleading, Hydrol. Earth Syst. Sci., 22, 4867–4873, https://doi.org/10.5194/hess-22-4867-2018, 2018a.

Maraun, D. and Widmann, M.: Statistical Downscaling and Bias Correction for Climate Research, Cambridge University Press, Cambridge, https://doi.org/10.1017/9781107588783, Online ISBN: 9781107588783, 2018b.

Maraun, D., Shepherd, T. G., Widmann, M., Zappa, G., Walton, D., Gutiérrez, J. M., Hagemann, S., Richter, I., Soares, P. M. M., Hall, A., and Mearns, L. O.: Towards process-informed bias correction of climate change simulations, Nat. Clim. Change, 7, 764–773, https://doi.org/10.1038/nclimate3418, 2017.

Maraun, D., Truhetz, H., and Schaffer, A.: Regional Climate Model Biases, Their Dependence on Synoptic Circulation Biases and the Potential for Bias Adjustment: A Process-Oriented Evaluation of the Austrian Regional Climate Projections, J. Geophys. Res.-Atmos., 126, e2020JD032824, https://doi.org/10.1029/2020JD032824, 2021.

Martin-Vide, J. and Gomez, L.: Regionalization of peninsular Spain based on the length of dry spells, Int. J. Climatol., 19, 537–555, https://doi.org/10.1002/(SICI)1097-0088(199904)19:5<537::AID-JOC371>3.0.CO;2-X, 1999.

Mazdiyasni, O. and AghaKouchak, A.: Substantial increase in concurrent droughts and heatwaves in the United States, P. Natl. Acad. Sci. USA, 37, 11484–11489, https://doi.org/10.1073/pnas.1422945112, 2015.

Orlowsky, B. and Seneviratne, S. I.: Global changes in extreme events: Regional and seasonal dimension, Climatic Change, 110, 669–696, https://doi.org/10.1007/s10584-011-0122-9, 2012.

Panofsky, H. and Brier, G.: Some Applications of Statistics to Meteorology, The Pennsylvania State University, University Park, PA, 1968.

Piani, C. and Haerter, J. O.: Two dimensional bias correction of temperature and precipitation copulas in climate models, Geophys. Res. Lett., 39, 1–6, https://doi.org/10.1029/2012GL053839, 2012.

Piani, C., Haerter, J. O., and Coppola, E.: Statistical bias correction for daily precipitation in regional climate models over Europe, Theor. Appl. Climatol., 99, 187–192, 2010.

Polade, S. D., Pierce, D. W., Cayan, D. R., Gershunov, A., and Dettinger, M. D.: The key role of dry days in changing regional climate and precipitation regimes, Sci. Rep., 4, 4364, https://doi.org/10.1038/srep04364, 2014.

Rajczak, J., Kotlarski, S., and Schär, C.: Does quantile mapping of simulated precipitation correct for biases in transition

probabilities and spell lengths?, J. Climate, 29, 1605–1615, https://doi.org/10.1175/JCLI-D-15-0162.1, 2016.

Riahi, K., Rao, S., Krey, V., Cho, C., Chirkov, V., Fischer, G., Kindermann, G., Nakicenovic, N., and Rafaj, P.: RCP 8.5-A scenario of comparatively high greenhouse gas emissions, Climatic Change, 109, 33, https://doi.org/10.1007/s10584-011-0149-y, 2011.

Salameh, A. A. M., Gámiz-Fortis, S. R., Castro-Díez, Y., Abu Hammad, A., and Esteban-Parra, M. J.: Spatio-temporal analysis for extreme temperature indices over the Levant region, Int. J. Climatol., 39, 5556–5582, https://doi.org/10.1002/joc.6171, 2019.

Sen, P. K.: Estimates of the Regression Coefficient Based on Kendall's Tau, J. Am. Stat. Assoc., 62, 1379–1389, https://doi.org/10.1080/01621459.1968.10480934, 1968.

Serrano-Notivoli, R., Beguería, S., Saz, M. Á., Longares, L. A., and de Luis, M.: SPREAD: a high-resolution daily gridded precipitation dataset for Spain – an extreme events frequency and intensity overview, Earth Syst. Sci. Data, 9, 721–738, https://doi.org/10.5194/essd-9-721-2017, 2017.

Serrano-Notivoli, R., Beguería, S., and de Luis, M.: STEAD: a high-resolution daily gridded temperature dataset for Spain, Earth Syst. Sci. Data, 11, 1171–1188, https://doi.org/10.5194/essd-11-1171-2019, 2019.

Sharma, S. and Mujumdar, P.: Increasing frequency and spatial extent of concurrent meteorological droughts and heatwaves in India, Sci. Rep., 7, 15582, https://doi.org/10.1038/s41598-017-15896-3, 2017.

Singh, D., Tsiang, M., Rajaratnam, B., and Diffenbaugh, N. S.: Observed changes in extreme wet and dry spells during the south Asian summer monsoon season, Nat. Clim. Change, 4, 456–461, https://doi.org/10.1038/nclimate2208, 2014.

Sousa, P. M., Trigo, R. M., Barriopedro, D., Soares, P. M., and Santos, J. A.: European temperature responses to blocking and ridge regional patterns, Clim. Dynam., 50, 457–477, https://doi.org/10.1007/s00382-017-3620-2, 2018.

Stocker, T. F., Qin, D., Plattner, G.-K., Tignor, M., Allen, S. K., Boschung, J., Nauels, A., Xia, Y., Bex, V., and Midgley, P. M. (Eds.): Climate change 2013: The physical science basis: Working Group I contribution to the Fifth assessment report of the Intergovernmental Panel on Climate Change, Cambridge University Press, Cambridge, 2014.

Teutschbein, C. and Seibert, J.: Bias correction of regional climate model simulations for hydrological climate-change impact studies: Review and evaluation of different methods, J. Hydrol., 456–457, 12–29, 2012.

Trenberth, K. E., Dai, A., Van Der Schrier, G., Jones, P. D., Barichivich, J., Briffa, K. R., and Sheffield, J.: Global warming and changes in drought, Nat. Clim. Chang., 4, 17–22, https://doi.org/10.1038/nclimate2067, 2014.

Turco, M., von Hardenberg, J., AghaKouchak, A., Llasat, M. C., Provenzale, A., and Trigo, R. M.: On the key role of droughts in the dynamics of summer fires in Mediterranean Europe, Sci. Rep., 7, 1–10, https://doi.org/10.1038/s41598-017-00116-9, 2017.

Vrac, M. and Friederichs, P.: Multivariate-intervariable, spatial, and temporal-bias correction, J. Climate, 28, 218–237, 2015.

Wilcke, R. A. I., Mendlik, T., and Gobiet, A.: Multi-variable error correction of regional climate models, Climatic Change, 120, 871–887, https://doi.org/10.1007/s10584-013-0845-x, 2013.

Wise, M., Calvin, K., Thomson, A., Clarke, L., Bond-Lamberty, B., Sands, R., Smith, S. J., Janetos, A., and Edmonds, J.: Implications of limiting CO_2 concentrations for land use and energy, Science, 324, 1183–1186, https://doi.org/10.1126/science.1168475, 2009.

Wu, X., Hao, Z., Hao, F., Singh, V. P., and Zhang, X.: Dry-hot magnitude index: A joint indicator for compound event analysis, Environ. Res. Lett., 14, 1–9, https://doi.org/10.1088/1748-9326/ab1ec7, 2019.

Wu, X., Hao, Z., Tang, Q., Singh, V. P., Zhang, X., and Hao, F.: Projected increase in compound dry and hot events over global land areas, Int. J. Climatol., 41, 393–403, https://doi.org/10.1002/joc.6626, 2020.

Ye, H. and Fetzer, E. J.: Asymmetrical Shift Toward Longer Dry Spells Associated with Warming Temperatures During Russian Summers, Geophys. Res. Lett., 46, 11455–11462, https://doi.org/10.1029/2019GL084748, 2019.

Zolina, O., Simmer, C., Belyaev, K., Gulev, S. K., and Koltermann, P.: Changes in the duration of European wet and dry spells during the last 60 years, J. Climate, 16, 2022–2047, https://doi.org/10.1175/JCLI-D-11-00498.1, 2013.

Zscheischler, J. and Seneviratne, S. I.: Dependence of drivers affects risks associated with compound events, Science Advances, 3, e17002, https://doi.org/10.1126/sciadv.1700263, 2017.

Zscheischler, J., Orth, R., and Seneviratne, S. I.: Bivariate return periods of temperature and precipitation explain a large fraction of European crop yields, Biogeosciences, 14, 3309–3320, https://doi.org/10.5194/bg-14-3309-2017, 2017.

Zscheischler, J., Westra, S., Van Den Hurk, B. J. J. M., Seneviratne, S. I., Ward, P. J., Pitman, A., Aghakouchak, A., Bresch, D. N., Leonard, M., Wahl, T., and Zhang, X.: Future climate risk from compound events, Nat. Clim. Change, 8, 469–477, https://doi.org/10.1038/s41558-018-0156-3, 2018.

Capítol 4. Conclusions

Aquesta secció presenta les conclusions finals derivades de la tasca duta a terme en aquesta tesi doctoral. El conjunt del treball s'ha vertebrat a partir de la consecució dels objectius generals proposats a la secció 1.3, els quals es recorden a continuació:

- OG1: caracteritzar els principals patrons pluviomètrics de l'àrea pirinenca des d'un punt de vista sinòptic.
- OG2: proveir un entorn repetible que permeti la caracterització pluviomètrica des d'un punt de vista sinòptic de qualsevol indret del planeta.
- OG3: Analitzar les característiques dels períodes perllongats d'absència de precipitació i d'altes temperatures.

A partir d'aquests objectius generals es detalla a continuació l'assoliment dels objectius específics, abordats en l'apartat de resultats. Posteriorment, es mostren alguns resultats en curs sobre els projectes de futur que possibilita aquesta tesi doctoral.

4.1. Conclusions finals

- OE1: Proposar una metodologia que permeti l'obtenció objectiva de regions pluviomètriques uniformes i autoexplicatives mitjançant el vincle dels patrons sinòptics amb la precipitació diària.

  S'ha presentat un flux de treball que permet vincular les quantitats diàries de precipitació a uns patrons de circulació determinats i, posteriorment, generar una classificació categòrica dels principals règims pluviomètrics a l'àrea del Pirineu. La prèvia síntesi dels estats atmosfèrics mitjançant una classificació sinòptica objectiva permet la derivació d'un breu nombre de situacions pluviomètriques. Aquest fet disminueix dràsticament el cost computacional del procés de clustering dut a terme a l'hora de generar la regionalització categòrica, ja que el nombre de mostres que entren en el còmput són una diminuta part de la població inicial. Tot i l'optimització computacional del procés, aquest flux de treball presenta algunes febleses. Una d'elles és que la regionalització categòrica depèn bàsicament del nombre de tipus de circulació i, per tant, del nombre de mapes de precipitació vinculats a aquests tipus, fent que les regions puguin variar a l'incrementar o disminuir el nombre de mostres a agrupar. D'altra banda, i tot i que les situacions pluviomètriques vinculades als tipus de circulació atmosfèrica són un bon resum de les principals situacions que es produeixen en un període llarg de temps, aquestes no capten tota la variabilitat temporal ni espacial de l'àrea d'estudi, fent que les regions generades mitjançant l'algoritme de clustering puguin no ser del tot homogènies. En aquest sentit, s'han proposat una sèrie de preprocessos a la realització del clustering per tal d'evitar discontinuïtats espacials en la regionalització categòrica, i evitar que efectes orogràfics, com els fons de vall, generin noves categories. Amb tot, aquests preprocessos impliquen la pèrdua de la resolució espacial original. Les noves

regions pluviomètriques esdevenen autoexplicatives mitjançant la generació de la seva sèrie regionalitzada, la qual permet conèixer el comportament climàtic regional de l'àrea. En el cas del Pirineu, les dues regions més meridionals mostren una disminució anual de la precipitació estadísticament significativa durant el període 1961-2010.

- OE2: Desenvolupar una llibreria en el llenguatge de programació R que permeti repetir l'objectiu OE1, i en definitiva l'OG2, en qualsevol punt del planeta de forma totalment automatitzada.

  Després de generar el flux metodològicament robust que dona resposta a l'OE1, es planteja maximitzar-ne la seva repetibilitat mitjançant la construcció d'una llibreria informàtica que brindi a l'usuari –investigador o tècnic–, de totes les eines necessàries per a realitzar: 1) el càlcul d'una classificació sinòptica objectiva; 2) la cartografia dels patrons pluviomètrics –o de la variable d'interès– associats als tipus de circulació atmosfèrica; 3) la consecució d'una regionalització categòrica explicativa de la variabilitat pluviomètrica –o de la variable d'interès– de l'àrea desitjada. Així doncs, aquesta llibreria, programada en el llenguatge de programació R, i que rep el nom de "synoptReg", conté 11 funcions que permeten dur a terme els processos anteriorment mencionats, juntament amb l'adquisició de dades de les reanàlisis atmosfèriques i el seu preprocessat abans d'executar la classificació sinòptica mitjançant algun dels mètodes implementats (ACP, Automàtica de Lamb i SOM). D'aquesta manera, i essent també un dels objectius principals de la construcció d'aquesta llibreria, es procura simplificar al màxim les tasques a l'usuari per a conduir tot el flux metodològic.

- OE3: Identificar les causes sinòptiques atribuïbles als esdeveniments torrencials.

  Bona part d'aquesta tesi doctoral analitza la variabilitat temporal i espacial de la circulació atmosfèrica i de la precipitació en una escala climatològica, amb l'objectiu de comprendre globalment els principals patrons als quals respon la precipitació a l'àrea del Pirineu. No obstant això, i, especialment, pel seu interès en l'operativa de la predicció meteorològica, és d'elevada importància conèixer els mecanismes físics que condueixen a situacions de risc, com ara l'ocurrència d'esdeveniments de precipitació torrencial. En aquest sentit, s'ha generat un catàleg sinòptic objectiu que descriu les principals situacions atmosfèriques que donen lloc a dies de precipitació $\geq$ 100 mm a l'àrea del Pirineu. Així, al nord i oest del Pirineu, les principals situacions causants d'esdeveniments torrencials es caracteritzen per adveccions del nord i del nord-est a nivell de superfície i una circulació més meridional del corrent en jet sobre l'àrea d'estudi, generalment acompanyada d'un important transport de vapor d'aigua entre 1000 i 300 hPa. Els vents de l'oest també poden provocar esdeveniments torrencials quan una profunda depressió se situa sobre el nord de la Península Ibèrica. En el sector centre-sud del Pirineu, els episodis torrencials estan dominats per un

sistema de baixes pressions al nord-oest de la Península Ibèrica, que impulsa vents de sud molt humits. D'altra banda, és l'àrea més oriental la que es troba sotmesa al major nombre d'esdeveniments torrencials quan es genera una situació de ciclogènesi a la Mediterrània Occidental, impulsant vents de l'est i de sud-est sobre la Península Ibèrica. Només una de les situacions definides en el catàleg sinòptic va vinculada amb processos a subescala: la situació isobàrica indefinida a nivell de superfície, però amb penetració d'aire més fred en altura durant la temporada d'estiu. Pel que respecta a l'origen de les partícules d'aire associades a aquests esdeveniments torrencials, a la zona més oriental dels Pirineus, aquestes procedeixen de latituds subtropicals i tenen una trajectòria curta. Contràriament, a l'àrea més occidental del Pirineu, la trajectòria de les masses d'aire és molt més llarga i sol originar-se en les costes orientals d'Amèrica del Nord. Les precipitacions més intenses als Pirineus estan vinculades, principalment, amb l'índex de la WeMO: les zones oriental i nord-occidental estan sota la influència de les fases negativa i positiva de la WeMO, respectivament. L'índex NAO no té cap efecte sobre l'aparició de fenòmens torrencials als Pirineus, excepte en zones aïllades de la façana sud i central d'aquesta serralada.

- OE4: Projectar al futur l'evolució de les ratxes seques de llarga durada conjuntament amb l'ocurrència de temperatures màximes extremes.

Els resultats per al període observat (1981-2015) han mostrat un augment generalitzat dels extrems tèrmics dins dels períodes secs de llarga durada, però sense detectar-se un increment en la longitud d'aquests últims. En un escenari intermedi d'emissions d'efecte hivernacle (RCP4.5), l'augment del risc induït per aquestes dues variables es veu, de nou, incrementat per un fort augment de la temperatura extrema en aquests períodes de sequera en totes les regions del Pirineu. En canvi, sota un escenari d'altes emissions (RCP8.5), els riscos futurs induïts per aquests extrems compostos seran conseqüència d'un increment, tant de la temperatura extrema interna, com de la duració d'aquestes ratxes seques extremes. A més, també s'ha quantificat que l'augment futur de la temperatura màxima extrema durant aquests episodis secs serà més pronunciat i ràpid que durant períodes sense sequera. Els resultats posen de manifest un augment potencial dels riscos mediambientals als Pirineus (incendis, pèrdues de rendiment dels cultius, efectes sobre la biodiversitat o en la disponibilitat de recursos hídrics, etc.), derivat de la major intensitat dels esdeveniments compostos per llargs períodes secs i temperatures extremes. Les regions situades en àrees d'elevada altitud i alhora més septentrionals podrien veure's afectades en major mesura, independentment de l'estació de l'any (primavera o estiu) per a un escenari d'altes emissions.

4.2. Treball en curs i futur

Arran de l'últim article del compendi, s'ha fet palès que no es disposa de projeccions climàtiques a molt alta resolució espacial per l'àrea dels Pirineus. En el transcurs final d'aquesta tesi doctoral, Amblar-Francés et al. (2020) publiquen un treball amb les projeccions de temperatura i precipitació diària a 5 km per a aquesta àrea d'estudi i mitjançant els models climàtics del CMIP5. Tot i realitzar un excel · lent treball, aquesta resolució espacial pot ser insuficient per analitzar processos de subescala, o per a treballar en subregions dins d'aquesta àrea (Andorra, Pirineu català, etc.). En aquest sentit, s'ha estat treballant en el downscaling estadístic de la temperatura màxima i mínima diàries per a aquesta àrea, a 1 km de resolució espacial i amb les projeccions derivades del CMIP6. Al mateix temps, també s'està treballant en projectar a alta resolució espacial la coberta de neu, una variable de molt alt interès en aquesta àrea. A la Figura 14 se'n mostra una primera aproximació dels resultats obtinguts mitjançant tècniques de downscaling estadístic.

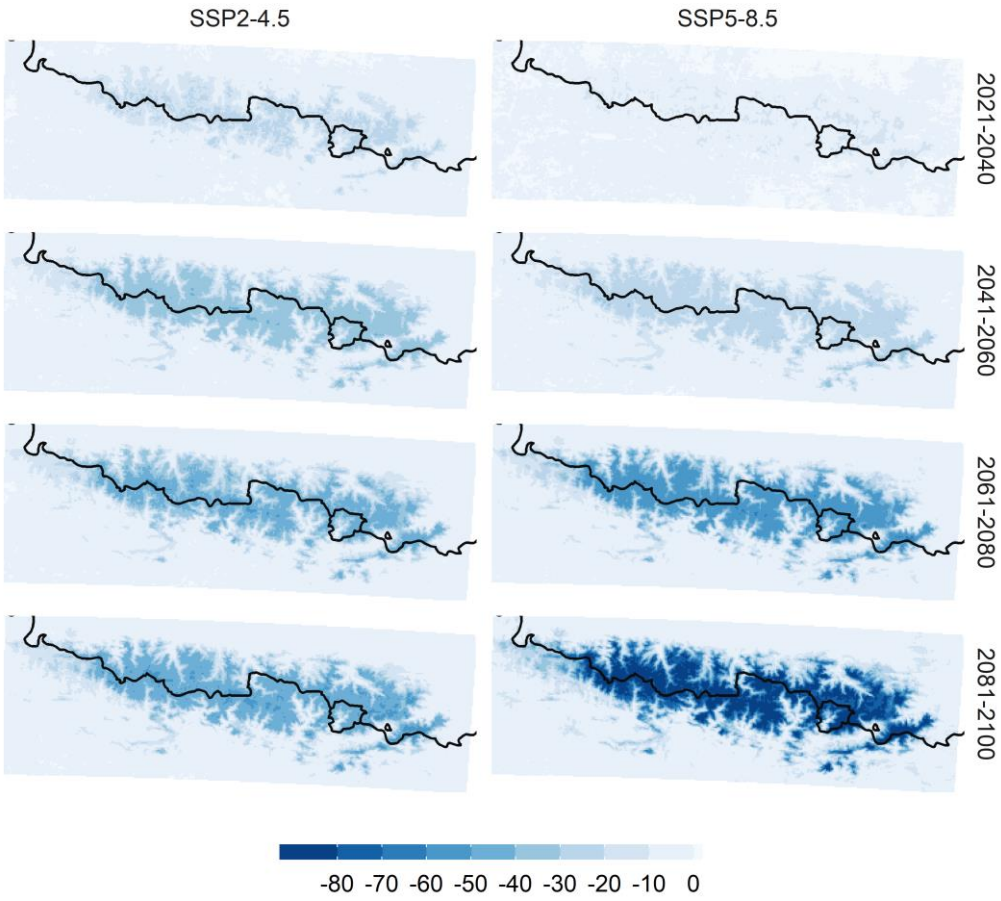

Figura 14. Projecció de la diferència entre el número de dies de neu al terra a 1km per als escenaris SSP2-4.5 i SSP5-8.5 del CMIP 6 i per a 4 subperíodes futurs, respecte el període de referència 1981-2015. A final de segle sota un escenari SSP5-8.5 el descens queda quantificat en més de 80 dies.

Realitzar el downscaling estadística d'aquestes variables a una elevada resolució espacial pel futur, pot proporcionar una font de dades per a molts estudis interessats en analitzar l'impacte del canvi climàtic en diverses disciplines, tals com:

- Ecologia: models de predicció de distribució d'espècies sota escenaris de canvi climàtic.
- Turisme: impacte en el turisme d'hivern.
- Salut: nits tropicals, dies càlids i modelització futura de la morbiditat/mortalitat en condicions futures de canvi climàtic.
- Canvi climàtic: períodes de retorns de grans episodis de calor.
- Incendis: base per a modelitzar la probabilitat d'incendis futurs.

D'altra banda, i en la línia de continuar treballant en el desenvolupament de la llibreria synoptReg, un dels proper treballs planejats és la creació d'una aplicació web mitjançant R per tal que qualsevol usuari, independentment del seu coneixement en aquest llenguatge, pugui implementar tot el flux metodològic simplement realitzant alguns clics.

Capítol 5. Conclusions (menció internacional)

This section presents the final conclusions derived from the task conducted in the present doctoral thesis. The project as a whole has been structured around the general objectives put forward in section 1.3, which are once again described as follows:

- GO1: characterising the principal pluviometric patterns in the Pyrenees area from a synoptic perspective.
- GO2: providing a reproducible environment to enable a pluviometric characterisation of any location on the planet from a synoptic perspective.
- GO3: Analysing the characteristics of prolonged periods of drought and high temperatures.

Based upon these general objectives, the specific objectives are now described in detail; they are addressed in the results section. Subsequently, some results of ongoing research projects are provided in relation to future studies deriving from this doctoral thesis.

5.1. Final conclusions

- SO1: To propose a methodology aimed at objectively establishing uniform pluviometric and self-explanatory regions by means of the link between synoptic patterns and daily precipitation.

A workflow is presented which enables daily rainfall patterns to be associated with certain circulation patterns and subsequently, which permits a categorical classification to be generated of the main pluviometric regimes in the Pyrenees area. Prior synthesis of the atmospheric conditions by means of objective synoptic classification enables a small number of pluviometric situations to be derived. This implies a drastic reduction of the computational cost of the clustering process conducted when generating a categorical regionalisation, because the number of samples in the computation are a minuscule part of the initial population. Despite the computational optimisation of the process proposed, this workflow presents certain weaknesses. One of these is that the categorical regionalisation basically depends upon the number of circulation types and therefore, on the number of rainfall maps associated with these types, which means that the regions can vary on increasing or reducing the number of samples to be grouped. Furthermore, and although the pluviometric situations associated with the atmospheric circulation types constitute a reliable summary of the principal situations occurring over a long time period, these do not capture all the temporal or spatial variability of the study area, which means that the regions generated by clustering algorithm may not be entirely homogeneous. In this sense, a series of pre-processes has been proposed prior to the clustering process in order to avoid spatial discontinuities in the categorical regionalisation and to prevent orographic effects, such as valley bottoms, from generating new categories. In summary, these pre-processes involve the loss of the original spatial resolution. The new pluviometric regions become self-explanatory by generation of their

regionalised series, which enables the regional climatic behaviour of the area to be established. In the case of the Pyrenees, the two southernmost regions exhibit a statistically significant annual decrease in rainfall during the 1961-2010 period.

- SO2: To develop a library in the R programming language to enable objective SO1 to be repeated, and finally GO2, at any point of the planet in a totally automated manner.

  Having generated the methodologically robust flow which addresses SO1, an attempt is made to maximise its repeatability through the construction of a software library aimed at providing the user –researcher or technician– with all the necessary tools to perform: 1) calculation of an objective synoptic classification; 2) cartography of pluviometric patterns –or of the variable of interest– associated with the types of atmospheric circulation; 3) an explanatory categorical regionalisation of the pluviometric variability –or of the variable of interest– of the desired area. Thus, this library, in the R programming language, known as "synoptReg", contains 11 functions that enable the aforementioned processes to be conducted, and that provide atmospheric reanalysis data and permit these to be pre-processed prior to executing the synoptic classification by means of any of the methods implemented (PCA, objective Lamb classification and SOM). Thus, as it is one of the main aims of this library, an attempt is made to make the tasks for the user as easy as possible on conducting the whole methodological flow.

- SO3: To identify the synoptic causes attributable to torrential events.

  Much of the present doctoral thesis analyses the temporal and spatial variability of atmospheric circulation and precipitation at the climatological scale in an attempt to provide a global understanding of the main patterns governing precipitation in this part of the Pyrenees. However, and particularly with regard to its use in meteorological forecasting, it is of great interest to establish the physical mechanisms underlying risk situations such as torrential rainfall events. In this sense, an objective synoptic catalogue has been developed which describes the main atmospheric situations giving rise to days with precipitation ≥ 100 mm in the Pyrenees area. Thus, to the north and west of the Pyrenees, the principal situations causing torrential events are characterised by advections from the north and northeast at surface level and a more southerly circulation of the jet stream over the study area, generally accompanied by abundant transport of water vapour between 1000 and 300 hPa. Westerly winds can also generate torrential events when a profound depression is situated over the north of the Iberian Peninsula. In the central-southern sector of the Iberian Peninsula, torrential episodes are dominated by a system of low pressures in the northwest of the Iberian Peninsula, which drives very moist southerly winds. Moreover, the easternmost area is the one that receives the highest number of torrential episodes when a situation of cyclogenesis arises in the Western Mediterranean, with easterly and south-easterly winds being driven

over the Iberian Peninsula. Only one of the situations described in the synoptic catalogue is associated with sub-scale processes: the isobaric situation that is undefined at surface level, but which involves penetration of colder air at high altitude during the summer. As for the origin of the air particles associated with these torrential events, in the easternmost area of the Pyrenees, these come from subtropical latitudes and present a short trajectory. On the contrary, in the westernmost area of the Pyrenees, the trajectory of the air masses is much longer, and these usually originate on the eastern coasts of North America. The most intense precipitation in the Pyrenees is mainly associated with the WeMO index: the eastern and north-western zones fall under the influence of the negative and positive phases of the WeMO, respectively. The NAO index has no influence in the appearance of torrential episodes in the Pyrenees, except in isolated areas of the south and central faces of these mountains.

- SO4: To project the evolution of long-lasting dry spells along with the occurrence of extreme temperature maxima.

  Results for the study period (1981-2015) reveal a generalised rise in temperature extremes within the prolonged dry periods, although no increase in the duration thereof was detected. In an intermediate scenario of greenhouse gas emissions (RCP4.5), the greater risk caused by the combination of these two variables is once again exacerbated by a sharp rise in extreme temperatures during these drought periods in the Pyrenees region. On the contrary, under a high-emissions scenario (RCP8.5), the future risks caused by these compound extremes will result from an increase both in maximum extreme temperatures and in the duration of these extreme dry spells. Additionally, it has been calculated that the future rise in maximum extreme temperatures during these dry events will be sharper and faster than during the periods with no drought. The results highlight a potential increase in environmental risks in the Pyrenees (wildfires, loss of crop yields, effects upon biodiversity or availability of water resources, etc.) deriving from the greater intensity of these events made up of long dry periods and extreme temperatures. Regions situated further north and at high altitudes could be affected to a greater degree, regardless of the season of the year (spring or summer) for a high-emissions scenario.

5.2. Work underway and future

The latest paper in the compendium highlights the lack of climate projections at very high spatial resolution for the Pyrenees area. During the final stage of the present doctoral thesis, Amblar-Francés et al. (2020) published a paper involving daily temperature and precipitation projections at 5 km for this study area and with the use of the CMIP5 climate models. Although these authors conducted an excellent study, this spatial resolution might be insufficient with regard to analysing sub-scale processes or for working in sub-regions within this area (Andorra, Catalan Pyrenees, etc.). In this sense, work is being conducted on statistical downscaling of daily temperature maxima and

minima for this area, at a spatial resolution of 1 km and with the use of projections from the CMIP6 Moreover, work is also underway to project snow cover, a variable of great interest in this area. Figure 15 shows an initial approach of the results obtained by means of statistical downscaling techniques.

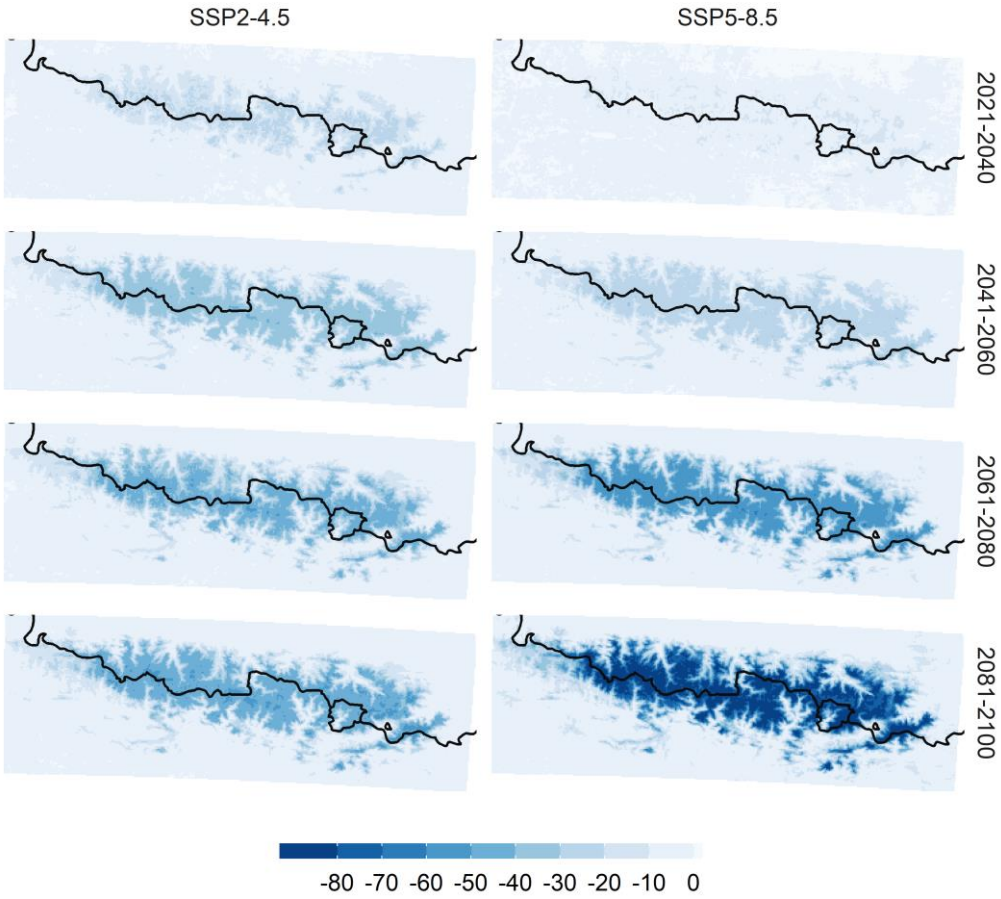

Figure 15. Projection of the difference between the number of days with snow at 1km for scenarios SSP2-4.5 and SSP5-8.5 of the CMIP 6 and for 4 future sub-periods, in relation to the 1981-2015 reference period. At the end of the century under a SSP5-8.5 scenario, the decrease is quantified as being greater than 80 days.

Performing statistical downscaling of these variables at a high spatial resolution for the future could provide a source of data for many studies attempting to analyse the impact of climate change in different disciplines, such as:

- Ecology: models for predicting species distribution under climate change scenarios.
- Tourism: impact upon winter tourism.
- Health: tropical nights, warm/hot days and future modelling of morbimortality under future climate change conditions.
- Climate change: return periods of extreme heat events.
- Wildfires: basis for modelling the likelihood of future fires.

Furthermore, and in order to continue working on the development of the synoptReg library, one of the planned research projects involves the creation of a web application with the use of R so that all users, regardless of their knowledge of this language, can implement the whole methodological flow with just a few clicks.

Referències

Aalto, J., Pirinen, P., Heikkinen, J., & Venäläinen, A. (2013). Spatial interpolation of monthly climate data for Finland: Comparing the performance of kriging and generalized additive models. Theoretical and Applied Climatology, 112(1–2), 99–111. https://doi.org/10.1007/s00704-012-0716-9

Abaurrea, J., Asín, J., Cebrián, A. C., & Centelles, A. (2004). Metodología para el control de calidad y homogeneidad de una base de datos de precipitación diaria.

Abercromby, R. (1883). On certain types of British weather. Quarterly Journal of the Royal Meteorological Society, 9(45), 1–25.

Aguilar, E., & Prohom, M. (n.d.). ExtraQC quality control software.

Amblar-Francés, M. P., Ramos-Calzado, P., Sanchis-Lladó, J., Hernanz-Lázaro, A., Peral-García, M. C., Navascués, B., Dominguez-Alonso, M., Pastor-Saavedra, M. A., & Rodríguez-Camino, E. (2020). High resolution climate change projections for the Pyrenees region. Advances in Science and Research, 17, 191–208. https://doi.org/10.5194/asr-17-191-2020

Anel, J. A., Ignacio Lopez-Moreno, J., Otto, F. E. L., Vicente-Serrano, S., Schaller, N., Massey, N., Buisan, S. T., & Allen, M. R. (2013). The extreme snow accumulation in the western spanish pyrenees during winter and spring 2013 vo - 95 rt - journal article. in bulletin of the american meteorological society op - S73-S76 (Issues 9 WP-).

Barry, R. G. (2005). Synoptic Climatology BT - Encyclopedia of World Climatology (J. E. Oliver (Ed.); pp. 700–704). Springer Netherlands. https://doi.org/10.1007/1-4020-3266-8_200

Barry, R. G., & Carleton, A. M. (2013). Synoptic and dynamic climatology. In Synoptic and Dynamic Climatology. Taylor and Francis. https://doi.org/10.4324/9780203218181

Baur, F., Hess, P., & Nagel, H. (1944). Kalender der grosswetterlagen Europas 1881–1939. Bad Homburg, 35.

Bonsoms, J., Salvador-Franch, F., & Oliva, M. (2021a). Snowfall and snow cover evolution in the Eastern Pre-Pyrenees (NE Iberian Peninsula). Cuadernos de Investigación Geográfica; Accepted Papers in PressDO - 10.18172/Cig.4879 . https://publicaciones.unirioja.es/ojs/index.php/cig/article/view/4879/3811

Bonsoms, J., Gonzalez, S., Prohom, M., Esteban, P., Salvador-Franch, F., López-Moreno, J. I., & Oliva, M. (2021b). Spatio-temporal patterns of snow in the Catalan Pyrenees (NE Iberia). International Journal of Climatology, n/a(n/a). https://doi.org/https://doi.org/10.1002/joc.7147

Brunetti, M., Maugeri, M., Nanni, T., Simolo, C., & Spinoni, J. (2014). High-resolution temperature climatology for Italy: Interpolation method intercomparison. International Journal of Climatology, 34(4), 1278–1296. https://doi.org/10.1002/joc.3764

Bücher, A., & Dessens, J. (1991). Secular Trend of Surface Temperature at an Elevated Observatory in the Pyrenees. Journal of Climate, 4(8), 859–868. https://doi.org/10.1175/1520-0442(1991)004<0859:STOSTA>2.0.CO;2

Buisan, S. T., Saz, M. A., & López-Moreno, J. I. (2015). Spatial and temporal variability of winter snow and precipitation days in the western and central Spanish Pyrenees. International Journal of Climatology, 35(2), 259–274. https://doi.org/10.1002/joc.3978

Buisan, S., López-Moreno, J., Saz, M., & Kochendorfer, J. (2016). Impact of weather type variability on winter precipitation, temperature and annual snowpack in the Spanish Pyrenees. Climate Research, 69(1), 79–92. https://doi.org/10.3354/cr01391

Camarero, J. J. (2017). The Multiple Factors Explaining Decline in Mountain Forests: Historical Logging and Warming-Related Drought Stress is Causing Silver-Fir Dieback in the Aragón Pyrenees. In Advances in Global Change Research. https://doi.org/10.1007/978-3-319-55982-7_6

Cannon, A. J. (2017). Multivariate quantile mapping bias correction: an N -dimensional probability density function transform for climate model simulations of multiple variables. Climate Dynamics 2017 50:1, 50(1), 31–49. https://doi.org/10.1007/S00382-017-3580-6

Cannon, A. J. (2016). Multivariate Bias Correction of Climate Model Output: Matching Marginal Distributions and Intervariable Dependence Structure. Journal of Climate, 29(19), 7045–7064. https://doi.org/10.1175/JCLI-D-15-0679.1

Cannon, A. J., Sobie, S. R., & Murdock, T. Q. (2015). Bias Correction of GCM Precipitation by Quantile Mapping: How Well Do Methods Preserve Changes in Quantiles and Extremes? Journal of Climate, 28(17), 6938–6959. https://doi.org/10.1175/JCLI-D-14-00754.1

Carleton, A. M. (1999). Methodology in climatology. Annals of the Association of American Geographers, 89(4), 713–735. https://doi.org/10.1111/0004-5608.00172

Carro-Calvo, L., Ordóñez, C., García-Herrera, R., & Schnell, J. L. (2017). Spatial clustering and meteorological drivers of summer ozone in Europe. Atmospheric Environment, 167, 496–510. https://doi.org/10.1016/j.atmosenv.2017.08.050

Casado, M. J., Pastor, M. A., & Doblas-Reyes, F. J. (2010). Links between circulation types and precipitation over Spain. Physics and Chemistry of the Earth, 35(9–12), 437–447. https://doi.org/10.1016/j.pce.2009.12.007

Casanueva, A., Bedia, J., Herrera, S., Fernández, J., & Gutiérrez, J. M. (2018). Direct and component-wise bias correction of multi-variate climate indices: the percentile adjustment function diagnostic tool. Climatic Change 2018 147:3, 147(3), 411–425. https://doi.org/10.1007/S10584-018-2167-5

Cattell, R. B. (1966). The scree test for the number of factors. Multivariate Behavioral Research, 1(2), 245–276. https://doi.org/10.1207/s15327906mbr0102_10

Climatologia, S. de. (2002). Avance datos climatologicos de catalunya.

Cortesi, N., Gonzalez-Hidalgo, J. C., Trigo, R. M., & Ramos, A. M. (2014). Weather types and spatial variability of precipitation in the Iberian Peninsula. International Journal of Climatology, 34(8), 2661–2677. https://doi.org/10.1002/joc.3866

Crespi, A., Callegari, M., Greifeneder, F., Notarnicola, C., Petitta, M., & Zebisch, M. (2020). Downscaling and bias correction of seasonal forecasts to support climate services for the Alpine regions. EGU

General Assembly Conference Abstracts, 10109. https://ui.adsabs.harvard.edu/abs/2020EGUGA..2210109C

Crespi, A., Lussana, C., Brunetti, M., Dobler, A., Maugeri, M., & Tveito, O. E. (2019). High-resolution monthly precipitation climatologies over Norway (1981–2010): Joining numerical model data sets and in situ observations. International Journal of Climatology, 39(4), 2057–2070. https://doi.org/10.1002/joc.5933

Cuadrat, J. M., Serrano, R., Saz, M. Á., Tejedor, E., Prohom, M., Cunillera, J., Esteban, P., Soubeyroux, J. M., & Deaux, N. (2014). Creación de una base de datos homogeneizada de temperaturas para los Pirineos (1950-2010). Geographicalia, 63–64, 63. https://doi.org/10.26754/ojs_geoph/geoph.201363-64854

Cuadrat, J. M., Serrano, R., Saz-Sánchez, M. Á., Tejedor, E., Prohom, M., Cunillera, J., SOuBEyROux, J.-Mic., Deaux, N., & Esteban, P. (2014). El clima de los Pirineos: base de datos y primeros resultados.

Cuadrat, J. M., Serrano-Notivoli, R., Tejedor, E., Saz, M. Á., Prohom, M., Cunillera, J., Llabrés, A., Trapero, L., Pons, M., López-Moreno, J. I., Copons, R., Gascoin, S., Luna, Y., Rodríguez, E., Ramos, P., Amblar, P., & Soubeyroux, J.-M. (2020). CLIMPY: Climate of the Pyrenees. https://doi.org/10.5281/ZENODO.3611127

Davies, T. D., Farmer, G., & Barthelmie, R. J. (1990). Use of simple daily atmospheric circulation types for the interpretation of precipitation composition at a site (Eskdalemuir) in Scotland, 1978-1984. Atmospheric Environment Part A, General Topics, 24(1), 63–72. https://doi.org/10.1016/0960-1686(90)90441-O

Dayan, U., & Levy, I. (2005). The influence of meteorological conditions and atmospheric circulation types on PM10 and visibility in Tel Aviv. Journal of Applied Meteorology, 44(5), 606–619.

Demory, M. E., Berthou, S., Fernández, J., Sørland, S. L., Brogli, R., Roberts, M. J., Beyerle, U., Seddon, J., Haarsma, R., Schär, C., Buonomo, E., Christensen, O. B., Ciarlo, J. M., Fealy, R., Nikulin, G., Peano, D., Putrasahan, D., Roberts, C. D., Senan, R., … Vautard, R. (2020). European daily precipitation according to EURO-CORDEX regional climate models (RCMs) and high-resolution global climate models (GCMs) from the High-Resolution Model Intercomparison Project (HighResMIP). Geoscientific Model Development, 13(11), 5485–5506. https://doi.org/10.5194/gmd-13-5485-2020

Dessens, J., & Bücher, A. (1997). A Critical Examination of the Precipitation Records at the Pic Du Midi Observatory, Pyrenees, France. In Climatic Change at High Elevation Sites (pp. 113–121). Springer Netherlands. https://doi.org/10.1007/978-94-015-8905-5_6

Diffenbaugh, N. S., & Ashfaq, M. (2010). Intensification of hot extremes in the United States. Geophysical Research Letters. https://doi.org/10.1029/2010GL043888

Dixon, P. G., Allen, M., Gosling, S. N., Hondula, D. M., Ingole, V., Lucas, R., & Vanos, J. (2016). Perspectives on the Synoptic Climate Classification and its Role in Interdisciplinary Research. Geography Compass, 10(4), 147–164. https://doi.org/10.1111/gec3.12264

Donat, M. G., Alexander, L. V., Yang, H., Durre, I., Vose, R., Dunn, R. J. H., Willett, K. M., Aguilar, E., Brunet, M., Caesar, J., Hewitson, B., Jack, C., Klein Tank, A. M. G., Kruger, A. C., Marengo, J., Peterson, T. C., Renom, M., Oria Rojas, C., Rusticucci, M., … Kitching, S. (2013). Updated analyses of

temperature and precipitation extreme indices since the beginning of the twentieth century: The HadEX2 dataset. Journal of Geophysical Research Atmospheres. https://doi.org/10.1002/jgrd.50150

Donoho, D. L. (2000). High-dimensional data analysis: The curses and blessings of dimensionality. AMS CONFERENCE ON MATH CHALLENGES OF THE 21ST CENTURY. https://citeseerx.ist.psu.edu/viewdoc/summary?doi=10.1.1.329.3392

Duda, R., & Hart, P. (1973). Pattern classification and scene analysis. A Wiley-Interscience Publication.

El Kenawy, A., Ló-Moreno, J. I., & Vicente-Serrano, S. M. (2011). Recent trends in daily temperature extremes over northeastern Spain (1960-2006). Natural Hazards and Earth System Science, 11(9), 2583–2603. https://doi.org/10.5194/nhess-11-2583-2011

Esteban, P., Jones, P. D., Martín-Vide, J., & Mases, M. (2005). Atmospheric circulation patterns related to heavy snowfall days in Andorra, Pyrenees. International Journal of Climatology, 25(3), 319–329. https://doi.org/10.1002/joc.1103

Esteban, P., Ninyerola, M., & Prohom, M. (2009). Spatial modelling of air temperature and precipitation for Andorra (Pyrenees) from daily circulation patterns. Theoretical and Applied Climatology, 96(1–2), 43–56. https://doi.org/10.1007/s00704-008-0035-3

Esteban, P., Prohom, M., Aguilar, E., & Mestre, O. (2010). Annual and seasonal analysis of temperature and precipitation in Andorra (Pyrenees) from 1934 to 2008: quality check, homogenization and trends.

Esteban Vea, P. (2012). Classificació de tipus de circulació atmosfèrica: proposta metodològica i aplicacions. TDX (Tesis Doctorals En Xarxa). http://www.tesisenred.net/handle/10803/93320

Esteban Vea, P., Prohom Duran, M., & Aguilar, E. (2012). Tendencias recientes e índices de cambio climático de la temperatura y la precipitación en Andorra, Pirineos (1935-2008). Pirineos, 167(0), 87–106. https://doi.org/10.3989/Pirineos.2012.167005

Eyring, V., Bony, S., Meehl, G. A., Senior, C. A., Stevens, B., Stouffer, R. J., & Taylor, K. E. (2016). Overview of the Coupled Model Intercomparison Project Phase 6 (CMIP6) experimental design and organization. Geoscientific Model Development, 9(5), 1937–1958. https://doi.org/10.5194/gmd-9-1937-2016

Fonseca, D., Carvalho, M. J., Marta-Almeida, M., Melo-Gonçalves, P., & Rocha, A. (2016). Recent trends of extreme temperature indices for the Iberian Peninsula. Physics and Chemistry of the Earth, Parts A/B/C, 94, 66–76. https://doi.org/10.1016/j.pce.2015.12.005

François, B., Vrac, M., Cannon, A. J., Robin, Y., & Allard, D. (2020). Multivariate bias corrections of climate simulations: Which benefits for which losses? Earth System Dynamics, 11(2), 537–562. https://doi.org/10.5194/ESD-11-537-2020

García, C., Martí, G., Oller, P., Moner, I., Gavaldà, J., Martínez, P., & Peña, J. C. (2009). Major avalanches occurrence at regional scale and related atmospheric circulation patterns in the Eastern Pyrenees. Cold Regions Science and Technology, 59(2–3), 106–118. https://doi.org/10.1016/j.coldregions.2009.07.009

Gazol, A., Sangüesa-Barreda, G., & Camarero, J. J. (2020). Forecasting Forest Vulnerability to Drought in Pyrenean Silver Fir Forests Showing Dieback. Frontiers in Forests and Global Change. https://doi.org/10.3389/ffgc.2020.00036

Giorgi, F. (2019). Thirty Years of Regional Climate Modeling: Where Are We and Where Are We Going next? Journal of Geophysical Research: Atmospheres, 124(11), 5696–5723. https://doi.org/10.1029/2018JD030094

Girs, A. A. (1948). Some aspects concerning basic forms of atmospheric circulation. Met. Gidr, 3, 9–11.

Glahn, H. R., & Lowry, D. A. (1972). The Use of Model Output Statistics (MOS) in Objective Weather Forecasting. Journal of Applied Meteorology and Climatology, 11(8), 1203–1211. https://doi.org/10.1175/1520-0450(1972)011<1203:TUOMOS>2.0.CO;2

González-Hidalgo, J. C., Vicente-Serrano, S. M., Peña-Angulo, D., Salinas, C., Tomas-Burguera, M., & Beguería, S. (2018). High-resolution spatio-temporal analyses of drought episodes in the western Mediterranean basin (Spanish mainland, Iberian Peninsula). Acta Geophysica, 66(3), 381–392. https://doi.org/10.1007/s11600-018-0138-x

Goodess, C. M., & Palutikof, J. P. (1998). Development of daily rainfall scenarios for southeast Spain using a circulation-type approach to downscaling. International Journal of Climatology, 18(10), 1051–1083. https://doi.org/https://doi.org/10.1002/(SICI)1097-0088(199808)18:10<1051::AID-JOC304>3.0.CO;2-1

Gudmundsson, L. (2016). qmap: Statistical transformations for post-processing climate model output.

Gudmundsson, L., Bremnes, J. B., Haugen, J. E., & Engen-Skaugen, T. (2012). Technical Note: Downscaling RCM precipitation to the station scale using statistical transformations – A comparison of methods. Hydrology and Earth System Sciences. https://doi.org/10.5194/hess-16-3383-2012

Gutowski, W. J., Decker, S. G., Donavon, R. A., Pan, Z., Arritt, R. W., & Takle, E. S. (2003). Temporal-spatial scales of observed and simulated precipitation in Central U.S. climate. Journal of Climate. https://doi.org/10.1175/1520-0442(2003)016<3841:TSOOAS>2.0.CO;2

Hao, Z., Hao, F., Xia, Y., Singh, V. P., & Zhang, X. (2019). A monitoring and prediction system for compound dry and hot events. Environmental Research Letters. https://doi.org/10.1088/1748-9326/ab4df5

Hastie, T. (2017). R package Gam: Generalized Additive Models. http://cran.r-project.org/package=gam

Hastie, T. J., & Tibshirani, R. J. (1990). Generalized Additive Models. CRC Press. https://books.google.pt/books?id=JFQPEAAAQBAJ

Hay, L. E., & Clark, M. P. (2003). Use of statistically and dynamically downscaled atmospheric model output for hydrologic simulations in three mountainous basins in the western United States. Journal of Hydrology, 282(1–4), 56–75. https://doi.org/10.1016/S0022-1694(03)00252-X

Haylock, M. R., Hofstra, N., Klein Tank, A. M. G., Klok, E. J., Jones, P. D., & New, M. (2008). A European daily high-resolution gridded data set of surface temperature and precipitation for 1950–2006. Journal of Geophysical Research: Atmospheres, 113(D20).

Hengl, T. (2009). A practical guide to geostatistical mapping.

Hengl, T., Heuvelink, G. B. M., & Rossiter, D. G. (2007). About regression-kriging: From equations to case studies. Computers & Geosciences, 33(10), 1301–1315.

Hewitson, B. C., & Crane, R. G. (1992). Large-scale atmospheric controls on local precipitation in tropical Mexico. Geophysical Research Letters, 19(18), 1835–1838. https://doi.org/10.1029/92GL01423

Hewitson, B. C., & Crane, R. G. (2002). Self-organizing maps: Applications to synoptic climatology. Climate Research, 22(1), 13–26. https://doi.org/10.3354/cr022013

Hulme, M., & Jones, P. D. (1991). Temperatures and windiness over the United Kingdom during the winters of 1988/89 and 1989/90 compared with previous years. Weather, 46(5), 126–136. https://doi.org/10.1002/j.1477-8696.1991.tb05724.x

Huth, R. (1996). Properties of the circulation classification scheme based on the rotated principal component analysis. Meteorology and Atmospheric Physics, 59(3–4), 217–233. https://doi.org/10.1007/BF01030145

Huth, R., Beck, C., Philipp, A., Demuzere, M., Ustrnul, Z., Cahynová, M., Kyselý, J., & Tveito, O. E. (2008). Classifications of atmospheric circulation patterns: Recent advances and applications. Annals of the New York Academy of Sciences, 1146(1), 105–152. https://doi.org/10.1196/annals.1446.019

Insua-Costa, D., Lemus-Cánovas, M., Miguez-Macho, G., & Llasat, M. C. (2021). Climatology and ranking of hazardous precipitation events in the western Mediterranean area. Atmospheric Research,

Jacob, D., Petersen, J., Eggert, B., Alias, A., Christensen, O. B., Bouwer, L. M., Braun, A., Colette, A., Déqué, M., Georgievski, G., Georgopoulou, E., Gobiet, A., Menut, L., Nikulin, G., Haensler, A., Hempelmann, N., Jones, C., Keuler, K., Kovats, S., … Yiou, P. (2014). EURO-CORDEX: New high-resolution climate change projections for European impact research. Regional Environmental Change. https://doi.org/10.1007/s10113-013-0499-2

Jenkinson, A. F., & Collison, F. P. (1977). An initial climatology of gales over the North Sea. Synoptic Climatology Branch Memorandum, 62, 18.

Jones, P. D., & Hulme, M. (1996). Calculating regional climatic time series for temperature and precipitation: methods and illustrations. International Journal of Climatology, 16(4), 361–377. https://doi.org/https://doi.org/10.1002/(SICI)1097-0088(199604)16:4<361::AID-JOC53>3.0.CO;2-F

Jones, P. D., Hulme, M., & Briffa, K. R. (1993). A comparison of Lamb circulation types with an objective classification scheme. International Journal of Climatology, 13(6), 655–663. https://doi.org/10.1002/joc.3370130606

Knutti, R., Furrer, R., Tebaldi, C., Cermak, J., & Meehl, G. A. (2010). Challenges in combining projections from multiple climate models. Journal of Climate, 23(10), 2739–2758. https://doi.org/10.1175/2009JCLI3361.1

Kohonen, T. (2001). Self-organizing maps (Vol. 30). Springer Science & Business Media.

Kotlarski, S., Keuler, K., Christensen, O. B., Colette, A., Déqué, M., Gobiet, A., Goergen, K., Jacob, D., Lüthi, D., Van Meijgaard, E., Nikulin, G., Schär, C., Teichmann, C., Vautard, R., Warrach-Sagi, K., &

Wulfmeyer, V. (2014). Regional climate modeling on European scales: A joint standard evaluation of the EURO-CORDEX RCM ensemble. Geoscientific Model Development, 7(4), 1297–1333. https://doi.org/10.5194/gmd-7-1297-2014

Kuhn, M. (2008). Building predictive models in R using the caret package. Journal of Statistical Software, 28(1), 1–26.

Lamb, H. H. (1950). Types and spells of weather around the year in the British Isles: Annual trends, seasonal structure of the year, singularities. Quarterly Journal of the Royal Meteorological Society, 76(330), 393–429.

Lamb, H. H. (1972). British Isles weather types and a register of the daily sequence of circulation patterns 1861-1971.

Lana, X., Martínez, M. D., Burgueño, A., Serra, C., Martín-Vide, J., & Gómez, L. (2008). Spatial and temporal patterns of dry spell lengths in the Iberian Peninsula for the second half of the twentieth century. Theoretical and Applied Climatology, 91(1–4), 99–116. https://doi.org/10.1007/s00704-007-0300-x

Lana, X., Martínez, M. D., Burgueño, A., Serra, C., Martín-Vide, J., & Gómez, L. (2006). Distributions of long dry spells in the iberian peninsula, years 1951–1990. International Journal of Climatology, 26(14), 1999–2021. https://doi.org/10.1002/joc.1354

LeDrew, E. F. (1984). The role of local heat sources in synoptic activity within the polar basin. Atmosphere-Ocean, 22(3), 309–327.

Lee, C. C., & Sheridan, S. C. (2015). Synoptic Climatology: An Overview. In Reference Module in Earth Systems and Environmental Sciences. Elsevier. https://doi.org/10.1016/b978-0-12-409548-9.09421-5

Lopez-Bustins, J. A., Martin-Vide, J., & Sanchez-Lorenzo, A. (2008). Iberia winter rainfall trends based upon changes in teleconnection and circulation patterns. Global and Planetary Change, 63(2–3), 171–176. https://doi.org/10.1016/j.gloplacha.2007.09.002

López-Moreno, J. I., Soubeyroux, J. M., Gascoin, S., Alonso-Gonzalez, E., Durán-Gómez, N., Lafaysse, M., Vernay, M., Carmagnola, C., & Morin, S. (2020). Long-term trends (1958–2017) in snow cover duration and depth in the Pyrenees. International Journal of Climatology, 40(14), 6122–6136. https://doi.org/10.1002/joc.6571

López-Moreno, J. I., Vicente-Serrano, S. M., Angulo-Martínez, M., Beguería, S., & Kenawy, A. (2010). Trends in daily precipitation on the northeastern Iberian Peninsula, 1955-2006. International Journal of Climatology, 30(7), 1026–1041. https://doi.org/10.1002/joc.1945

López-Moreno, J. I., & Vicente-Serrano, S. M. (2007). Atmospheric circulation influence on the interannual variability of snow pack in the Spanish Pyrenees during the second half of the 20th century. Nordic Hydrology, 38(1), 33–44. https://doi.org/10.2166/nh.2007.030

Lu, Y., Hu, H., Li, C., & Tian, F. (2018). Increasing compound events of extreme hot and dry days during growing seasons of wheat and maize in China. Scientific Reports. https://doi.org/10.1038/s41598-018-34215-y

Maheras, P., & Anagnostopoulou, C. (2003). Circulation Types and Their Influence on the Interannual Variability and Precipitation Changes in Greece. In Mediterranean Climate (pp. 215–239). Springer Berlin Heidelberg. https://doi.org/10.1007/978-3-642-55657-9_12

Mann, H. B. (1945). Nonparametric Tests Against Trend. Econometrica, 13(3), 245. https://doi.org/10.2307/1907187

Manning, C., Widmann, M., Bevacqua, E., Van Loon, A. F., Maraun, D., & Vrac, M. (2019). Increased probability of compound long-duration dry and hot events in Europe during summer (1950-2013). In Environmental Research Letters. https://doi.org/10.1088/1748-9326/ab23bf

Maraun, D. (2013). Bias correction, quantile mapping, and downscaling: Revisiting the inflation issue. Journal of Climate. https://doi.org/10.1175/JCLI-D-12-00821.1

Maraun, D., Shepherd, T. G., Widmann, M., Zappa, G., Walton, D., Gutiérrez, J. M., Hagemann, S., Richter, I., Soares, P. M. M., Hall, A., & Mearns, L. O. (2017). Towards process-informed bias correction of climate change simulations. Nature Climate Change. https://doi.org/10.1038/nclimate3418

Maraun, D., & Widmann, M. (2018). Statistical Downscaling and Bias Correction for Climate Research. In Statistical Downscaling and Bias Correction for Climate Research. https://doi.org/10.1017/9781107588783

Maraun, D., & Widmann, M. (2018). Cross-validation of bias-corrected climate simulations is misleading. Hydrology and Earth System Sciences, 22(9), 4867–4873. https://doi.org/10.5194/HESS-22-4867-2018

Maris, M. N. A., Giraud, G., Durand, Y., Navarre, J.-P., & Mérindol, L. (2009). Results of 50 years of climate reanalysis in the French Pyrenees (1958-2008) using the SAFRAN and CROCUS models. In International Snow Science Workshop (Vol. 219).

Martin-Vide, J., Sanchez-Lorenzo, A., Lopez-Bustins, J. A., Cordobilla, M. J., Garcia-Manuel, A., & Raso, J. M. (2008). Torrential rainfall in northeast of the Iberian Peninsula: synoptic patterns and WeMO influence. Advances in Science and Research, 2(1), 99–105. https://doi.org/10.5194/asr-2-99-2008

Martin-Vide, J., & Gomez, L. (1999). Regionalization of peninsular Spain based on the length of dry spells. International Journal of Climatology. https://doi.org/10.1002/(SICI)1097-0088(199904)19:5<537::AID-JOC371>3.0.CO;2-X

Marwick, B. (2017). Computational reproducibility in archaeological research: Basic principles and a case study of their implementation. Journal of Archaeological Method and Theory, 24(2), 424–450.

Maugeri, M., Brunetti, M., Monti, F., & Nanni, T. (2004). Sea-level pressure variability in the Po Plain (1765–2000) from homogenized daily secular records. International Journal of Climatology, 24(4), 437–455. https://doi.org/https://doi.org/10.1002/joc.991

Mazdiyasni, O., & AghaKouchak, A. (2015). Substantial increase in concurrent droughts and heatwaves in the United States. Proceedings of the National Academy of Sciences of the United States of America. https://doi.org/10.1073/pnas.1422945112

McCullagh, P., & Nelder, J. A. (2019). Generalized linear models. Routledge.

Meseguer-Ruiz, O., Ponce-Philimon, P. I., Baltazar, A., Guijarro, J. A., Serrano-Notivoli, R., Olcina Cantos, J., Martin-Vide, J., & Sarricolea, P. (2020). Synoptic attributions of extreme precipitation in the Atacama Desert (Chile). Climate Dynamics, 55(11–12), 3431–3444. https://doi.org/10.1007/s00382-020-05455-4

Modala, N. R. (2014). Assessing the impacts of climate change on cotton production in the Texas High Plains and Rolling Plains.

Morata, A., Martín, M. L., Luna, M. Y., & Valero, F. (2006). Self-similarity patterns of precipitation in the Iberian Peninsula. Theoretical and Applied Climatology, 85(1–2), 41–59. https://doi.org/10.1007/s00704-005-0175-7

Ninyerola, M., Pons, X., & Roure, J. M. (2000). A methodological approach of climatological modelling of air temperature and precipitation through GIS techniques. International Journal of Climatology, 20(14), 1823–1841. https://doi.org/10.1002/1097-0088(20001130)20:14<1823::AID-JOC566>3.0.CO;2-B

Nishiyama, K., Endo, S., Jinno, K., Bertacchi Uvo, C., Olsson, J., & Berndtsson, R. (2007). Identification of typical synoptic patterns causing heavy rainfall in the rainy season in Japan by a Self-Organizing Map. Atmospheric Research, 83(2-4 SPEC. ISS.), 185–200. https://doi.org/10.1016/j.atmosres.2005.10.015

Orlowsky, B., & Seneviratne, S. I. (2012). Global changes in extreme events: Regional and seasonal dimension. Climatic Change. https://doi.org/10.1007/s10584-011-0122-9

Páscoa, P., Gouveia, C. M., Russo, A., & Trigo, R. M. (2017). Drought trends in the Iberian Peninsula over the last 112 years. Advances in Meteorology, 2017. https://doi.org/10.1155/2017/4653126

Páscoa, P., Russo, A., Gouveia, C. M., Soares, P. M. M., Cardoso, R. M., Careto, J. A. M., & Ribeiro, A. F. S. (2021). A high-resolution view of the recent drought trends over the Iberian Peninsula. Weather and Climate Extremes, 32, 100320. https://doi.org/10.1016/j.wace.2021.100320

Pebesma, E. J. (2004). Multivariable geostatistics in S: the gstat package. Computers & Geosciences, 30(7), 683–691. https://doi.org/10.1016/J.CAGEO.2004.03.012

Peng, R. D. (2011). Reproducible research in computational science. Science, 334(6060), 1226–1227.

Peña-Angulo, D., Trigo, R. M., Cortesi, N., & González-Hidalgo, J. C. (2016). The influence of weather types on the monthly average maximum and minimum temperatures in the Iberian Peninsula. In Atmospheric Research (Vols. 178–179, pp. 217–230). Elsevier Ltd. https://doi.org/10.1016/j.atmosres.2016.03.022

Pepin, N., & Kidd, D. (2006). Spatial temperature variation in the Eastern Pyrenees. Weather, 61(11), 300–310. https://doi.org/10.1256/wea.106.06

Pérez-Zanón, N., Sigró, J., & Ashcroft, L. (2017). Temperature and precipitation regional climate series over the central Pyrenees during 1910-2013. International Journal of Climatology, 37(4), 1922–1937. https://doi.org/10.1002/joc.4823

Pesquer, L., Masó, J., & Pons, X. (2007). Integración S.I.G. de regresión multivariante, interpolación de residuos y validación para la generación de rásters continuos de variables meteorológicas. Revista de Teledetección, 28, 69–76.

Piani, C., & Haerter, J. O. (2012). Two dimensional bias correction of temperature and precipitation copulas in climate models. Geophysical Research Letters, 39(20). https://doi.org/10.1029/2012GL053839

Piani, C., Weedon, G., Best, M., Gomes, S., Viterbo, P., Hagemann, S., & Haerter, J. (2010). Statistical Bias Correction of Global Simulated Daily Precipitation and Temperature for the Application of Hydrological Models. Journal of Hydrology, 395, 199–215. https://doi.org/10.1016/j.jhydrol.2010.10.024

Pons, X., & Ninyerola, M. (2008). Mapping a topographic global solar radiation model implemented in a GIS and refined with ground data. International Journal of Climatology: A Journal of the Royal Meteorological Society, 28(13), 1821–1834.

Quéno, L., Vionnet, V., Dombrowski-Etchevers, I., Lafaysse, M., Dumont, M., & Karbou, F. (2016). Snowpack modelling in the Pyrenees driven by kilometric-resolution meteorological forecasts. The Cryosphere, 10(4), 1571–1589. https://doi.org/10.5194/tc-10-1571-2016

Rajczak, J., Kotlarski, S., Salzmann, N., & Schär, C. (2016). Robust climate scenarios for sites with sparse observations: A two-step bias correction approach. International Journal of Climatology, 36(3), 1226–1243. https://doi.org/10.1002/joc.4417

Rajczak, J., Kotlarski, S., & Schär, C. (2016). Does quantile mapping of simulated precipitation correct for biases in transition probabilities and spell lengths? Journal of Climate. https://doi.org/10.1175/JCLI-D-15-0162.1

Ramos, A. M., Cortesi, N., & Trigo, R. M. (2014). Circulation weather types and spatial variability of daily precipitation in the Iberian Peninsula. Frontiers in Earth Science, 2, 25. https://doi.org/10.3389/feart.2014.00025

Salameh, A. A. M., Gámiz-Fortis, S. R., Castro-Díez, Y., Abu Hammad, A., & Esteban-Parra, M. J. (2019). Spatio-temporal analysis for extreme temperature indices over the Levant region. International Journal of Climatology, 39(15), 5556–5582. https://doi.org/10.1002/joc.6171

Sánchez, E., Domínguez, M., Romera, R., de la Franca, N. L., Gaertner, M. A., Gallardo, C., & Castro, M. (2011). Regional modeling of dry spells over the Iberian Peninsula for present climate and climate change conditions. Climatic Change, 107(3), 625–634. https://doi.org/10.1007/s10584-011-0114-9

Sanchez-Lorenzo, A., Calbó, J., & Martin-Vide, J. (2009). Reply to comment by HJ Hendricks Franssen et al. on" Winter'weekend effect'in southern Europe and its connections with periodicities in atmospheric dynamics". Geophysical Research Letters, 36(13).

Sen, P. K. (1968). Estimates of the Regression Coefficient Based on Kendall's Tau. Journal of the American Statistical Association, 63(324), 1379–1389. https://doi.org/10.1080/01621459.1968.10480934

Serrano-Notivoli, R., Beguería, S., & de Luis, M. (2019). STEAD: a high-resolution daily gridded temperature dataset for Spain. Earth System Science Data, 11(3), 1171–1188. https://doi.org/10.5194/essd-11-1171-2019

Serrano-Notivoli, R., Beguería, S., Saz, M. Á., Longares, L. A., & Luis, M. de. (2017). SPREAD: a high-resolution daily gridded precipitation dataset for Spain–an extreme events frequency and intensity overview. Earth System Science Data, 9(2), 721–738.

Serrano-Notivoli, R., Buisan, S. T., Abad Perez, L. M., Sierra Álvarez, E., Rodriguez Ballesteros, C., López-Moreno, J. I., & Cuadrat, J. M. (2018). (PDF) Tendencias recientes en precipitación, temperatura y nieve de alta montaña en los Pirineos (Refugio de Góriz, Huesca). In El clima: aire, agua, tierra y fuego (pp. 267–280). Asociación Española de Climatología. https://www.researchgate.net/publication/328415318_Tendencias_recientes_en_precipitacion_temperatura_y_nieve_de_alta_montana_en_los_Pirineos_Refugio_de_Goriz_Huesca

Serrano-Notivoli, R., Llabrés Brustenga, A., Prohom, M., Cuadrat, J., Cunillera, J., Trapero, L., Pons, M., Tejedor, E., Saz, M., López-Moreno, J., copons llorens, R., Gascoin, S., Luna, M. Y., Rodriguez-Camino, E., Ramos-Calzado, P., Amblar-Francés, P., & Soubeyroux, J.-M. (2019, April 7). Observed climatic trends in the Pyrenees (1950-2015). European Geosciens Union Assembly 2019. https://doi.org/10.13140/RG.2.2.17306.29125

Sharma, S., & Mujumdar, P. (2017). Increasing frequency and spatial extent of concurrent meteorological droughts and heatwaves in India. Scientific Reports. https://doi.org/10.1038/s41598-017-15896-3

Sheridan, S. C., & Lee, C. C. (2011). The self-organizing map in synoptic climatological research. Progress in Physical Geography, 35(1), 109–119. https://doi.org/10.1177/0309133310397582

Singh, D., Tsiang, M., Rajaratnam, B., & Diffenbaugh, N. S. (2014). Observed changes in extreme wet and dry spells during the south Asian summer monsoon season. Nature Climate Change. https://doi.org/10.1038/nclimate2208

Spandre, P., François, H., Verfaillie, D., Pons, M., Vernay, M., Lafaysse, M., George, E., & Morin, S. (2019). Winter tourism under climate change in the pyrenees and the French alps: Relevance of snowmaking as a technical adaptation. Cryosphere, 13(4), 1325–1347. https://doi.org/10.5194/tc-13-1325-2019

Stauffer, R., Mayr, G. J., Messner, J. W., Umlauf, N., & Zeileis, A. (2017). Spatio-temporal precipitation climatology over complex terrain using a censored additive regression model. International Journal of Climatology, 37(7), 3264–3275. https://doi.org/10.1002/joc.4913

Stein, A. F., Draxler, R. R., Rolph, G. D., Stunder, B. J. B., Cohen, M. D., & Ngan, F. (2015). Noaa's hysplit atmospheric transport and dispersion modeling system. In Bulletin of the American Meteorological Society (Vol. 96, Issue 12, pp. 2059–2077). American Meteorological Society. https://doi.org/10.1175/BAMS-D-14-00110.1

Suriano, Z. J., Leathers, D. J., & Benjamin, A. E. (2020). Regionalization of Northeast US moisture conditions: Analysis of synoptic-scale atmospheric drivers. Climate Research, 79(3), 193–206. https://doi.org/10.3354/CR01588

Taylor, K. E., Stouffer, R. J., & Meehl, G. A. (2012). An overview of CMIP5 and the experiment design. In Bulletin of the American Meteorological Society (Vol. 93, Issue 4, pp. 485–498). American Meteorological Society. https://doi.org/10.1175/BAMS-D-11-00094.1

Teutschbein, C., & Seibert, J. (2012). Bias correction of regional climate model simulations for hydrological climate-change impact studies: Review and evaluation of different methods. Journal of Hydrology, s 456–457, 12–29. https://doi.org/10.1016/j.jhydrol.2012.05.052

Trigo, R. M., & Dacamara, C. C. (2000). Circulation weather types and their influence on the precipitation regime in Portugal. Int. J. Climatol, 20, 1559–1581.

van Bebber, W. J., & Köppen, W. P. (1895). Die Isobarentypen des Nordatlantischen Ozeans und Westeuropas, ihre Beziehungen zur Lage und Bewegung der barometrischen Maxima und Minima.

Vicente-Serrano, S. M., López-Moreno, J. I., & Beguería, S. (2007). La precipitación en el Pirineo español: diversidad espacial en las tendencias y escenarios futuros. Pirineos, 162(0 SE-Artículos), 43–69. https://doi.org/10.3989/pirineos.2007.v162.12

Vicente-Serrano, S. M., & Cuadrat-Prats, J. M. (2007). Trends in drought intensity and variability in the middle Ebro valley (NE of the Iberian peninsula) during the second half of the twentieth century. Theoretical and Applied Climatology, 88(3–4), 247–258. https://doi.org/10.1007/s00704-006-0236-6

Vicente-Serrano, S. M., Peña-Angulo, D., Murphy, C., López-Moreno, J. I., Tomas-Burguera, M., Domínguez-Castro, F., Tian, F., Eklundh, L., Cai, Z., Alvarez-Farizo, B., Noguera, I., Camarero, J. J., Sánchez-Salguero, R., Gazol, A., Grainger, S., Conradt, T., Boincean, B., & El Kenawy, A. (2021). The complex multi-sectoral impacts of drought: Evidence from a mountainous basin in the Central Spanish Pyrenees. Science of the Total Environment, 769, 144702. https://doi.org/10.1016/j.scitotenv.2020.144702

Vicente-Serrano, S. M. (2006). Spatial and temporal analysis of droughts in the Iberian Peninsula (1910-2000). Hydrological Sciences Journal, 51(1), 83–97. https://doi.org/10.1623/hysj.51.1.83

Vicente-Serrano, S. M. (2006). Differences in spatial patterns of drought on different time scales: An analysis of the Iberian Peninsula. Water Resources Management, 20(1), 37–60. https://doi.org/10.1007/s11269-006-2974-8

Vrac, M., & Friederichs, P. (2015). Multivariate—Intervariable, Spatial, and Temporal—Bias Correction. Journal of Climate, 28(1), 218–237. https://doi.org/10.1175/JCLI-D-14-00059.1

Wilby, R. L., & Wigley, T. M. L. (1997). Downscaling general circulation model output: A review of methods and limitations. In Progress in Physical Geography (Vol. 21, Issue 4, pp. 530–548). Arnold. https://doi.org/10.1177/030913339702100403

Wilcke, R. A. I., Mendlik, T., & Gobiet, A. (2013). Multi-variable error correction of regional climate models. Climatic Change 2013 120:4, 120(4), 871–887. https://doi.org/10.1007/S10584-013-0845-X

Wilks, D. (2019). Statistical Methods in the Atmospheric Sciences. In Statistical Methods in the Atmospheric Sciences. https://doi.org/10.1016/c2017-0-03921-6

Willmott, C. J. (1982). Some comments on the evaluation of model performance. Bulletin of the American Meteorological Society, 63(11), 1309–1313.

Wise, M., Calvin, K., Thomson, A., Clarke, L., Bond-Lamberty, B., Sands, R., Smith, S. J., Janetos, A., & Edmonds, J. (2009). Implications of limiting CO2 concentrations for land use and energy. Science. https://doi.org/10.1126/science.1168475

Wu, X., Hao, Z., Hao, F., & Zhang, X. (2019). Variations of compound precipitation and temperature extremes in China during 1961–2014. Science of the Total Environment. https://doi.org/10.1016/j.scitotenv.2019.01.366

Wu, X., Hao, Z., Tang, Q., Singh, V. P., Zhang, X., & Hao, F. (2021). Projected increase in compound dry and hot events over global land areas. International Journal of Climatology, 41(1), 393–403. https://doi.org/10.1002/joc.6626

Yarnal, B. (1993). Synoptic climatology in environmental analysis: a primer. CRC Press.

Yarnal, B., Comrie, A. C., Frakes, B., & Brown, D. P. (2001). Developments and prospects in synoptic climatology. International Journal of Climatology, 21(15), 1923–1950. https://doi.org/10.1002/joc.675

Zhang, X., & Yang, F. (2004). RClimDex (1.0) user manual. Climate Research Branch Environment Canada, 22.

Zolina, O., Simmer, C., Belyaev, K., Gulev, S. K., & Koltermann, P. (2013). Changes in the duration of European wet and dry spells during the last 60 years. Journal of Climate. https://doi.org/10.1175/JCLI-D-11-00498.1

Zscheischler, J., Mahecha, M. D., & Harmeling, S. (2012). Climate classifications: The value of unsupervised clustering. Procedia Computer Science, 9, 897–906. https://doi.org/10.1016/j.procs.2012.04.096

Zscheischler, J., & Seneviratne, S. I. (2017). Dependence of drivers affects risks associated with compound events. Science Advances. https://doi.org/10.1126/sciadv.1700263

Zscheischler, J., Westra, S., Van Den Hurk, B. J. J. M., Seneviratne, S. I., Ward, P. J., Pitman, A., Aghakouchak, A., Bresch, D. N., Leonard, M., Wahl, T., & Zhang, X. (2018). Future climate risk from compound events. In Nature Climate Change. https://doi.org/10.1038/s41558-018-0156-3

Apèndix A. Material suplementari

A.1. Suplement original de l'article: Combining circulation weather types and daily precipitation modelling to derive climatic precipitation regions in the Pyrenees

Fig. S1. Results of the GLM interpolation method for each model related to each circulation weather type.

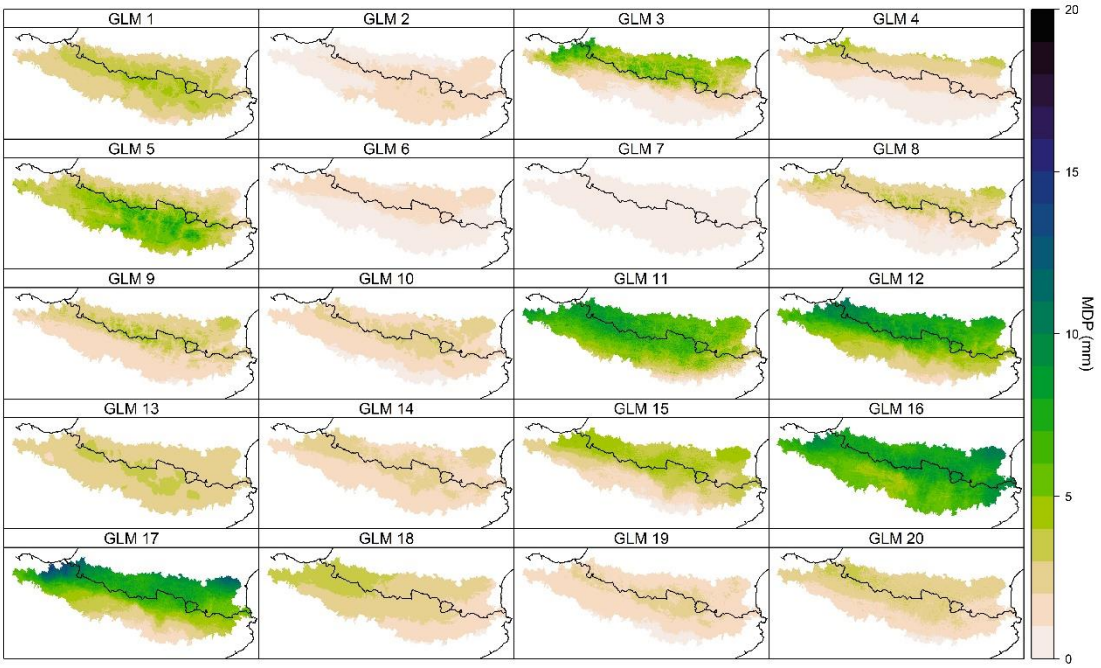

Fig. S2. K-means Clustering iteration for GAM and RK models.

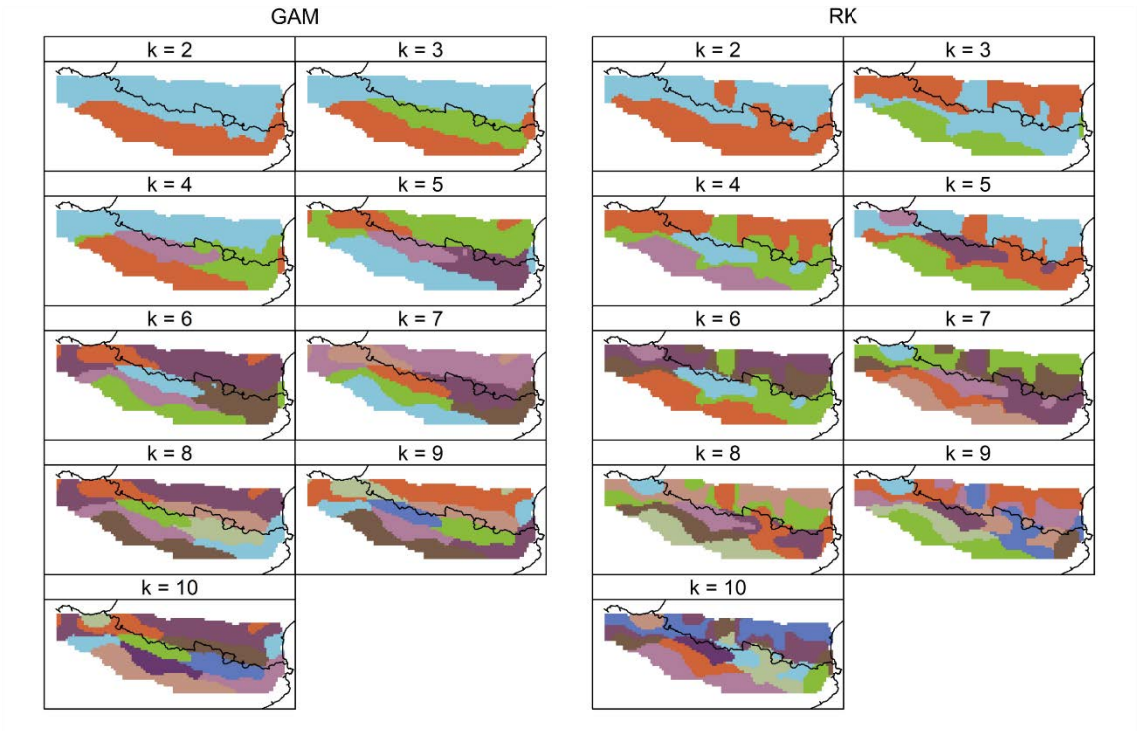

A.2. Suplement original de l'article: Characterisation of Extreme Precipitation Events in the Pyrenees: From the Local to the Synoptic Scale

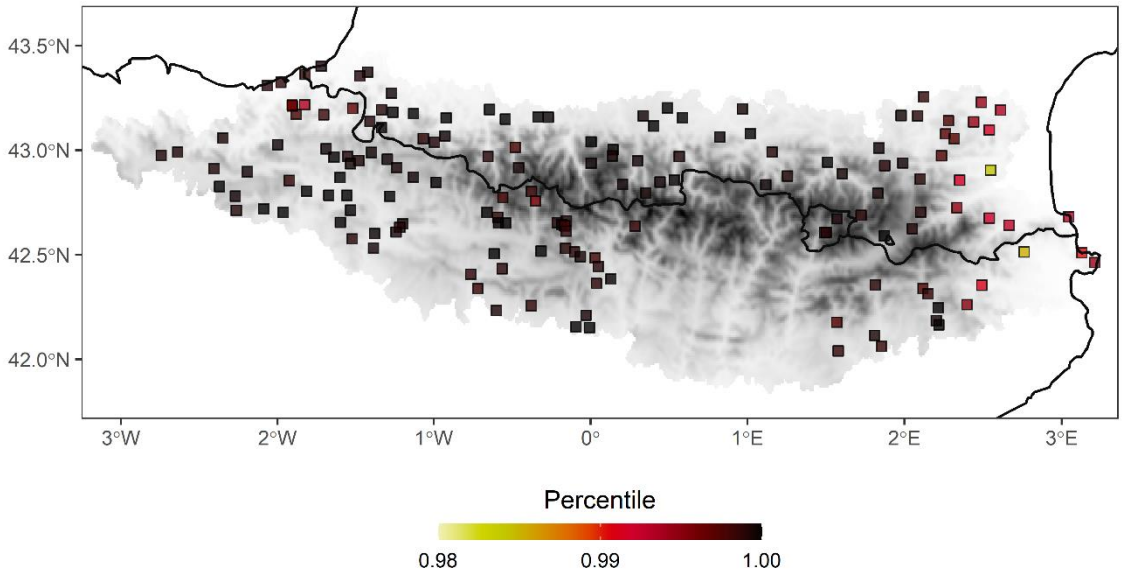

Fig S1. Percentile for a daily precipitation equal to or greater than 100 mm day^{-1}. For its estimation, daily precipitation values of less than 1 mm were eliminated.

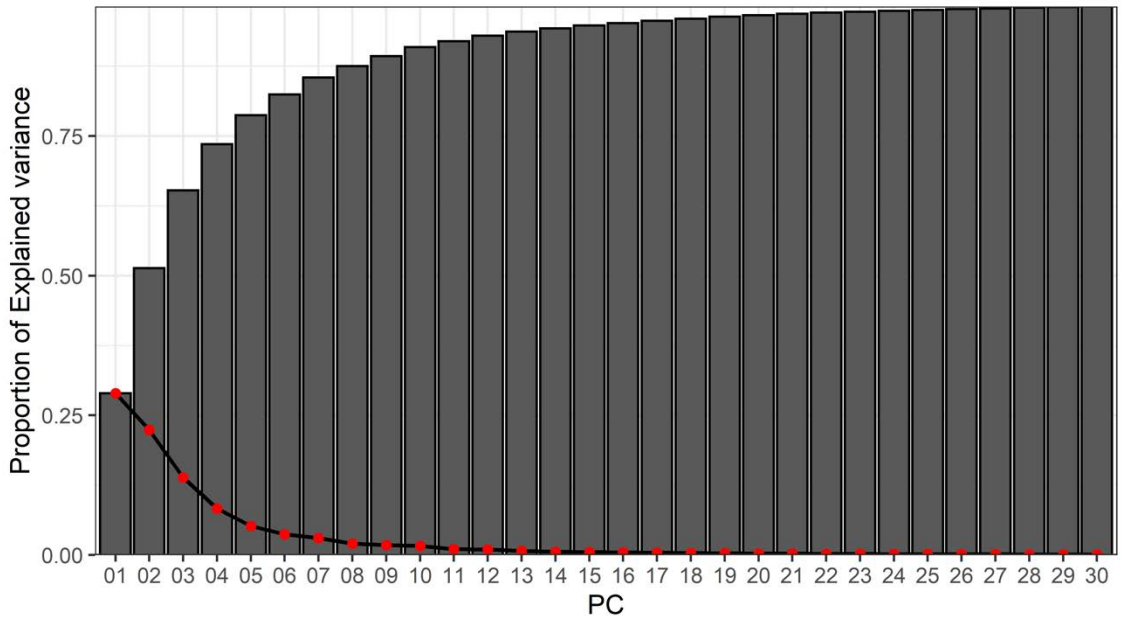

Fig S2. Scree test for the first 30 principal components (PCs). The red dots show the explained variance (%) for each principal component, while the grey bars show the cumulative explained variance.

Figure S3. Relative monthly frequencies in percentages of each weather type (WT) for the 1981-2015 period

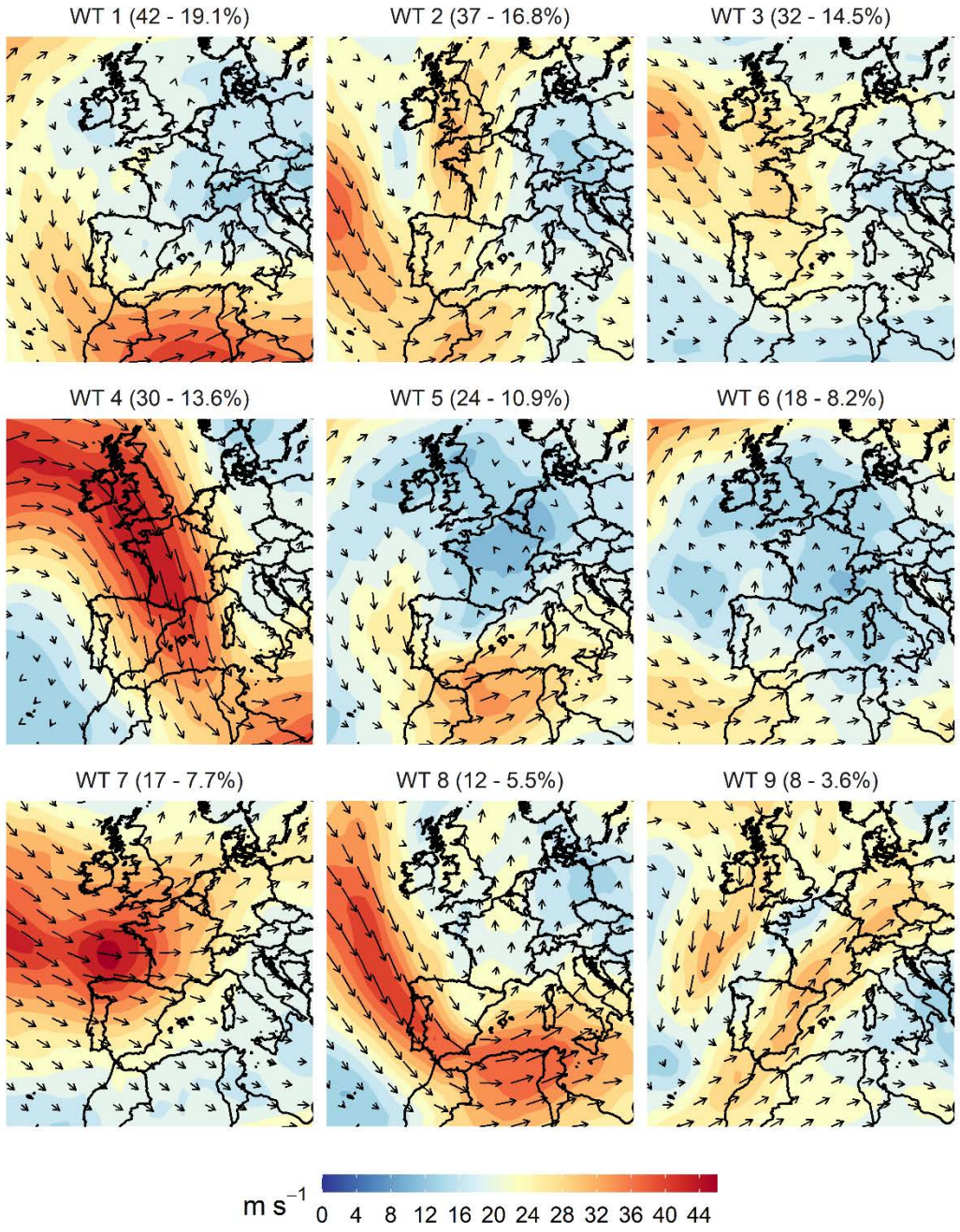

Figure S4. Daily mean 300 hPa wind direction and speed (m s^{-1}) of the 9 most frequent weather types associated with torrential precipitation in the western Mediterranean region. Above each map, the number of days assigned to each synoptic pattern and their percentages with respect to the total are shown in parentheses.

A.3. Suplement original de l'article: synoptReg: An R package for computing a synoptic climate classification and a spatial regionalization of environmental data

We provided an example code for easy use of the synoptReg package at: https://github.com/lemuscanovas/synoptReg. The example provided uses the preloaded datasets in the package. However, As shown in Fig. S4, we provided the R code for performing all calculations and designing all the figures in this paper.

Fig. S1. Scree test obtained with the function pca_decision.

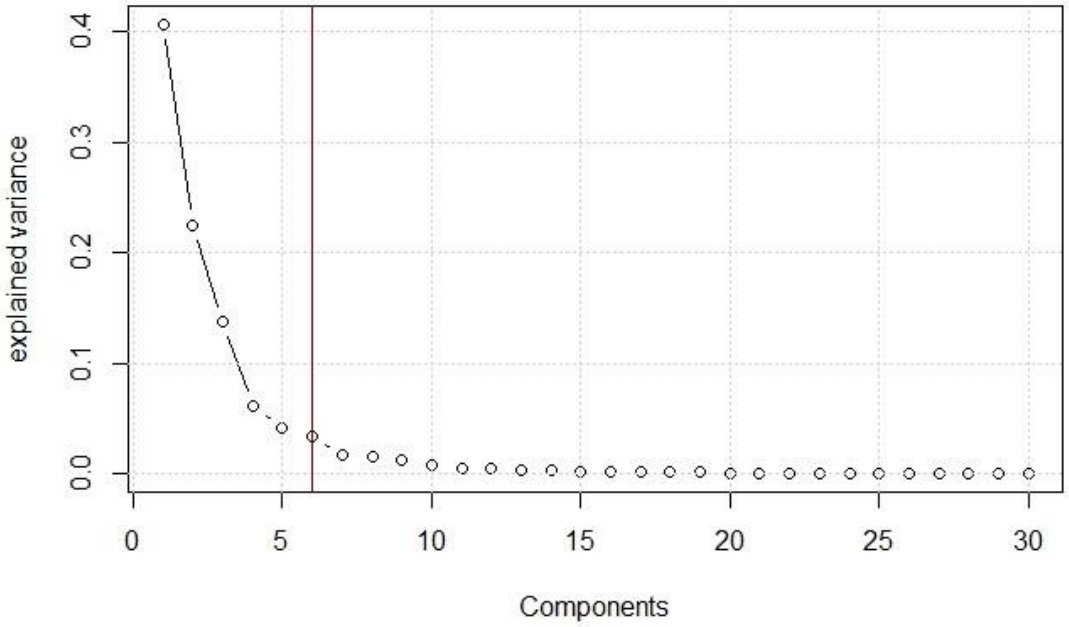

Fig. S2. Annual trend of the daily frequency by circulation type (CT).

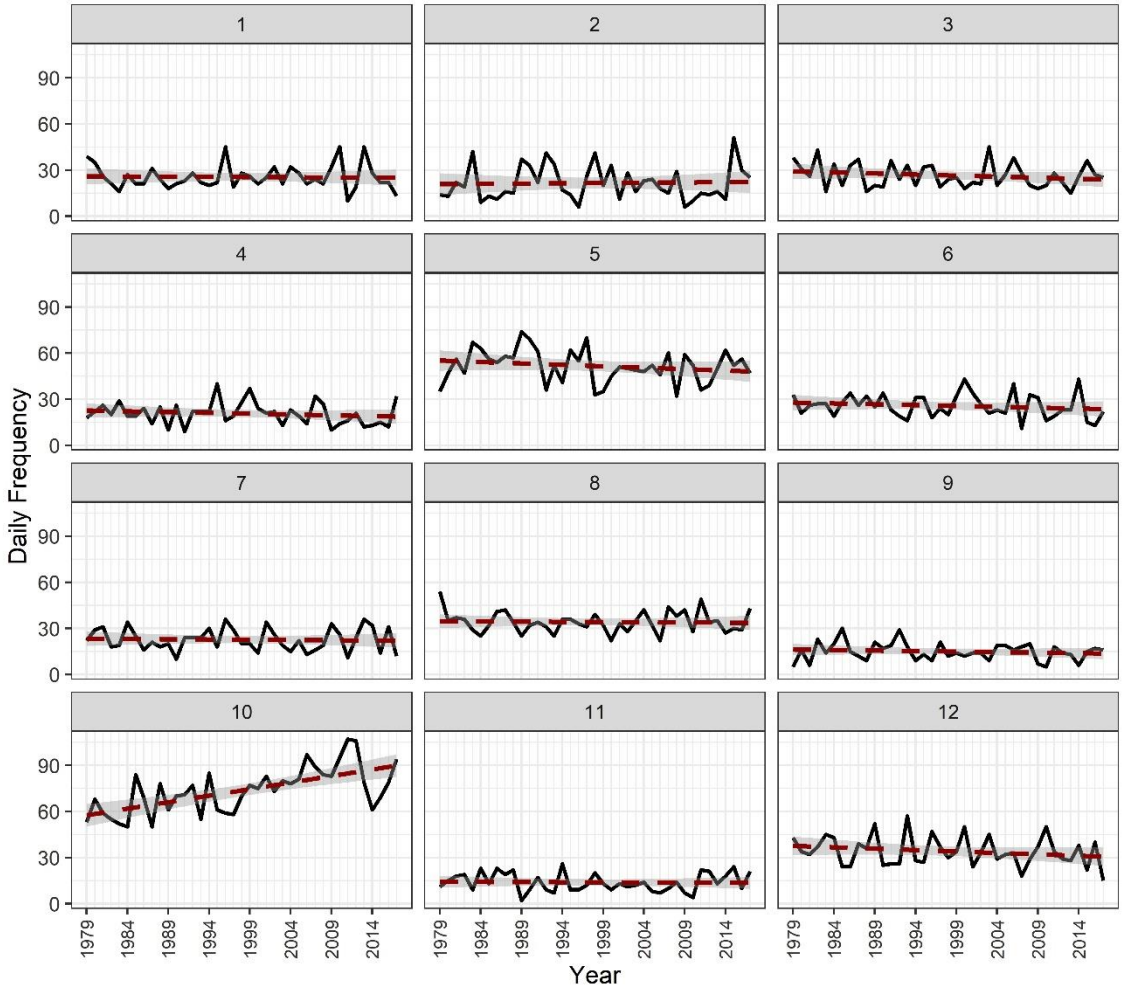

Fig. S3. Number of days per CT and month. This plot enables the seasonality of some of the CT to be visualized. Note that the CT 10 is an example of high summer seasonality.

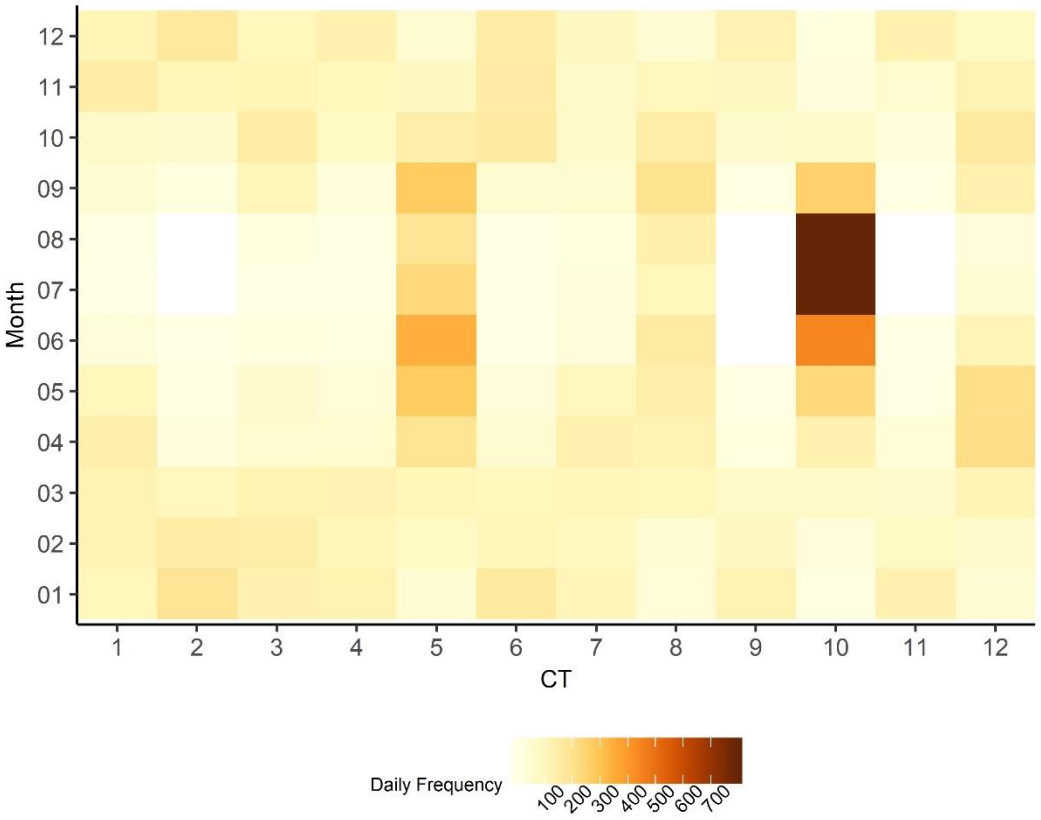

Fig. S4. PCA applied to the RasterStack object containing the MDP rasters. Visualization of these PCs provides the most frequent spatial patterns of precipitation.

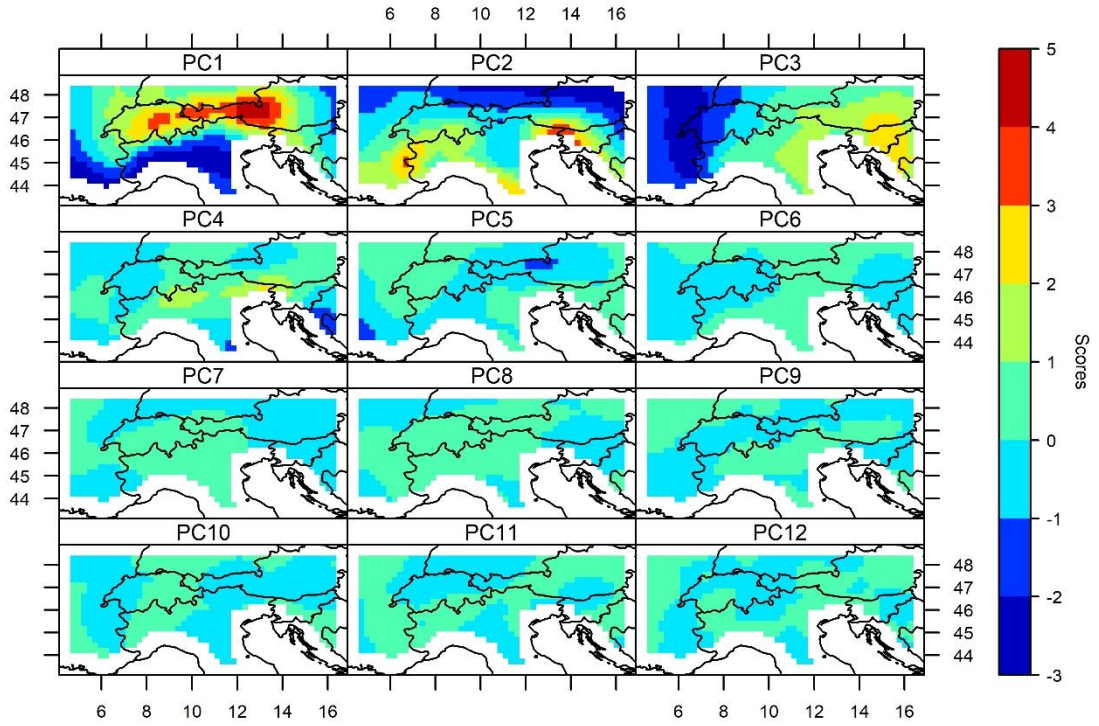

```
library(synoptReg)
library(maptools)
library(ggplot2)
library(RColorBrewer)
library(sp)
library(grid)
library(raster)


# Set working directory
setwd("C:/set_working_directory")

# Using read_nc to read the atmospheric and environmental data ------------
mslp <- read_nc(nc_input = "slp_1979_2017.nc",
                name_coord = c("longitude","latitude","time"),
                initial_date = "1979-01-01")

precp_grid <- read_nc(nc_input = "alps_rr_0.125deg_1979_2017.nc",
                      name_coord = c("longitude","latitude","time"),
                      initial_date = "1979-01-01")

# We now need to convert our mslp and precipitation data
# into S-mode data frame --------------------------------------------------
mslp_smode <- tidy_cuttime_nc(datalist = mslp)

precp_grid_s <- tidy_cuttime_nc(datalist = precp_grid)

# Requesting the suitable number of principal components ------------------
info_pca_mslp <- pca_decision(smode_data = mslp_smode$smode_data)

# Once we have established the number of components (6), we proceed
# with the synoptic classification ----------------------------------------
mslp_s_clas <- synoptclas(smode_data = mslp_smode$smode_data,
                          ncomp =  6)

# Converting the synoptic classification into a RasterStack object --------
raster_ct_clas <-raster_clas(longitude = mslp$lon,
                             latitude = mslp$lat,
                             grouped_data = mslp_s_clas$grouped_data)


# Figure 1 ----------------------------------------------------------------

# Reading the world shapefile (low resolution borders)
limit <-readShapeSpatial("TM_WORLD_BORDERS_SIMPL-0.3.shp")

# Converting to hPa
raster_ct_clas <- raster_ct_clas/100

# Plotting the synoptic classification
jpeg("ct_eu.jpg", width = 180, height = 160,
     quality = 100, res = 600, units = "mm")
spplot(raster_ct_clas,
       sp.layout = list(limit, first = FALSE),
       names.attr=names(raster_ct_clas),
       at = seq(round(min(minValue(raster_ct_clas)))-2,
                round(max(maxValue(raster_ct_clas)))+2, 2),
       zlim = c(round(min(minValue(raster_ct_clas)))-2,
```

```
                round(max(maxValue(raster_ct_clas)))+2),
       col.regions=colorRamps::matlab.like2(100),
       par.settings = list(strip.background=list(col="white"),
                           fontsize = list(text = 7)),
       contour=TRUE,
       colorkey = F,
       col='black',
       pretty=TRUE,
       scales=list(draw = TRUE),
       labels=TRUE)
dev.off()

# Converting the environmental data into a RasterStack object
# based on the CTs ----------------------------------------------------------

result_ct_env <- raster_ct2env(longitude = precp_grid$lon,
                               latitude = precp_grid$lat,
                               clas =  mslp_s_clas$clas,
                               grid_data = precp_grid_s$smode_data)


# Figure 2 ------------------------------------------------------------------

# Reading the world shapefile (high resolution borders)

limit <- readShapeSpatial("TM_WORLD_BORDERS-0.3.shp")

jpeg("pcp_alps_ct.jpg", width = 155, height = 110,
     quality = 100, res = 600, units = "mm")
spplot(result_ct_env,
       sp.layout = list(limit, first = FALSE),
       names.attr=names(result_ct_env),
       at = seq(round(min(minValue(result_ct_env))),
                round(max(maxValue(result_ct_env))+1),1),
       col.regions=rev(colorRamps::matlab.like2(100)),
       par.settings = list(strip.background=list(col="white"),
                           fontsize = list(text = 8)),
       contour=FALSE,
       colorkey = TRUE,
       col='black',
       pretty=TRUE,
       scales=list(draw = TRUE),
       labels=TRUE)
grid.text("MDP (mm)",
          x=unit(0.993,"npc"),
          y=unit(0.50, "npc"),
          rot = -90,
          gp=gpar(fontsize=7))
dev.off()

# Raster PCA (R-mode) -------------------------------------------------------

pca_result <- raster_pca(raststack = result_ct_env,
                         aggregate = 0,
                         focal = 5)


# Computing the spatial regionalization -------------------------------------

# Selecting the first 4 PC of the raster PCA object
```

```r
sel<-pca_result$rasterPCA[[1:4]]



# For loop for obtaining the regions from k = 2 to k = 10
pseudoMAE<-c()
reg_results<-list()
raster_region<-stack()

for (ii in 2:10) {
  reg_results[[ii]] <- regionalization(sel,ii)
  pseudoMAE [ii] <- reg_results[[ii]]$pseudoMAE
  raster_region <- stack(raster_region, reg_results[[ii]]$regionalization)
}

# Names raster layers:
v = list()
for (i in 2:10){
  v[[i]] = paste0("k = ",i)
}

name_layers = unlist(v, use.names=FALSE)


# Figure 3 ------------------------------------------------------------

ColorRamp <- colorRampPalette(c("#89C5DA", "#DA5724", "#74D944",
                                "#CE50CA", "#3F4921", "#C0717C",
                                "#CBD588", "#5F7FC7","#673770"))

jpeg("regionalization_alps.jpg", width = 155, height = 90,
     quality = 100, res = 600, units = "mm")
spplot(raster_region,
       sp.layout = list(limit, first = FALSE),
       names.attr=name_layers,
       at = seq(min(minValue(raster_region)-1),
                max(maxValue(raster_region)), 1),
       col.regions=ColorRamp,
       par.settings = list(strip.background=list(col="white"),
                           fontsize = list(text = 7)),
       contour=F,
       colorkey = F,
       col='black',
       pretty=TRUE,
       scales=list(draw = TRUE),
       labels=TRUE)
dev.off()



# Figure 4 ------------------------------------------------------------

# Pseudo-MAE plot
jpeg("pseudoMAE.jpg", width = 190, height = 140,
     quality = 100, res = 600, units = "mm")
plot(pseudoMAE,
     type="b", lwd = 1.8, pch =16,
     xlim = c(2,10), xlab = "number of clusters (k)",
     ylab = "Pseudo-MAE (dimensionless)")
grid()
abline(v = c(3,4,8,9))
```

```
dev.off()
# Supplementary figures ------------------------------------------------

# Figure S1 is obtained by running the pca_decision function.

# Figure S2
lab <- seq(1979, 2017, 5)
mslp_s_clas$annual_freq$Year <- as.numeric(mslp_s_clas$annual_freq$Year)

jpeg("annual_trend_ct.jpg", width = 180, height = 160,
     quality = 100, res = 600, units = "mm")
ggplot(data = mslp_s_clas$annual_freq, aes(x = Year,
                                           y = Counts,
                                           group = CT)) +
  geom_line(size = 0.8) +
  scale_x_continuous(labels = lab,
                     breaks = seq(1979,2017,5),
                     minor_breaks = seq(1979,2017,1))  +
  stat_smooth(method = "lm",
              formula = y ~ x,
              size = 1,
              color = "red4",
              linetype = "dashed") +
  facet_wrap(~ CT, nrow = 4, ncol = 3) +
  theme_bw() +
  theme(axis.text.x = element_text(colour="grey20",
                                   size=8,
                                   angle=90,
                                   hjust=.5,
                                   vjust=.5),
        axis.text.y = element_text(colour="grey20",
                                   size=8),
        text = element_text(size=10)) +
  ylab("Daily Frequency")
dev.off()

# Figure S3

jpeg("monthly_matrix_ct.jpg", width = 140, height = 120,
     quality = 100, res = 600, units = "mm")
ggplot(data = mslp_s_clas$monthly_freq, aes(x=CT,y=Month)) +
  geom_tile(aes(fill=Counts)) +
  scale_fill_gradientn(colours= brewer.pal(9, "YlOrBr"),
                       guide = "colourbar",
                       name = "Daily Frequency",
                       breaks = seq(0,800, by = 100),1) +
  scale_x_continuous(name="CT",
                     breaks = seq(1,12,1),
                     expand=c(0,0)) +
  ggtitle("") +
  theme_classic()+
  theme(plot.title = element_text(color="black",
                                  size=10,
                                  face="bold"),
        axis.text=element_text(size=8),
        axis.title.x = element_text(size = 8),
        axis.title.y = element_text(size = 8),
        legend.title=element_text(size=6),
        legend.text=element_text(size= 5),
        legend.position="bottom")
```

```
dev.off()

# Figure S4 ------------------------------------------------------------

jpeg("PCA_pcp_alps.jpg", width = 155, height = 110,
     quality = 100, res = 600, units = "mm")
spplot(pca_result$rasterPCA,
       sp.layout = list(limit, first = FALSE),
       names.attr=names(pca_result$rasterPCA),
       at = seq(round(min(minValue(pca_result$rasterPCA))),
                round(max(maxValue(pca_result$rasterPCA))),1),
       col.regions=colorRamps::blue2green2red(100),
       par.settings = list(strip.background=list(col="white"),
                           fontsize = list(text = 8)),
       contour=FALSE,
       colorkey = TRUE,
       col='black',
       pretty=TRUE,
       scales=list(draw = TRUE),
       labels=TRUE)
grid.text("Scores",
          x=unit(0.993,"npc"),
          y=unit(0.50, "npc"),
          rot = -90,
          gp=gpar(fontsize=7))
dev.off()
```

A.4. Suplement original de l'article: Assessing internal changes in the future structure of dry–hot compound events: the case of the Pyrenees

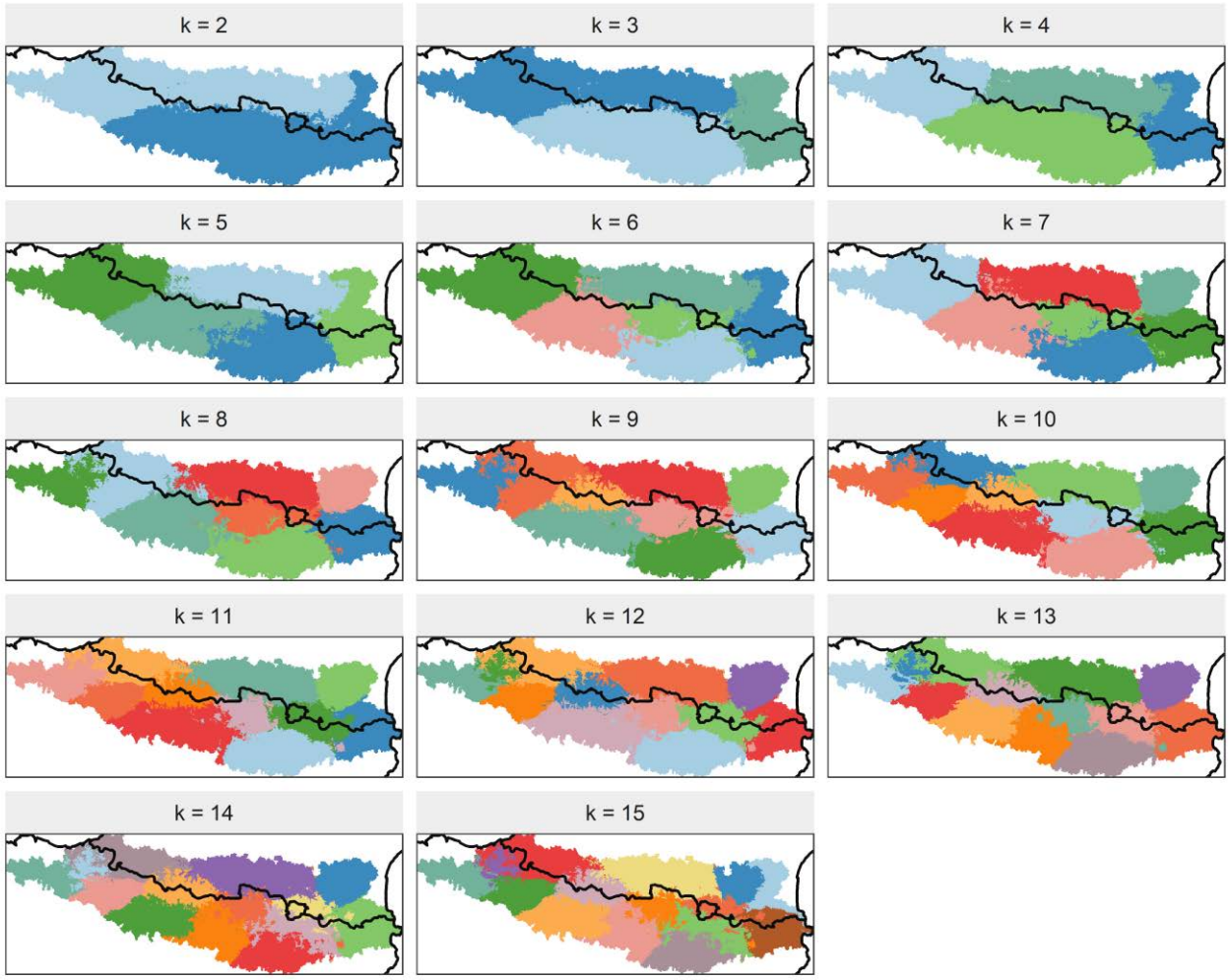

Figure S15. Regionalization of spring and summer precipitation and temperature during the 1981–2015 period for k = 2, 3..., 15 clusters.

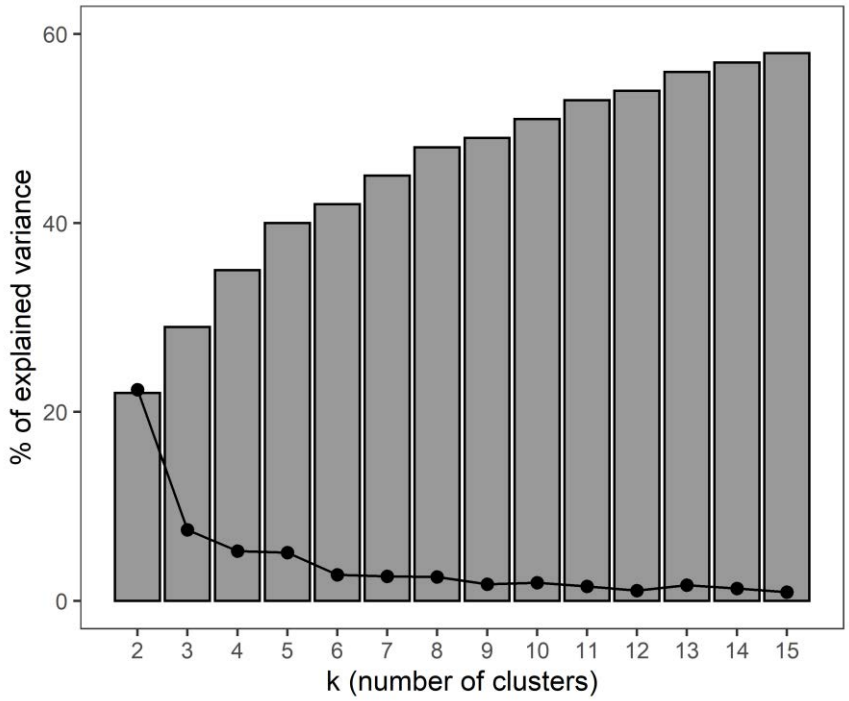

Figure S16. Scree test for the number of clusters. The slope changes considered for the selection of the number of regions were k = 5 and k = 8, the latter being the definitive number of regions.

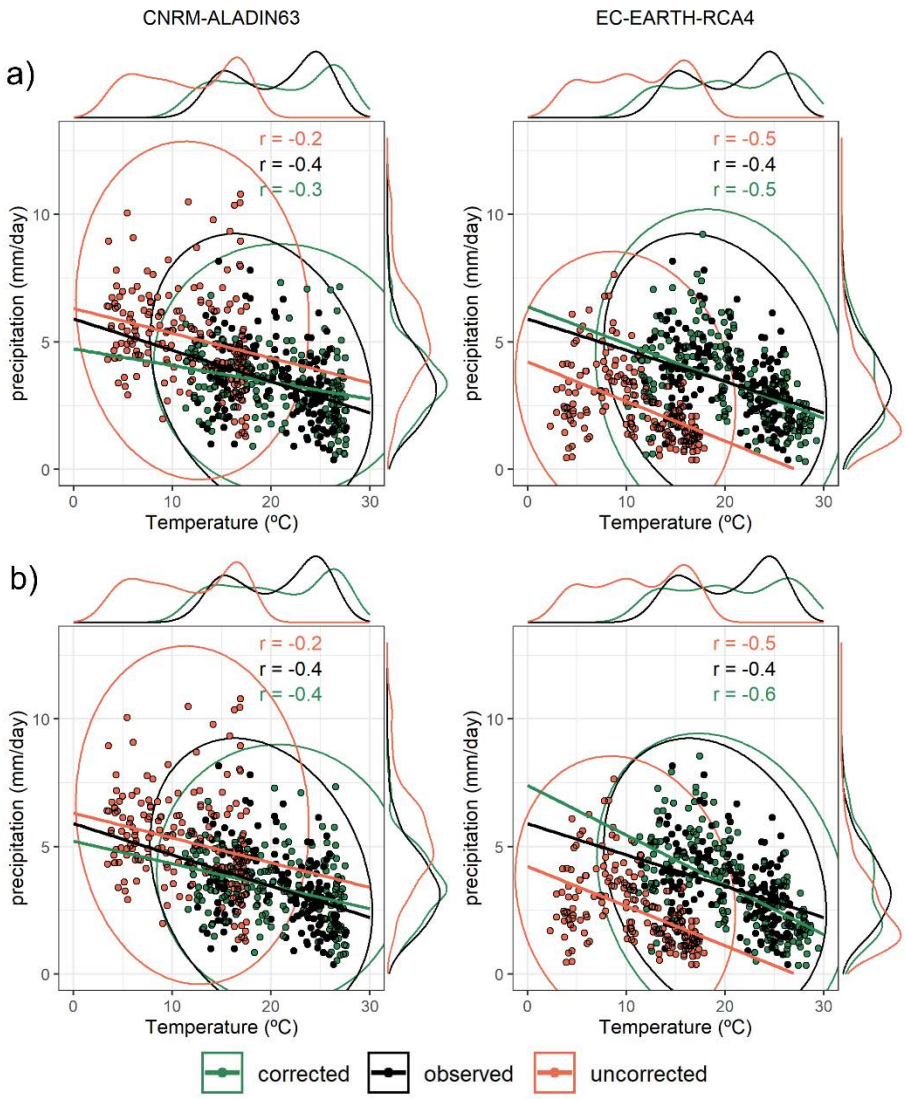

Figure S17. Distribution of mean daily temperature versus mean daily precipitation from March to August (1981–2005) for the NMED region and for two RCM: CNRM-ALADIN63 and EC-EARTH-RCA4. UBC method (a); MBC method (b). Fitted lines, area of distribution and density distributions in green color are referred to bias corrected model, in black are referred to observed data, and in red are referred to raw/uncorrected model. Pearson correlation values (r) are also shown.

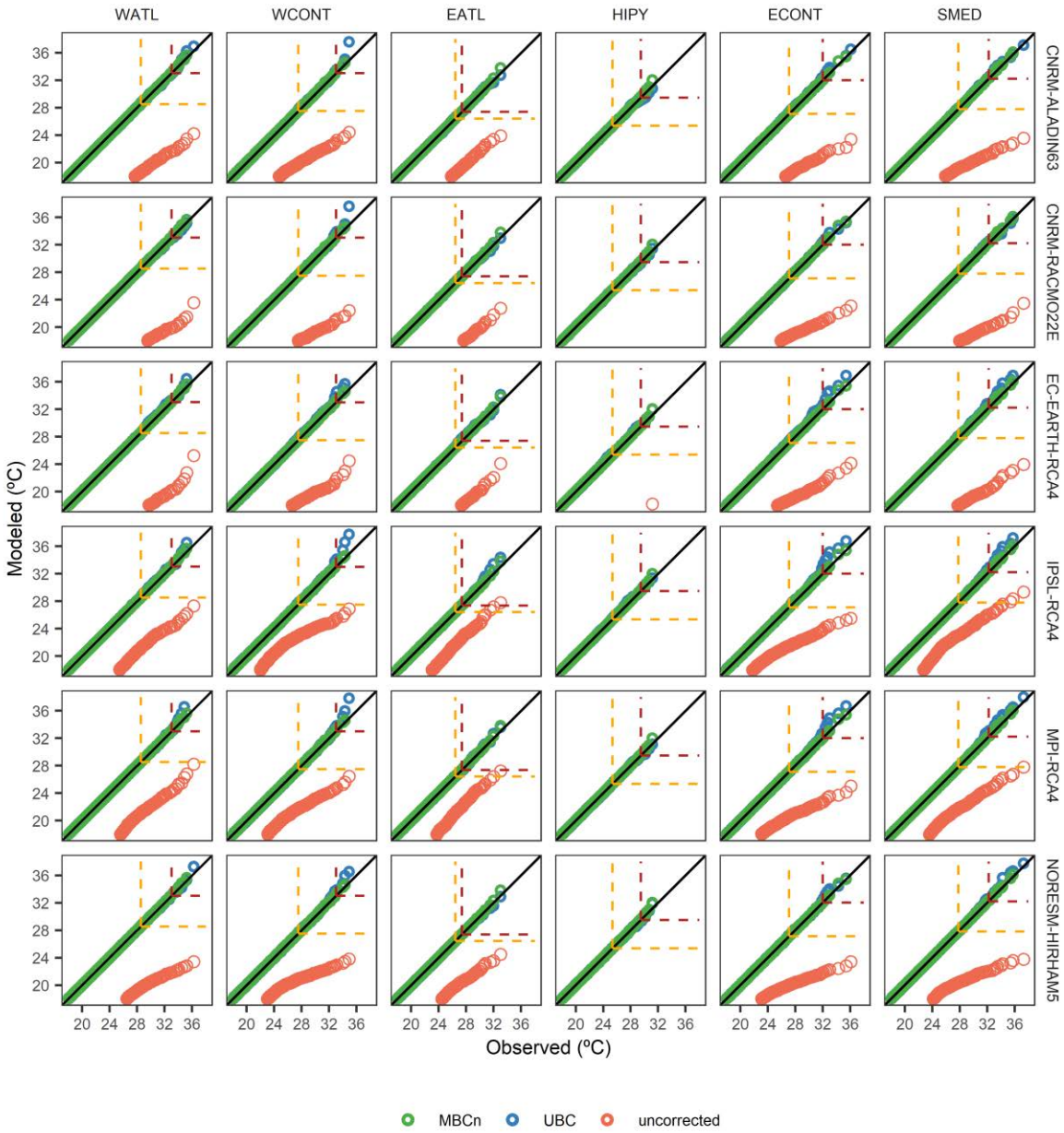

Figure S4. Quantile–quantile plot of observed versus modeled values for temperature for WATL, WCONT, EATL, HIPY,ECONT and SMED regions and all RCMs; green and blue circles are referred to MBCn and UBC methods, respectively. Red circles correspond to the uncorrected RCM series. The yellow top right dashed box shows the 95th percentile of observed daily temperature, while the dark red top right dashed box shows the 95th percentile of observed daily temperature during the occurrence of dry spells of extreme length (95th percentile).

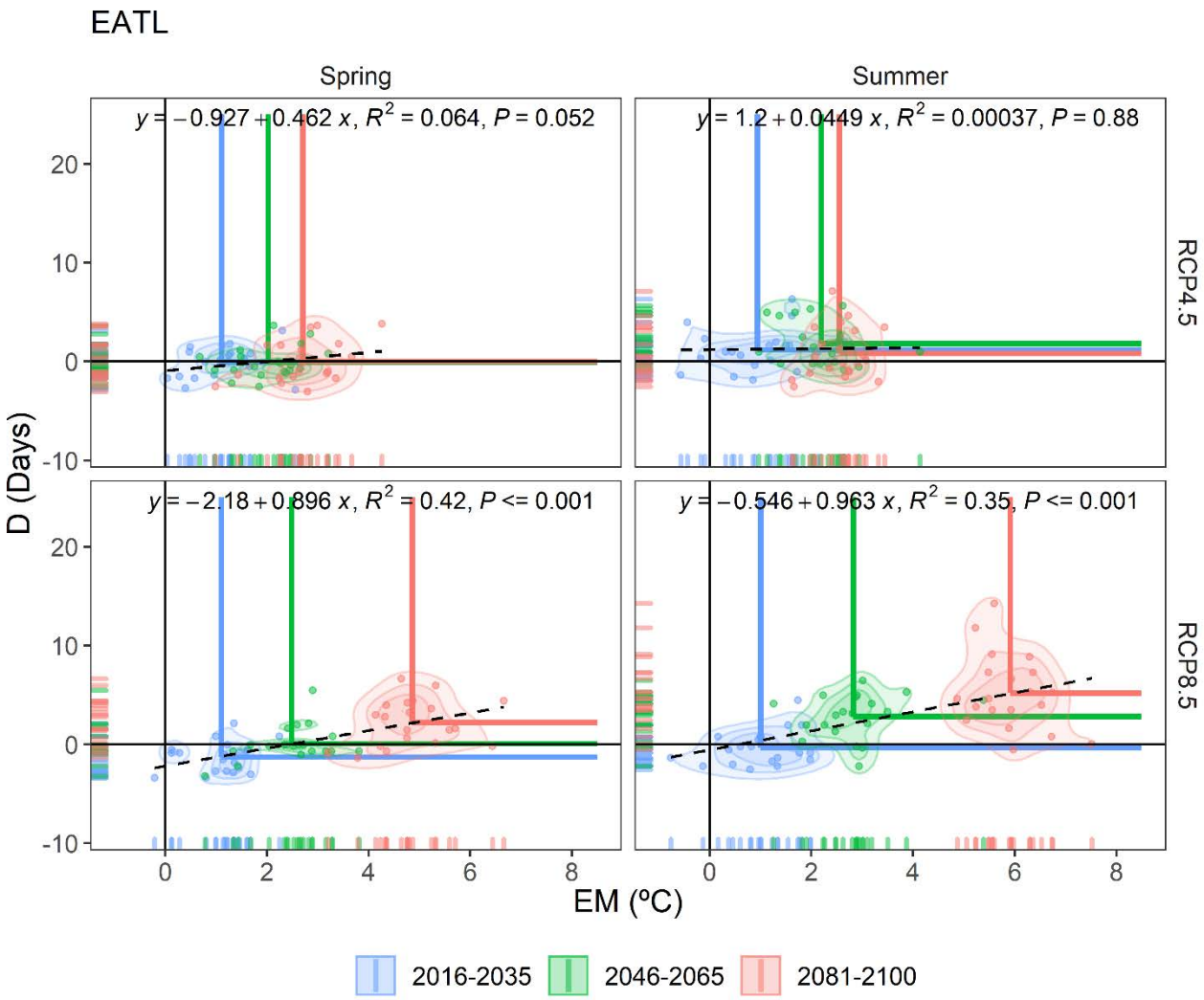

Figure S5. Bivariate probability density functions of D and EM anomalies for the three future periods (2016-2035, 2046-2065 and 2081-2100) and for the two emission and seasonal scenarios with respect to the historical period (1981-2005) for the EATL region. Each point in the scatter plot represents the multi-model annual mean of D and EM in a given year. The intersections of the blue, green and red horizontal and vertical lines indicate the mean anomaly value of the bivariate distribution for each period. The linear fit regression was computed using the annual mean anomalies of EM and D for the 2016-2100 period. Each plot possesses a regression equation and its statistical significance (P, p-value). The figure is generated using the ensemble of all RCMs.

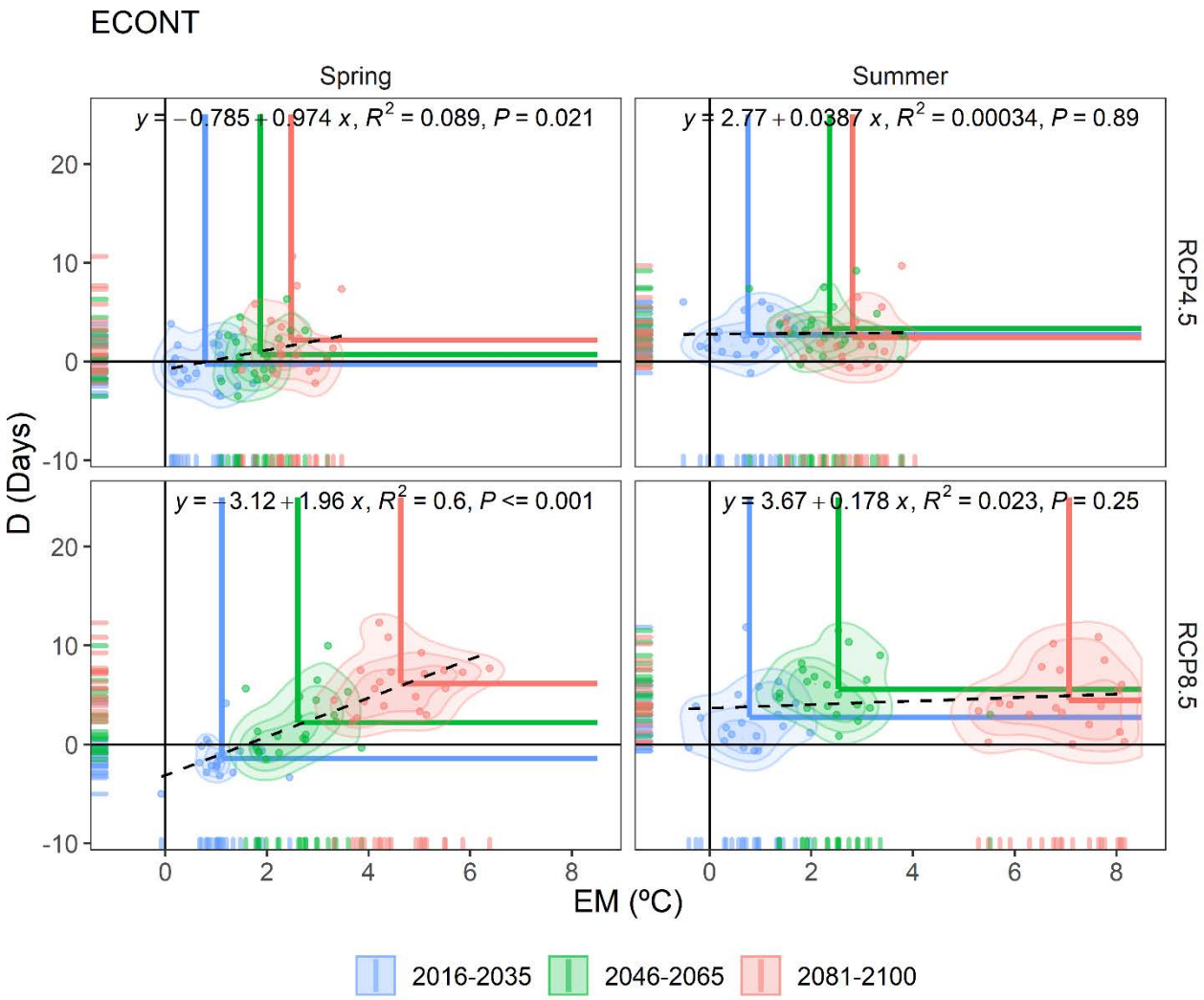

Figure S6. Same as Fig. S5, but for the ECONT region.

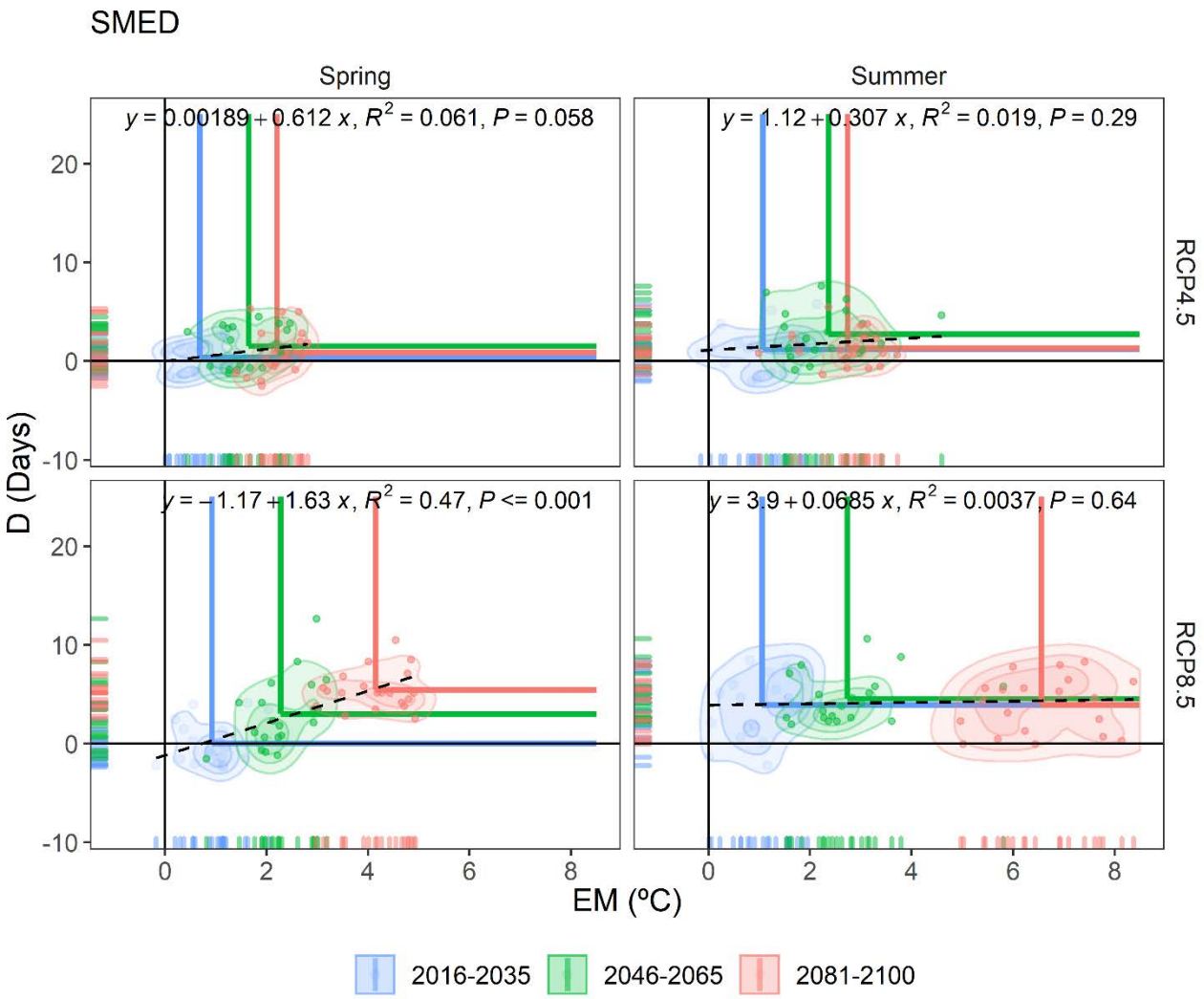

Figure S7. Same as Fig. S5, but for the SMED region.

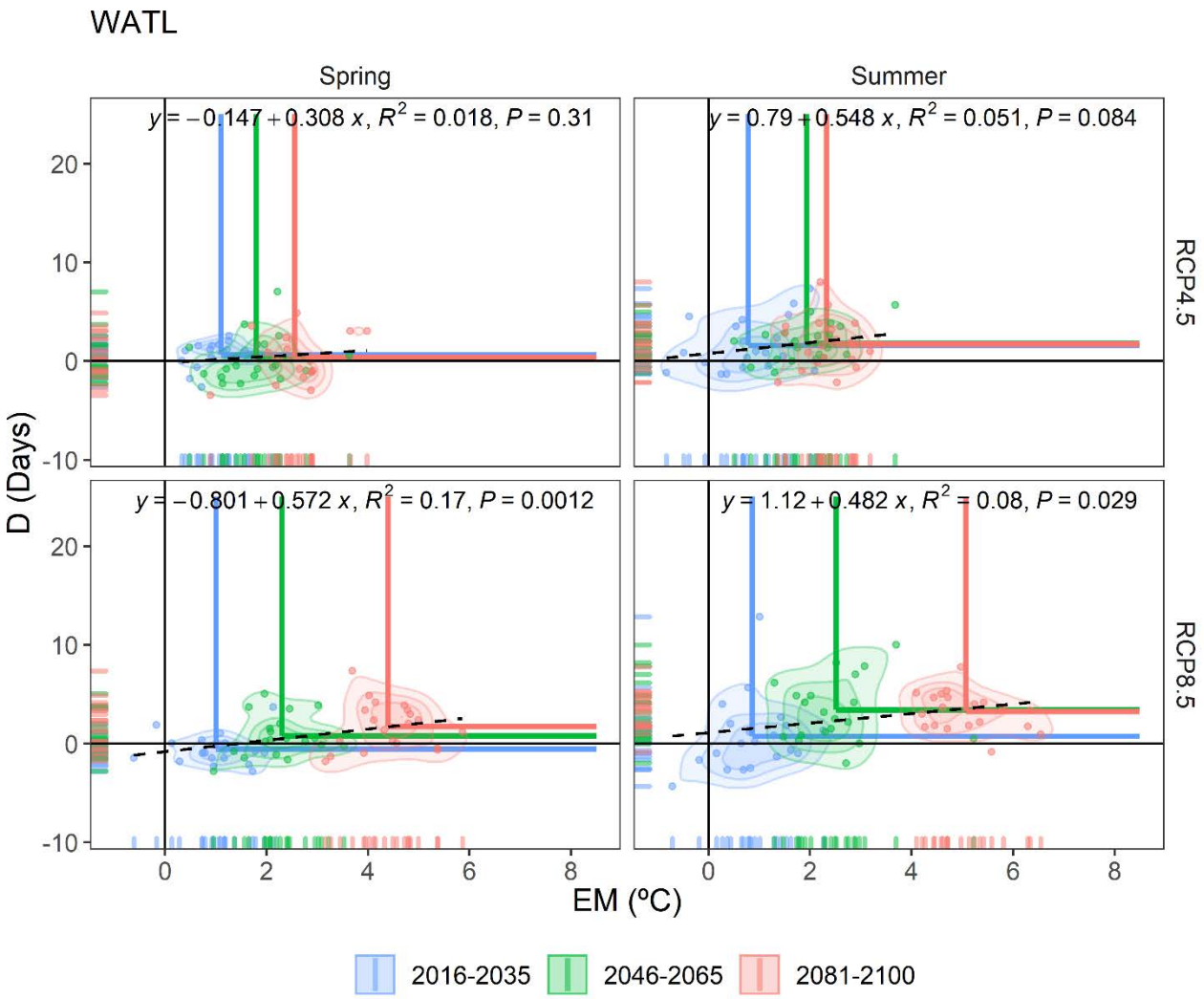

Figure S8. Same as Fig. S5, but for the WATL region.

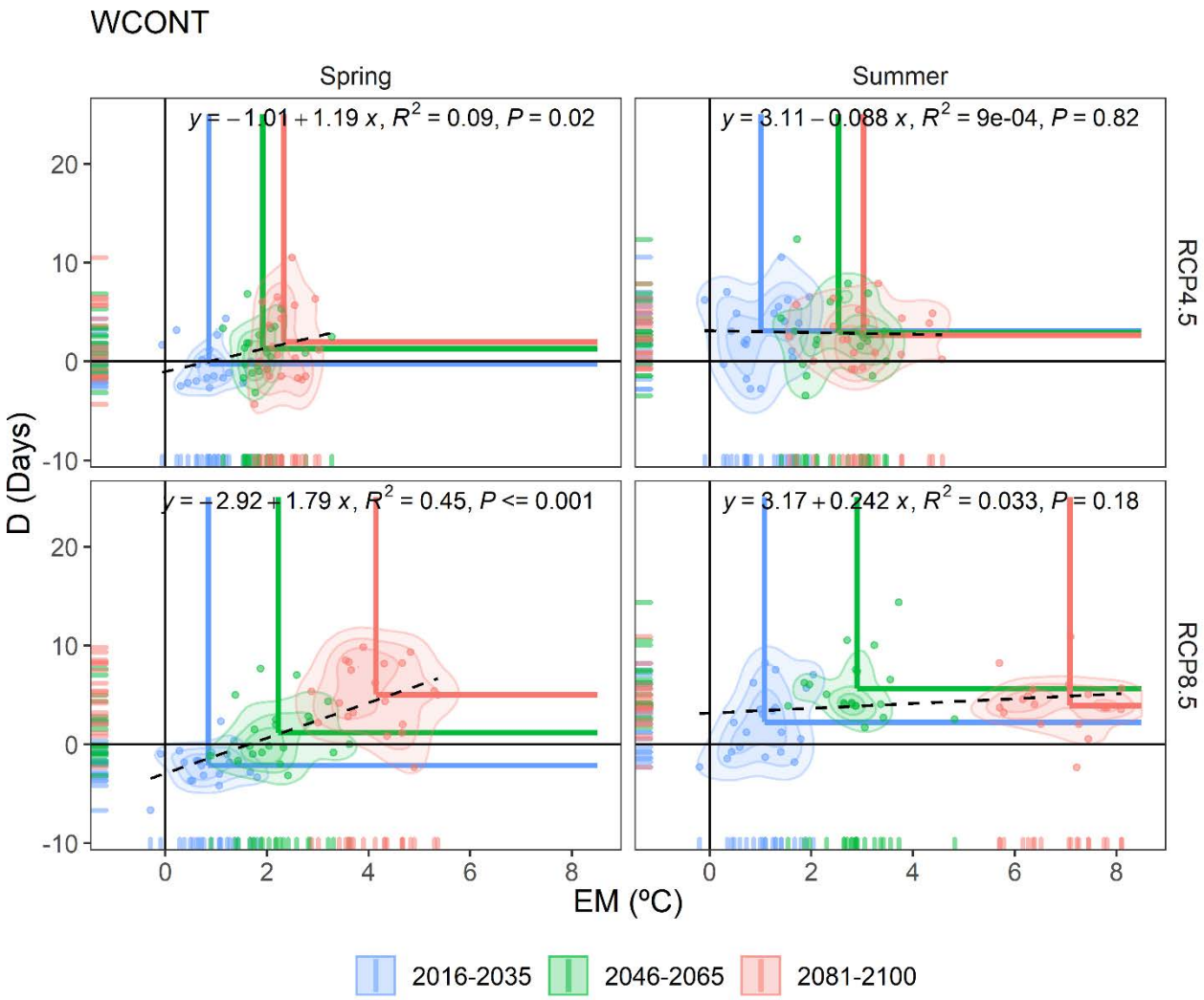

Figure S9. Same as Fig. S5, but for the WCONT region.

Apèndix B. Contribucions durant el període doctorat

En aquesta secció es llisten, ordenades cronològicament, les contribucions realitzades durant el període predoctoral en format d'article, de presentació oral i de pòster en congressos i seminaris, així com la docència impartida durant aquest període.

B.1. Articles

Publicats

- Lemus-Canovas, M. (2021). Barcelona intense urban activity greatly limited the role of the atmosphere in driving NO_2 concentration in 2018. Environmental Research Communications. https://doi.org/10.1088/2515-7620/ac2fbb
- Insua-Costa, D., Lemus-Canovas, M., Miguez-Macho, G., & Llasat, M. C. (2021). Climatology and ranking of hazardous precipitation events in the western Mediterranean area. Atmospheric Research, 255, 105521. https://doi.org/10.1016/j.atmosres.2021.105521
- Martinez-Artigas, J., Lemus-Canovas, M., & Lopez-Bustins, J. A. (2021). Precipitation in peninsular Spain: Influence of teleconnection indices and spatial regionalisation. International Journal of Climatology, 41(S1), E1320–E1335. https://doi.org/10.1002/joc.6770
- Lemus-Canovas, M., & Lopez-Bustins, J. A. (2021). Assessing internal changes in the future structure of dry–hot compound events: the case of the Pyrenees. Natural Hazards and Earth System Sciences, 21(6), 1721–1738. https://doi.org/10.5194/nhess-21-1721-2021
- Lemus-Canovas, M., Lopez-Bustins, J. A., Martín-Vide, J., Halifa-Marin, A., Insua-Costa, D., Martinez-Artigas, J., Trapero, L., Serrano-Notivoli, R., & Cuadrat, J. M. (2021). Characterisation of Extreme Precipitation Events in the Pyrenees: From the Local to the Synoptic Scale. Atmosphere, 12(6), 665. https://doi.org/10.3390/atmos12060665
- Peña-Angulo, D., Gonzalez-Hidalgo, J. C., Sandonís, L., Beguería, S., Tomas-Burguera, M., López-Bustins, J. A., Lemus-Canovas, M., & Martin-Vide, J. (2021). Seasonal temperature trends on the Spanish mainland: A secular study (1916–2015). International Journal of Climatology, 41(5), 3071–3084.
- Lopez-Bustins, J. A., & Lemus-Canovas, M. (2020). The influence of the Western Mediterranean Oscillation upon the spatio-temporal variability of precipitation over Catalonia (northeastern of the Iberian Peninsula). Atmospheric Research, 236. https://doi.org/10.1016/j.atmosres.2019.104819
- Lemus-Canovas, M., Martin-Vide, J., Moreno-Garcia, M. C., & Lopez-Bustins, J. A. (2020). Estimating Barcelona's metropolitan daytime hot and cold poles using Landsat-8 Land Surface Temperature. Science of the Total Environment, 699. https://doi.org/10.1016/j.scitotenv.2019.134307
- Lemus-Canovas, M., Lopez-Bustins, J. A., Trapero, L., & Martin-Vide, J. (2019). Combining circulation weather types and daily precipitation modelling to derive climatic precipitation

regions in the Pyrenees. Atmospheric Research, 220. https://doi.org/10.1016/j.atmosres.2019.01.018

- Lemus-Canovas, M., Lopez-Bustins, J. A., Martin-Vide, J., & Royé, D. (2019). synoptReg: An R package for computing a synoptic climate classification and a spatial regionalization of environmental data. Environmental Modelling and Software. https://doi.org/10.1016/j.envsoft.2019.04.006
- Lemus-Canovas, M., Ninyerola, M., Lopez-Bustins, J. A., Manguan, S., & Garcia-Sellés, C. (2018). A mixed application of an objective synoptic classification and spatial regression models for deriving winter precipitation regimes in the Eastern Pyrenees. International Journal of Climatology. https://doi.org/10.1002/joc.5948

En preparació/revisió

- Lemus-Canovas, M., & Brands, S. Very high-resolution temperature projections for the Pyrenees based on CMIP6 and robust statistical downscaling. En preparació per a Earth System Dynamics.
- Lemus-Canovas, M. (Under Review). Changes in compound monthly precipitation and temperature extremes and its relationship with teleconnection patterns in the Mediterranean. Journal of Hydrology.

B.2. Comunicacions en congressos

- Marc Lemus-Canovas and Swen Brands. Assessing several downscaling methods for daily minimum and maximum temperature in a mountainous area. Are we able to statistically simulate a warmer climate in the Pyrenees? On-line. EGU General Assembly. Maig 2020
- Marc Lemus-Canovas. Combinant els tipus de circulació atmosfèrica i la interpolació de la precipitació diària per a l'obtenció de regions pluviomètriques en zones de muntanya. Jornada Tècnica del Grup d'Experts del Canvi Climàtica a Catalunya (GECC).Barcelona, Gener del 2020.
- Marc Lemus Cánovas, Joan Albert López Bustins i Javier Martín Vide. An R package for computing a synoptic classification and spatial regionalization ofprecipitation data. 7th International Conference on Meteorology and Climatology of the Mediterranean. Palma de Mallorca, Illes Balears, Espanya. Març del 2019.
- Marc Lemus Cánovas, Joan Albert López Bustins, Laura Trapero Bagué i Javier Martin Vide. Mixing weather types and daily precipitation modelling as an approach to obtain climatic precipitation regions in mountain areas. European Geosciences Union General Assembly. Viena, Àustria. Abril 2019.
- Marc Lemus Canovas, José Manuel Garrido Pérez, Carlos Ordóñez i Ricardo Garcia Herrera. Impact of the extratropical jet on air quality in Europe. European Geosciences Union General Assembly. Viena, Àustria. Març 2018.
- Marc Lemus Canovas. Modelització de la precipitació hivernal al Pirineu de Catalunya en base a diferents situacions sinòptiques. Una eina operativa per a la predicció d'allaus. 3rd

IdRA Young Researchers Seminar. Water Research Institute. Universitat de Barcelona, Barcelona. Espanya. Maig 2018.

B.3. Estades en centres de recerca

- Instituto Dom Luiz. Universidade de Lisboa. Portugal. (3 mesos).
- Geography and Spatial Planning Research Centre. Universidade do Porto. porto. Portugal. (1 mes)
- Grupo de Física No Lineal. Universidade de Santiago de Compostela. Santiago de Compostela. (1 mes)

B.4. Docència impartida

Docència en Graus i màsters universitaris (180 hores):

- Estadística (Grau en Geografia)
- Geografia Física i Climatologia (Grau en Ciències Ambientals)
- Canvi Global (Grau en Geografia)
- Seminaris del Canvi Global (Màster en Ecologia)
- Tractament i anàlisi de dades climàtiques amb R (Màster en Climatologia Aplicada i Mitjans de Comunicació)
- Anàlisi de sèries climàtiques (Màster en Climatologia Aplicada i Mitjans de Comunicació)

Cursos extra curriculars (100 hores)

- Introducció a R per a l'anàlisi i visualització de dades estadístiques i espacials. (2 edicions presencials (Gener 2019, Febrer 2020) i 2 edicions online (Abril i Novembre, 2021). 25 hores per curs.

B.5. Desenvolupament de llibreries i aplicacions R

- synoptReg, Synoptic Climate Classification and Spatial Regionalization of Environmental Data, Set of functions to compute different types of synoptic classification methods and for analysing their effect on environmental variables. https://lemuscanovas.github.io/synoptreg/
- meteoclimaticR, Descàrrega de dades de la xarxa d'estacions Meteoclimatic (https://www.meteoclimatic.net/). meteoclimaticR permet la descàrrega de dades meteorològiques proporcionades per la xarxa d'estacions de Meteoclimatic. Es poden obtenir les dades actuals i històriques de temperatura, humitat relativa, precipitació, vent i pressió atmosfèrica. https://github.com/lemuscanovas/meteoclimaticR .
- Shiny app Càlcul del Període de Retorn. Càlcul del Període de retorn per a diferents llindars de temperatura a 850 i 500 hPa. https://lemuscanovas.shinyapps.io/app_periode_retorn/.

B.6 Altres mèrits

Recull en mitjans de premsa

- Com respondrà el Pirineu a les situacions d'extrema sequera i l'ambient calorós del futur? 3/24. CCMA. Juliol, 2021. https://bit.ly/3hPaQrF
- Nou estudi sobre l'impacte del canvi climàtic als Pirineus en un futur més sec i càlid. RTVE. Juliol, 2021. https://bit.ly/3Bm9aOh
- El canvi climàtic als Pirineus: temperatures extremes més altes i sequeres més llargues. Barcelona Televisió, BTV. Juliol, 2021 https://bit.ly/3AUhnZC
- L'escalfament global farà augmentar les morts per calor a Catalunya. Juliol, 2021. Barcelona. Onda Cero. https://bit.ly/3r2G7dE
- Un equip de la UB analitza l'impacte del canvi climàtic en els períodes secs i càlids als Pirineus. Premsa Universitat de Barcelona. Juliol, 2021. https://bit.ly/3BmQiP5
- Pot donar-se una onada de calor com la del Canadà a Barcelona? Juliol, 2021. Barcelona Televisió, BTV. https://bit.ly/3dP2JZQ
- Les barres pel clima de tot Catalunya, obertes a tothom. Juny, 2020. Barcelona Televisió, BTV. https://bit.ly/2SQBKFY
- Les àrees urbanes s'escalfen fins a 2.5 ºC més que les zones amb verd urbà. Setembre, 2019. Barcelona Televisió, BTV. https://bit.ly/3dQDN4k
- Detecten un descens significatiu de la precipitació anual al vessant sud del Pirineu. Febrer, 2019. Portal de Notícies 324. https://bit.ly/2STQaFx
- Alguns episodis anticiclònics al Pirineu són quatre vegades més freqüents ara que fa 50 anys. Febrer, 2019. MeteoMauri. Catalunya Radio. https://bit.ly/3yxri5C
- El canvi climàtic a Barcelona en un cop d'ull: els anys més càlids a partir del 2000. Juny, 2018. Barcelona Televisió. https://bit.ly/3xrAKaC

Premis

- Best Student Poster Presentation. 7th International Conference on Meteorology and Climatology of the Mediterranean (2019)

Altres

- Assistant Guest Editor of the Special Issue: "Spatiotemporal Variability of Precipitation Concentration and Drought Events in the Mediterranean Basin". https://www.mdpi.com/journal/atmosphere/special_issues/variability_of_precipitation_concentration_and_drought_events
- Reviewer of the Second Order Draft of the IPCC Sixth Assessment Report Climate Change 2021: The Physical Science Basis, by the Working Group I. Maig, 2020.
- Col · laborador en l'organització tècnica del 3rd IdRA Young Researchers Seminar. Barcelona, Maig, 2018.
- Participació al 1r workshop CLIM'PY: Base de dades climàtiques en zones de muntanya. Ordino, Andorra. Gen 2018